THE DEVELOPMENT OF A CATALYTIC PROCESS FOR THE HYDROTREATMENT OF HALOARENES

SANTIAGO GÓMEZ QUERO

A dissertation submitted for the degree of Doctor of Philosophy

Heriot-Watt University

School of Engineering and Physical Sciences

September 2009

Abstract

The abatement of halogenated compounds released from various processes into the environment is now recognized as a pressing environmental issue. Catalytic hydrodehalogenation (HDH) has emerged as a potential technology that can facilitate waste transformation and reuse. In this thesis, a comprehensive study of the critical reaction/catalyst variables is considered for the HDH of a range of haloarenes (chloro- and bromo-phenols and chlorobenzenes) using (commercial) Pd/Al_2O_3 and (laboratory synthesised) Au supported on α-Fe_2O_3 and Fe_3O_4. Aqueous phase (T = 303 K) HDH is demonstrated to be structure sensitive where smaller Pd particles are intrinsically more active and metal/support interactions have a major impact on reaction selectivity (notably at pH = 3). HDH follows an electrophilic aromatic substitution mechanism: the rate of C–Br bond(s) scission is an order of magnitude greater relative to C–Cl (due to the lower bond dissociation energy). The presence of a second halogen substituent has a deactivating effect (by lowering electron density in the aromatic ring). Solvent (water, organic and water/organic mixtures) effects have been established where, in absence of mass transport limitations, reaction in water delivers significantly higher HDH rates and selectivity is unaffected by solvent composition. A mathematical analysis demonstrates that these effects are principally (*ca.* 80 % contribution) the result of the variations in solvent dielectric constant where the molar volume represents a secondary consideration. The advantages of a shift from batch to continuous HDH are established in terms of: (i) more efficient gas to liquid H_2 transfer; (ii) enhanced HDH rates; (iii) prolongued catalyst lifetime. The potential of HDH as a means of waste transformation to a commercial product is demonstrated in the gas phase (T = 423 K) hydroconversion of 2,4-dichlorophenol into cyclohexanone (over Pd) and 4-chlorophenol (over iron-oxide supported Au). In both cases, a contribution due to spillover hydrogen is established. A comprehensive programme of (Au) catalysts synthesis and characterization, in terms of TPR, H_2 chemisorption/TPD, XRD, DRS UV-Vis, SEM/TEM and BET/pore volume measurements is provided and correlated with HDH kinetics. The results presented in this thesis demonstrate the feasibility and flexibility (in terms of operation, rate/selectivity control and product reuse) of catalytic HDH as a progressive means of haloarene waste treatment.

Dedication

To

Emilio Gómez Gutiérrez

Victoriano Quero Castro

Julia Díaz Sastre

María Rueda López

Acknowledgements

I would like to express my sincere gratitude to Professor Mark A. Keane for his patience, belief, encouragement and uncomparable commitment to research and science, providing the background to fullfil the academic excellence that a PhD requires. He was, is and will always be such an inspiration to me. My laboratory colleague and friend, Dr. Fernando Cárdenas Lizana, also deserves attention and recognition. Inherent ability to consider alternative points of view, willingness to work and positive attitude are the main characteristics of an unprecedent support that will be etched on my memory. I am indebted to him for much more than the PhD.

I would also like to acknowledge the assistance of the Heriot-Watt University staff, special thanks are due to Curtis L. Abbott, Anne Blyth, Craig Bell, Rebecca Crawford, Eileen M. McEvoy, Malcolm McWilliams, Marian K. Millar, Ronald Millar and Cameron Smith.

I also owe this thesis to the pleasant environment created by people I had the chance to meet during the three and a half years of laboratory work: Dimitra Gouliari, Romain Charbonnel, Craig Burnett, Maria Luz Pérez Cuevas, Fisher Millard, Antonio Nieto-Márquez Ballesteros, Elena Díaz Nieto, Zahara Martínez de Pedro, Noémie Perret and Sofía Marín Mallo. Gracias/thanks/merçi/ευχαριστώ. I would also like to thank the cheerful spirit of my friends, those in Spain and the new ones I got to know in Scotland, notably Amalia, Camino, Charis, Christos, Elena, Emilio, Gerard, Gianlucca, Isaela, Iwona, Jacek, James, Julien, Nick, Rafa, Robert, Simon, Úrsula, Verónica and Víctor. María Lucía Romero Pérez, Patricia Leyva Bailén and Alberto Campos Zataraín deserve a separate mention, as they were my family during these years in Scotland.

Last, but not least, I would like to give a special place to my beloved parents (Santiago Gómez Díaz and Maria Victoria Quero Rueda) and sister (Mavi) and other members of my family. It is only thanks to your education and day-to-day example that I learnt to surmount difficulties with hard work, perseverance, psychological resilience and, most importantly, that this is not in contradiction with being a kind-hearted (good) person. This thesis would have not been possible to do without them.

This PhD project was funded by the EPSRC through grant No. 0231 110525, whom I would also like to thank.

Table of Contents

List of Tables

List of Figures

Glossary

Roman Letters

Symbol	*Physical Meaning*	*Units*
a_{ε}	Fitting parameter	$mmol_{2,4\text{-DCP}}\ g_{Pd}^{-1}\ min^{-1}$ $mmol_{X}\ g_{Pd}^{-1}\ min^{-1}$
a_g	Gas/liquid interfacial area per unit volume of liquid	$m^2\ m^{-3}$
$a_{\bar{v}}$	Fitting parameter	$mmol_{2,4\text{-DCP}}\ mol_{Solvent}^{\ b_{\bar{v}}}\ g_{Pd}^{-1}\ min^{-1}\ cm^{-(3+b_{\bar{v}})}$ $mmol_{X}\ mol_{solvent}^{\ b_{\bar{v}}}\ g_{Pd}^{-1}\ min^{-1}\ dm^{-(3+b_{\bar{v}})}$
a_T	Fitting parameter	$mmol_{2,4\text{-DCP}}\ cm^{(3+b_T)}\ g_{Pd}^{-1}\ min^{-1}\ mol_{solvent}^{\ -b_T}$ $mmol_{X}\ dm^{(3+b_T)}\ g_{Pd}^{-1}\ min^{-1}\ mol_{solvent}^{\ -b_T}$
b_{ε}	HDH/HDC rate dependence factor on solvent dielectric constant	dimensionless
$b_{\bar{v}}$	HDH/HDC rate dependence factor on solvent molar volume	dimensionless
b_T	HDH/HDC rate dependence factor on both solvent dielectric constant and molar volume	dimensionless
C_{HX}	Concentration of inorganic halogen	$mol_{HX}\ dm^{-3}$, $mmol_{HX}\ dm^{-3}$
$(C_{H_2})_{bulk}$	H_2 concentration in the bulk liquid	$mmol_{H_2}\ dm^{-3}$
$(C_{H_2})_{saturation}$	H_2 saturation concentration	$mmol_{H_2}\ dm^{-3}$
C_i	Concentration of compound *i*	$mol_i\ dm^{-3}$, $mmol_i\ dm^{-3}$
$C_{i,0}$	Initial concentration of compound *i*	$mol_i\ dm^{-3}$, $mmol_i\ dm^{-3}$
$C_i\ (t)$	Concentration of compound *i* at time *t*	$mol_i\ dm^{-3}$
C_X	Concentration of organic halogen	$mol_X\ dm^{-3}$, $mmol_X\ dm^{-3}$
$C_{X,0}$	Initial concentration of organic halogen	$mol_X\ dm^{-3}$, $mmol_X\ dm^{-3}$
Ca	Carberry number	dimensionless
D	Metal dispersion	dimensionless
$D_{Eff,i}$	Effective diffusivity of compound *i*	$m^2\ s^{-1}$
D_i	Diffusivity of compound *i*	$m^2\ s^{-1}$
d	Catalyst particle diameter	μm
d_{Chem}	Metal particle size estimated from H_2 chemisorption analysis	nm
d_i	Diameter of the i^{th} metal particle	nm
d_{TEM}	Surface area weighted metal particle size estimated from TEM analysis	nm
$\Delta\bar{H}$	Enthalpy of vaporization	$kJ\ mol^{-1}$

Symbol	*Physical Meaning*	*Units*
$\Delta\bar{H}_{T_b}$	Boiling point enthalpy of vaporization	kJ mol^{-1}
Δt	Integral time	h
$EC_{50,i}$	Median effective concentration of compound *i*	mg dm^{-3}
F	Molar flow of 2,4-DCP	$mol_{2,4\text{-DCP}}$ h^{-1}
F_{Cl}	Molar flow of organic chlorine	mol_{Cl} h^{-1}
F_{OH}	Molar flow of (chloro-)phenol	mol_{OH} h^{-1}
$f^0_{H_2}$	Fugacity of H_2 gas	MPa
$f^L_{H_2}$	Fugacity of H_2	MPa
g	Volume fraction of the solvent	dimensionless
K	Ratio of 2-CP consumption and formation constants	dimensionless
K_j	Equilibrium constant of step j	dimensionless, atm^{-1}, atm^{-2}
k	Pseudo first order 2,4-DCP consumption rate constant	$mol_{2,4\text{-DCP}}$ h^{-1} mol_{Au}^{-1}
k_j	Pseudo first order rate constant for reaction step j	min^{-1}
k_L	liquid film mass transfer coefficient	m min^{-1}
k_X	Pseudo first order HDH rate constant	min^{-1}
k'	Specific pseudo first order 2,4-DCP consumption rate constant	$mol_{2,4\text{-DCP}}$ h^{-1} m_{Au}^{-2}
k'_{Cl}	Specific HDC rate constant	mol_{Cl} h^{-1} m_{Au}^{-2}
L	Fitting parameter	dimensionless
M	Fitting parameter	dimensionless
M_M	Atomic mass of metal M	dimensionless
m	Catalyst concentration	g dm^{-3}
m_{Pd}	Catalyst Pd loading	g_{Pd} g^{-1}
N_{H_2}	H_2 mass transfer rate	$mmol_{H_2}$ min^{-1} dm^{-3}
n_{Cl}	Number of moles of organic chlorine	$mmol_{Cl}$
$n_{2,4\text{-DCP}}$	Number of moles of 2,4-DCP	$mol_{2,4DCP}$
n_{HCl}	Number of moles of inorganic chlorine	$mmol_{HCl}$
n_i	Number of metal particles of diameter d_i	dimensionless
n_M	Number of moles of metal M	mol_M
P	Pressure	atm
P_i	Partial pressure of compound i	atm
P/P_0	Relative pressure	dimensionless
pH_{acid}	pH maintained at acid conditions	dimensionless
pH_{basic}	pH maintained at basic conditions	dimensionless
$pH_{l/s}$	pH at the bulk liquid/catalyst surface interface	dimensionless
pH_{pzc}	pH of the point of zero charge	dimensionless
pK	Acid-base equilibria dissociation constant	dimensionless
R	Universal gas constant	J mol^{-1} K^{-1}

Symbol	*Physical Meaning*	*Units*
r	Pore radius	Å
$(R_{C6ONE})_0$	Initial C6ONE production rate	$mol_{C6ONE}\ mol_{Pd}^{-1}\ h^{-1}$
$(R'_{C6ONE})_0$	Specific initial C6ONE production rate	$mol_{C6ONE}\ m_{Pd}^{-2}\ h^{-1}$
$(R_{2\text{-}CP})$	2-CP production rate	$mmol_{2\text{-}CP}\ g_{Pd}^{-1}\ min^{-1}$
$(-R_{2,4\text{-}DCP})$	2,4-DCP consumption rate	$mmol_{2,4\text{-}DCP}\ g_{Pd}^{-1}\ min^{-1}$
$(-R_{2,4\text{-}DCP})_0$	Initial 2,4-DCP consumption rate	$mmol_{2,4\text{-}DCP}\ g_{Pd}^{-1}\ min^{-1}$
$(-R'_{2,4\text{-}DCP})_0$	Specific initial 2,4-DCP consumption rate	$mmol_{2,4\text{-}DCP}\ m_{Pd}^{-2}\ min^{-1}$
$(-R_{2,4\text{-}DCP})_0^E$	Excess initial 2,4-DCP consumption rate in a water+organic solvent mixture	$mmol_{2,4\text{-}DCP}\ g_{Pd}^{-1}\ min^{-1}$
$(-R_{2,4\text{-}DCP})_0^{Predicted}$	Initial 2,4-DCP consumption rate in a water+organic solvent mixture, as predicted assuming an ideal mixing rule	$mmol_{2,4\text{-}DCP}\ g_{Pd}^{-1}\ min^{-1}$
$(R_{HDC})_0$	Initial HDC rate	$mmol_{Cl}\ g_{Pd}^{-1}\ min^{-1}$
$(R'_{HDC})_0$	Speficic initial HDC rate	$mmol_{Cl}\ m_{Pd}^{-2}\ min^{-1}$
$(R_{HDH})_0$	Initial HDH rate	$mmol_{X}\ g_{Pd}^{-1}\ min^{-1}$
$(-R_i)_0$	Consumption rate of compound *i*	$mol\ g^{-1}\ s^{-1}$
S_i	Reaction selectivity with respect to product *i*	dimensionless
$S_{i,0}$	Initial reaction selectivity with respect to product *i*	dimensionless
S_M	Specific surface area of metal *M*	$m_M^2\ g_M^{-1}$
T	Temperature	K
$T.U._{Mixture}\ (t)$	Toxicity units of the reaction mixture at time *t*	dimensionless
t	Reaction time, contact time	min
V_{N_2}	Volume of N_2 adsorbed during pore volume measurements	cm^3_{STP}
W	Catalyst mass	g
W_{Pd}	Pd concentration	$g_{Pd}\ dm^{-3}$
X_i	Fractional conversion of compound *i*	dimensionless
$X_{i,0}$	Initial fractional conversion of compound *i*	dimensionless
$X_{i,5h}$	Fractional conversion of compound *i* after 5 h time-on-stream hydroprocessing	dimensionless
x_i	Molar fraction of compound *i*	dimensionless
$x_{i,0}$	Initial molar fraction of compound *i*	dimensionless
x_X	Fractional degree of HDH	dimensionless
Y_i	Yield of compound *i*	dimensionless
$Y_{i,0}$	Initial yield of compound *i*	dimensionless

Greek Letters

Symbol	*Physical Meaning*	*Units*
α	Fitting parameter	dimensionless
β	Heating rate	K min^{-1}
δ	Solubility parameter for the solvent	$kJ^{1/2}$ $m^{-3/2}$
δ_{H_2}	Solubility parameter for H_2	$kJ^{1/2}$ $m^{-3/2}$
ε	Dielectric constant	dimensionless
ε_c	Corrected dielectric constant of a water+organic solvent mixture	dimensionless
$\varepsilon_{catalyst}$	Catalyst porosity	dimensionless
ε_m	Dielectric constant of a water+organic solvent mixture	dimensionless
ε_i	Dielectric constant of compound *i*	dimensionless
ε^E	Excess dielectric constant of a water+organic solvent mixture	dimensionless
η	Effectiveness factor	dimensionless
η_S	Dynamic viscosity of solvent *S*	mPa s^{-1}
$\overline{v}$	Molar volume	cm^3 mol^{-1}
$\overline{v}_c$	Corrected molar volume of a water+organic solvent mixture	cm^3 mol^{-1}
$\overline{v}_i$	Molar volume of compound *i*	cm^3 mol_i^{-1}
$\overline{v}^E$	Excess molar volume of a water+organic solvent mixture	cm^3 mol^{-1}
ρ	Catalyst bulk density	kg m^{-3}
ρ_M	Density of metal *M*	g_M cm_M^{-3}
τ	Catalyst tortuosity	dimensionless
Φ	Weisz-Prater number	dimensionless
ϕ	Thiele modulus	dimensionless
Ψ	HDH/HDC fractional dependence on the solvent dielectric constant	dimensionless

Nomenclature

Acronim	*Meaning*
BET	Brunauer-Emmet-Teller
BP	Bromophenol
CB	Chlorobenzene
CFC	ChloroFluoro Carbon
C6OH	Cyclohexanol
C6ONE	Cyclohexanone
CP	Chlorophenol
CSTR	Continuous Stirred-Tank Reactor
CTC	Carbon Tetrachloride
DBP	Dibromophenol
DCB	Dichlorobenzene
DCP	Dichlorophenol
DRS UV-Vis	Diffuse Reflectance Spectroscopy in the Ultraviolet-Visible region
EDX	Energy Dispersive X-ray
EPA	Environmental Protection Agency
EXAFS	Extended X-ray Atomic Fine Structure
FID	Flame Ionization Detector
FTIR	Fourier Transform InfraRed spectroscopy
GHSV	Gas Hourly Space Velocity
HDC	Hydrodechlorination
HDH	Hydrodehalogenation
IARC	International Agency for Research Cancer
ICP-OES	Inductively Coupled Plasma-Optical Emission Spectrometry
JCPDS-ICDD	Joint Committee on Powder Diffraction Standards – International Center for Diffraction Data
PCDD / PCDF	Polychlorodibenzodioxins / Polychlorodibenzofurans
PhOH	Phenol
SEM	Scanning Electron Microscopy
TCD	Thermal Conductivity Detector
TCP	Trichlorophenol
TEM	Transmission Electron Microscopy
TPD	Temperature-Programmed Desorption
TPR	Temperature-Programmed Reduction
TSCA	Toxic Substance Control Act
UTW	Ultra-Thin Window
WHO	World Health Organisation
XPS	X-ray Photoelectron Spectroscopy
XRD	X-Ray Diffraction

List of Publications by the Candidate

1) S. Gómez-Quero, F. Cárdenas-Lizana, M. A. Keane, Effect of Metal Dispersion on the Liquid Phase Hydrodechlorination of 2,4-Dichlorophenol over Pd/Al_2O_3, Ind. Eng. Chem. Res., 47, 6841 (2008).

2) S. Gómez-Quero, F. Cárdenas-Lizana, M. A. Keane, Solvent Effects in the Liquid Phase Hydrodechlorination of 2,4-Dichlorophenol over Pd/Al_2O_3, AIChe J., Accepted.

3) S. Gómez-Quero, E. Díaz, F. Cárdenas-Lizana, M. A. Keane, Solvent Effects in the Catalytic Hydrotreatment of Haloaromatics over Pd/Al_2O_3 in Water Organic Mixtures, Chem. Eng. Sci., submitted for publication.

4) S. Gómez-Quero, F. Cárdenas-Lizana, M. A. Keane, Liquid Phase Catalytic Hydrodechlorination of 2,4-Dichlorophenol over Pd/Al_2O_3: Batch *vs.* Continuous Operation, manuscript ready for submission.

5) S. Gómez-Quero, F. Cárdenas-Lizana, M. A. Keane, Gas Phase Hydrotreatment of Chlorophenols as an Alternative Route to Cyclohexanone, manuscript ready for submission.

6) S. Gómez-Quero, F. Cárdenas-Lizana, M. A. Keane, Selective Hydrodechlorination of 2,4-Dichlorophenol over Iron Oxide Supported Au, manuscript ready for submission.

7) S. Gómez-Quero, F. Cárdenas-Lizana, M. A. Keane, Au/Fe_3O_4: Characterization and Application in Gas Phase Hydrodechlorination, manuscript ready for submission.

List of Presentations by the Candidate

1) "Solvent and Particle Size on the Hydrodechlorination of 2,4-Dichlorophenol over Pd/Al_2O_3", 5th International Conference in Environmental Catalysis; University of Belfast, August 2008.

2) "Solvent Effects in Catalytic Hydrodechlorination", SURCAT Ecosse Conference; University of Aberdeen, May 2008.

3) "Solvent and Particle Size Effects in Liquid Phase Catalytic Hydrodechlorination", Mechanical and Chemical Engineering Department Seminar Series; Heriot-Watt University (Edinburgh), February 2008.

4) "Metal Dispersion in 2,4-Dichlorophenol Catalytic Hydrodechlorination", SURCAT Ecosse Conference; University of St. Andrews, May 2007.

5) "Metal Dispersion in 2,4-Dichlorophenol Catalytic Hydrodechlorination", ScotCHEM Materials Conference; Heriot-Watt University (Edinburgh), March 2007.

List of Posters by the Candidate

1) "The Hydrotreatment of Chlorophenols: An Alternative Route to Cyclohexanone", IChemE Conference on Applied Catalysis: Towards Sustainable Chemical Industry; University of Bath, November 2008.

2) "Catalytic Hydrodechlorination of Chlorophenols over Palladium", 9th UK Particle Technology Forum; Heriot-Watt University (Edinburgh), June 2008.

3) "Catalytic Hydrodechlorination of Chlorophenols over Palladium", 1st Year PhD Progress Meeting; Heriot-Watt University (Edinburgh), October 2006.

Chapter 1

Introduction and Scope of the Thesis

This Chapter presents a short overview of the environmental implications associated with the release of halogenated compounds and available methods of control/disposal, highlighting the significance of catalytic hydrodehalogenation as a progressive approach to environmental remediation. The objectives of this PhD research are defined and the approach taken is described.

1.1 Halogenated Compounds

Halogen-containing organics (particularly chlorinated compounds) have long been used in the chemical industry for the manufacture of fine chemicals, notably personal care formulations and microorganism/plant/insect control (see **Table 1.1**). Lack of stringent production controls has resulted in the release of these compounds into the environment as a result of uncontrolled emissions and/or accidental spills [1,2]. Due to their low biodegradability and deleterious ecological and environmental effects (see **Table 1.2**), they are now identified as high priority pollutants in terms of treatment [2-4] and heavily legislated by the EPA Toxic Substance Control Act (TSCA), the International Agency for Research Cancer (IARC) and the World Health Organization (WHO) [5,6].

Table 1.1: Typical products manufactured using halogenated compounds as starting materials or additives.

Category	Products	Refs.
Health/personal care	Pharmaceuticals Deodorants Mouthwashes and toothpastes Fragances	[7,8]
Microorganism control	Biocides Antiseptics Fungicides Molluskicides Antimicrobial finishing of textiles and paper	[7-13]
Plant/insect control	Herbicides Algae control in water circulating systems Repellents for plant-feeding insects	[7,8,14-16]
Other	Preservative for metal working lubricants Flame retardant additives in unsaturated polyester and epoxy resins Fire extinguishing agents Solvents for oil, waxes, resins, greases and rubbers Wood preservation	[1,7,8,14,17]

Table 1.2: Impact of halogenated chemicals on human health and the environment.

Category	Effect	Refs.
Health[a]	Irritation of skin, eyes and lung Kidney/liver damage Cardiovascular effects Carcinogenic Neuropathies and behavioral disturbances Death	[4,6-8,11,14,18,19]
Environment[b]	Global warming O_3 depletion Contamination of agriculture Animal disease	[4,6,8,20-23]

[a]detailed information can be found in refs. [4] (for a range of compounds) and [17] and [8] for specific chlorinated and brominated organics, respectively
[b]concise examples can be found in refs [20] and [23] for dioxin(s) and chlorobenzene(s) presence/effects in the Great Lakes (USA) and UK rivers, respectively

Several methods of halogenated waste control/disposal have been considered and are summarised in **Table 1.3**. Cumulative methods are typically inexpensive and are the preferred option for the treatment of individual compounds when present in high concentrations (> 2 g dm^{-3} [24]). This approach serves to concentrate the pollutant(s). Oxidative methods generate CO_2, H_2O and the corresponding hydrogen halide (HX, X = Cl, Br, I) [2,25] and are the most widely used due to their proven efficiency (*e.g.* incineration [26]). Nevertheless, oxidative treatments present decided drawbacks in terms of (i) the requirement of expensive reactants (*e.g.* photo-oxidation [27,28]) and/or equipment (*e.g.* sono- [29,30] and electrochemical [31,32] oxidation) and (ii) the potential production of even more toxic by-products as a result of incomplete combustion (*e.g.* incineration [33,34]). Bioremediation, either aerobic (oxidative) or anaerobic (reductive), can be successfully used for the treatment of a wide range of compounds (halogenated dioxins, benzenes and phenols) but only at low concentrations (*e.g.* $< 6\times10^{-3}$ mol_{Cl} dm^{-3} in the case of chlorinated compounds [35,36]). Furthermore, effective practical application of bioremediation can be hampered by the requirement of careful control of the moisture content and the inclusion of C/N/P nutrients [37]. In order to minimise environmental effects and ensure conservation of resources, the ideal abatement option should be the recovery/reuse of raw material [4,38]. This is facilitated by the last reductive method included in **Table 1.3** and the focus of this thesis: catalytic hydrodehalogenation.

Table 1.3: Short overview of principal methods for halogenated waste control/disposal.

Nature	Method	Resume	Refs.
Cumulative	Adsorption	Pollutant capture from a gas/liquid stream onto a solid (typically activated carbon or resins)	[39-41]
	Absorption	Pollutant capture from a gas stream into a liquid stream where it can react.	[42,43]
	Air stripping	Pollutant capture from a liquid stream into air	[43-45]
	Permeation	Concentration from a liquid stream into another by membrane separation	[46,47]
Oxidative	Incineration	Pollutant combustion at high temperatures ($T \geq 1200$ K)	[26,33,34]
	Wet air oxidation	Treatment of a liquid stream containing the pollutant with O_2 at $T \geq 433$ K and $P \geq 2$ atm	[48-50]
	Advanced	Pollutant oxidation by OH· radicals generated by chemical redox processes (Fe, H_2O_2, O_3), UV radiation, ultrasound or high voltages	[27-32,51]
	Aerobic biodegradation	Treatment with microorganisms in the presence of air	[35-37]
Reductive	Anaerobic biodegradation	Treatment with microorganisms in the absence of oxygen	[37,52]
	Hydrodehalogenation	Transformation of the C–X bond into C–H using a range of reducing agents: (notably, inorganic salts, formic acid, secondary alcohols or H_2)	-[a]

[a]literature review provided in section **1.2**

1.2 Catalytic Hydrodehalogenation

Hydrodehalogenation (HDH) involves the H_2-mediated cleavage of the carbon-halogen bond to form an alkane (*via* an electrophilic mechanism [53,54], see **Table 1.3**), with the release of the corresponding HX [54-56]. A distinction should be made bewteen HDH and dehydrohalogenation, the latter involving internal halogen elimination with the production of an alkene [57,58]. HDH is a thermodynamically favourable and exothermic process [59,60] where the use of a catalyst results in an appreciable enhancement of HDH rate. This feature of catalytic HDH will be reviewed, analysed and discussed throughout this thesis. The main body of work dealing with catalytic HDH research has been developed over the past decade where Pd has been identified as the most effective metal due to its H_2 chemisorptive ability [61,62] and resistance to HX-induced deactivation [63,64]. The effect of process variables relating to the catalyst (support [65-68], metal particle size [67-77] and electronic state [78,79]) and reaction conditions (temperature/pressure [70,80-87], solvent/carrier [82-86,88-97], contact time [70,78,81,95,98]) has now been studied. Nevertheless, there is still no general consensus regarding the role of such variables as metal dispersion and solvent.

Moreover, few published studies have included detailed kinetic measurements with an explicit analysis of mass transport phenomena. Indeed, there is a dearth of studies that have provided any clear correlation of catalyst performance with catalyst structure/surface chemistry. This lack of fundamental information has limited the actual deployment of catalytic HDH in environmental pollution control.

1.3 Scope and Organization of the Thesis

The objective of this research is to carry out a systematic and comprehensive study of critical variables that can underpin catalytic HDH and to demonstrate the potential of this approach as a progressive haloarene waste abatement technology.

The liquid phase catalytic hydrodechlorination of 2,4-dichlorophenol over Pd/Al_2O_3 has been taken as starting point because it is a relatively well characterized system and total dechlorination can be achieved under mild conditions (P = 1 atm; T = 303 K; [99-104]). The effect of variations in Pd dispersion is first established in **Chapter 2** where the Pd particle size is adjusted by means of controlled thermal sintering at different temperatures (423 - 1273 K) and heating rates (1 - 50 K min^{-1}); the action of bulk (unsupported) Pd is also considered for comparative purposes. The effect of the solvent is next considered in **Chapters 3** and **4** using water and organic (alcohols, cyclohexane, *n*-hexane, benzene and THF) solvents and extending the study to a range of mono- and di-chlorophenols, bromophenols and chlorobenzenes. Since the vast majority of liquid phase HDH studies have been carried out in batch (discontinuous) operation, the feasibility and advantages of a shift to continuous HDH is addressed in **Chapter 5**. Finally, the feasability of product recovery/reuse from catalytic HDH is examined in **Chapters 6**, **7** and **8**, focusing on the gas phase production of cyclohexanone and 4-chlorophenol over Pd and iron oxide supported Au, respectively. A detailed catalyst characterization program (in tems of TPR, H_2 chemisorption/TPD, BET/pore volume, XRD, SEM/TEM and DRS UV-Vis) has been performed in each instance to link critical catalyst structural features with the observed catalytic response(s). A comprehensive assessment of mass transfer limitations has ensured operation under a kinetically controlled regime. In short, this thesis is a compilation of fundamental HDH studies with the practical deliverable of halogenated waste control/disposal/recovery.

1.4 References

[1.1] E. J. Kormondy, International Handbook of Pollution Control, Gower Publishing Company, Aldershot, 1989.

[1.2] G. W. Dawson, B. W. Mercer, Hazardous Waste Management, John Wiley & Sons, New York, 1986.

[1.3] USEPA, The Inventory of Sources of Dioxin in the United States. EPA/600/P-98/00A2, 1998.

[1.4] M. D. Lagrega, P. L. Buckingham, J. C. Evans, Hazardous Waste Management, Mc. Graw-Hill, Singapore, 1994.

[1.5] R. J. Lewis, Hazardous Chemicals Desk Reference, Van Nostrand Reinhold, New York, 1997.

[1.6] USEPA, Advisory Document No. 8EHQ-14302, 2000.

[1.7] W. Paulus, Ullmann's Encyclopedia of Industrial Chemistry. "Phenol Derivates", Wiley-VCH Verlag GmbH & Co. KGaA, Weinheim, 2005.

[1.8] M. J. Dagani, H. J. Barda, T. J. Benya, D. C. Sanders, Ullmann's Encyclopedia of Industrial Chemistry. "Bromine Compounds", Wiley-VCH Verlag GmbH & Co. KGaA, Weinheim, 2005.

[1.9] P. Ackermann, P. Margot, F. Müller, Ullmann's Encyclopedia of Industrial Chemistry. "Fungicides, Agricultural", Wiley-VCH Verlag GmbH & Co. KGaA, Weinheim, 2005.

[1.10] G. J. Gendimenico, Ullmann's Encyclopedia of Industrial Chemistry. "Dermatotherapeutic Agents", Wiley-VCH Verlag GmbH & Co. KGaA, Weinheim, 2006.

[1.11] H.-J. Schnorbach, H.-D. Matthaei, F. Müller, Ullmann's Encyclopedia of Industrial Chemistry. "Molluskicides", Wiley-VCH Verlag GmbH & Co. KGaA, Weinheim, 2008.

[1.12] H. A. Wittcoff, B. G. Reuben, J. S. Plotkin, Industrial Organic Chemicals, 2nd ed., Witey-Interscience Publication, New Jersey, 2004.

[1.13] F. Muller, L. Caillard, Ullmann's Encyclopedia of Industrial Chemistry. "Chlorophenols", Wiley-VCH Verlag GmbH & Co. KGaA, Weinheim, 2000.

[1.14] M. L. Leng, Ullmann's Encyclopedia of Industrial Chemistry. "Chlorophenoxyalkanoic Acids", Wiley-VCH Verlag GmbH & Co. KGaA, Weinheim, 2005.

[1.15] R. L. Metcalf, Ullmann's Encyclopedia of Industrial Chemistry. "Insect Control", Wiley-VCH Verlag GmbH & Co. KGaA, Weinheim, 2005.

[1.16] International Agency for Research on Cancer: World Health Organisation, IARC Monographs on The Evaluation of Carcinogenic Risks to Humans. Volume 52: Chlorinated Drinking-Water; Chlorination By-Products; Some Other Halogenated Compounds; Cobald and Cobalt Compounds, Check, Check, 1991.

[1.17] M. Rossberg, W. Lendle, G. Pfleiderer, A. Tögel, E.-L. Dreher, E. Langer, H. Rassaerts, P. Kleinschmidt, H. Strack, R. Cook, U. Beck, K.-A. Lipper, T. R. Torkelson, E. Löser, K. K. Beutel, T. Mann, Ullmann's Encyclopedia of Industrial Chemistry. "Chlorinated Hydrocarbons", Wiley-VCH Verlag GmbH & Co. KGaA, Weinheim, 2006.

[1.18] P. Kintz, A. Tracqui, P. Mangin, Arch. Toxicol., 66, 298 (1992)

[1.19] A. Schecter, L. Birnbaum, J. J. Ryan, J. D. Constable, Environ. Res., 101, 419 (2006)

[1.20] R. E. Hester, R. M. Harrison, Chlorinated Organic Micropollutants, Bookcraft, Cambridge, 1996.

[1.21] C. A. Kan, G. A. L. Meijer, Anim. Feed Sci. Technol., 133, 84 (2007)

[1.22] Pollution Handbook 2005: The Esssential Guide to UK and European Pollution Control Legislation, Environmental Protection UK, 2005.

[1.23] A. A. Meharg, J. Wright, D. Osborn, Sci. Total Environ., 251-252, 243 (2000)

[1.24] W. Ying, R. R. Bonk, S. C. Hannam, Q. D. Li, Environ. Prog., 13, 192 (1994)

[1.25] W. S. Trahanovsky, Oxidation in Organic Chemistry, Academic Press, London, 1982.

[1.26] L. Theodore, J. Reynolds, Introduction to Hazardous Waste Incineration, John Wiley & Sons, New York, 1987.

[1.27] M. Pera-Titus, V. García-Molina, M. A. Baños, J. Giméneza, S. Esplugas, Appl. Catal. B: Environmental, 47, 219 (2004)

[1.28] L. Wu, A. Li, G. Gao, Z. Fei, S. Xu, Q. Zhang, J. Mol. Catal. A: Chemical, 269, 183 (2007)

[1.29] R. Kidak, N. H. Ince, Ultrason. Sonochem., 13, 195 (2006)

[1.30] O. Hamdaoui, E. Naffrechoux, Ultrason. Sonochem., 15, 981 (2008)

[1.31] H. Cheng, K. Scott, P. A. Christensen, Appl. Catal. A: General, 261, 1 (2004)

[1.32] G. Chen, Z. Wang, D. Xia, Electrochim. Acta, 50, 933 (2004)

[1.33] V. Nicolas, S. Jean-Pierre, Chemosphere, 67, S144 (2007)

[1.34] L. Khachatryan, S. Lomnicki, B. Dellinger, Chemosphere, 68, 1741 (2007)

[1.35] M. Dilaver, F. Kargi, Bioresour. Technol., 100, 1459 (2009)

[1.36] S. Eker, F. Kargi, J. Hazard. Mater., 159, 306 (2008)

[1.37] G. R. Chaudhry, Biological Degradation and Bioremediation of Toxic Chemicals, Colorcraft, Hong Kong, 1994.

[1.38] M. A. Keane, J. Chem. Technol. Biotechnol., 82, 787 (2007)

[1.39] A. Derylo-Marczewska, A. Swiatkowski, S. Biniak, M. Walczyk, Colloids Surf,. A, 327, 1 (2008)

[1.40] C. Namasivayam, D. Sangeetha, R. Gunasekaran, Process Saf. Environ. Prot., 85, 181 (2007)

[1.41] M. S. Bilgili, J. Hazard. Mater. B, 137, 157 (2006)

[1.42] B. J. Kim, S. Qi, Water Environ. Res., 67, 560 (1995)

[1.43] M. L. Davis, D. A. Cornwell, Introduction to Environmental Engineering, McGraw-Hill, New York, 1998.

[1.44] C. A. Cole, D. A. Long, Hazardous and Industrial Wastes, Technomic Publishing Company, Pennsylvania, 1989.

[1.45] R. L. Gross, S. G. Termaath, Environ. Prog., 4, 119 (1985)

[1.46] S. B. Kulkarni, A. A. Kittur, S. S. Kulkarni, M. Y. Kariduraganavar, Desalination, 196, 43 (2006)

[1.47] S. H. Lin, C. L. Pan, H. G. Leu, J. Hazard. Mater. B, 65, 289 (1999)

[1.48] V. García-Molina, J. Kallas, S. Esplugas, Chem. Eng. J., 126, 59 (2007)

[1.49] M. E. Suárez-Ojeda, A. Fabregat, F. Stüber, A. Fortuny, J. Carrera, J. Font, Chem. Eng. J., 132, 105 (2007)

[1.50] M. E. Suárez-Ojeda, J. Carrera, I. S. Metcalfe, J. Font, Chem. Eng. J., 144, 205 (2008)

[1.51] W. Simmler, Ullmann's Encyclopedia of Industrial Chemistry. "Wastewater", Wiley-VCH Verlag GmbH & Co. KGaA, Weinheim, 2005.

[1.52] P. S. Majumder, S. K. Gupta, Bioresour. Technol., 100, 1881 (2009)

[1.53] Y. A. Serguchev, Y. V. Belokopytov, Kinet. Catal., 42, 174 (2001)

[1.54] K. V. Murthy, P. M. Patterson, M. A. Keane, J. Mol. Catal. A: Chemical, 225, 149 (2005)

[1.55] T. Yoneda, T. Takido, K. Konuma, Appl. Catal. B: Environmental, 84, 667 (2008)

[1.56] F. Alonso, I. P. Beletskaya, M. Yus, Chem. Rev., 102, 4009 (2002)

[1.57] G. Tavoularis, M. A. Keane, J. Mol. Catal. A: Chemical, 142, 187 (1999)

[1.58] G. Tavoularis, M. A. Keane, Appl. Catal. A: General, 182, 309 (1999)

[1.59] A. Converti, M. Zilli, D. M. de Faveri, G. Ferraiolo, J. Hazard. Mater., 27, 127 (1991)

[1.60] J. Dolfing, B. K. Harrison, Environ. Sci. Technol., 26, 2213 (1992)

[1.61] G. Centi, J. Mol. Catal. A: Chemical, 173, 287 (2001)

[1.62] P. N. Rylander, Catalytic Hydrogenation Over Platinum Metals, Academic Press, New York, 1967.

[1.63] F. J. Urbano, J. M. Marinas, J. Mol. Catal. A: Chemical, 173, 329 (2001)

[1.64] P. Albers, J. Pietsch, S. F. Parker, J. Mol. Catal. A: Chemical, 173, 275 (2001)

[1.65] L. Prati, M. Rossi, Appl. Catal. B: Environmental, 23, 135 (1999)

[1.66] J. L. Benítez, G. del Angel, React. Kinet. Catal. Lett., 66, 13 (1999)

[1.67] M. A. Keane, C. Park, C. Menini, Catal. Lett., 88, 89 (2003)

[1.68] M. A. Aramendia, V. Boráu, I. M. García, C. Jiménez, F. Lafont, A. Marinas, J. M. Marinas, F. J. Urbano, J. Catal., 187, 392 (1999)

[1.69] Z. Karpiński, K. Early, J. L. d'Itri, J. Catal., 164, 378 (1996)

[1.70] C. Menini, C. Park, E.-J. Shin, G. Tavoularis, M. A. Keane, Catal. Today, 62, 355 (2000)

[1.71] R. Gopinath, K. N. Rao, P. S. S. Prasad, S. S. Madhavendra, S. Narayanan, G. Vivekanandan, J. Mol. Catal. A: Chemical, 181, 215 (2002)

[1.72] W. Juszczyk, A. Malinowski, Z. Karpiński, Appl. Catal. A: General, 166, 311 (1998)

[1.73] B. Coq, G. Ferrat, F. Figuéras, J. Catal., 101, 434 (1986)

[1.74] E.-J. Shin, M. A. Keane, React. Kinet. Catal. Lett., 69, 3 (2000)

[1.75] P. S. S. Prasad, N. Lingaiah, S. Chandrasekhar, K. S. R. Rao, P. K. Rao, K. V. Raghavan, F. J. Berry, L. E. Smart, Catal. Lett., 66, 201 (2000)

[1.76] A. D. L. Ramos, P. S. Alves, D. A. G. Aranda, M. Schmal, Appl. Catal. A: General, 277, 71 (2004)

[1.77] J. Estellé, J. Ruz, Y. Cesteros, R. Fernández, P. Salagre, F. Medina, J.-E. Sueiras, J. Chem. Soc., Faraday Trans., 92, 2811 (1996)

[1.78] K. V. Murthy, P. M. Patterson, G. Jacobs, B. H. Davis, M. A. Keane, J. Catal., 223, 74 (2004)

[1.79] L. M. Gómez-Sainero, X. L. Seoane, J. L. G. Fierro, A. Arcoya, J. Catal., 209, 279 (2002)

[1.80] J. D. Oxley, M. M. Mdleleni, K. S. Suslick, Catal. Today, 88, 139 (2004)

[1.81] K. Yang, B. Wang, L. Chen, X. Wang, Catal. Commun., 9, 431 (2008)

[1.82] J. Chae, S. L. Buchwald, J. Org. Chem., 69, 3336 (2004)

[1.83] M. A. Fakhfakh, X. Franck, R. Hocquemiller, B. Figadère, J. Organomet. Chem., 624, 131 (2001)

[1.84] Y. Monguchi, A. Kume, K. Hattori, T. Maegawa, H. Sajiki, Tetrahedron, 62, 7926 (2006)

[1.85] C. Xia, J. Xu, W. Wu, X. Liang, Catal. Commun., 5, 383 (2004)

[1.86] J.-W. Bae, E.-J. Jang, D.-H. Jo, J.-S. Lee, K.-H. Lee, J. Mol. Catal. A: Chemical, 206, 225 (2003)

[1.87] P. D. Vaidya, V. V. Mahajani, Appl. Catal. B: Environmental, 51, 21 (2004)

[1.88] S. S. Zinovyev, A. Perosa, P. Tundo, J. Catal., 226, 9 (2004)

[1.89] N. C. Concibido, T. Okuda, W. Nishijima, M. Okada, React. Kinet. Catal. Lett., 90, 127 (2007)

[1.90] N. C. Concibido, T. Okuda, W. Nishijima, M. Okada, Appl. Catal. B: Environmental, 71, 64 (2007)

[1.91] N. C. Concibido, T. Okuda, W. Nishijima, M. Okada, React. Kinet. Catal. Lett., 89, 369 (2006)

[1.92] Y. Ukisu, T. Miyadera, React. Kinet. Catal. Lett., 89, 341 (2006)

[1.93] Y. Mitoma, N. Tasaka, M. Takase, T. Masuda, H. Tashiro, N. Egashira, T. Oki, Environ. Sci. Technol., 40, 1849 (2006)

[1.94] N. C. Concibido, T. Okuda, Y. Nakano, W. Nishijima, M. Okada, Tetrahedron Lett., 46, 3613 (2005)

[1.95] G. Evdokimova, S. Zinovyev, A. Perosa, P. Tundo, Appl. Catal. A: General, 271, 129 (2004)

[1.96] W. Nishijima, Y. Ochi, T.-Y. Tsai, Y. Nakano, M. Okada, Appl. Catal. B: Environmental, 51, 135 (2004)

[1.97] P. P. Cellier, J.-F. Spindler, M. Taillefer, H.-J. Cristau, Tetrahedron Lett., 44, 7191 (2003)

[1.98] M. A. Aramendía, V. Boráu, I. M. García, C. Jiménez, J. M. Marinas, F. J. Urbano, Appl. Catal. B: Environmental, 20, 101 (1999)

[1.99] G. Yuan, M. A. Keane, Ind. Eng. Chem. Res., 46, 705 (2007)

[1.100] G. Yuan, M. A. Keane, Catal. Today, 88, 27 (2003)

[1.101] G. Yuan, M. A. Keane, Catal. Commun., 4, 195 (2003)

[1.102] G. Yuan, M. A. Keane, J. Catal., 225, 510 (2004)

[1.103] G. Yuan, M. A. Keane, Appl. Catal. B: Environmental, 52, 301 (2004)

[1.104] G. Yuan, M. A. Keane, Chem. Eng. Sci., 58, 257 (2003)

Chapter 2

Effect of Metal Dispersion on the Liquid Phase Hydrodechlorination of 2,4-Dichlorophenol over Pd/Al_2O_3

The effect of varying Pd metal particle size on catalytic hydrodechlorination is studied in this Chapter, where two (alumina) supported Pd catalysts are considered and compared with bulk (unsupported) Pd. The catalysts are subjected to a comprehensive programme of characterization and their catalytic performance is established. The results demonstrate that hydrodechlorination is structure sensitive where smaller Pd particles deliver a greater intrinsic activity and solution pH is a paramount factor that controls selectivity.

2.1 Introduction

Catalytic hydrodechlorination (HDC) has emerged over the last 20 years as a viable non-destructive approach for the treatment of toxic chlorinated waste [1] including chlorobenzenes [2-8], chlorophenols [1,3,9-16], chlorotoluenes [3,17], CFCs [18-21] and pesticides based on chloro-derivates [12,22]. In HDC, chlorine is replaced by hydrogen with the subsequent release of HCl as by-product. Catalytic studies have been carried out in both gas [1-3,5-7,13,15,16,18-21,23-27] and liquid [4,8-12,14,22,28] phases, where Pd has been identified as the most efficient metal with regard to activity and resistance to deactivation [29,30]. In terms of the structural properties that control HDC performance, metal dispersion which determines specific metal surface area and is dependent on particle size, has been identified as critical. Supported metal particle size can be altered by the synthesis method [4,12,28], nature of the precursor [4,23,31], the support [3,32], loading [3,15,16,33], catalyst pre-treatment [6,7,25,33,34] and/or reduction conditions [5,24]. Furthermore, an increase in metal particle size by agglomeration during HDC, ascribed to metal-chlorine interactions, has also been reported [26,27]. **Table 2.1** contains a compilation of studies available in the open literature that have quoted a catalytic response towards changes in metal dispersion in HDC.

Table 2.1: A compilation of the pertinent literature on metal particle size effects in HDC. Nomenclature: CB = Chlorobenzene; 1,2-DCB = 1,2-Dichlorobenzene; 2-CP = 2-Chlorophenol; 2,4-DCP = 2,4-Dichlorophenol; 2,6-DCP = 2,6-Dichlorophenol; 2,4,5-TCP = 2,4,5-Trichlorophenol; PCP = Pentachlorophenol; CFC-12 = Dichlorodifluoromethane; CFC-114a = Dichlorotetrafluoroethane; CTC = Carbon tetrachloride.

Phase	Catalyst	Reactant(s)	Procedure for metal particle size modification	Size (nm)	Rates (*T* (K), units)		S.S.[a]	Ref.
Gas	Ni[b]	CB; 1,2-DCB	TT[c]: Uncalcined/calcined to 523 K	47-60[d]	3.0-14.0	($493, \times 10^{3}$ $mol_{Reactant}$ s^{-1} mol_{Ni}^{-1})	+	[25]
	Ni/C	CB	TT: Reduction, 673-973 K	9-57	1.8-1.3	($573, \times 10^{-6}$ mol_{CB} s^{-1} g^{-1})	-	[24]
	Ni/CeO_2	CB	MP[c]: $Ni(NO_3)_2$, $Ni(Acetylacetonate)_2$	5-7	6.2-5.5	($573, \times 10^{-3}$ mol_{CB} h^{-1} g^{-1})	-	[23]
	Ni/SiO_2	CB; 2-CP	ML[c]: 1.5-15.2 % w/w	1-3	0.9-5.0	($573, \times 10^{-9}$ $mol_{Reactant}$ s^{-1} g_{Ni} m_{Ni}^{-2})	+	[3]
		CB	ML: 1.5-15.2 % w/w TT: Calcined/uncalcined to 623 K	1-12	0.8-6.0	($523, \times 10^{-5}$ mol_{CB} s^{-1} g_{Ni} m_{Ni}^{-2})	+	[7]
		2-CP; 2,6-DCP 2,4,5-TCP; PCP	ML: 1.5-15.2 % w/w	1-3	1.0-3.7	($573, \times 10^{-4}$ $mmol_{Reactant}$ min^{-1} m_{Ni}^{-2})[d]	+	[16]
	Pd/Al_2O_3	CB	TT: Reduction, 423-673 K	6-37[d]	2.2-1.0	($453, \times 10^{-5}$ mol_{CB} s^{-1} g^{-1})	-	[5]
		CFC-12	ML: 1-5 % w/w MP: $PdCl_2$, $Pd(NO_3)_2$ TT: Reduction, 573-873 K	2-18[d]	4.7-27.0	($453, \times 10^{-3}$ mol_{CFC-12} s^{-1} mol_{Pd}^{-1})	+	[18]
		CFC-12	TT: With/without microwave to 433 K	5-23	7.1-88.0	($473, \times 10^{-3}$ mol_{CFC-12} s^{-1} mol_{Pd}^{-1})	+	[19]
		CFC-114a	TT: Reduction, 573-873 K	11-53	0.8-3.6	($473, mol_{CFC-1114a}$ s^{-1} mol_{Pd}^{-1})	+	[21]
	Pd/C	CFC-12	ST[c]: Contact with HCl/HNO_3	1-4[d]	5.2-11.0	($453, \times 10^{-3}$ mol_{CFC-12} s^{-1} mol_{Pd}^{-1})	+	[20]
	Pd/Nb_2O_5	CB	TT: With/without microwave to 473 K	25-38	4.0-4.7	($473, \times 10^{-1}$ $mmol_{CB}$ min^{-1} m_{Pd}^{-2})[d]	+	[6]
	Pt/Al_2O_3	CTC	TT: Untreated/treated with NH_4Cl after reduction	2-7	1.3-4.9	($363, \times 10^{-1}$ $mmol_{CTC}$ min^{-1} m_{Pd}^{-2})[d]	+	[34]
Liquid	Pd/C	CTC	ML: 0.2-1.6 % w/w TT: Reduction, 423-823 K	5-14[d]	0.5-12.0	($373, \times 10^{+2}$ μmol_{CTC} min^{-1} g^{-1})	+	[33]
	$Pd/AlPO_4$-SiO_2	CB	ML: 0.5-3 % w/w MP: $PdCl_2$, $Pd(Acetylacetonate)_2$ TT: Reduction, 493-873 K	2-16[d]	2.1-72.0	($313, \times 10^{-2}$ $mmol_{CB}$ s^{-1} g_{Pd}^{-1})	+	[4]

[a]Structure Sensitivity: "+" indicates activity increase with increasing particle size, "-" indicates activity decrease with increasing particle size.
[b]Bulk Ni catalyst prepared from $2NiCO_3 \cdot 3Ni(OH)_2 \cdot 4H_2O$.
[c]TT = Thermal treatment; ML = Metal Loading; MP = Metal Precursor; ST = Support Treatment.
[d]Calculated from data source.

Some consensus emerges that points to higher activity for larger particle sizes but this conclusion is by no means irrefutable [3-7,16,18-21,25,33,34]; indeed, Kopinke and co-workers [28], studying the liquid phase chlorobenzene (CB) HDC over Pd-Fe/TiO_2 quoted similar HDC rates (0.3 $mmol_{CB}$ m_{Pd}^{-2} min^{-1}) over catalysts bearing 8 - 11 nm Pd clusters. As shown in **Table 2.1**, CB has been the model reactant in the majority of cases where variations in metal loading and thermal treatment have been employed to modify metal surface area. Differences in reaction rates by up to an order of magnitude have been recorded when the particle sizes are in the mitohedrical region (1 - 5 nm) [4,19] and catalytic activity can be governed by particle morphology and support-induced electronic effects [35]. In gas phase operation, Coq *et al.* [5], studying CB HDC over Pd/Al_2O_3 (6 - 37 nm), reported (an up to two-fold) higher activity over smaller metal particles due to their associated electron-deficient character. Studying the same reaction, Chary *et al.* [23] reached a similar conclusion for a co-precipitated Ni/CeO_2 (5 - 7 nm). On the other hand, Gopinath *et al.* [6], using Pd/Nb_2O_5 (25 - 38 nm), suggested that larger Pd particles are more active due to better resistance to HCl deactivation. Juszczyk *et al.* [18], examining CFC-12 HDC over Pd/Al_2O_3 (2 - 18 nm), linked the same tendency to a more facile carbiding of less dispersed Pd. In an earlier study [3] of the gas phase HDC of a range of halo-arenes over Ni/SiO_2 (1 - 3 nm), Keane *et al.* recorded dechlorination rates up to five times higher on larger Ni particles and ascribed this response to an ensemble effect. The role of metal dispersion has not been studied to the same extent in liquid phase applications and the available literature is not only scant but also inconclusive. Aramendia *et al.* [4], taking the HDC of CB over Pd/$AlPO_4$-SiO_2 (2 - 16 nm), reported rates up to an order of magnitude higher over bigger particles and attributed this to a lesser deactivation by HCl and the contribution of Pd hydride as an alternative source of active hydrogen at lower dispersion. Gómez-Sainero *et al.* [33], examining CCl_4 HDC over Pd/C (5 - 14 nm), linked differences in activity to a different distribution of metallic (Pd^0) and cationic (Pd^{+n}) metal species that was dependent on metal size. We have omitted other studies involving dehydrochlorination of 1,2-dichloroethane [36,37] and 1,2-dichloropropane [38], as it does not require an external H_2 supply but an internal elimination of HCl with the formation of the pertinent olefin [2]; *i.e.* different reaction mechanism that can lead to different particle size dependence.

The aim of this study is to address the effect of metal particle size in liquid phase HDC. 2,4-Dichlorophenol (2,4-DCP) HDC over Pd/Al_2O_3 has been chosen as a model catalytic system, as it has been demonstrated elsewhere [9] that complete dechlorination can be achieved. The metal surface area has been modified by catalyst activation under well controlled conditions (temperature/heating rate) and the action of bulk Pd has also been considered to establish the influence of the support. Following an exhaustive search through the literature, this is the first reported study of liquid phase HDC over an unsupported metal. This Chapter sets out a comprehensive examination of HDC structure sensitivity that includes an explicit correlation of catalytic surface characteristics with HDC kinetics. In addition, it is also attempted to quantify the efficiency of catalytic HDC to reduce the toxicity associated with the starting aqueous chlorophenol solution.

2.2 Experimental

2.2.1 Catalyst Activation and Characterization

1 and 5 % w/w Pd/Al_2O_3 (labelled in this paper as Pd/Al_2O_3-A and Pd/Al_2O_3-B, respectively) and PdO were supplied by Aldrich, sieved (ATM fine test sieves) into batches of 38 μm average particle diameter and activated using the commercial CHEM-BET 3000 (Quantachrome Instruments) unit. The samples were loaded into a U-shaped (100 × 3.76 mm) pyrex-glass or quartz cell, contacted with 5 % v/v H_2/N_2 (17 cm^3 min^{-1}, Brooks mass flow controlled) and subjected to a temperature-programmed reduction (TPR) treatment at different heating rates (β = 1, 10 or 50 K min^{-1}) to a final temperature in the range 423 - 1273 K. The effluent gas was directed through a liquid N_2 trap and H_2 consumption/release was monitored by a thermal conductivity detector (TCD) with data acquisition and manipulation using the TPR Win™ software. After TPR, the reduced samples were swept with dry N_2 (65 cm^3 min^{-1}) at the final reduction temperature for 90 min, cooled to room temperature and subjected to H_2 chemisorption analysis: 50 μL H_2 pulses, under conditions where Pd hydride formation does not occur, *i.e.* H_2 partial pressure < 9 Torr [26]. Post-activation, the samples were passivated at room temperature in (17 cm^3 min^{-1}) 1 % v/v O_2/He. BET surface area analysis and pore size distribution were performed using a commercial Micromeritics Flowsorb II 2300. Prior to analysis, the samples were outgassed at 423 K for 1 h in 20 cm^3 min^{-1} dry N_2. BET area was obtained in 30 % v/v N_2/He (20 cm^3 min^{-1}) with at least three cycles of N_2 adsorption-desorption using the standard single-point BET method.

N_2 adsorption/desorption isotherms were performed over the relative pressure range $0.05 \leq P/P_0 \leq 0.98$, where the total pore volume and size distribution were obtained according to the method of Dollimore and Heal [39]. The BET areas and H_2 uptake values were reproducible to within ± 6 % and the values quoted in this paper are the mean. Pd particle size and morphology were determined by transmission electron microscopy (TEM): JEOL 2000 TEM microscope operated at an accelerating voltage of 200 kV. The catalyst sample was dispersed in 1-butanol by ultrasonic vibration, deposited on a lacey-carbon/Cu grid (200 Mesh) and dried at 383 K for 12 h. At least 650 individual Pd particles were counted for each catalyst and the mean surface area-weighted Pd particle sizes (d_{TEM}) are quoted in this paper as:

$$d_{TEM} = \frac{\sum_i n_i d_i^3}{\sum_i n_i d_i^2} \qquad \textbf{(2.1)}$$

where n_i is the number of particles of diameter d_i and $\Sigma_i\, n_i > 650$. X-ray diffraction (XRD) analysis was conducted using a Bruker/Siemens D500 incident X-ray diffractometer with Cu Kα radiation. The samples were scanned at a rate of 0.02º step^{-1} over the range $20º \leq 2\theta \leq 80º$ (scan time = 2 s step^{-1}). The diffractograms were compared with the JCPDS-ICDD references for comparative purposes (Card No. 05-0681 (Pd), 16-0394 (δ-Al_2O_3) and 10-0425 (γ-Al_2O_3)). The pH associated with the point of zero charge (pH_{pzc}) was determined using the potentiometric mass titration (PMT) technique [40]. Three different masses of catalyst were immersed in 50 cm^3 0.1 M NaCl to which a known amount of NaOH (0.1 M) was added to adjust initial pH to *ca.* 11. Titration of the samples was performed under continuous agitation in a He atmosphere with HCl (0.1 M) as titrant. The pH of the slurry was measured with a pH meter (Corning, Model 440) equipped with a polymer-body, liquid-filled combination electrode: calibration was performed before each titration with standard buffer solutions (pH 4.0 and 10.0).

2.2.2 Catalytic Procedure

Stock aqueous solutions of 2,4-DCP (Aldrich) and NaOH (Riedel-de Haën), both ≥ 99.0 %, were prepared with distilled water. All the gases used in this study (H_2 and He) were of ultra high purity (> 99.99 %, BOC).

Liquid phase HDC reactions were carried out in a modified commercial stirred glass reactor (Ken Kimble Reactors Ltd.) equipped with a H_2 supply at a constant (Brooks mass flow controlled) volumetric flow rate (150 cm^3 min^{-1}), a simplified experimental scheme is provided in **Figure 2.1**.

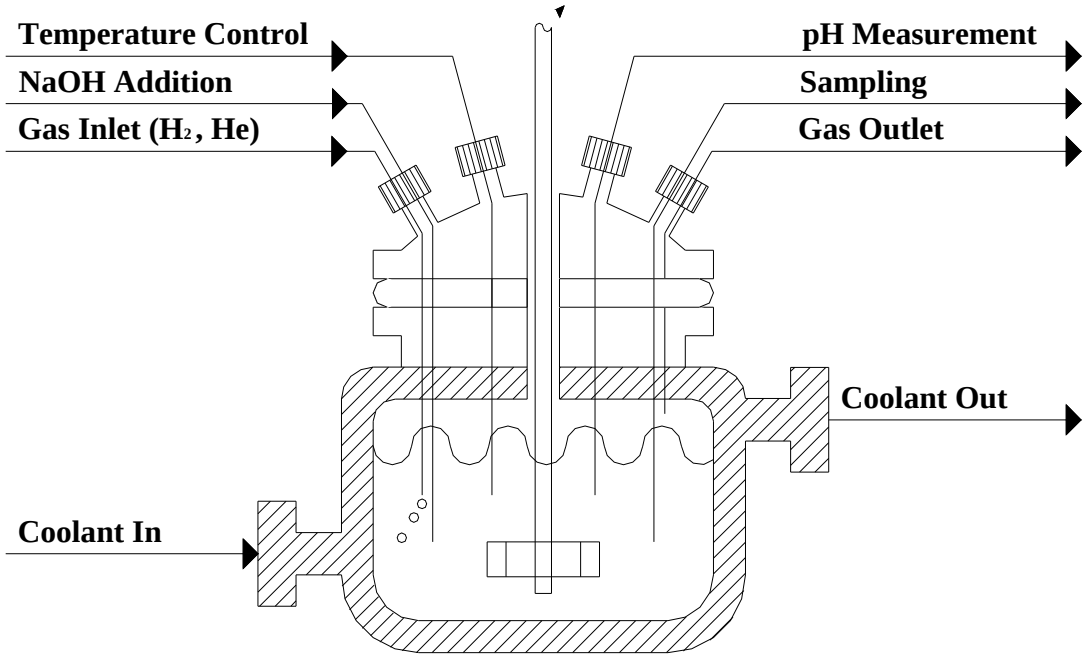

Figure 2.1: Simplified experimental scheme of the three-phase slurry (scaled vessel) reactor.

A glass impeller provided effective agitation at a stirring speed of 1100 rpm. The choice of H_2 flow rate and stirring speed served to minimize transport limitations as established elsewhere [9]. A recirculator (Julabo HD-4) was used to stabilize the reaction temperature at $T = 303 \pm 1$ K with water as coolant (293 K); loss of the reactor liquid contents in the H_2 flow was negligible (< 0.5 % v/v). At the beginning of each experiment, the catalyst and 0.1 dm^3 of 2,4-DCP stock solution were charged and agitated in a He flow (50 cm^3 min^{-1}); the temperature was allowed to stabilize (15 min) and H_2 was then introduced (time $t = 0$ for reaction). As blank tests, experiments carried out under He, *i.e.* in the absence of H_2, did not result in any measurable conversion. Three different strategies were employed for pH studies: (i) uncontrolled pH during reaction, where a known amount of NaOH was added in the preparation of the 2,4-DCP stock solution such that $C_{Cl,0}/C_{NaOH,0} = 1$ mol_{Cl} mol_{NaOH}^{-1}; (ii) pH maintained at basic conditions ($pH_{basic} = 13$), where an aqueous NaOH solution (2.4 mol_{NaOH} dm^{-3}) was fed to the reactor using a Model 100 (kd Scientific) microprocessor-

controlled infusion pump to bring the initial pH of the reaction mixture to the desired value, which was maintained during reaction by adding the same NaOH solution (≤ 5 % of the total liquid volume) with adjustment of the inlet flow rate; (iii) pH kept under acid conditions (pH_{acid} = 3) where solution pH decreased rapidly (t < 1 min) to acid conditions as a result of the HCl produced [41]. The pH of the reaction mixture was monitored continuously using a Dow-Corning pencil electrode coupled to a data logging and collection system (Pico Technology Ltd.). The initial 2,4-DCP concentrations ($C_{2,4\text{-}DCP,0}$) were in the range 25.8 - 47.5 mmol dm^{-3} where the initial Cl/Pd molar ratio = 23 - 1728 mol_{Cl} mol_{Pd}^{-1}. A non-invasive liquid sampling system *via* syringe/in-line filters allowed a controlled removal of aliquots (≤ 0.5 cm^3) of reactant/product(s). Prior to analysis, the samples were neutralized with dilute acetic acid (0.2 mol dm^{-3}). The composition of the reaction/product mixture was analyzed by gas chromatography (Perkin-Elmer Auto System XL), employing an FID and a DB-1 (J&W Scientific) capillary column (i.d. = 0.2 mm, length = 50 m, film thickness = 0.33 μm) [9]. The concentration of organic species (2,4-DCP, 2-chlorophenol (2-CP), phenol (PhOH) and cyclohexanone (C6ONE)) in the bulk liquid phase were determined from the total molar balance in the reaction mixture, where the effect of uptake on the support was negligible [9,42]. The HCl produced (mol dm^{-3}) during reaction was calculated from the molar balance based on GC analysis. The fractional conversion of 2,4-DCP ($X_{2,4\text{-}DCP}$) is defined as

$$X_{2,4\text{-}DCP} = \frac{C_{2,4\text{-}DCP,0} - C_{2,4\text{-}DCP}}{C_{2,4\text{-}DCP,0}} \qquad \textbf{(2.2)}$$

and selectivity with respect to 2-CP ($S_{2\text{-}CP}$) is given in terms of the total moles of product formed, *i.e.*

$$S_{2\text{-}CP} = \frac{C_{2\text{-}CP}}{C_{2,4\text{-}DCP,0} - C_{2,4\text{-}DCP}} \qquad \textbf{(2.3)}$$

Repeated reactions with different samples of catalyst delivered raw data reproducibility that was better than ± 7 %.

2.3 Results and Discussion

2.3.1 Catalyst Characterization

The TPR profiles (up to 1273 K) generated for Pd/Al_2O_3-A (Profile I) and γ-Al_2O_3 (Profile II) are shown in **Figure 2.2**.

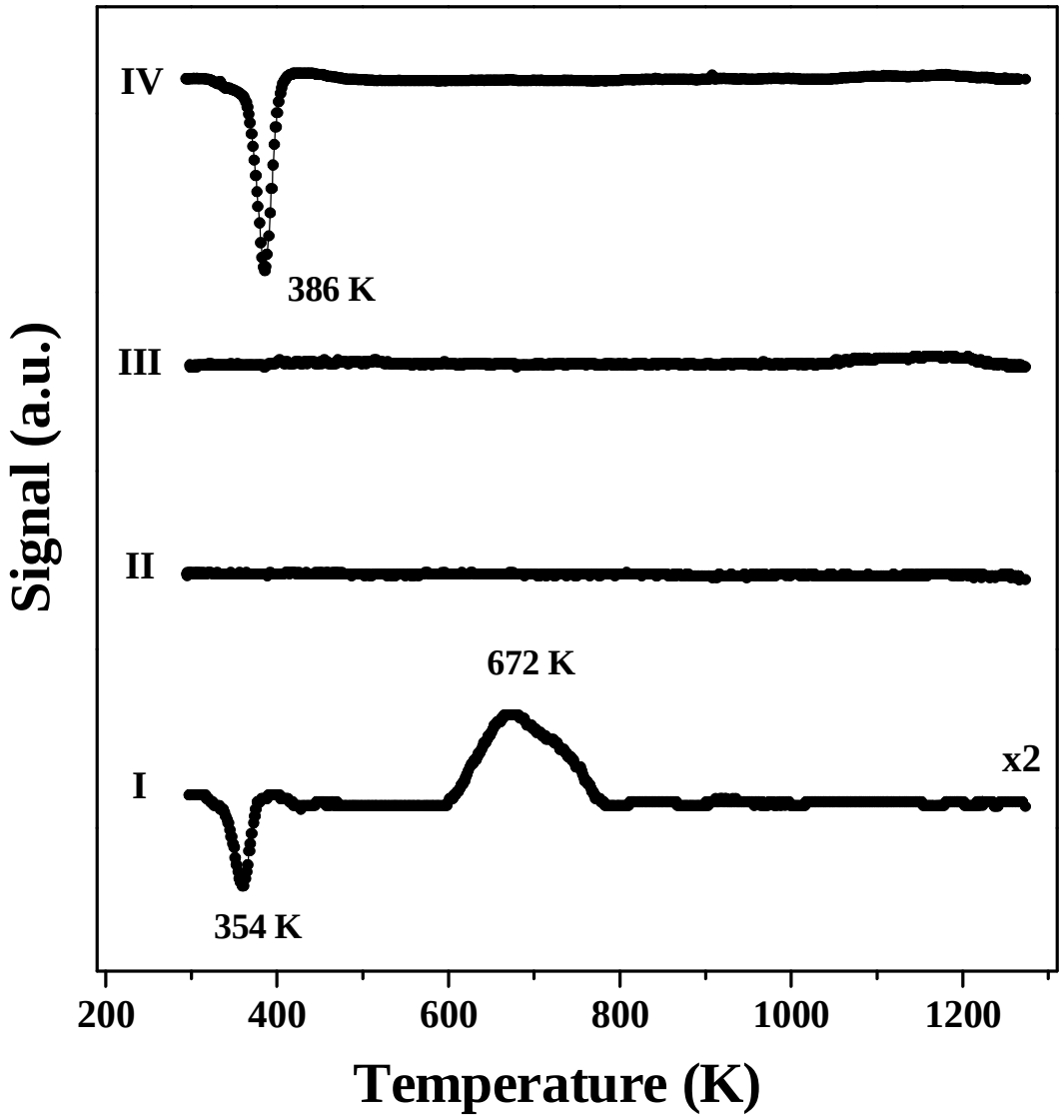

Figure 2.2: Temperature-programmed reduction (TPR) profiles for Pd/Al_2O_3-A (I) and γ-Al_2O_3 (II), TCD response for the thermal treatment of Pd/Al_2O_3-A in N_2 (III) and TPR of $PdO+Al_2O_3$ (IV).

The TPR profile for the support is featureless but Pd/Al_2O_3-A shows two distinct peaks. The appearance of a negative peak at 354 K corresponds to H_2 release as a result of β-palladium hydride (β-PdH_x) decomposition. It is well established that, at room temperature, Pd can absorb H_2 when the partial pressure exceeds 0.02 atm [43,44].

The absence of any H_2 consumption preceding hydride decomposition suggests the formation of zero valent Pd at room temperature [45,46]. Subjecting Pd/Al_2O_3-A to the same temperature ramp but in the absence of H_2 (in N_2) did not result in any TCD signal (see Profile III). The positive peak at T_{max} = 672 K can be linked to a secondary reduction of an oxidized Pd component that interacts strongly with the support [44,47]. Otto and co-workers [48,49] reported (based on XPS measurements) the presence of unreduced PdO in activated Pd/γ-Al_2O_3 and attributed this effect to support/metal electron transfer that stabilises the metal oxide, rendering it less susceptible to reduction. In a very recent study, Babu *et al.* [50] attributed H_2 consumption at T = 673 K by Pd/Al_2O_3 (prepared by deposition-precipitation) to the reduction of a PdO surface phase. TPR of a physical mixture of $PdO+Al_2O_3$ was carried out and the resultant profile (Profile IV) is characterized by a sole negative peak at 386 K which can again be ascribed to β-PdH_x decomposition. The higher decomposition temperature (ΔT = 32 K) for bulk (relative to supported) β-PdH_x can be accounted for in terms of metal particle size. Indeed, a clear increase was observed in this temperature for catalysts subjected to higher temperature activation (see **Table 2.2**), *i.e.* a shift in hydride decomposition temperature to higher values for larger Pd particles. Nag [51], studying the formation of β-PdH_x over Pd/C, reported an increase in the decomposition temperature (ΔT = 20 K) with increasing reduction temperature (from 303 to 973 K) and attributed this to a change in the electronic state of Pd particles that is dependent on metal dispersion. The shift to higher decomposition temperature suggests some inhibition of H_2 diffusion from larger particles. Indeed, H_2 diffusivity in transition metal hydrides has been reported to decrease with increasing metal size [52] and this has been linked to a higher H_2 concentration in these particles [53]. Metal dispersion post-thermal treatment was estimated by H_2 chemisorption where an increase in the activation temperature from 423 K to 1273 K was accompanied by an appreciable decrease in dispersion (see **Table 2.2**). The same tendency has been previously reported with a six-fold [5] and five-fold [21] decrease in dispersion recorded over the temperature ranges 423 - 673 K and 573 - 873 K, respectively (see **Table 2.1**). Hydrogen chemisorption data for Pd/Al_2O_3-A activated to the same final temperature using different heating rates (β) reveals a measurable decrease in dispersion at higher β values, which must serve to induce metal sintering [54]. Activation to a higher final temperature (at a fixed β) was accompanied by an appreciable decrease in dispersion, notably where T > 823 K as a direct consequence of a more facile agglomeration of metal particles [55].

Table 2.2: Temperature of Pd hydride decomposition (T_{max}), metal dispersion (D), Pd particle size obtained from H_2 chemisorption (d_{Chem}) analysis, specific Pd surface area (S_{Pd}), BET area and pH of point of zero charge (pH_{pzc}) for the activated Pd/Al_2O_3 catalysts and bulk Pd.

Catalyst	Activation Procedure		T_{max} (K)	D[a] (%)	d_{Chem}[a] (nm)	S_{Pd}[b] ($m_{Pd}^2\ g_{Pd}^{-1}$)	BET ($m^2\ g^{-1}$)	pH_{pzc}
	Temperature (K)	**β (K min^{-1})**						
Pd/Al_2O_3-A	423	10	355	55	2.0	250	152	-
	573	1	356	67	1.6	312	160	-
		10	355	59	1.9[c]	263	160	7.7
		50	355	51	2.2	227	157	-
	723	10	355	60	1.8	277	155	-
	823	10	355	54	2.1	238	150	-
	1023	10	356	39	2.7	185	145	-
	1123	10	365	25	4.5	111	142	-
	1273	1	371	8	13.1	38	138	-
		10	371	8	13.1[d]	38	137	7.6
		50	370	9	12.1	41	128	-
Pd/Al_2O_3-B	573	10	369	51	1.9	263	117	7.7
Pd	573	10	386	-	250	2	2	-

[a]based on H_2 chemisorption analysis.
[b]$S_{Pd} = 6 / (\rho_{Pd} \times d_{chem})$ where $\rho_{Pd} = 12.02$ g cm^{-3}.
[c]$d_{TEM} = 3.0$ nm.
[d]$d_{TEM} = 9.6$ nm.

The correlation between the hydrogen absorbed to generate the hydride (H_{ab}/Pd) and the hydrogen chemisorbed on the Pd surface (H_{ad}/Pd) is shown in **Figure 2.3**, where there is a clear decrease in H_{ab}/Pd with increasing metal dispersion (increasing H_{ad}/Pd). Boudart and Hwang [56] reported a linear decline in H_2 solubility with decreasing Pd particle size, which approaches zero as dispersion reaches 100 %. Bulk Pd delivered a maximum value of H_{ab}/Pd = 0.69 which agrees with the literature [56]. However, higher values have been reported and attributed to H_2 spillover effects [57]. Hydrogen absorption/adsorption data for the thermally treated Pd/Al_2O_3-B show the same tendency (see **Figure 2.3**), demonstrating the applicability of this analysis regardless of metal loading.

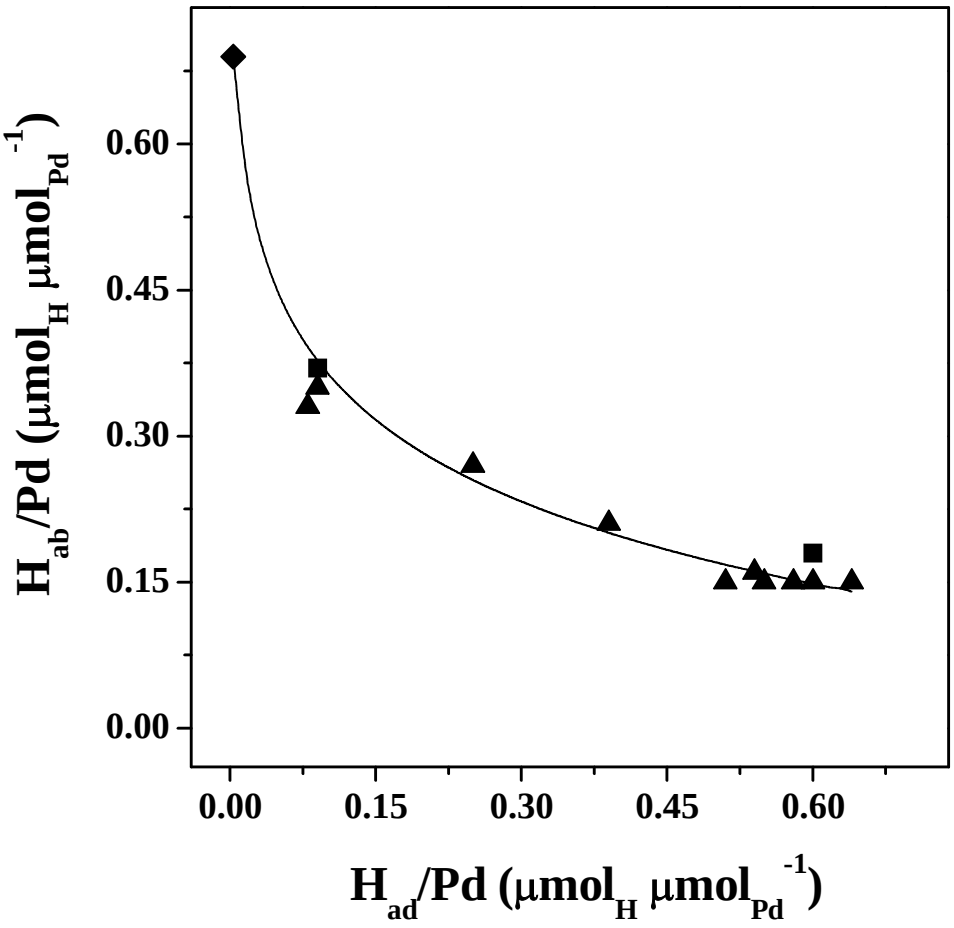

Figure 2.3: β-Pd hydride composition (H_{ab}/Pd) as a function of specific dissociative hydrogen chemisorption (H_{ad}/Pd) for activated Pd/Al_2O_3 (▲: A, ■: B) and bulk Pd (◆).

An increase in Pd particle size with increasing activation temperature was confirmed by TEM analysis; representative images are presented in **Figure 2.4**(a) which also includes TEM derived particle size distributions for two representative activation temperatures (**Figure 2.4**(b)).

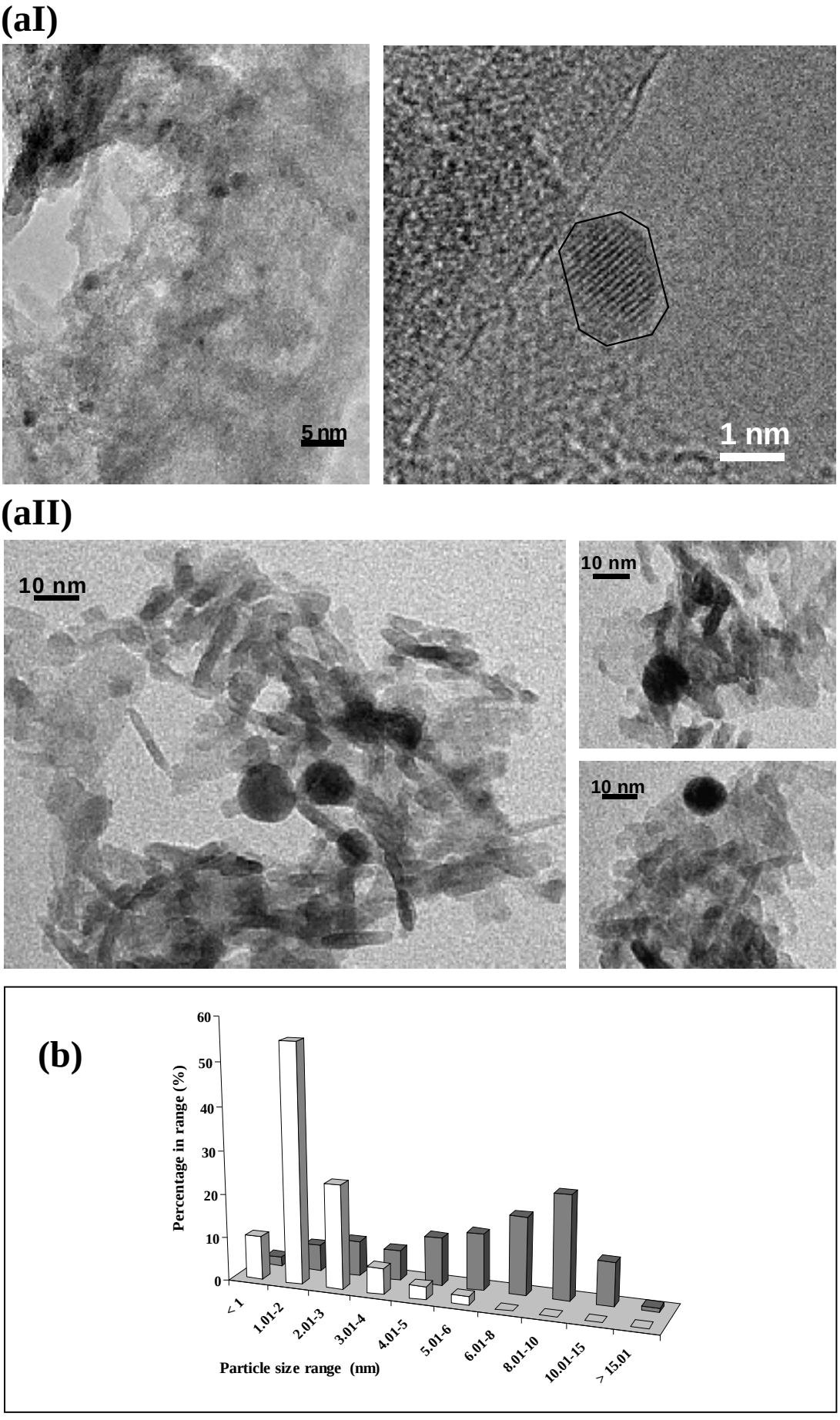

Figure 2.4: (a) Representative TEM images and (b) Pd particle size distributions associated with Pd/Al_2O_3-A activated (β = 10 K min^{-1}) at 573 K (I, open bars) and 1273 K (II, solid bars).

A significant number of metal particles smaller than 1 nm in size were observed at the lower temperature with visible faceting (see **Figure 2.4**(a)I), as noted previously [58]. Such faceting is diagnostic of stronger metal/support interactions and can be linked to electron transfer between Al_2O_3 and Pd. An increase in activation temperature (from 573 to 1273 K) resulted in an appreciable broadening of the particle size distribution (**Figure 2.4**(b)) with a shift in surface-weighted mean size from 3.0 to 9.6 nm (**Table 2.2**), consistent with a temperature-induced metal sintering. Palladium particles with diameters up to 20 nm were detected at the higher temperature and the particles exhibited a pseudo-spherical morphology (**Figure 2.4**(a)II). Pd particle sizes derived from H_2 chemisorption and TEM analysis (see **Table 2.2**) are in reasonable agreement; we have adopted an exclusive dissociative adsorption of hydrogen on Pd (H/Pd = 1) as applied elsewhere [8,59].

XRD analyses were also conducted (see **Figure 2.5**) to establish metal particle sintering. The diffractogram for Pd/Al_2O_3-A activated up to 573 K (Profile I) does not present any peak associated with a Pd phase, *i.e.* the metal size is below the detection limit (< *ca.* 5 nm) [60]. In contrast, the catalyst activated at 1273 K (Profile II) exhibited a peak at 40º that corresponds to the (111) Pd plane with an associated particle size (obtained from standard line broadening analysis) of 7 nm. The XRD pattern of bulk Pd (Profile III) presents peaks at 40º, 45º and 68º corresponding to (111), (200) and (220) Pd planes, consistent with a cubic symmetry. In the case of the supported catalyst, the signal at 67º is associated with the (440) plane of cubic γ-Al_2O_3 and the two peaks at 32º and 45º correspond, respectively, to the (222) and (400) planes of tetragonal δ-Al_2O_3. The appearance of these peaks, not present at the lower activation temperature, is due to a partial allotropic transformation of the support at T = 1273 K [61]. This temperature induced phase change of Al_2O_3 was not accompanied by any significant modification to the bimodal pore size distribution, shown as an inset in **Figure 2.5**. Indeed, N_2 adsorption/desorption isotherms were consistent with a combination of the type I (microporosity) and type IV (mesoporosity) IUPAC classification which is characteristic of γ-Al_2O_3 [62,63]. The total pore volume decreased from 0.56 (at 573 K) to 0.47 $cm^3\ g^{-1}$ (at 1273 K) which can be due, in part, to a partial occlusion of the pores by the larger (sintered) Pd particles, as noted by Jusczcyk *et al.* [18] and Babu and co-workers [50]. As a direct consequence of the decease in total pore volume, the BET areas are lower (see **Table 2.2**).

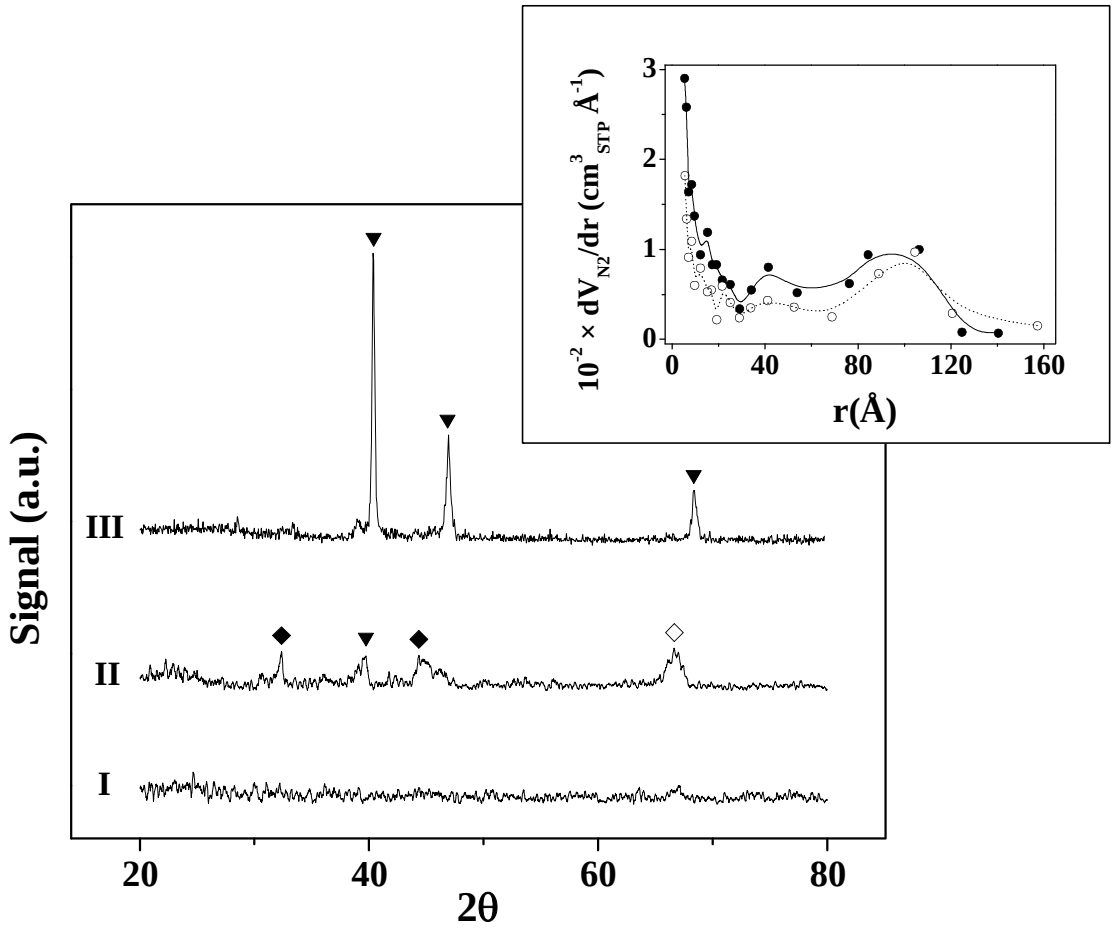

Figure 2.5: XRD patterns for Pd/Al_2O_3-A activated (β = 10 K min^{-1}) at 573 K (I) and 1273 K (II), and bulk Pd activated (β = 10 K min^{-1}) at 573 K (III); (▼) indicates peak assignment based on JCPDS-ICDD for *fcc* Pd (Card No. 06-0581), (◇) for cubic γ-Al_2O_3 (Card No. 10-0425) and (◆) for tetragonal δ-Al_2O_3 (Card No. 16-0394). Inset: Pore size distributions for Pd/Al_2O_3-A activated at 573 K (○) and 1273 K (●) (β = 10 K min^{-1}).

The pH point of zero charge (pH_{pzc}) has been shown to be an important catalyst characteristic in determining liquid phase catalytic HDC performance [41,58]. The effect of thermal treatment on the pH_{pzc} was accordingly considered and representative titration curves are presented in **Figure 2.6**. The pH_{pzc} value (7.6 - 7.7) was insensitive to activation temperature and Pd loading (**Table 2.2**) and fits within the range previously reported for γ-Al_2O_3 (6 - 9) [32,64].

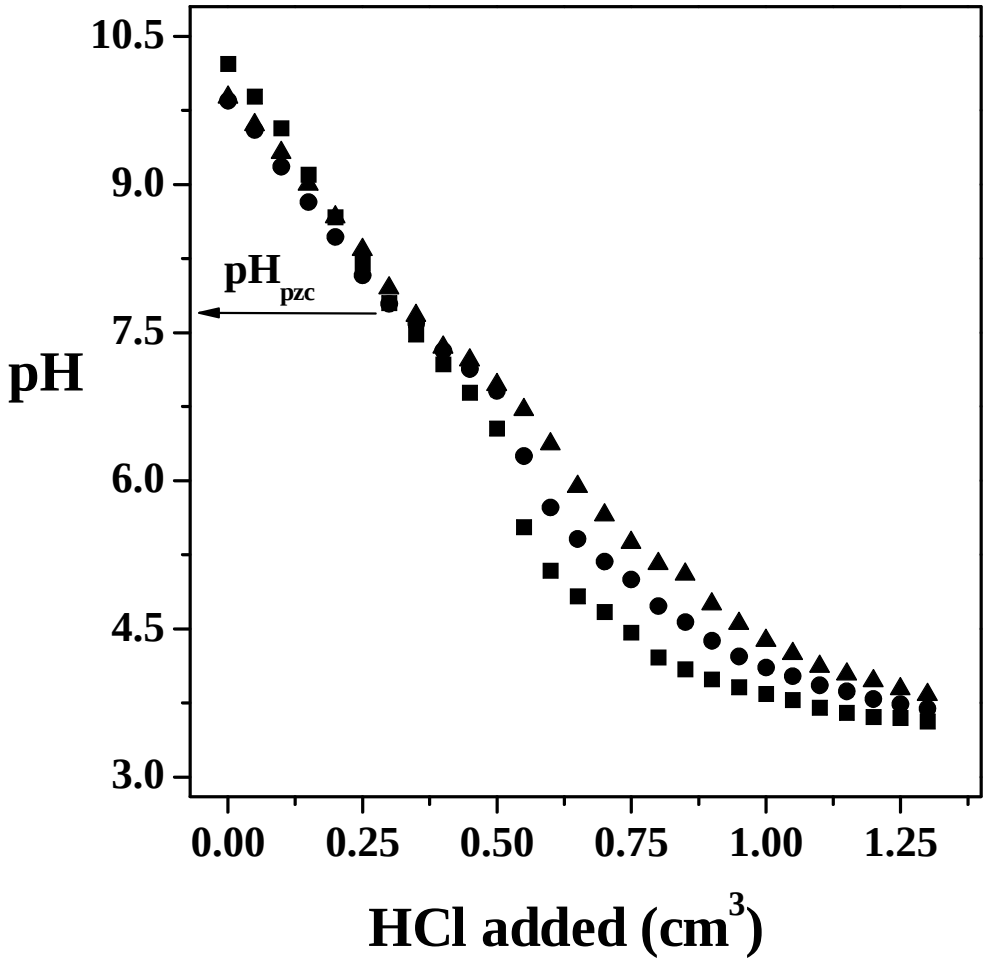

Figure 2.6: pH profiles associated with the pH of point of zero charge (pH_{pzc}) determination for 0.025 g (■), 0.050 g (●) and 0.075 g (▲) of Pd/Al_2O_3-A activated at 1273 K (β = 10 K min^{-1}).

2.3.2 HDC of 2,4-DCP over Pd/Al_2O_3 and Pd: Influence of Metal Dispersion on Product Composition and HDC Rate

The catalytic response to variations in Pd particle size was initially tested by monitoring bulk solution composition and associated temporal pH changes for 2,4-DCP HDC, which proceeds according to the reaction network shown in **Figure 2.7**. The composition *vs.* time profiles for Pd/Al_2O_3-A activated at 573 K are given in **Figure 2.8**(a) where 2-chlorophenol (2-CP) was the only partial 2,4-DCP HDC product. This can be explained on the basis of steric hindrance where the *ortho*- positioned Cl is less susceptible to attack [9]. Phenol (PhOH) was the predominant product of total dechlorination but further hydrogenation to cyclohexanone (C6ONE) was also detected with a selectivity ≤ 7 %, *i.e.* ($k_3 + k_5 + k_6$) <<< ($k_1 + k_2 + k_4$), a result that finds agreement in an earlier report [65].

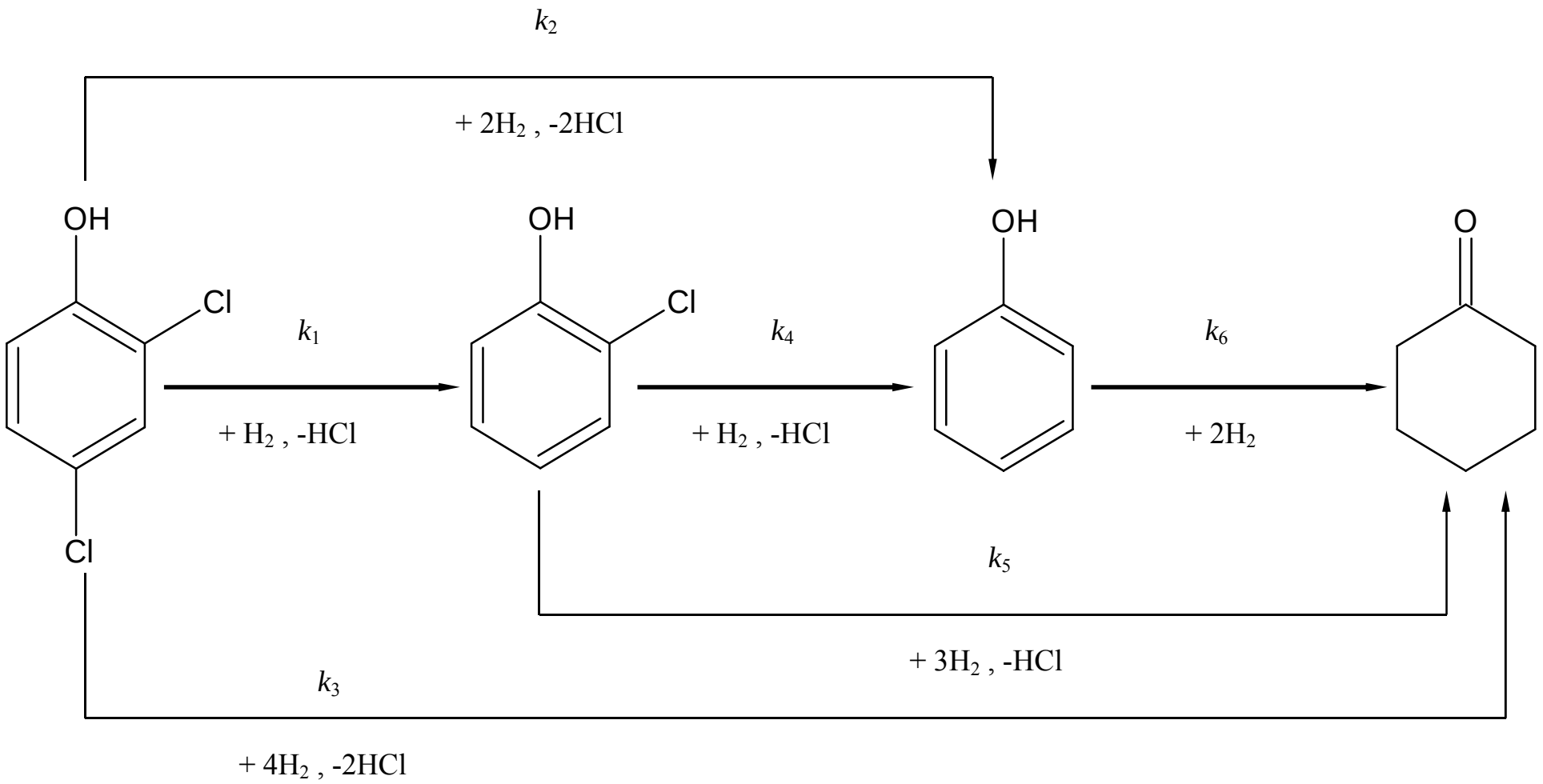

Figure 2.7: Simplified reaction network for 2,4-DCP HDC (stepwise mechanism is highlighted by bold arrows).

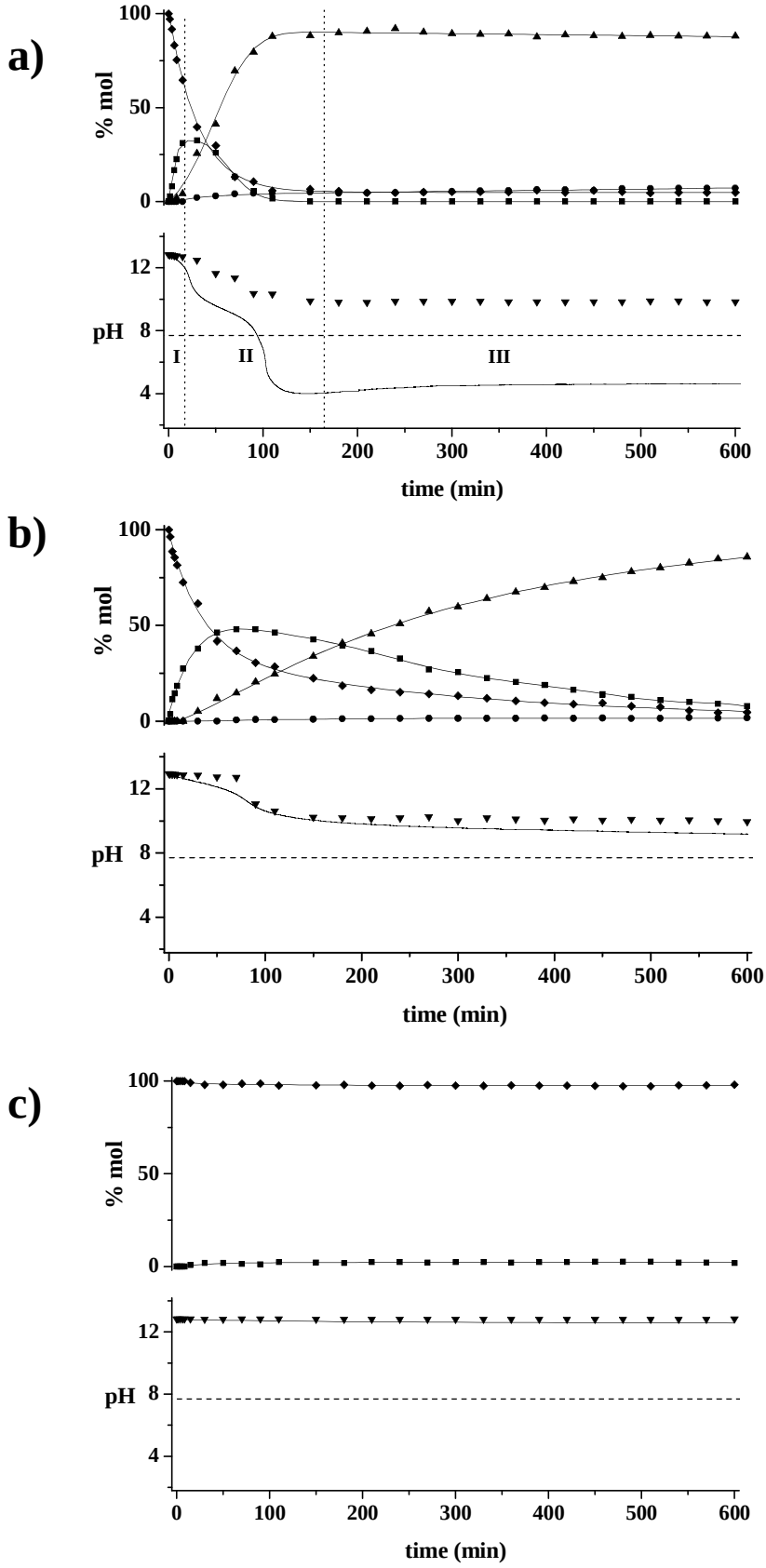

Figure 2.8: Bulk liquid composition (% mol 2,4-DCP (◆), 2-CP (■), PhOH (▲), C6ONE (●)) as a function of time for reaction over Pd/Al_2O_3-A activated (β = 10 K min^{-1}) at (a) 573 K, (b) 1123 K and (c) 1273 K with associated pH profiles where the lines represent measured and the symbols (▼) estimated (from HCl molar balance) values: dashed line represents pH_{pzc}; initial (Cl/Pd) = 1234 mol_{Cl} mol_{Pd}^{-1}.

Although liquid phase chlorophenol HDC is strongly influenced by solution pH, which impacts on catalyst/reactant interactions [41,58,66-68], there are many instances in the literature where the operational pH and/or temporal variations have not been recorded/quoted [10,14,42,69-74]. The actual (experimentally determined) pH response is illustrated in **Figure 2.8** by the solid lines (pH_{pzc} is denoted by the dashed line) while the symbols show the predicted pH based on the HCl molar balance (see experimental section). The predicted values take into consideration the NaOH consumed to neutralise the HCl produced and the dissociation of the species present; *pK* values = 7.89 (2,4-DCP), 8.56 (2-CP), 10.0 (PhOH) and 17.4 (C6ONE) [68]. The predicted and measured pH values shown in **Figure 2.8**(a) clearly deviate and, in order to account for this, the temporal response can be differentiated into three regions or zones. In zone I, where initial 2,4-DCP yields 2-CP as the predominant product, there is reasonable agreement between the measured and the predicted pH. In zone II there is an immediate mismatch where the actual pH is appreciably lower than the expected values. To explain this apparent anomaly, it is necessary to consider pH_{pzc} (7.7, dashed line), which establishes the pH at which the accessible wetted catalyst surface is electrically neutral, *i.e.* when pH > pH_{pzc} the catalyst surface bears a negative charge and presents an unfavourable surface for interaction with anions in solution [41]. At the beginning of zone II, where pH = 12, a repulsion can be expected as a result of electrostatic interactions between the dissociated 2-chlorophenolate species and the negatively charged Al_2O_3 surface and this should limit the production of PhOH from 2-CP. However, the composition profile (**Figure 2.8**(a)) shows the opposite effect, *i.e.* enrichment of the bulk liquid with PhOH (in moving from zone I to zone II). We must also take into account the HCl released during HDC, which can adsorb on the Al_2O_3 surface [5,26,34] to generate a liquid/solid interface with an associated pH ($pH_{l/s}$) that can be quite different from that of the bulk liquid (pH) and the support surface (pH_{pzc}). Where $pH_{l/s} < pH_{pzc} <$ pH, the γ-Al_2O_3 surface develops a positive charge, favouring interaction with the 2-chlorophenolate species and, furthermore, the adsorption of OH^- ions (from H_2O dissociation) on the catalyst surface. The observed increase in the acidity of the bulk liquid can then arise as the result of two effects: (i) higher PhOH production leading to a high HCl content; (ii) greater concentration of H^+ as a consequence of the removal of OH^- from the reaction medium. This can account for the apparent disagreement between the measured and calculated pH. When the pH of the bulk solution reaches a value such that pH < pH_{pzc} (mid-point of zone II), the development of an increasingly positively charged surface will enhance OH^- interactions leading to a further decrease in bulk solution pH.

Zone III is essentially pH invariant where the only reaction is the secondary hydrogenation of PhOH to C6ONE. The measured and predicted bulk solution pH agree to a greater extent for reaction over Pd/Al_2O_3-A activated at 1123 K (**Figure 2.8**(b)). This system is characterised by higher 2-CP contents at prolonged reaction times, where the rate of HCl production is appreciably lower than that associated with the better dispersed catalysts and, accordingly, $pH_{l/s}$ did not drop below $pH_{pzc.}$ Reaction over Pd/Al_2O_3-A activated at 1273 K (**Figure 2.8**(c)) resulted in a low conversion of 2,4-DCP exclusively to 2-CP with a negligible temporal change to the bulk solution pH. In order to quantify HDC activity dependence on Pd particle size, the initial 2,4-DCP consumption rates ($(-R_{2,4\text{-}DCP})_0$) were determined from a linear regression of the temporal 2,4-DCP concentration profiles (see **Figure 2.9**) where $X_{2,4\text{-}DCP} < 0.24$, *i.e.* NaOH in excess relative to the HCl produced ($C_{NaOH}/C_{HCl} \geq 4$).

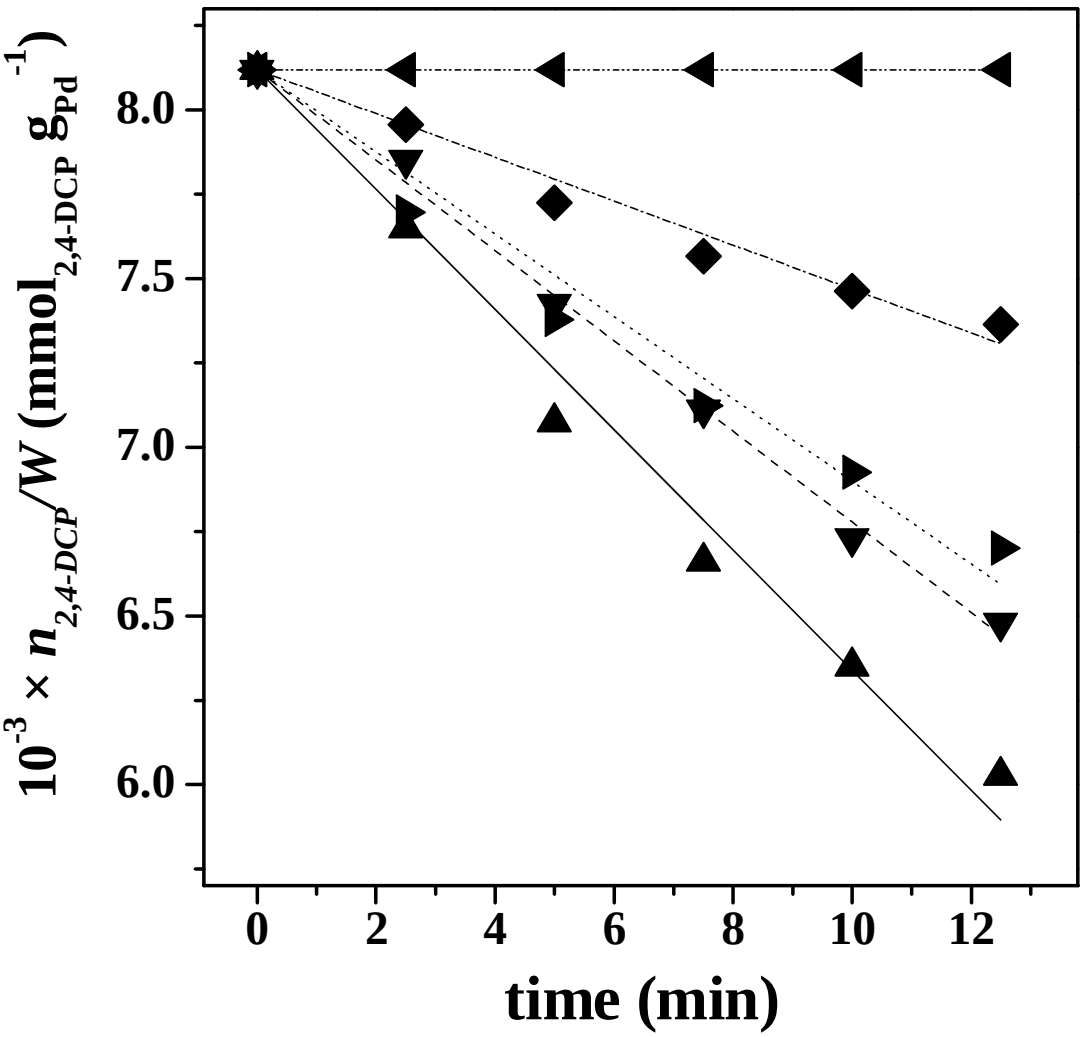

Figure 2.9: Linear fitting of initial 2,4-DCP consumption rates for Pd/Al_2O_3-A activated (β = 10 K min^{-1}) at 723 K (▲), 823 K (▼), 1023 K (▶), 1123 K (◆) and 1273 K (◀): initial (Cl/Pd) = 1728 mol$_{Cl}$ mol$_{Pd}^{-1}$.

Under these conditions, Yuan and Keane have demonstrated [58] that any contribution due to catalyst deactivation is negligible and the initial rate represents a true measure of the intrinsic catalyst activity. Initial 2,4-DCP consumption and HDC ($(R_{HDC})_0$) rates can be compared in **Table 2.3**. The tabulated rates fall within the range that has been established [68] for reaction operated under chemical control. An appreciable decrease in $(-R_{2,4\text{-}DCP})_0$ over Pd/Al_2O_3-A is immediately apparent with a decrease in Pd dispersion from 67 to 25 % with only residual activity associated with the catalyst treated at the highest temperature (8 % dispersion).

The equivalency of the $(-R_{2,4\text{-}DCP})_0$ and $(R_{HDC})_0$ values suggest that chlorine removal occurs predominantly in a stepwise fashion, *i.e.* PhOH formation *via* simultaneous removal of both Cl substituents is not significant [75]. The initial 2-CP yields ($Y_{2\text{-}CP,0}$), calculated from [68]

$$Y_{2\text{-}CP} = \frac{(R_{2\text{-}CP})}{(-R_{2,4\text{-}DCP})} = Y_{2\text{-}CP,0} - \left(\frac{k_4}{k_1}\right)\left(\frac{C_{2\text{-}CP}}{C_{2,4\text{-}DCP}}\right) = Y_{2\text{-}CP,0} - K\left(\frac{C_{2\text{-}CP}}{C_{2,4\text{-}DCP}}\right) \qquad \textbf{(2.4)}$$

are close to unity (see **Table 2.3**), consistent with a stepwise Cl removal; where the value of $K = k_4/k_1 = 1.30 - 1.36$ suggests a faster 2-CP HDC (when compared to 2,4-DCP, see **Figure 2.7**) that is in line with an increase in reactivity when decreasing the number of chlorines in the parent phenolic ring [68,76]. It should be noted that $(-R_{2,4\text{-}DCP})_0$, $Y_{2\text{-}CP,0}$ and K values delivered by Pd/Al_2O_3-B are close to those obtained from Pd/Al_2O_3-A at the same degree of dispersion (**Table 2.3**), while bulk Pd was inactive under the same reaction conditions. In order to explicitly compare the catalytic action of samples bearing different metal particle sizes, specific (per m_{Pd}^2) initial 2,4-DCP consumption ($(-R'_{2,4\text{-}DCP})_0$) and HDC ($(R'_{HDC})_0$) rates were calculated based on specific Pd surface area values (S_{Pd}, see **Table 2.2**) and the results are presented in **Figure 2.10**. There was a measurable decrease in the specific rates over the Pd particle size range 1.9 - 4.5 nm and a greater than 20-fold drop in specific activity for the catalyst activated at 1273 K (mean particle diameter = 13.1 nm). This response is indicative of structure sensitivity where smaller Pd particles (< 5 nm) are intrinsically more active.

Table 2.3: Initial 2,4-DCP consumption $(-R_{2,4\text{-}DCP})_0$ and HDC $(R_{HDC})_0$ rates, initial 2-CP yield ($Y_{2\text{-}CP,0}$, see eqn. (2.4)) and ratio of 2-CP consumption and formation constants (K, see eqn. (2.4)) over Pd/Al_2O_3 catalysts; initial (Cl/Pd) = 1728 mol_{Cl} mol_{Pd}^{-1}.

Catalyst	Activation Procedure		$(-R_{2,4\text{-}DCP})_0$ ($mmol_{2,4\text{-}DCP}$ g_{Pd}^{-1} min^{-1})	$(R_{HDC})_0$ ($mmol_{Cl}$ g_{Pd}^{-1} min^{-1})	$Y_{2\text{-}CP,0}$	K
	Temperature (K)	β (K min^{-1})				
Pd/Al_2O_3-A	423	10	150	171	1.07	1.36
	573	1	204	205	1.02	1.34
		10	192	204	1.04	1.35
		50	183	185	1.00	1.33
	723	10	178	180	1.01	1.30
	823	10	145	145	1.05	1.35
	1023	10	110	110	1.06	1.36
	1123	10	64	62	1.00	1.31
	1273	1	2	2	1.00	1.31
		10	1	1	1.00	1.32
		50	<1	<1	1.00	1.31
Pd/Al_2O_3-B	573	10	146	148	1.01	1.33

In marked contrast, Gómez-Sainero *et al.* [33], studying CCl_4 HDC over Pd/C, recorded an increase (by a factor of 25) in the initial CCl_4 consumption rate when increasing the metal size from 5 to 14 nm (see **Table 2.1**). Aramendia *et al.* [4] (CB HDC over Pd/$AlPO_4$-SiO_2 (2 - 16 nm)) recorded a 36-fold increase in the reaction rate with increasing Pd particle diameter. In the mitohedrical region (1 - 5 nm), the activity of supported metals is governed by the size, shape and number of coordinatively unsaturated atoms comprising the metal particle and is sensitive to the number of face/edge sites [35]. The mitohedrical region applies to the catalyst activated at 573 K, which is characterized by a narrow particle size distribution (**Figure 2.3**(b)) with a mean particle size of 3 nm. In this size range, electron transfer to the γ-Al_2O_3 support can result in strong metal-support interactions [31], leading to electron-deficient metal sites.

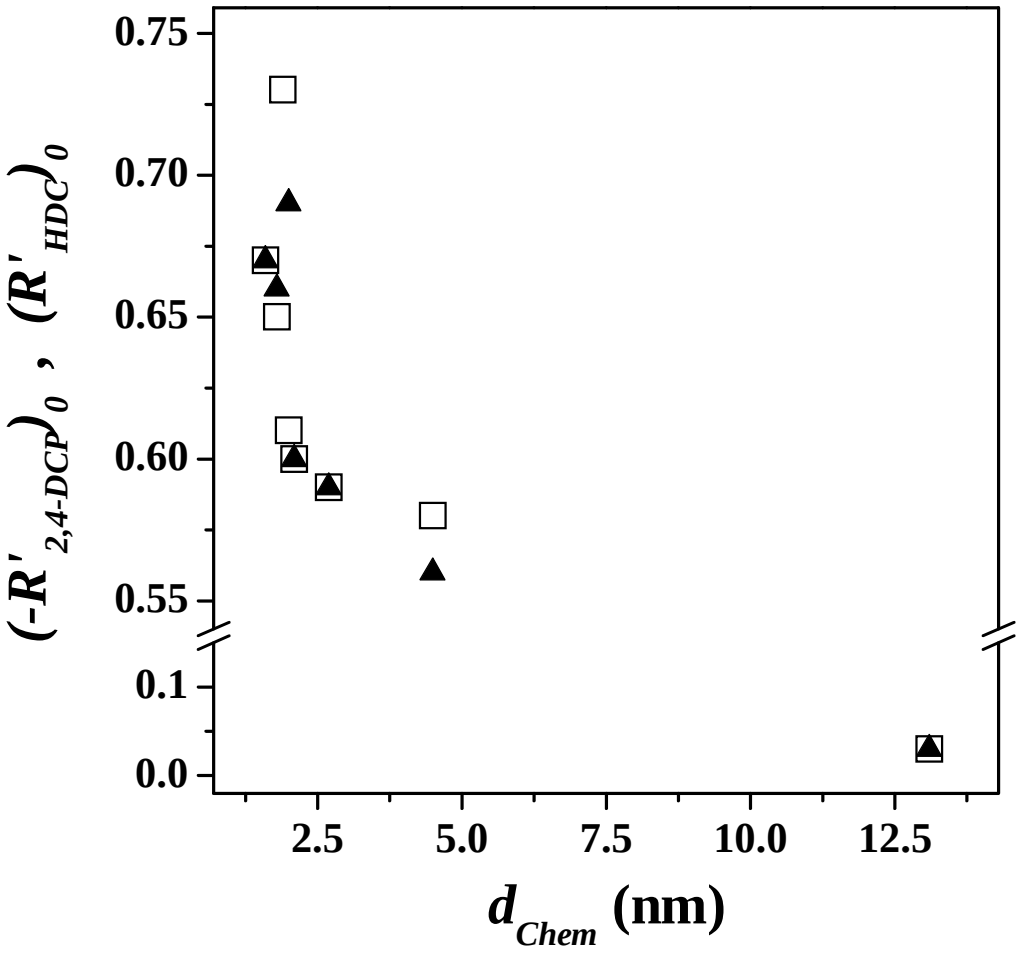

Figure 2.10: Specific initial 2,4-DCP consumption (□, $(-R'_{2,4\text{-}DCP})_0$, units = $mmol_{2,4\text{-}DCP}\ m_{Pd}^{-2}\ min^{-1}$) and HDC (▲, $(R'_{HDC})_0$, units = $mmol_{Cl}\ m_{Pd}^{-2}\ min^{-1}$) rates as a function of metal particle size (d_{Chem}) for Pd/Al_2O_3-A.

Metal sintering at 1273 K shifted the particle size distribution outside the mitohedrical region (see **Figure 2.3**(b)) with a subsequent increase in the coordination number for the exposed Pd atoms and a lesser degree of support interaction [35]. Gómez-Sainero *et al.* [33] have proposed that a HDC-active Pd site bears both metallic (Pd^0) and electron-deficient (Pd^{+n}) atoms, where the ratio Pd^{+n}/Pd^0 decreases (from 2.5 to 0) with decreasing dispersion (from 30 to 10 %) with an associated maximum in activity where $Pd^{+n}/Pd^0 \cong 1$. Moreover, they suggested that metal particles composed of only one of these species (metallic/cationic Pd) are inactive. However, a base was not used in that work to neutralize the HCl produced and the possibility of contributions due to catalyst deactivation can not be ruled out. Under conditions of strong inhibition by chloride ions, the reaction rate can become a strong function of conversion [4], where larger metal particles have been reported to maintain higher reaction rates at extended reaction times [8]. Indeed, Aramendia *et al.* [4] have associated higher reaction rates over larger particles to a lesser degree of metal deactivation. The gas phase HDC work included in **Table 2.1** also supports this tendency but differences in reaction temperature and contact time do not allow a direct comparison between gas and liquid phase operations. The results show a clear increase in specific HDC activity for smaller Pd particles (< 5 nm), demonstrating sensitivity to the electronic/geometric nature of supported Pd particles under conditions where inhibition by HCl can be discounted.

2.3.3 HDC of 2,4-DCP over Pd/Al_2O_3 and Pd: Influence of Metal Dispersion on the HDC Pathway

Dependence of HDC pathway on Pd dispersion can be effectively proved from a consideration of 2-CP selectivity ($S_{2\text{-}CP}$) as a function of 2,4-DCP conversion ($X_{2,4\text{-}DCP}$); the corresponding data for different dispersions are presented in **Figure 2.11**. At a similar degree of dispersion (51 *vs.* 59 %), the activity/selectivity profiles for Pd/Al_2O_3-A and Pd/Al_2O_3-B overlapped, which suggest that for the same metal particle size the reaction pathway is independent of Pd loading. However, the $S_{2\text{-}CP}$ *vs.* $X_{2,4\text{-}DCP}$ profiles for Pd/Al_2O_3-A activated at 573 and 1123 K do not coincide, indicating that Pd particle size can impact on the reaction network, *i.e.* concerted (k_2) *vs.* consecutive (k_1, k_4) Cl removal (see **Figure 2.7**).

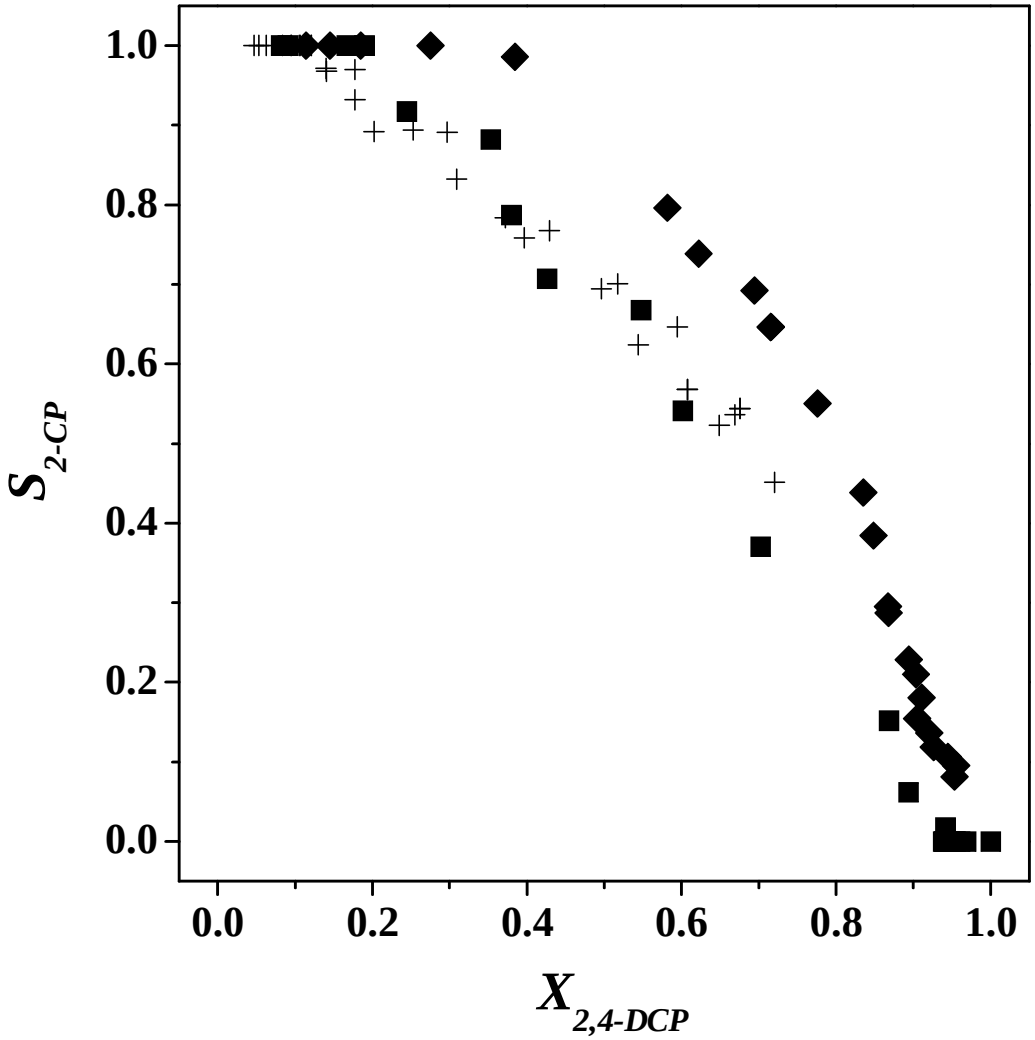

Figure 2.11: 2-CP Selectivity ($S_{2\text{-}CP}$) as a function of 2,4-DCP conversion ($X_{2,4\text{-}DCP}$) for reaction over Pd/Al_2O_3-A activated (β = 10 K min^{-1}) at 573 K (■) and 1123 K (◆) and Pd/Al_2O_3-B activated at 573 K (+).

The higher values of $S_{2\text{-}CP}$ at a given $X_{2,4\text{-}DCP}$ for the sintered Pd/Al_2O_3-A can be accounted for on the basis of the electrostatic repulsion between the 2-chlorophenolate species and the negatively charged γ-Al_2O_3 surface, *i.e.* pH > pH_{pzc}. A higher 2-CP content, maintained over prolonged reaction time, in the bulk liquid under basic conditions (pH > 8.5) is evident in **Figure 2.8**(b). In contrast, for reaction over the smaller Pd particles, the pH in bulk solution (**Figure 2.8**(a)) evolves from initially basic (pH = 12.9) to ultimately acidic (pH = 4.7) with a consequent decrease in $S_{2\text{-}CP}$. The $S_{2\text{-}CP}$ *vs.* $X_{2,4\text{-}DCP}$ profiles are then determined by the interaction between the γ-Al_2O_3 surface (negatively/positively charged) and the reacting species in solution (chlorophenolate/chlorophenolic). Solution pH is the reaction variable controlling the HDC pathway and this, in effect, masks the impact of Pd size variations.

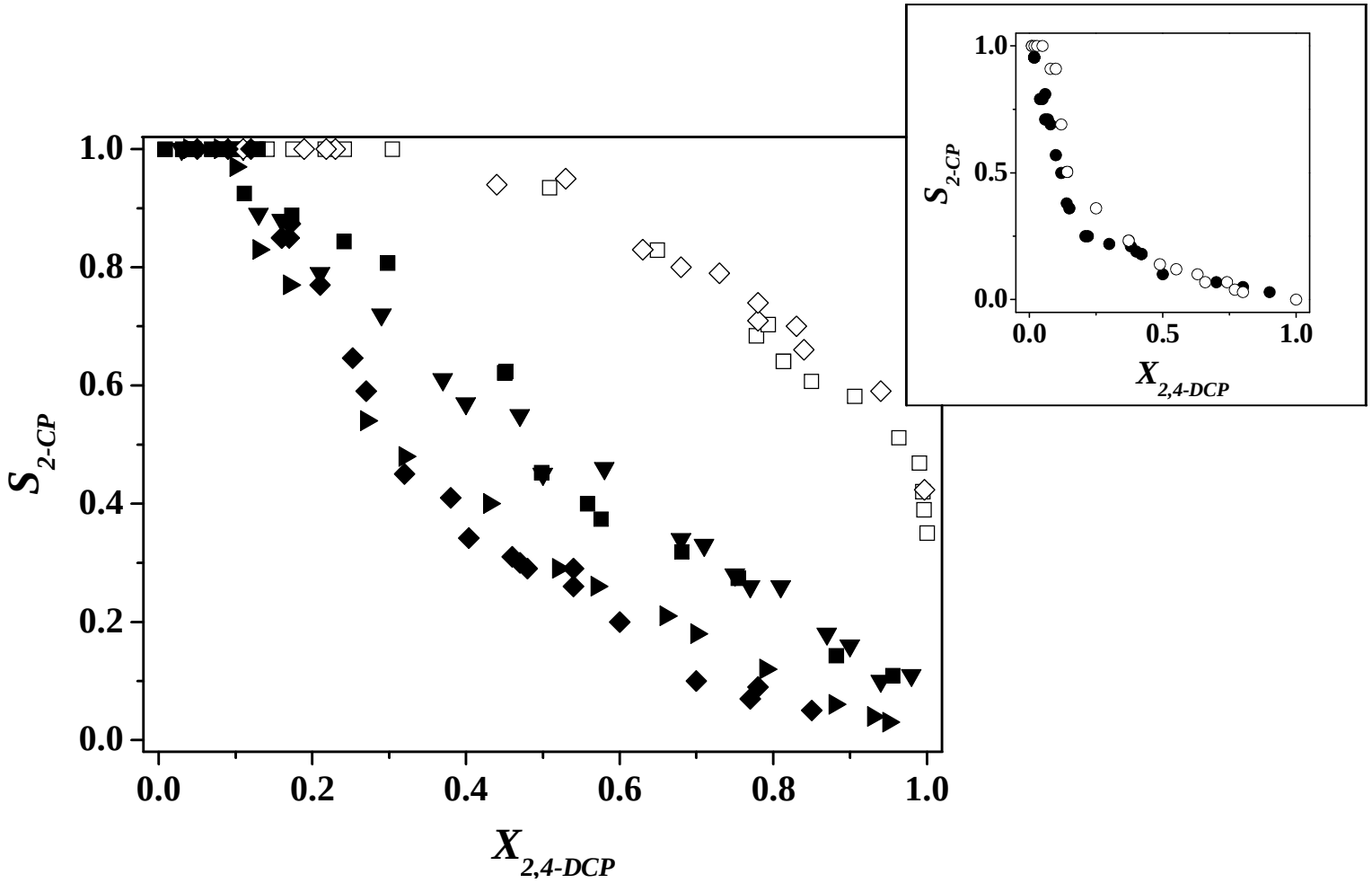

Figure 2.12. 2-CP Selectivity ($S_{2\text{-}CP}$) as a function of 2,4-DCP conversion ($X_{2,4\text{-}DCP}$) for reaction over Pd/Al_2O_3-A activated (β = 10 K min^{-1}) at 573 K (■,□), 823 K (▼), 1023 K (▶) and 1123 K (◆,◇). Inset: $S_{2\text{-}CP}$ *vs.* $X_{2,4\text{-}DCP}$ profiles for bulk Pd activated at 573 K (●,○). Note: pH maintained at pH_{acid} = 3 (solid symbols) and pH_{basic} = 13 (open symbols).

In order to decouple the possible metal particle size effects from pH contributions, experiments were carried out where the pH was maintained at a constant value. Reactions conducted at pH_{basic} = 13 (> pH_{pzc} and reactant/product *pK*) show overlapping $S_{2\text{-}CP}$ *vs.* $X_{2,4\text{-}DCP}$ trends (**Figure 2.12**): the HDC pathway was unaffected by Pd particle size, *i.e.* similar k_j. This does not apply under acidic conditions, *i.e.* pH_{acid} = 3 (< pH_{pzc} and reactant/product *pK*), where the less dispersed catalysts delivered lower selectivities with respect to 2-CP at a given fractional conversion, *i.e.* $k_2 > k_1$. Under such acidic conditions, all the species in the reaction medium are non-dissociated and the catalyst surface bears a positive charge, inhibiting the adsorption of chlorophenolic species. As pH_{pzc} was insensitive to thermal treatment (see **Table 2.2**) differences in $S_{2\text{-}CP}$ must be due to Pd particle size and, critically, to the electron-deficient nature of the smaller supported Pd particles. There is evidence in the literature [33] that the presence of electron-deficient Pd species can lead to the formation of a Pd–H^+ adduct during HDC over Pd/C (≥ 4 nm). The higher values of $S_{2\text{-}CP}$ for the more dispersed catalysts can then be linked to a lower intrinsic efficiency of supported Pd–H^+ to dechlorinate protonated 2-chlorophenolic species to PhOH, *i.e.* $k_4 < k_1$. Such particle size effects are not prevalent at pH_{basic} due to the dissociated nature of the species in solution (chlorophenolate) and the lower concentration of H^+ to form the metal adduct.

Initial 2,4-DCP consumption rates under controlled pH are given in **Table 2.4** where, again, the better dispersed catalysts consistently deliver higher specific activities; at a given dispersion, a higher rate is obtained at pH_{basic}. This observation is in agreement with the findings of Felis *et al.* [70], who claimed that chlorophenolate species are more reactive due to resonance effects, *i.e.* charge delocalisation within the aromatic ring, which results in stable resonant forms that undergo a more facile dechlorination.

Table 2.4: Initial 2,4-DCP consumption rates $(-R_{2,4\text{-}DCP})_0$ over activated Pd/Al_2O_3-A and bulk Pd (β = 10 K min^{-1}) where pH is controlled. Initial (Cl/Pd) = 1234 (Pd/Al_2O_3) and 32 (Pd) mol_{Cl} mol_{Pd}^{-1}.

Catalyst	Activation Temperature (K)	$(-R_{2,4\text{-}DCP})_0$ ($mmol_{2,4\text{-}DCP}$ g_{Pd}^{-1} min^{-1})	
		pH_{acid} = 3	pH_{basic} = 13
Pd/Al_2O_3-A	573	80	143
	823	76	120
	1023	54	86
	1123	30	58
Pd	573	19×10^{-2}	5×10^{-2}

The results demonstrate that the metal support plays a key role in determining 2,4-DCP HDC through both metal/support interactions (critical for Pd particles < 5 nm) and reactant/support interactions that are dependent on pH variations. Consequently, the reaction over bulk Pd was also carried out. To the best of the author's knowledge, this is the first reported instance of liquid phase HDC promoted by an unsupported metal. The selectivity/activity response for bulk Pd under controlled pH is shown as an inset to **Figure 2.12**. The $S_{2\text{-}CP}$ values at each $X_{2,4\text{-}DCP}$ were markedly lower than those obtained for the supported systems and the activity/selectivity profiles coincided for reaction under acidic and basic conditions. In the absence of support, any catalyst/reactant interactions by electrostatic forces can be discounted and reactant adsorption on bulk Pd must occur *via* the delocalized π-system. The lower 2-CP selectivities suggest a predominant concerted removal of both Cl substituents. In contrast, Rioux *et al.* [77], studying the HDC of CFCs over Pd/C and Pd black, recorded lower selectivities towards dechlorinated products over the non-supported system and attributed this to the presence of impurities (traces of other metals) on the bulk catalyst surface. van de Sandt *et al.* [78], in the HDC of CFC-12 over the same catalysts, observed a similar trend and linked this to a carbiding of the Pd phase.

In terms of initial 2,4-DCP consumption rates, bulk Pd delivered smaller (by two orders of magnitude) values than those obtained with Pd/Al_2O_3-A (**Table 2.4**). It has been reported [77,78] that bulk metals can achieve the same degree of HDC (in gas phase applications) compared with corresponding supported systems. In contrast to Pd/Al_2O_3, HDC rate over bulk Pd in basic media was lower than that recorded under acidic conditions. This response can be tentatively attributed to a more effective interaction of chlorophenolic species with the metal surface *via* the π-delocalized ring relative to the adsorption of chlorophenolate species (present at pH_{basic}).

2.3.4 HDC of 2,4-DCP over Pd/Al_2O_3: Correlation of HDC with Ecotoxicity

From the results presented it can be concluded that higher Pd dispersions deliver more efficient Cl removal, a critical finding in the treatment of organochlorinated waste *via* "green catalysis" [66]. Despite the growing corpus of literature dealing with catalytic HDC, there is still a dearth of work that provides a quantification of such "green efficiency".

In this respect ecotoxicity, *i.e.* the relationship between the exposure/effects of a chemical or effluent under controlled laboratory conditions [79], can be used as a benchmark to determine impact on the aquatic environment.

Here, for the first time, the efficiency of a catalytic HDC process is quantified on the basis of a reduction in toxicity. The ecotoxicity of the reaction medium was evaluated in terms of toxicity units, applying the approach of Chen and Lu [80] for a concentration addition effect where all the compounds impact independently on a model biological system with no synergistic/antagonistic effects:

$$T.U._{Mixture}(t) = \sum_i \left(\frac{C_i(t)}{EC_{50,i}} \right) \qquad \textbf{(2.5)}$$

The parameter $T.U._{Mixture}(t)$ represents the toxicity units of the mixture at time t, $C_i(t)$ is the concentration of compound i at time t and $EC_{50,i}$ is the median effective concentration of compound i, *i.e.* the concentration necessary to kill 50 % of the population of a particular microorganism. The $EC_{50,i}$ values (for *Daphnia Magna* after 24 h contact) were taken from reference sources [81]: $EC_{50,i}$ = 3 (2,4-DCP), 6 (4-CP), 12 (2-CP and PhOH) and 820 (C6ONE) mg dm^{-3}.

The temporal decrease in the ecotoxicity of the bulk reaction liquid for the most and least dispersed Pd/Al_2O_3-A under controlled pH (pH_{basic} and pH_{acid}) are shown in **Figure 2.13**. For a given dispersion, reaction under basic conditions generated a less toxic reaction medium and, regardless of the operational pH, the final toxicity generated by smaller Pd particles was significantly lower than that obtained with the sintered catalyst. HDC using the highest Pd dispersion under basic conditions resulted in an 81 % reduction in liquid toxicity, a result that can serve as the basis for the development of an effective detoxification unit operation.

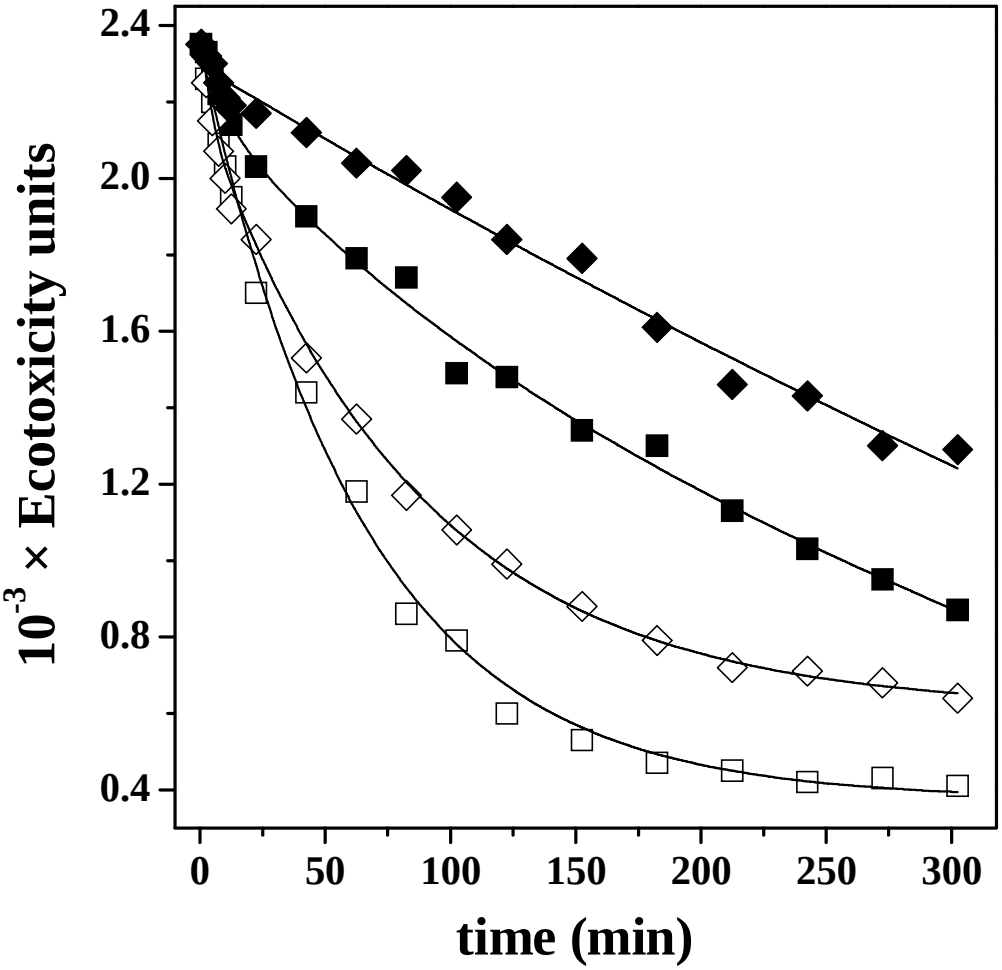

Figure 2.13. Temporal variation of the ecotoxicity of the reaction medium (see eqn (1.5)) for 2,4-DCP HDC over Pd/Al_2O_3-A activated to 573 K (■,□) and 1123 K (◆,◇) (β = 10 K min^{-1}) under pH_{acid} = 3 (solid symbols) and pH_{basic} = 13 (open symbols).

2.4 Conclusions

The data presented in this Chapter support the following conclusions:

(i) Thermal treatment of Pd/Al_2O_3 over the temperature range 573 - 1273 K results in a decrease in metal dispersion from 59 to 8 %; metal sintering has been confirmed by TEM, H_2 chemisorption and XRD measurements. The Pd particles at the higher dispersion fall within the mitohedrical region (1 - 5 nm) and exhibit a faceted morphology while the sintered particles are characterised by a pseudo-spherical shape. Metal sintering resulted in a slight decrease in BET area and pore volume but the pH_{pzc} remained unchanged.

(ii) Liquid phase HDC of 2,4-DCP under kinetic control yielded 2-CP and PhOH *via* a predominantly stepwise reaction pathway. Structure sensitivity has been established where smaller Pd particles (≤ 5 nm) delivered a higher specific (per m_{Pd}^2) HDC rate.

(iii) Solution pH values (relative to *pK* and pH_{pzc}) determine reactant/catalyst interactions, ultimately impacting on HDC pathway. At a controlled pH ($pH_{acid} < 7 < pK$, pH_{pzc}), reaction selectivity is dependent on Pd particle size whereas HDC selectivity at pH_{basic} is insensitive to Pd dispersion.

(iv) Bulk Pd was inactive under the same reaction conditions and lower Cl/Pd molar ratios were necessary to deliver measurable conversions, where the removal of both chlorines was favoured relative to the supported system.

(v) Pd/Al_2O_3 promoted aqueous phase HDC (under basic conditions and at high Pd dispersions) resulted in a decrease in solution ecotoxicity by up to 81%.

2.5 References

[2.1] E.-J. Shin, M. A. Keane, Chem. Eng. Sci., 54, 1109 (1999)

[2.2] G. Tavoularis, M. A. Keane, J. Mol. Catal. A: Chemical, 142, 187 (1999)

[2.3] C. Menini, C. Park, E.-J. Shin, G. Tavoularis, M. A. Keane, Catal. Today, 62, 355 (2000)

[2.4] M. A. Aramendia, V. Boráu, I. M. García, C. Jiménez, F. Lafont, A. Marinas, J. M. Marinas, F. J. Urbano, J. Catal., 187, 392 (1999)

[2.5] B. Coq, G. Ferrat, F. Figuéras, J. Catal., 101, 434 (1986)

[2.6] R. Gopinath, K. N. Rao, P. S. S. Prasad, S. S. Madhavendra, S. Narayanan, G. Vivekanandan, J. Mol. Catal. A: Chemical, 181, 215 (2002)

[2.7] M. A. Keane, C. Park, C. Menini, Catal. Lett., 88, 89 (2003)

[2.8] J. L. Benitez, G. del Angel, React. Kinet. Catal. Lett., 70, 67 (2000)

[2.9] G. Yuan, M. A. Keane, Chem. Eng. Sci., 58, 257 (2003)

[2.10] L. Calvo, M. A. Gilarranz, J. A. Casas, A. F. Mohedano, J. J. Rodríguez, Appl. Catal. B: Environmental, 67, 68 (2006)

[2.11] H. Cheng, K. Scott, P. A. Christensen, Appl. Catal. A: General, 261, 1 (2004)

[2.12] S. S. Zinovyev, N. A. Shinkova, A. Perosa, P. Tundo, Appl. Catal. B: Environmental, 55, 49 (2005)

[2.13] E. Baumgarten, A. Fiebes, A. Stumpe, React. Funct. Polym., 33, 71 (1997)

[2.14] J. Morales, R. Hutcheson, I. F. Cheng, J. Hazard. Mater. B, 90, 97 (2002)

[2.15] G. Pina, C. Louis, M. A. Keane, Phys. Chem. Chem. Phys., 5, 1924 (2003)

[2.16] E.-J. Shin, M. A. Keane, React. Kinet. Catal. Lett., 69, 3 (2000)

[2.17] G. Tavoularis, M. A. Keane, J. Chem. Technol. Biotechnol., 74, 60 (1999)

[2.18] W. Juszczyk, A. Malinowski, Z. Karpiński, Appl. Catal. A: General, 166, 311 (1998)

[2.19] P. S. S. Prasad, N. Lingaiah, S. Chandrasekhar, K. S. R. Rao, P. K. Rao, K. V. Raghavan, F. J. Berry, L. E. Smart, Catal. Lett., 66, 201 (2000)

[2.20] A. D. L. Ramos, P. S. Alves, D. A. G. Aranda, M. Schmal, Appl. Catal. A: General, 277, 71 (2004)

[2.21] Z. Karpiński, K. Early, J. L. d'Itri, J. Catal., 164, 378 (1996)

[2.22] Y. Ukisu, T. Miyadera, Appl. Catal. A: General, 271, 165 (2004)

[2.23] K. V. R. Chary, P. V. R. Rao, V. Vishwanathan, Catal. Commun., 7, 974 (2006)

[2.24] N. Lingaiah, Md. A. Uddin, A. Muto, T. Iwamoto, Y. Sakata, Y. Kusano, J. Mol. Catal. A: Chemical, 161, 157 (2000)

[2.25] J. Estellé, J. Ruz, Y. Cesteros, R. Fernández, P. Salagre, F. Medina, J.-E. Sueiras, J. Chem. Soc., Faraday Trans., 92, 2811 (1996)

[2.26] A. Gampine, D. P. Eyman, J. Catal., 179, 315 (1998)

[2.27] C. Park, C. Menini, J. L. Valverde, M. A. Keane, J. Catal., 211, 451 (2002)

[2.28] D. Fritsch, K. Kuhr, K. Mackenzie, F.-D. Kopinke, Catal. Today, 82, 105 (2003)

[2.29] F. J. Urbano, J. M. Marinas, J. Mol. Catal. A: Chemical, 173, 329 (2001)

[2.30] P. Albers, J. Pietsch, S. F. Parker, J. Mol. Catal. A: Chemical, 173, 275 (2001)

[2.31] A. Y. Stakheev, L. M. Kustov, Appl. Catal. A: General, 188, 3 (1999)

[2.32] M. L. Toebes, J. A. Dillen, K. P. de Jong, J. Mol. Catal. A: Chemical, 173, 75 (2001)

[2.33] L. M. Gómez-Sainero, X. L. Seoane, J. L. G. Fierro, A. Arcoya, J. Catal., 209, 279 (2002)

[2.34] Z. C. Zhang, B. C. Beard, Appl. Catal. A: General, 174, 33 (1998)

[2.35] G. C. Bond, Chem. Soc. Rev., 20, 441 (1991)

[2.36] S. Lambert, C. Cellier, P. Grange, J.-P. Pirard, B. Heinrichs, J. Catal., 221, 335 (2004)

[2.37] S. Lambert, J.-F. Polard, J.-P. Pirard, B. Heinrichs, Appl. Catal. B: Environmental, 50, 127 (2004)

[2.38] Y. H. Choi, W. Y. Lee, Catal. Lett., 67, 155 (2000)

[2.39] D. Dollimore, G.R. Heal, J. Colloid Interface Sci., 33, 508 (1970)

[2.40] J. Vakros, C. Kordulis, A. Lycourghiotis, J. Chem. Soc. Chem. Commun., 17, 1980 (2002)

[2.41] G. Yuan, M. A. Keane, J. Catal., 225, 510 (2004)

[2.42] Y. Shindler, Y. Matatov-Meytal, M. Sheintuch, Ind. Eng. Chem. Res., 40, 3301 (2001)

[2.43] J. E. Benson, H. S. Hwang, M. Boudart, J. Catal., 30, 146 (1973)

[2.44] V. Ferrer, A. Moronta, J. Sánchez, R. Solano, S. Bernal, D. Finol, Catal. Today, 107-108, 487 (2005)

[2.45] C.-B. Wang, H.-K. Lin, C.-M. Ho, J. Mol. Catal. A: Chemical, 180, 285 (2002)

[2.46] G. M. Tonetto, D. E. Damiani, J. Mol. Catal. A: Chemical, 202, 289 (2003)

[2.47] F. Pinna, F. Menegazzo, M. Signoretto, P. Canton, G. Fagherazzi, N. Pernicone, Appl. Catal. A: General, 219, 195 (2001)

[2.48] K. Otto, L. P. Haack, J. E. de Vries, Appl. Catal. B: Environmental, 1, 1 (1992)

[2.49] P. J. Schmitz, K. Otto, J. E. de Vries, Appl. Catal. A: General, 92, 59 (1992)

[2.50] N. S. Babu, N. Lingaiah, R. Gopinath, P. S. S. Reddy, P. S. S. Prasad, J. Phys. Chem. C, 111, 6447 (2007)

[2.51] N. K. Nag, J. Phys. Chem. B, 105, 5945 (2001)

[2.52] Y. Suzuki, T. Haraki, H. Uchida, J. Alloys Compd., 330-332, 488 (2002)

[2.53] T. Haraki, N. Inomata, H. Uchida, J. Alloys Compd., 293-295, 407 (1999)

[2.54] P. Burattin, M. Che, C. Louis, J. Phys. Chem. B, 104, 10482 (2000)

[2.55] R. Strobel, F. Krumeich, W. J. Stark, S. E. Pratsinis, A. Baiker, J. Catal., 222, 307 (2004)

[2.56] M. Boudart, H. S. Hwang, J. Catal., 39, 44 (1975)

[2.57] A. Rose, S. Maguinet, R. J. Mathew, C. Slater, J. Yao, A. E. Russell, Phys. Chem. Chem. Phys., 5, 3220 (2003)

[2.58] G. Yuan, M. A. Keane, Appl. Catal. B: Environmental, 52, 301 (2004)

[2.59] A. L. Bonivardi, M. A. Baltanas, J. Catal., 138, 500 (1992)

[2.60] S. Díaz-Moreno, D. C. Koningsberger, A. Muñoz-Páez, Nucl. Instrum. Methods Phys. Res., Sect. B, 133, 15 (1997)

[2.61] N. E. Bogdanchikova, S. Fuentes, M. Avalos-Borja, M. H. Farías, A. Boronin, G. Díaz, Appl. Catal. B: Environmental, 17, 221 (1998)

[2.62] S. Storsæter, B. Tøtdal, J. C. Walmsley, B. S. Tanem, A. Holmen, J. Catal., 236, 139 (2005)

[2.63] J. Sanchez-Valente, X. Bokhimi, J. A. Toledo, Appl. Catal. A: General, 264, 175 (2004)

[2.64] M. Trueba, S. P. Trasatti, Eur. J. Inorg. Chem., 17, 3393 (2005)

[2.65] G. Yuan, M. A. Keane, Catal. Today, 88, 27 (2003)

[2.66] M. A. Keane, J. Chem. Technol. Biotechnol., 80, 1211 (2005)

[2.67] J. Wei, X. Xu, Y. Liu, D. Wang, Water Res., 40, 348 (2006)

[2.68] G. Yuan, M. A. Keane, Ind. Eng. Chem. Res., 46, 705 (2007)

[2.69] J. B. Hoke, G. A. Gramiccioni, E. N. Balko, Appl. Catal. B: Environmental, 1, 285 (1992)

[2.70] V. Felis, C. de Bellefon, P. Fouilloux, D. Schweich, Appl. Catal. B: Environmental, 20, 91 (1999)

[2.71] H. M. Roy, C. M. Wai, T. Yuan, J.-K. Kim, W. D. Marshall, Appl. Catal. A: General, 271, 137 (2004)

[2.72] T. T. Bovkun, Y. Sasson, J. Blum, J. Mol. Catal. A: Chemical, 242, 68 (2005)

[2.73] G. S. Pozan, I. Boz, J. Hazard. Mater. B, 136, 917 (2006)

[2.74] J. W. da Silva, R. E. Bruns, A. J. G. Cobo, Chem. Eng. J., 131, 59 (2007)

[2.75] G. Yuan, M. A. Keane, Catal. Commun., 4, 195 (2003)

[2.76] E.-J. Shin, M. A. Keane, J. Chem. Technol. Biotechnol., 75, 159 (2000)

[2.77] R. M. Rioux, C. D. Thompson, N. Chen, F. H. Ribeiro, Catal. Today, 62, 269 (2000)

[2.78] E. J. A. X. van de Sandt, A. Wiersma, M. Makkee, H. Van Bekkum, J. A. Moulijn, Appl. Catal. A: General, 155, 59 (1997)

[2.79] J. C. Chapman, Aust. J. Ecol., 20, 20 (1995)

[2.80] C.-Y. Chen, C.-L. Lu, Sci. Total Environ., 289, 123 (2002)

[2.81] Material and Safety Data Sheet; Section 12: Ecological Information: Ecotoxicological Effects. In *Directive 91/155/EEC, Official Journal L76/91*, (2006)

Chapter 3

Solvent Effects in the Hydrodechlorination of 2,4-Dichlorophenol over Pd/Al_2O_3

In this Chapter, the role of the solvent in determining hydrodechlorination performance is examined. Single component water and organic solvents and solvent mixtures have been considered and the catalytic response determined under reaction conditions where hydrodechlorination operates under kinetic control. While selectivity is found to be insensitive to the solvent, catalytic activity is governed by the solvent dielectric constant (with *ca.* 80 % contribution to the overall rate); the molar volume provides a secondary contribution.

3.1 Introduction

Catalytic hydrodechlorination (HDC), the controlled removal of organic chlorine with H_2, is finding increasing acceptance as a low energy, alternative chlorinated waste abatement methodology [1]. Supported palladium is now established as the most effective HDC catalyst due to its inherent capacity to promote C–Cl bond hydrogenolytic scission and resistance to deactivation by HCl [2]. Among the factors that can influence HDC performance, which include metal dispersion [3,4], nature of the support [5] and use of additives [6,7], solvent usage is a critical variable [8,9] that has yet to be examined in any appreciable detail. In liquid phase operations, water [10-15], methanol [15-19] and ethanol [19-22] have been the most commonly used solvents due to environmental applicability and/or reactant solubility considerations. The ideal role of the solvent should be to facilitate heat transfer and/or serve as an inert reaction medium to bring the reactants in close contact [23]. Nevertheless, there is evidence in the literature demonstrating that HDC rate [10-22,24] and product distribution [15,21] can be affected by the nature of the solvent. The reason for this response is still a matter of some debate as the HDC studies that have considered the role of solvent have also exhibited (i) secondary reactions, (ii) catalyst deactivation and (iii) mass-transfer limitations.

Indeed, there are many instances where the solvent has participated in the HDC process by (a) serving as a second reactant (*via* H_2 donation, particularly when using iso-propanol) [25-28] or (b) reacting with the chloroaromatic leading to by-product formation [29]. In the absence of such effects, variations in HDC rate/mechanism have been linked to a solvent-dependent catalyst deactivation by the HCl by-product [16,17] where differences in solubility [30] impact on HCl removal from the catalyst surface to varying degrees [9,21]. Water/alcohol [12,13] and binary alcohol [6,18] mixtures have been employed to circumvent deleterious HCl/catalyst interactions but these studies did not attempt to provide a quantitative relationship between the catalytic response and solvent physical/chemical properties. It should be flagged the work of Xia *et al.* [31] who, studying the HDC of 2,4,4'-trichloro-2'-hydroxyphenylether over Pd/C using a range of organic solvents, linked variations in turnover frequency to solvent-reactant steric and π-resonance interactions that influenced reactant adsorption on the catalyst. The addition of a base (typically NaOH) [14,20,22] has been employed to neutralize the HCl generated but lower HDC rates have also been attained and associated with active site occlusion by the precipitated chlorinated salt [12,18]. Few HDC studies have taken into consideration possible contributions due to mass-transfer limitations [19,31] with the result that the available kinetic data may be masked by H_2 and chloroaromatic transport [12,32] and/or solubility [10,15] constraints.

In this work, the effect of the solvent is addressed in the absence of secondary reactions and under negligible catalyst deactivation or transport limitations. In order to achieve this goal, a range of solvents (water, methanol, ethanol, *n*-propanol, THF, benzene, cyclohexane and *n*-hexane) have been considered and solvent combinations with varying properties in terms of solvation power and solvent-solvent interactions, *i.e.* dielectric constant, molar volume, viscosity and enthalpy of vaporization [23]. The HDC of 2,4-dichlorophenol (2,4-DCP) over Pd/Al_2O_3 has been chosen as a suitable model catalytic reaction [33] and provide the first comprehensive quantitative treatment of HDC performance that is correlated to solvent physical/chemical characteristics.

3.2 Experimental

3.2.1 Materials

The 2,4-DCP reactant (Aldrich, 98.0 %) and organic solvents (methanol: Riedel-de Haën, 99.9 %; ethanol: Aldrich, 99.9 %; *n*-propanol: Aldrich, 99.7 %; THF: Aldrich, 99.9 %; benzene: Aldrich, 99.9 %; cyclohexane: Fluka, 99.8 %; *n*-hexane: Aldrich, 99.9 %) were used as received without further purification. Stock solutions with an initial 2,4-DCP concentration ($C_{2,4\text{-}DCP,0}$) = 0.025 $mol_{2,4\text{-}DCP}$ dm^{-3} were employed. The catalyst, 1.2 % w/w Pd/Al_2O_3, was purchased from Sigma-Aldrich and sieved (ATM fine test sieves) into batches of 38 μm average particle diameter. A constant starting Cl/Pd molar ratio (= 900 mol_{Cl} mol_{Pd}^{-1}) was employed throughout this study.

3.2.2 Catalyst Characterization

BET surface area and pore size distribution analyses were performed using a commercial Micromeritics Flowsorb II 2300 unit. Prior to analysis, the samples were outgassed at 423 K for 1 h in 20 cm^3 min^{-1} dry N_2. BET area was obtained in 30 % v/v N_2/He (20 cm^3 min^{-1}) with at least three cycles of N_2 adsorption/desorption using the standard single-point BET method. N_2 adsorption/desorption isotherms were performed over the relative pressure range $0.05 \leq P/P_0 \leq 0.98$, where the total pore volume and size distribution were obtained according to the method of Dollimore and Heal [34]. The BET areas and N_2 uptake/release values were reproducible to within ± 4 % and the values quoted in this paper are the mean. Pd particle size and morphology were determined by transmission electron microscopy (TEM): JEOL JEM 2011 TEM unit with a UTW energy-dispersive X-ray detector (Oxford Instruments) operated at an accelerating voltage of 200 kV and using Gatan DigitalMicrograph 3.4 for data acquisition/manipulation. The samples were dispersed in acetone and deposited on a holey-carbon/Cu grid (300 Mesh). At least 650 individual Pd particles were counted and the Pd particle size quoted in this paper represents the surface area-weighted mean value as explained in detail elsewhere [35].

3.2.3 Catalytic Procedure

The liquid phase HDC reactions were carried out in a modified, commercial glass reactor (Ken Kimble Reactors Ltd.), equipped with a H_2 supply at a constant volumetric flow rate (Brooks mass flow-controlled at 150 cm^3 min^{-1}) and a glass impeller providing effective agitation at 1100 rpm. It has been demonstrated elsewhere [36,37] that this choice of H_2 flow and stirring speed served to minimize external H_2 transport limitations. A water-recirculating bath (Julabo HD-4) was used to stabilize the reaction temperature at T = 303 ± 1 K, where loss of the reactor liquid contents in the H_2 flow was negligible (< 0.5 % v/v) using water as coolant (*ca.* 293 K). At the beginning of each experiment, the catalyst and 100 cm^3 of the stock solution were charged and agitated in a He flow (50 cm^3 min^{-1}) while the temperature was allowed to stabilize (15 min) and hydrogen was then introduced (time t = 0 for reaction). As a blank test, experiments carried out under He, *i.e.* in the absence of H_2, did not result in any detectable conversion. A non-invasive liquid sampling *via* a syringe with in-line filters allowed a controlled removal of aliquots (< 0.5 cm^3) from the reactor. The composition of these samples was determined by gas chromatography using a Perkin-Elmer Auto System XL GC, equipped with an FID and a DB-1 capillary column (J&W Scientific: i.d. = 0.2 mm, length = 50 m, film thickness = 0.33 μm). The concentration of organic (2,4-DCP, 2-chlorophenol (2-CP), phenol (PhOH)) and inorganic (HCl) species in the bulk liquid phase were obtained from the total molar balance in the reaction mixture, where the effect of uptake on the support was negligible [36,38]. The fractional conversion of 2,4-DCP ($X_{2,4\text{-}DCP}$) is defined as

$$X_{2,4\text{-}DCP} = \frac{C_{2,4\text{-}DCP,0} - C_{2,4\text{-}DCP}}{C_{2,4\text{-}DCP,0}} \quad \textbf{(3.1)}$$

where $C_{2,4\text{-}DCP}$ represents the concentration of 2,4-DCP. The selectivity with respect to 2-CP ($S_{2\text{-}CP}$) is given in terms of the total moles of product formed

$$S_{2\text{-}CP} = \frac{C_{2\text{-}CP}}{C_{2,4\text{-}DCP,0} - C_{2,4\text{-}DCP}} \quad \textbf{(3.2)}$$

where $C_{2\text{-}CP}$ is the concentration of 2-CP.

HDC activity is expressed in terms of initial rate of 2,4-DCP consumption ($(-R_{2,4\text{-}DCP})_0$, units: $mmol_{2,4\text{-}DCP}\ g_{Pd}^{-1}\ min^{-1}$), as calculated from the temporal profiles for $C_{2,4\text{-}DCP}$ and $X_{2,4\text{-}DCP} \leq 0.25$ [37]. Repeated reactions with different samples of catalyst/reactant stock solution delivered raw data reproducibility that was better than ± 7 %.

3.3 Results and Discussion

3.3.1 Catalyst Characterization

The N_2 adsorption/desorption isotherms presented in **Figure 3.1**a present an hystersis loop at high relative pressures ($P/P_0 > 0.8$), consistent with a type IV adsorption according to the IUPAC classification, which is typical for γ-Al_2O_3 [39,40]. The associated pore size distribution (see inset to **Figure 3.1**a), shows significant microporous structure (pore size < 20 Å) with an appreciable contribution (35 % of total volume) due to the presence of mesopores. The BET surface area (160 $m^2\ g^{-1}$) and total pore volume (0.56 $cm^3\ g^{-1}$) values are within the range reported [41] for γ-Al_2O_3-supported catalysts, *i.e.* 150 - 250 $m^2\ g^{-1}$ and 0.45 - 0.75 $cm^3\ g^{-1}$, respectively. Catalyst porosity ($\varepsilon_{catalyst}$) and tortuosity (τ) were determined according to

$$\varepsilon_{catalyst} = \rho \times (Pore\ Volume) \tag{3.3}$$

$$\tau = \frac{1}{\varepsilon_{catalyst}} \tag{3.4}$$

where ρ is the bulk density (1154 kg m^{-3}). The resultant values for $\varepsilon_{catalyst}$ (0.65) and τ (1.54) are indicative of low impedance with respect to reactant/product diffusion where at τ values approaching unity, the actual (average) path traversed by the species in the interstitial fluid within the pores is similar to that for free diffusion in the bulk fluid [42]. Representative low (I) and high (II) magnification TEM images are given in **Figure 3.1**b. The Pd phase is present as well dispersed particles with a surface area-weighted mean particle size of 2.4 nm, corresponding to a specific metal surface area of 208 $m_{Pd}^2\ g_{Pd}^{-1}$.

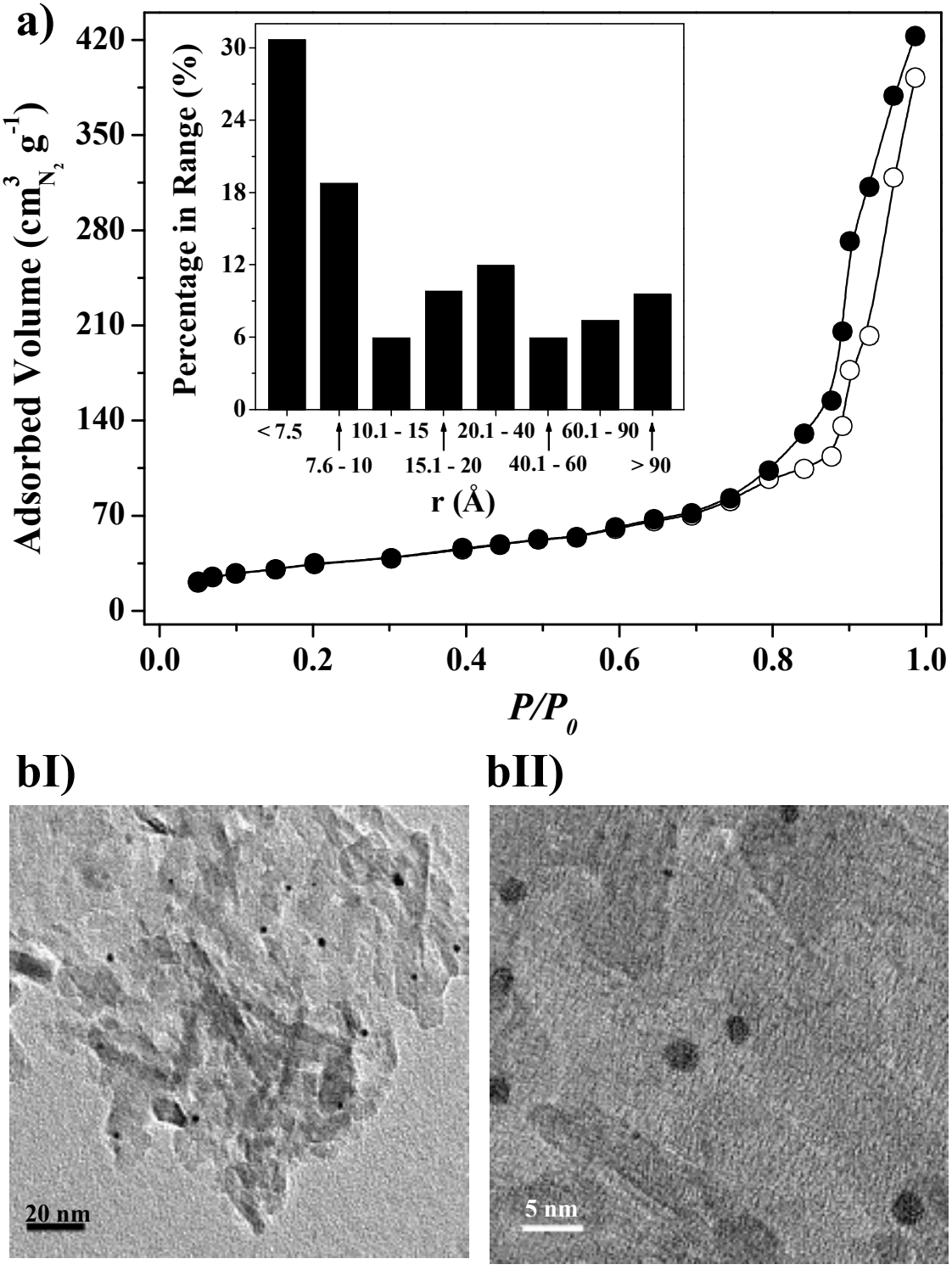

Figure 3.1: a) N_2 adsorption (○) and desorption (●) isotherms with associated pore volume distribution (inset) and b) representative (I) low and (II) high magnification TEM images of the Pd/Al_2O_3 catalyst.

3.3.2 Estimation of Transport Limitations

The catalytic HDC reaction requires the diffusion of both reactants to the catalyst surface and, if the rate of mass transfer is lower than that of the chemical step, a measurement of true kinetics is compromised. In this three phase system, the critical mass transport steps that must be considered occur in the bulk solvent, the liquid film at the external catalyst surface and within the pores. These three contributions will be denoted as zones I, II and III, respectively, and the crucial quantitative parameters that must be considered for each zone are compiled in **Table 3.1** [43,44], identifying the critical limiting values and our actual experimental results. In zone I, transport constrains are conditioned by the solubility of both reactants in each solvent. There are no associated transport constraints for 2,4-DCP as it is soluble in each solvent (water, methanol, ethanol, *n*-propanol, THF, benzene, cyclohexane and *n*-hexane) at the concentration (0.025 $mol_{2,4\text{-DCP}}$ dm^{-3}) used in this study but H_2 transport must be addressed. It has been demonstrated elsewhere [36] that, at the rate of gas supply employed, reaction in water is not hindered by H_2 solubility. Therefore, reaction in organic solvents will not be limited provided H_2 availability is at least equivalent to that in water. The molar fraction of H_2 (x_{H_2}) in each solvent was estimated according to the method of Prausnitz-Shair [45], using a solubility parameter for the particular solvent (δ) that was calculated applying Lemcoff's relationship [46]

$$\delta = \sqrt{\frac{\Delta\bar{H} - RT}{\bar{v}}} \qquad \textbf{(3.8)}$$

where $\Delta\bar{H}$ is the enthalpy of vaporization (estimated by the method of Watson) [47] and $\bar{v}$ is the molar volume (based on the Redlich-Kwong equation of state). It should be noted that the concentration of 2,4-DCP is low enough to discount any interference in the H_2 solubility calculations. The results demonstrate a wide range of H_2 molar fractions in the bulk solvent with the highest value for cyclohexane (44×10^{-5}) and lowest (8×10^{-5}) for methanol. As the range of molar fractions are well above the limiting value in water (1×10^{-5}), the available H_2 is sufficiently high that any restrictions to transport through the bulk solution are not significant.

Table 3.1: Summary of the estimation of mass transport resistances in the HDC of 2,4-DCP over Pd/Al_2O_3 in different solvents.

Zone	**I (Bulk liquid)**	**II (Liquid film at the catalyst surface)**	**III (Liquid in the catalyst pores)**
Parameter	H_2 solubility	Carberry number	Effectivenes factor
Expression	$-\ln x_{H_2} = \ln\left(\frac{f_{H_2}^L}{f_{H_2}^0}\right) + \frac{g^2 \overline{v}_{H_2}\left(\delta - \delta_{H_2}\right)^2}{RT}$ **(3.5)**	$Ca = \frac{\rho\, m_{Pd}\, d^2}{12\, C_i\, D_i} \times (-R_i)_0$ **(3.6)**	$\eta = \frac{1}{\phi} \times \left(\frac{1}{\tanh(3\phi)} - \frac{1}{3\phi}\right)$ **(3.7)**
Variables	$f_{H_2}^L$: fugacity of H_2 (57 MPa).[a,b] $f_{H_2}^0$: fugacity of H_2 (0.1 MPa). g : volume fraction of the solvent (≈ 1). $\overline{v}_{H_2}$: molar volume of H_2 (37 $cm^3\ mol^{-1}$).[a,c] δ_{H_2} : solubility parameter of H_2 (248 $kJ^{1/2}\ m^{-3/2}$).[a,c] δ : solubility parameter of the solvent ($kJ^{1/2}\ m^{-3/2}$). R : universal gas constant (8.314 $J\ mol^{-1}\ K^{-1}$). T : temperature (303 K).	ρ : bulk catalyst density (1154 $kg\ m^{-3}$). d : catalyst particle diameter (38 μm). m_{Pd} : catalyst Pd loading (0.012 $g_{Pd}\ g^{-1}$). C_i : bulk liquid concentration ($mol\ dm^{-3}$). D_i : diffusivity ($m^2\ s^{-1}$). $(-R_i)_0$: initial consumption rate ($mol\ g^{-1}\ s^{-1}$).	ϕ : Thiele modulus.
Limiting values	$x_{H_2} < 1 \times 10^{-5}$	$Ca > 0.1$	$\eta < 0.9$
Results	$x_{H_2} = 8 \times 10^{-5}$ - 44×10^{-5}	$Ca = 9 \times 10^{-2}$ - 5×10^{-7}	η = 0.96 - 1

[a]value at T = 303 K.
[b]as estimated from Jáuregui-Haza *et al.*[43].
[c]from Yen and McKetta [44].

The possibility of mass transfer limitations in zone II was evaluated for both H_2 and 2,4-DCP by applying the Carberry number (*Ca*) approach which, assuming (i) isothermal conditions, (ii) spherical catalyst particle morphology and (iii) the absence of concentration gradients, takes the form of the expression given in **Table 3.1**. The diffusivity of H_2 was calculated using the Wilke-Chang method [48] while 2,4-DCP diffusivity calculations were dependent on the nature of the solvent and drew on the Hayduk and Laudie equation in the case of water [49], whereas the method of King *et al.* [50] was employed for the organic solvents. The *Ca* numbers, ranging from 9×10^{-2} (2,4-DCP in water) to 5×10^{-7} (2,4-DCP in benzene), are consistent with operation under conditions of negligible reactant transport constraints. Finally, the possibility of transfer limitations in zone III was evaluated using the effectiveness factor (η, see **Table 3.1**), where the Thiele modulus (ϕ) was calculated from

$$\phi = \sqrt{\frac{(-R_i)_0 \rho m_{Pd} \left(d/6\right)^2}{C_i D_{Eff,i}}} \qquad \textbf{(3.9)}$$

where and $D_{Eff,i}$ ($m^2\ s^{-1}$) is the effective diffusivity ($D_{Eff,i} = D_i \times (\varepsilon_{catalyst})^2$ [51]). For each reactant/solvent system, the value of η is close to unity, indicating that the rate of transport in the catalyst pores is such that the HDC step is rate-determining. The results presented in this section confirm that the HDC of 2,4-DCP over Pd/Al_2O_3, in each of the solvents used, is free from mass transport constraints and our catalytic data were obtained under conditions of kinetic control.

3.3.3 2,4-DCP HDC in Single Component (Water or Organic) Solvents

The HDC of 2,4-DCP in all the solvents under consideration generated 2-CP and PhOH as the only products, resulting from partial and complete HDC, respectively. There was no evidence of 4-chlorophenol formation, hydrodeoxygenation or ring reduction. The formation of 2-CP and PhOH is possible either *via* a consecutive or parallel mechanism, as shown in **Figure 3.2**a.

In order to establish the preferred HDC pathway, a mass balance (in batch operation) was applied assuming pseudo-first order kinetics for each individual step,

$$\frac{1}{W}\frac{dx_{2,4\text{-}DCP}}{dt} = -\left(k_1 + k_3\right) x_{2,4\text{-}DCP} \quad \textbf{(3.10)}$$

$$\frac{1}{W}\frac{dx_{2\text{-}CP}}{dt} = k_1 x_{2,4\text{-}DCP} - k_2 x_{2\text{-}CP} \quad \textbf{(3.11)}$$

$$\frac{1}{W}\frac{dx_{PhOH}}{dt} = k_2 x_{2\text{-}CP} + k_3 x_{2,4\text{-}DCP} \quad \textbf{(3.12)}$$

where x_i represents the molar fraction of compound i, W is the catalyst mass and k_j is the rate constant of step j. Taking water as a representative solvent, the applicability of this model is demonstrated in **Figure 3.2**b where the experimentally determined and predicted product compositions converge. The resultant rate constants values (in $mmol_{Reactant}\ g_{Pd}^{-1}\ min^{-1}$) are k_1 = 385, k_2 = 513 and k_3 = 213. The k_2/k_1 ratio (1.3) is consistent with an electrophilic aromatic substitution mechanism where the dechlorination rate of 2,4-DCP is lower than that of 2-CP as a result of the deactivating electron withdrawing effect of the second Cl substituent. The k_1/k_3 ratio (1.8) is indicative of a preferentially stepwise (as opposed to concerted) HDC route.

The selectivity response was largely insensitive to the nature of the solvent as shown in **Figure 3.3**a where, for a given fractional 2,4-DCP conversion ($X_{2,4\text{-}DCP}$ = 0.1), 2-CP selectivity was essentially invariant ($S_{2\text{-}CP}$ = 0.77 ± 0.04). HDC selectivity has been reported to be both, dependent [15,21] and independent [18,20] on the sovent usage, but this response has not been discussed to any significant extent beyond reporting solvent choice to establish conditions for optimal chlorine removal. In the HDC of 4-chloroanisole over Pd/C, Ukisu and Miyadera [18] reported similar anisole selectivities, *i.e.* 99 % and 97 %, when using *i*-propanol and methanol, respectively, while Cellier *et al.* [20] recorded selectivities of 99 % and 96 % in THF and ethanol. In contrast, Concibido *et al.* [15], studying the HDC of tetrachloroethylene over Pd/C, suggested a distinct reaction pathway when using methanol or water as solvent due to the appearance of trichloroethane (as intermediate) in the former case.

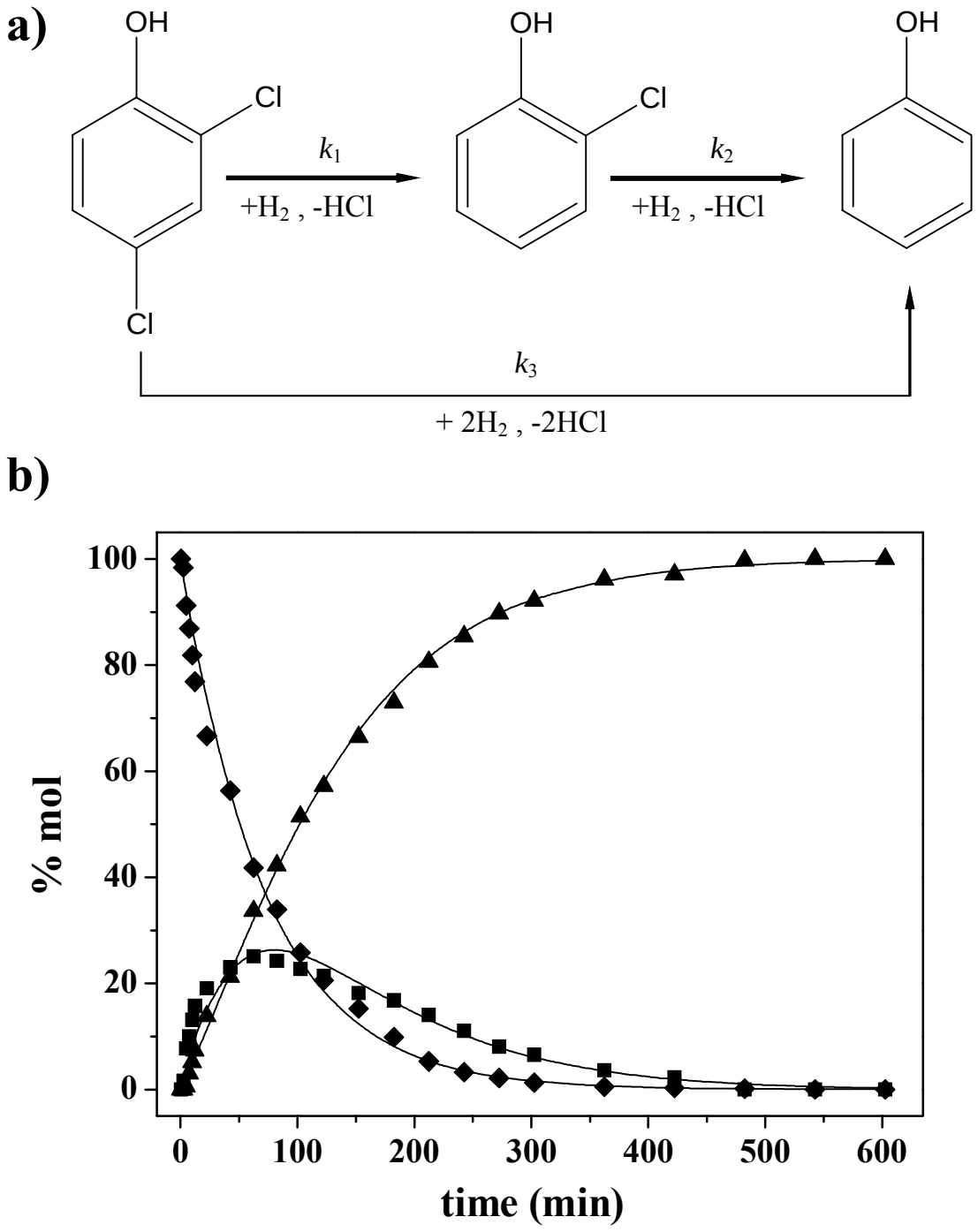

Figure 3.2: a) Simplified 2,4-DCP HDC reaction scheme (stepwise pathway is highlighted in bold) and b) bulk liquid composition as a function of reaction time, in terms of % mol 2,4-DCP (◆), 2-CP (■) and PhOH (▲) for reaction in water as solvent; lines represent fit to eqns. (3.10 - 3.12).

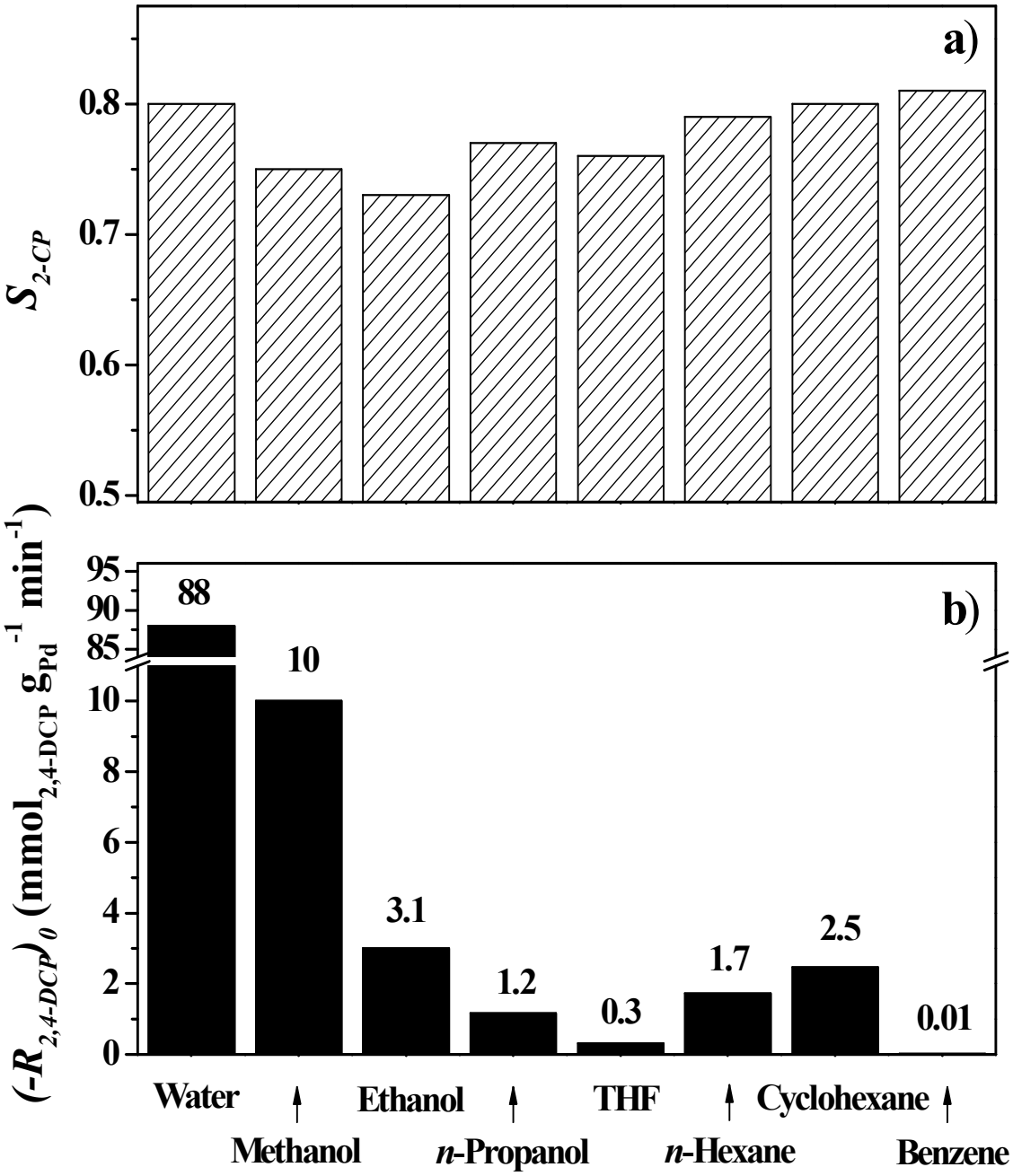

Figure 3.3: 2,4-DCP HDC in different solvents: a) selectivity with respect to 2-CP ($S_{2\text{-}CP}$) at $X_{2,4\text{-}DCP}$ = 0.1; b) initial 2,4-DCP consumption rates ($(-R_{2,4\text{-}DCP})_0$).

It is worth flagging the work of Bae *et al.* [21] who, studying the HDC of CCl_4 over Pd/C, recorded a selectivity to $CHCl_3$ of 97 % in ethanol that was significantly higher than that (74 %) obtained in acetonitrile and attributed this response to a proton-donation effect in the case of ethanol. The initial 2,4-DCP consumption rate ($(-R_{2,4\text{-}DCP})_0$) exhibited a strong dependence on the solvent with the following sequence of decreasing activity: water > methanol > ethanol ≈ cyclohexane ≈ *n*-hexane ≈ *n*-propanol > THF > benzene (see **Figure 3.3**b). The coupled catalytic response, *i.e.* selectivity invariance and significant activity dependence, suggests that each HDC step (partial *vs.* complete HDC) is affected to the same extent in each of the solvents. Having established a kinetic regime, the relationship between catalytic activity and solvent properties was examined in some detail where we considered dielectric constant (ε), molar volume ($\overline{v}$), dynamic viscosity (η_S) and the boiling point enthalpy of vaporization ($\Delta\overline{H}_{T_b}$) as critical solvent properties (see **Figure 3.4**). The relevance of these properties is as follows: ε provides a measure of the capacity of the solvent to stabilize ions in solution and is linked to polarity; $\overline{v}$ represents the volume of one mole of solvent and its ability to form organized structures; η_S and $\Delta\overline{H}_{T_b}$ are the macroscopic expressions of the strength of solvent-solvent physical and chemical interactions, respectively. Our results demonstrate a dependence of $(-R_{2,4\text{-}DCP})_0$ on solvent polarity and structure (see **Figure 3.4**a and **3.4**b, respectively) but no clear relationship with respect to differences in the degree of the solvent-solvent interactions (**Figure 3.4**c and **3.4**d) is apparent. HDC of 2,4-DCP proceeds *via* an electrophilic mechanism with the formation of a cationic reactive intermediate that is stabilized when the positive charge is delocalized due to resonance effects [52,53]. A dependence of HDC rate on the nature of the solvent can then result from differences in the stabilization of the electropositive intermediate due to solute-solvent interactions. The increase in $(-R_{2,4\text{-}DCP})_0$ with ε can be linked to the increased strength in the ionic (coulomb) forces due to solvation. Moreover, the increase in $(-R_{2,4\text{-}DCP})_0$ with decreasing $\overline{v}$ can be associated with the greater number of solvent molecules (per unit volume) available to interact with the charged reaction intermediate. The highest $(-R_{2,4\text{-}DCP})_0$ was observed for reaction in water, which is known to dissolve ions in solution and form well organized structures *via* H-bonding, *i.e.* highest/lowest values of ε and $\overline{v}$ in **Figure 3.4**. Lower $(-R_{2,4\text{-}DCP})_0$ were recorded in those solvents (*n*-hexane, cyclohexane, benzene and THF) with a lesser ion solvation capability and H-bonding (if any) [23].

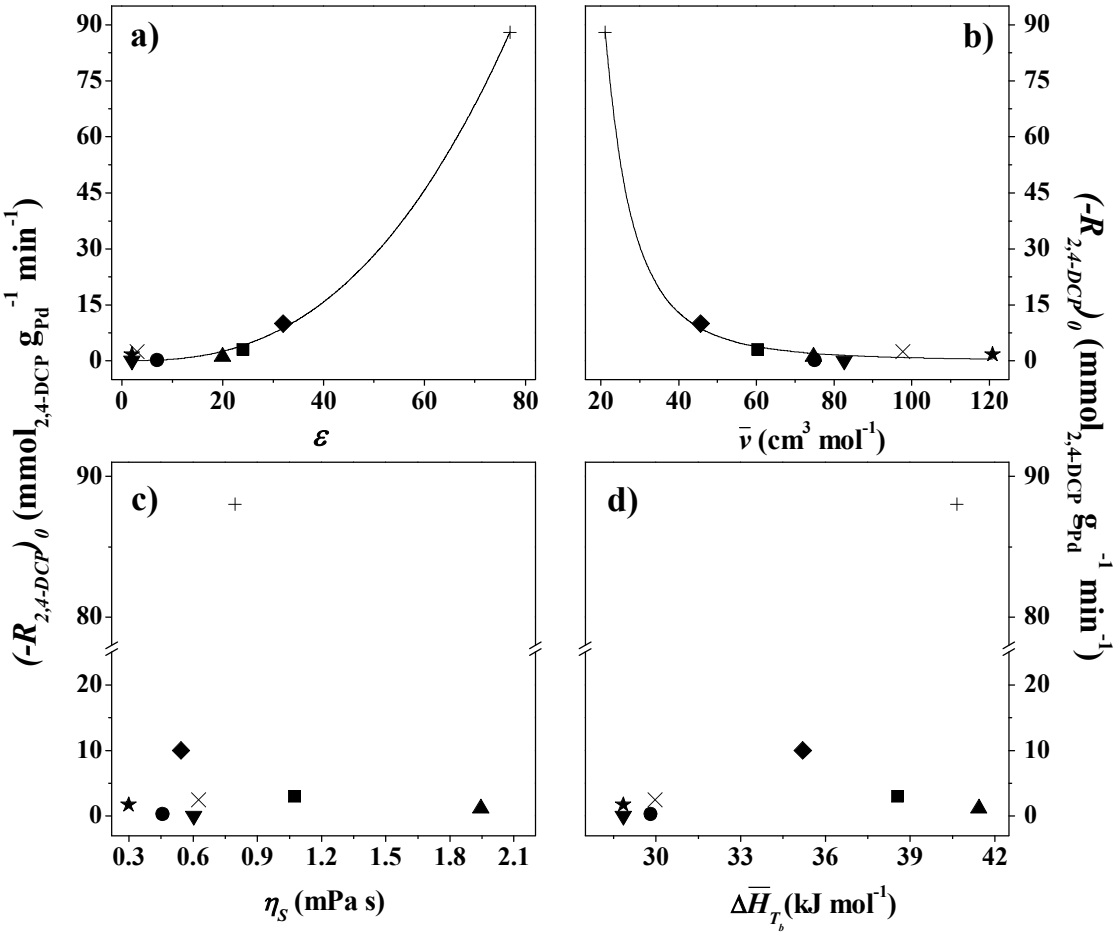

Figure 3.4: Initial 2,4-DCP consumption rates ($(-R_{2,4\text{-DCP}})_0$) as a function of a) solvent dielectric constant (ε), b) molar volume ($\bar{v}$), c) dymanic viscosity (η_S) and d) molar enthalpy of vaporization at normal boiling point ($\Delta\bar{H}_{T_b}$) for reaction in water (+), methanol (◆), ethanol (■), *n*-propanol (▲), THF (●), benzene (▼), cyclohexane (×) and *n*-hexane (★). Note: lines represent fit to eqns. (3.13) (for a)) and (3.14) (for b)).

Although there are instances in the literature where HDC rate has been linked to variations in ε [8,17,21], this response has not been quantified. Furthermore, this is the first reported study where HDC has also been shown to vary with $\bar{v}$. As a general rule, a solvent with high ε presents a low $\bar{v}$ with the result that a decoupling of the contribution of each parameter to the observed variation in rate is not straightforward and the author could not identify any practical solvent(s) that exhibit similar ε values but differing $\bar{v}$ (or *vice versa*).

As an alternative approach, a mathematical solution has been adopted here where $(-R_{2,4\text{-}DCP})_0$ has been adjusted to the empirical relationships

$$\left(-R_{2,4\text{-}DCP}\right)_0 = a_{\varepsilon}\left(\varepsilon\right)^{b_{\varepsilon}} \tag{3.13}$$

$$\left(-R_{2,4\text{-}DCP}\right)_0 = a_{\bar{v}}\left(\bar{v}\right)^{b_{\bar{v}}} \tag{3.14}$$

where a and b are fitting parameters. Given the direct and inverse dependence of $(-R_{2,4\text{-}DCP})_0$ on ε and $\bar{v}$, respectively, it follows that

$$\left(-R_{2,4\text{-}DCP}\right)_0 = a_T\left(\varepsilon/\bar{v}\right)^{b_T} \tag{3.15}$$

and the relationship between the ε and $\bar{v}$ factors (b_T) can be presented as

$$b_T = b_{\varepsilon}\Psi + b_{\bar{v}}\left(1-\Psi\right) \tag{3.16}$$

where Ψ serves to quantify the fractional contribution due to ε. The applicability of this approach is demonstrated in **Figures 3.4**a, **3.4**b and **Figure 3.5**, while the relevant parameters are given in **Table 3.2**. The high R^2 (0.998) illustrates the goodness of fit and the value of Ψ (*ca.* 0.8) establishes that the major source of the rate variation is ε. This result suggests that the strength of the solute-solvent interactions is more important than the actual (average) number of solvent molecules participating in the solvation process. In terms of practical application, in order to achieve elevated HDC rates, the choice of solvent must be prioritized, in the first instance, in terms of higher ε values where a lower $\bar{v}$ represents a secondary consideration. These findings are significant not only in terms of establishing the important solvent characteristics in catalytic HDC but also as an effective quantitative approach to tackling solvent effects in catalytic systems.

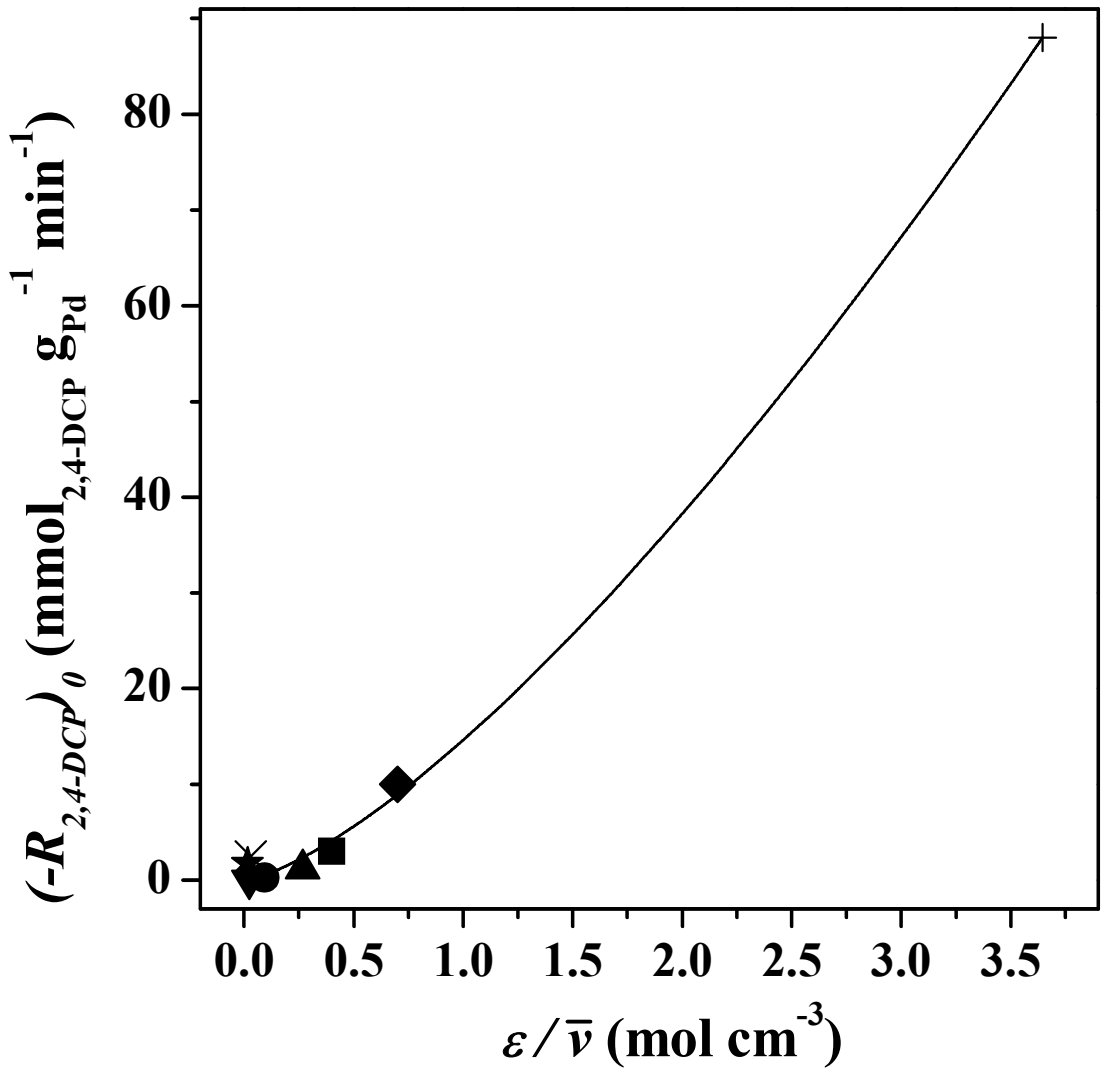

Figure 3.5: Initial 2,4-DCP consumption rate ($(-R_{2,4\text{-DCP}})_0$) as a function of the ratio between the solvent dielectric constant (ε) and associated molar volume ($\bar{v}$) for reaction in water (+), methanol (◆), ethanol (■), *n*-propanol (▲), THF (●), benzene (▼), cyclohexane (×) and *n*-hexane (★). Note: line represents fit to eqn. (3.15).

Table 3.2: Fitting results for the relationship between initial 2,4-DCP consumption rate $(-R_{2,4\text{-DCP}})_0$ and dielectric constant (b_ε), molar volume ($b_{\bar{v}}$) and the ratio of both parameters (b_T) with relative uncertainties (R^2) and the fractional dependence on the dielectric constant (Ψ) for reaction over Pd/Al_2O_3 in different solvents.

Reaction media	b_ε	R^2	$b_{\bar{v}}$	R^2	b_T	R^2	Ψ
Single component solvent	2.631	0.998	-3.006	0.998	1.388	0.998	0.779
Water+organic[a]	2.555	0.933	-3.365	0.906	1.443	0.926	0.812
Water+organic[b]	2.350	0.942	-2.908	0.956	1.298	0.951	0.800

[a]including water+THF
[b]excluding water+THF

3.3.4 2,4-DCP HDC in Water+Alcohol and Water+THF Mixtures

The results have established that water is the most effective HDC solvent due to its high and low associated ε and $\bar{v}$ values, respectively. However, its applicability in a wide range of HDC reactions is limited by the low solubility of non-polar chloroaromatics. The use of water+organic mixtures represents a compromise solution to extend the range of chloroarene concentrations that can be considered and ensure higher dechlorination rates. Such is the premise on which this study of binary solvent mixtures in 2,4-DCP HDC is based. The variation of $(-R_{2,4\text{-}DCP})_0$ in water+methanol (I), water+ethanol (II), water+*n*-propanol (III) and water+THF (IV) systems in terms of the dielectric constant of the solvent combinations (ε_m) is shown in **Figure 3.6**a. The corresponding data for single component solvents (connected by dotted lines) are identified in the figure. The impact of switching to solvent mixtures on reaction selectivity is illustrated in **Figure 3.6**b. The values of ε_m have been estimated according to:

$$\varepsilon_m = \left(\varepsilon_{water}\, x_{water}\right) + \left(\varepsilon_{organic}\left(1 - x_{water}\right)\right) \qquad \textbf{(3.17)}$$

where x_{water} is the molar fraction of water in the mixture. Regardless of the organic solvent or water content, the use of aqueous+organic mixtures delivered lower $(-R_{2,4\text{-}DCP})_0$ than that predicted ($(-R_{2,4\text{-}DCP})_0^{Predicted}$) on the basis of a linear correlation of the single constituents (moving along the dotted line), while all the selectivity/activity profiles were superimposable. The latter response supports our prior contention that the solvent does not influence the HDC pathway as it impacts on each individual dechlorination step to the same extent. Following our discussion in section **3.3.3**, the decrease in $(-R_{2,4\text{-}DCP})_0$ with dielectric constant can be linked to a lesser stabilization of the reaction intermediate. The deviation in the $(-R_{2,4\text{-}DCP})_0$ *vs.* ε_m profiles from the $(-R_{2,4\text{-}DCP})_0^{Predicted}$ response is significant.

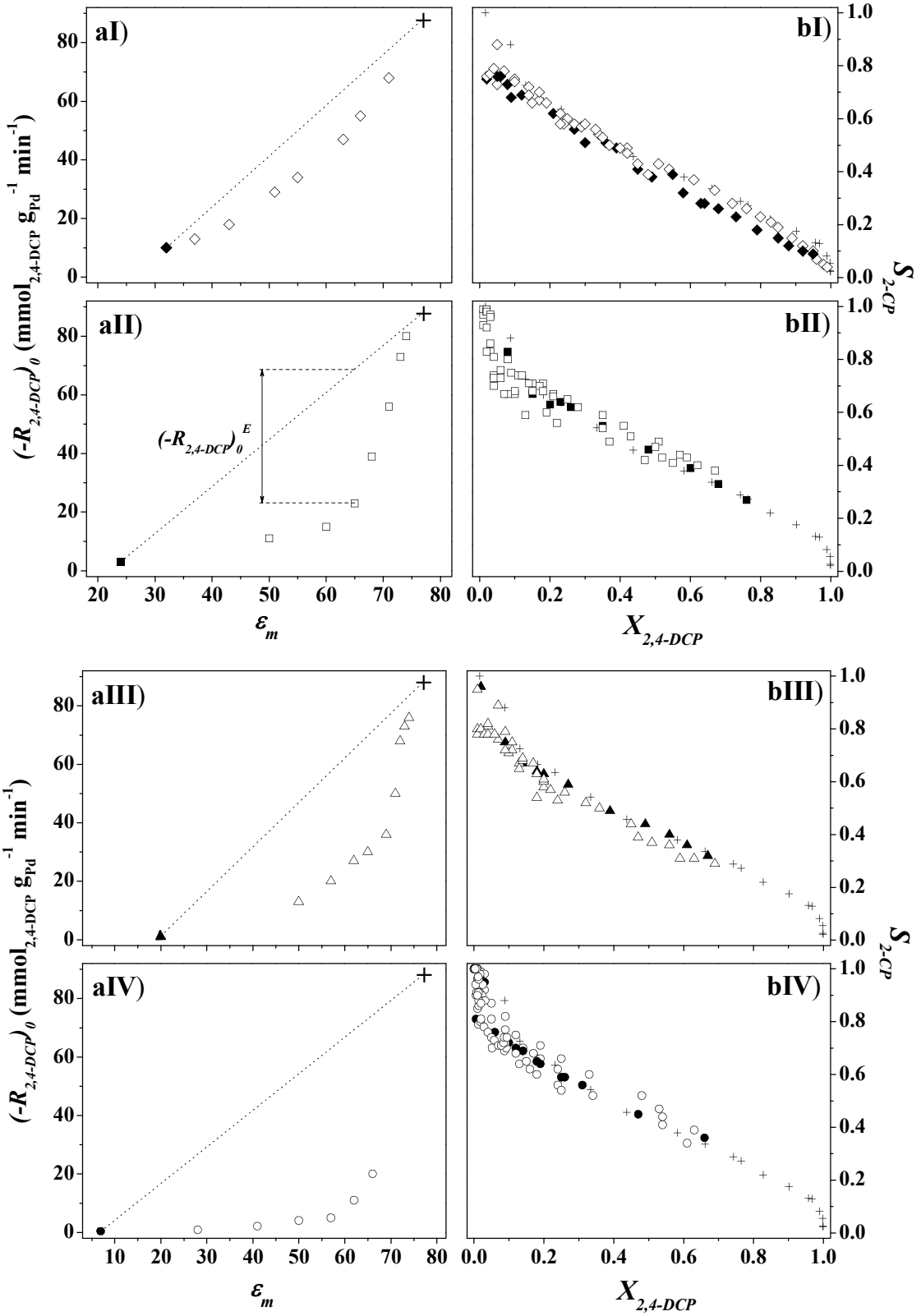

Figure 3.6: Initial 2,4-DCP consumption rate ($(-R_{2,4\text{-DCP}})_0$) as a function of dielectric constant (ε_m) and b) selectivity with respect to 2-CP ($S_{2\text{-CP}}$) as a function of 2,4-DCP conversion ($X_{2,4\text{-DCP}}$) for reaction in water+methanol (I,◇), water+ethanol (II,□), water+*n*-propanol (III,△) and water+THF (IV,○). Note: dotted line connects the data for reaction in a single component solvent: water (+); methanol (◆); ethanol (■); *n*-propanol (▲); THF (●).

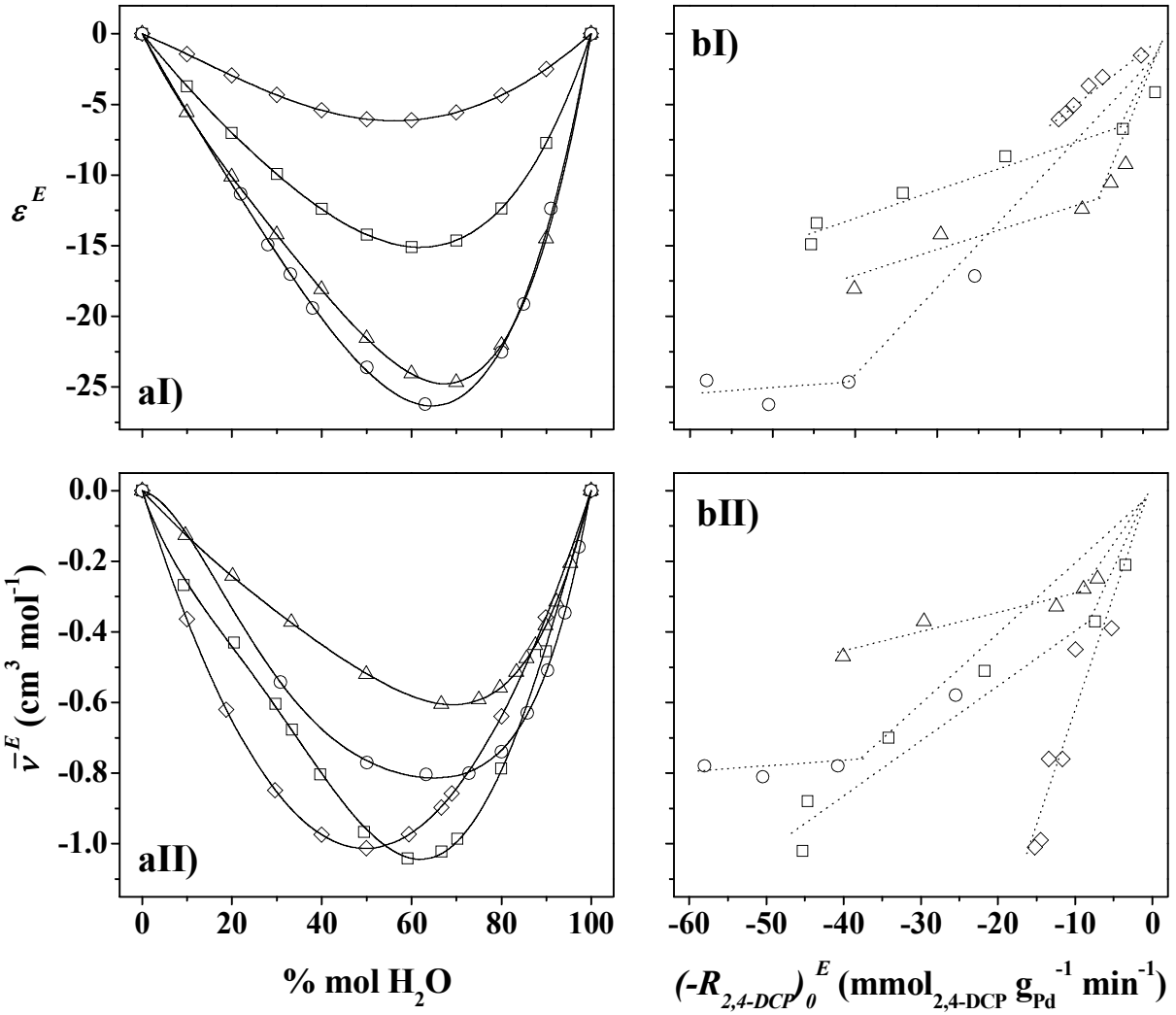

Figure 3.7: a) Variation of the excess dielectric constant (ε^E,I) and excess molar volume ($\bar{v}^E$,II) of the reaction media with water content (% mol H_2O) for water+methanol (◇), water+ethanol (□), water+*n*-propanol (△) and water+THF (○) mixtures. b) Relationship of the excess initial 2,4-DCP consumption rate ($(-R_{2,4\text{-}DCP})_0^E$, see eqn. (3.18)) with ε^E (I) and $\bar{v}^E$ (II) for the same solvent mixtures.

Indeed, there is evidence in the literature demonstrating that, when mixing water with alcohols [54-56] or THF [57], a reorganization of the overall solution structure occurs forming cooperative domains or clusters, where water accommodates the hydrophilic/hydrophobic organic components *via* H-bonding/physical interactions [54,58]. The continuous formation/destruction of these domains (known as *relaxation*) ultimately results in an excess of the thermodynamic properties (including ε and $\overline{v}$) in the mixture, *i.e.* the actual values of these properties differ from those predicted on the basis of an ideal mixing rule (as assumed when using eqn **(3.17)**) [59]. To assess the possible contribution of such an effect in our measurements, the excess dielectric constants (ε^E) and molar volumes ($\overline{v}^E$) were estimated by drawing on reference data [60-63]. These values were then correlated to the (negative) excess in initial 2,4-DCP consumption rate ($(-R_{2,4\text{-}DCP})_0^E$, see **Figure 3.6**aII), as defined by

$$\left(-R_{2,4\text{-}DCP}\right)_0^E = \left(-R_{2,4\text{-}DCP}\right)_0 - \left(-R_{2,4\text{-}DCP}\right)_0^{Predicted} \qquad \textbf{(3.18)}$$

The variation in ε^E and $\overline{v}^E$ with water content in the mixture is presented in **Figure 3.7**aI and **3.7**aII, while the impact on $(-R_{2,4\text{-}DCP})_0^E$ is shown in **Figure 3.7**bI and **3.7**bII, respectively. The occurrence of a minimum for both ε^E and $\overline{v}^E$ is well documented in the literature [58,59,64,65] for water+organic mixtures that facilitate H-bonding and is related to the formation of cooperative domains. In aqueous solutions, water molecules are arranged in tetrahedral clusters maintaining high void volumes [59,64]. If an even number of organic molecules is introduced, water forms semiclathrate-like structures within which the organic rotates freely [58,65]. As a direct consequence, part of the void volume is lost (due to a contraction in the overall water network/structure) leading to negative values of $\overline{v}^E$ and, at the same time, the number of effective dipoles decreases resulting in a negative ε^E [64,66]. It follows that the position and extent of the minima (in terms of % mol water) are dependent on the nature of the organic component, where the lowest $\overline{v}^E$ (**Figure 3.7**aII) occurs at higher water contents when increasing the alcohol chain length (methanol → *n*-propanol). Moreover, such a loss in the reaction medium structure and polarity seems to be directly related to the lower HDC activity, as can be inferred from **Figure 3.7**b, where the magnitude of $(-R_{2,4\text{-}DCP})_0^E$ is larger for mixture composition displaying larger ε^E and/or $\overline{v}^E$ values.

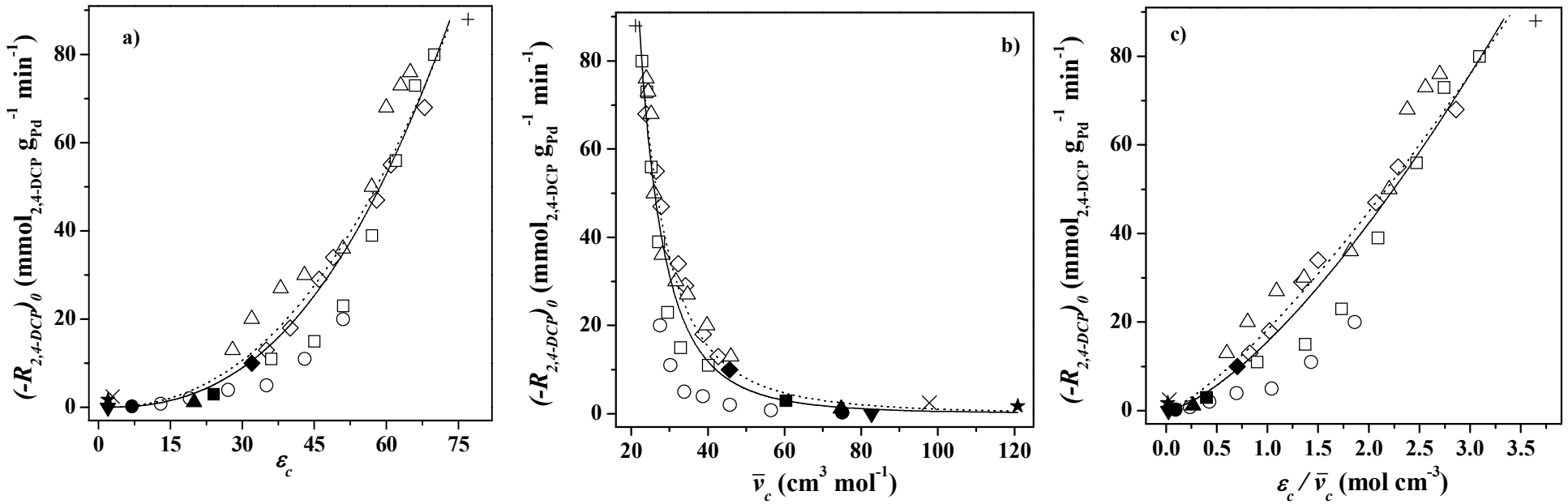

Figure 3.8. Initial 2,4-DCP consumption rate ($(-R_{2,4\text{-DCP}})_0$) as a function of (a) the corrected dielectric constant of the solvent (ε_c), (b) the corrected molar volume of the solvent ($\bar{v}_c$) and (c) the ratio of both properties ($\varepsilon_c/\bar{v}_c$) for single component (water (+), methanol (◆), ethanol (■), *n*-propanol (▲), THF (●), benzene (▼), cyclohexane (×) and *n*-hexane (★)) and binary water+organic mixtures (water+methanol (◇), water+ethanol (□), water+*n*-propanol (△) and water+THF (○)). Note: lines represent fits for all solvents including (dotted line) and excluding (solid line) water+THF mixtures according to eqns. (3.13 - 3.15).

These results suggest that, to achieve an optimum HDC rate in water+organic mixtures, the choice of water content must be made with a consideration that the composite ε and $\overline{v}$ values will be lower than those predicted from an ideal mixing rule. In order to assess the possible impact of the use of solvent mixtures on Ψ (the fractional contribution of ε to HDC rate), a corrected dielectric constant (ε_c) was calculated according to

$$\varepsilon_c = \varepsilon_m + \varepsilon^E \qquad \textbf{(3.19)}$$

and plotted against the experimentally determined $(-R_{2,4\text{-}DCP})_0$ in **Figure 3.8**a, which also includes data for the single component solvents with fitting to eqn **(3.13)**. The same approach was also taken for an estimation of the corrected molar volume ($\overline{v}_c$, **Figure 3.8**b, fitted to eqn **(3.14)**) and $\varepsilon_c/\overline{v}_c$ (**Figure 3.8**c, fitted to eqn **(3.15)**). A visual inspection of the three graphs serves to establish the validity of our approach, where all the experimental data for single component and solvent mixtures are consistent with increasing HDC rate with increasing/decreasing $\varepsilon_c/\overline{v}_c$; the relevant fitting parameters are given in **Table 3.2**. It should be noted that water+THF mixtures deviate somewhat from the general trend, possibly a result of steric effects in the case of the bulky THF. Data fitting that included and excluded the water+THF dataset delivered high R^2 values, demonstrating again goodness of fit for all the systems (including water+THF). This is significant, considering the possible secondary source of error associated with the ε^E and $\overline{v}^E$ values taken from the literature. The extracted (applying eqn **(3.16)**) values of Ψ yielded an (average) value of 0.806 ± 0.006, which is essentially the same to that obtained for HDC in single component solvent media and establishes that the critical solution property controlling HDC rate is the extent of solvent-solute interaction. This study represents a novel systematic approach to examining solvent effects associated with liquid phase catalytic HDC, where higher rates were consistently obtained with reaction media characterised by higher ε, where $\overline{v}$ plays a secondary role. This analysis is valid for both single component and binary solvent mixtures. In the latter case, the composition must be chosen considering that the actual values of ε for the mixture will be lower due to *relaxation* effects. These findings warrant further study to establish the generic features of this approach when dealing with solvent effects in liquid phase heterogeneous catalysis.

3.4 Conclusions

The results in this Chapter have provided, for the first time, a comprehensive quantitative analysis of solvent effects in the liquid phase (P = 1 atm; T = 303 K) HDC of 2,4-DCP over Pd/Al_2O_3 using water, methanol, ethanol, *n*-propanol, THF, benzene, cyclohexane and *n*-hexane as reaction media. Reaction conditions have been established where catalytic HDC was conducted under chemical/kinetic control, free from mass transport and diffusion constraints. In the absence of secondary reactions and negligible catalyst deactivation, 2-CP and PhOH were generated as products of partial and complete HDC *via* a stepwise electrophilic mechanism. While reaction selectivity was insensitive to the nature of the solvent, the initial 2,4-DCP consumption rate increased in the order: benzene < THF < *n*-hexane < cyclohexane < alcohols < water. Higher HDC rates were obtained in solvents with higher dielectric constants (ε = 2 - 77) and/or lower molar volumes ($\bar{v}$ = 20 - 120 cm^3 mol^{-1}). The analysis of HDC kinetics has revealed that the major (*ca.* 80 %) contribution to the observed HDC rate variation is ε. This response is attributed to stronger ionic forces (at higher ε) that serve to stabilize the electropositive arenium intermediate and this contribution is more important than the actual number of molecules available for solvation. This effect extends to reaction in water+alcohol and water+THF mixtures. The results establish (quantitatively) the solvent effects associated with the catalytic hydrotreatment of 2,4-DCP and the presented treatment represents a new approach to studying the role of solvent in liquid phase hydrogenolysis reactions.

3.5 References

[3.1] K. Pirkanniemi, M. Sillanpää, Chemosphere, 48, 1047 (2002)

[3.2] F. J. Urbano, J. M. Marinas, J. Mol. Catal. A: Chemical, 173, 329 (2001)

[3.3] L. M. Gómez-Sainero, X. L. Seoane, J. L. G. Fierro, A. Arcoya, J. Catal., 209, 279 (2002)

[3.4] M. A. Aramendia, V. Boráu, I. M. García, C. Jiménez, F. Lafont, A. Marinas, J. M. Marinas, F. J. Urbano, J. Catal., 187, 392 (1999)

[3.5] M. L. Toebes, J. A. Dillen, K. P. de Jong, J. Mol. Catal. A: Chemical, 173, 75 (2001)

[3.6] Y. Mitoma, N. Tasaka, M. Takase, T. Masuda, H. Tashiro, N. Egashira, T. Oki, Environ. Sci. Technol., 40, 1849 (2006)

[3.7] G. Evdokimova, S. Zinovyev, A. Perosa, P. Tundo, Appl. Catal. A: General, 271, 129 (2004)

[3.8] L. Lassová, H. K. Lee, T. S. A. Hor, J. Mol. Catal. A: Chemical, 144, 397 (1999)

[3.9] N. C. Concibido, T. Okuda, W. Nishijima, M. Okada, React. Kinet. Catal. Lett., 89, 369 (2006)

[3.10] Y. Monguchi, A. Kume, K. Hattori, T. Maegawa, H. Sajiki, Tetrahedron, 62, 7926 (2006)

[3.11] J. L. Benítez, G. del Angel, React. Kinet. Catal. Lett., 66, 13 (1999)

[3.12] C. Xia, J. Xu, W. Wu, X. Liang, Catal. Commun., 5, 383 (2004)

[3.13] H.-Y. Wee, J. A. Cunningham, J. Hazard. Mater., 155, 1 (2008)

[3.14] T. Hara, T. Kaneta, K. Mori, T. Mitsudome, T. Mizugaki, K. Ebitani, K. Kaneda, Green Chem., 9, 1246 (2008)

[3.15] N. C. Concibido, T. Okuda, Y. Nakano, W. Nishijima, M. Okada, Tetrahedron Lett., 46, 3613 (2005)

[3.16] N. C. Concibido, T. Okuda, W. Nishijima, M. Okada, React. Kinet. Catal. Lett., 90, 127 (2007)

[3.17] N. C. Concibido, T. Okuda, W. Nishijima, M. Okada, Appl. Catal. B: Environmental, 71, 64 (2007)

[3.18] Y. Ukisu, T. Miyadera, React. Kinet. Catal. Lett., 89, 341 (2006)

[3.19] W. Nishijima, Y. Ochi, T.-Y. Tsai, Y. Nakano, M. Okada, Appl. Catal. B: Environmental, 51, 135 (2004)

[3.20] P. P. Cellier, J.-F. Spindler, M. Taillefer, H.-J. Cristau, Tetrahedron Lett., 44, 7191 (2003)

[3.21] J.-W. Bae, E.-J. Jang, D.-H. Jo, J.-S. Lee, K.-H. Lee, J. Mol. Catal. A: Chemical, 206, 225 (2003)

[3.22] Y. Ukisu, T. Miyadera, J. Mol. Catal. A: Chemical, 125, 135 (1997)

[3.23] D. Stoye, Ullmann's Encyclopedia of Industrial Chemistry. "Solvents", Wiley-VCH Verlag GmbH & Co. KGaA, Weinheim, 2005.

[3.24] V. de Jong, R. Louw, Appl. Catal. A: General, 271, 153 (2004)

[3.25] Y. Ukisu, T. Miyadera, Appl. Catal. B: Environmental, 40, 141 (2003)

[3.26] V. A. Yakovlev, V. V. Terskikh, V. I. Simagina, V. A. Likholobov, J. Mol. Catal. A: Chemical, 153, 231 (2000)

[3.27] F.-D. Kopinke, K. Mackenzie, R. Koehler, A. Georgi, Appl. Catal. A: General, 271, 119 (2004)

[3.28] Y. Ukisu, Appl. Catal. A: General, 349, 229 (2008)

[3.29] W. D. Marshall, A. Kubátová, A. J. M. Lagadec, D. J. Miller, S. B. Hawthorne, Green Chem., 4, 17 (2002)

[3.30] D. R. Lide, Handbook of Chemistry and Physics, 90th ed., Taylor and Francis Group, Boca Raton, 2009.

[3.31] C. Xia, J. Xu, W. Wu, Q. Luo, J. Chen, Q. Zhang, X. Liang, Appl. Catal. B: Environmental, 45, 281 (2003)

[3.32] K. Mackenzie, H. Frenzel, F.-D. Kopinke, Appl. Catal. B: Environmental, 63, 161 (2006)

[3.33] G. Yuan, M. A. Keane, Ind. Eng. Chem. Res., 46, 705 (2007)

[3.34] D. Dollimore, G.R. Heal, J. Colloid Interface Sci., 33, 508 (1970)

[3.35] C. Amorim, M. A. Keane, J. Colloid Interface Sci., 322, 196 (2008)

[3.36] G. Yuan, M. A. Keane, Chem. Eng. Sci., 58, 257 (2003)

[3.37] S. Gómez-Quero, F. Cárdenas-Lizana, M. A. Keane, Ind. Eng. Chem. Res., 47, 6841 (2008)

[3.38] Y. Shindler, Y. Matatov-Meytal, M. Sheintuch, Ind. Eng. Chem. Res., 40, 3301 (2001)

[3.39] S. Storsæter, B. Tøtdal, J. C. Walmsley, B. S. Tanem, A. Holmen, J. Catal., 236, 139 (2005)

[3.40] J. Sanchez-Valente, X. Bokhimi, J. A. Toledo, Appl. Catal. A: General, 264, 175 (2004)

[3.41] M. Trueba, S. P. Trasatti, Eur. J. Inorg. Chem., 17, 3393 (2005)

[3.42] L. Shena, Z. Chen, Chem. Eng. Sci., 62, 3748 (2007)

[3.43] U. J. Jáuregui-Haza, E. J. Pardillo-Fontdevila, A. M. Wilhelm, H. Delmas, Lat. Am. Appl. Res., 34, 71 (2004)

[3.44] L. C. Yen, J. J. McKetta, AIChE J., 8, 501 (1962)

[3.45] J. M. Prausnitz, F. H. Shair, AIChE J., 7, 682 (1961)

[3.46] N. O. Lemcoff, J. Catal., 46, 356 (1977)

[3.47] K. M. Watson, Ind. Eng. Chem., 35, 398 (1943)

[3.48] S. Mukherjee, M. A. Vannice, J. Catal., 243, 108 (2006)

[3.49] R. P. Danner, T. E. Daubert, Manual for Predicting Chemical Process Design Data, Design Institute for Physical Property Data, New York, 1983.

[3.50] C. J. King, L. Hsueh, K.-W. Mao, J. Chem. Eng. Data, 10, 348 (1965)

[3.51] J. M. Smith, Chemical Engineering Kinetics, McGraw-Hill, Singapore, 1981.

[3.52] M. A. Keane, Appl. Catal. A: General, 271, 109 (2004)

[3.53] F. Alonso, I. P. Beletskaya, M. Yus, Chem. Rev., 102, 4009 (2002)

[3.54] R. J. Sengwa, M. Abhilasha, J. Mol. Liq., 123, 92 (2006)

[3.55] A. Jouyban, S. Soltanpour, H.-K. Chan, Int. J. Pharm., 269, 353 (2004)

[3.56] T. Sato, A. Chiba, R. Nozaki, J. Chem. Phys., 110, 2508 (1999)

[3.57] F. Goffredi, M. Goffredi, V. T. Liveri, J. Solution Chem., 24, 813 (1995)

[3.58] S. Sudo, N. Shinyashiki, Y. Kitsuki, S. Yagihara, J. Phys. Chem. A, 106, 458 (2002)

[3.59] T. Sato, A. Chiba, R. Nozaki, J. Mol. Liq., 96-97, 327 (2002)

[3.60] R. L. Smith, S. B. Lee, H. Komori, K. Arai, Fluid Phase Equilib., 144, 315 (1998)

[3.61] J. V. Herráez, R. Belda, J. Solution Chem., 35, 1315 (2006)

[3.62] J. N. Nayak, M. I. Aralaguppi, B. V. K. Naidu, T. M. Aminabhavi, J. Chem. Eng. Data, 49, 468 (2004)

[3.63] A. Chaudhari, P. Khirade, R. Singh, S. N. Helambe, N. K. Narain, S. C. Mehrotra, J. Mol. Liq., 82, 245 (1999)

[3.64] R. J. Sengwa, Madhvi, S. Sankhla, S. Sharma, J. Solution Chem., 35, 1037 (2006)

[3.65] W. Marczak, M. Spurek, J. Solution Chem., 33, 99 (2004)

[3.66] V. P. Pawar, S. C. Mehrotra, J. Mol. Liq., 115, 17 (2004)

Chapter 4

Solvent Effects in the Catalytic Hydrotreatment of Haloaromatics over Pd/Al_2O_3 in Water+Organic Mixtures

In the previous Chapter, solvent effects associated with the hydrodechlorination of 2,4-dichlorophenol were established and a novel, systematic approach served to quantify the contribution of dielectric constant and molar volume to variations in hydrodechlorination rate. That work is extended in this Chapter with a demonstration of generic solvent effects for the hydrodehalogenation of a range of brominated and chlorinated aromatics.

4.1 Introduction

Catalytic hydrodehalogenation (HDH) has emerged as a viable approach to the treatment of toxic halogenated waste [1,2], where halogen removal in aromatic systems has been found to be dependent on the nature [3,4], number [5,6] and position [7,8] of the substituent(s). The scission of C–Cl [6,9-12] and C–Br [13-17] bonds has now been promoted using Fe [6,16], Ni [9,13], Pt [10,14] and Pd [11,12,15,17] catalysts, where the latter has been demonstrated to be the most efficient in terms of specific rate and resistance to deactivation [18,19]. It is established that catalytic HDH is influenced by the nature of the catalyst support [14,20], metal dispersion [15,21] and use of additives [13,22]. Nevertheless, the possible role of the solvent still remains unresolved and the author could not find any study in the open literature dealing with solvent effects in hydrodebromination applications. With regard to hydrodechlorination, the reaction medium has been claimed to influence reaction rate [23-25] and product distribution [25,26], where water [24,26] and methanol [23,25] have been the most commonly used solvents. The apparent activity/selectivity solvent dependence may be masked by the occurrence of (i) secondary reactions [27,28], (ii) catalyst deactivation [23,29] and (iii) mass-transfer constraints [30-32]. In the previous Chapter, the liquid phase conversion of 2,4-dichlorophenol in various solvents over Pd/Al_2O_3 was studied, where reaction rate showed a dependence on solvent dielectric constant [33].

This Chapter represents an extension to that work where it is set out to establish generic features of solvent dependency in the catalytic dehalogenation of both chlorinated and brominated aromatics. In liquid phase catalytic transformations, hydrodebromination has been generally found to proceed at higher rates than hydrodechlorination [34,35]. Indeed, Aramendia and co-workers [36] considered the aqueous phase HDH of 4-chlorobromobenzene over $Pd/AlPO_4$-SiO_2 and isolated chlorobenzene as the only product, *i.e.* C–Br bond cleavage was preferred. Zinovyev *et al.* [11] recorded a higher HDH rate for bromobenzene when compared with chlorobenzene (7.2×10^{-3} *vs.* 8.8×10^{-3}, mol dm^{-3} min^{-1}) for reaction in methanol over Pd/C, which they attributed to differences in reactant/catalyst interaction. It should be noted that the opposite trend, *i.e.* higher HDH rates for chlorinated aromatics, has also been reported [37,38] in gas phase operation and linked to the lower electron affinity of Br compared with Cl that results in less effective activation on the catalyst surface [39,40]. In this study, the catalytic action of Pd/Al_2O_3 is monitored to promote the HDH of a range of halogenated (benzene and PhOH) reactants in water+organic mixtures and account quantitatively for the observed dependence of rate on solvent composition.

4.2 Materials and Methods

4.2.1 Materials

The reactants (2-chlorophenol (2-CP, +99%), 3-CP (98%), 4-CP (+99%), 2,3-dichlorophenol (2,3-DCP, 98%), 2,4-DCP (99%), 2,5-DCP (+98%), 2,6-DCP (99%), 3,4-DCP (99%), 3,5-DCP (97%), 2-bromophenol (2-BP, 98%), 3-BP (98%), 4-BP (99%), 2,4-DBP (95%), chlorobenzene (CB, 99.9%) and 1,3-DCB (+99%)) and the organic solvents (methanol (+99.9%) and THF (99.9%)) were obtained from Aldrich and used as received. All gases used in this study (H_2 and He) were of ultra high purity (> 99.99 %, BOC). The catalyst as supplied (1.2 % w/w Pd/Al_2O_3, Aldrich) was sieved (ATM fine test sieves) into batches of 38 μm average particle diameter.

4.2.2 Catalyst Characterization

BET surface area and pore volume measurements were performed using the commercial Micromeritics Flowsorb II 2300 unit.

Prior to analysis, the samples were outgassed at 423 K for 1 h in 20 cm^3 min^{-1} dry N_2. BET area was obtained in 30 % v/v N_2/He (20 cm^3 min^{-1}) with at least three cycles of N_2 adsorption/desorption using the standard single-point BET method; total pore volume was obtained at a relative pressure of P/P_0 = 0.95. The BET areas and pore volume values were reproducible to within ± 4 % and the values quoted in this study are the mean. Catalyst reducibility was assessed by temperature programmed reduction (TPR) using the CHEM-BET 3000 (Quantachrome Instruments) unit. The samples were loaded into a U-shaped (100 × 3.76 mm) Pyrex cell, contacted with 5 % v/v H_2/N_2 (17 cm^3 min^{-1}, Brooks mass flow controlled) and subjected to TPR to 423 K (2 K min^{-1}). The effluent gas was directed through a liquid N_2 trap and H_2 consumption/release was monitored by a thermal conductivity detector with data acquisition and manipulation using the TPR Win™ software. Bulk catalyst structure was evaluated by X-ray diffraction (XRD) analysis, using a Bruker/Siemens D500 incident X-ray diffractometer with Cu Kα radiation. The samples were scanned at 0.02º $step^{-1}$ over the range 20º ≤ 2θ ≤ 90º (scan time = 5 s $step^{-1}$) and the diffractogram patterns were compared with the JCPDS-ICDD references for comparative purposes (Card No. 10-0425 (γ-Al_2O_3) and 05-0681 (Pd)). Metal particle size was determined by transmission electron microscopy (TEM) analysis: JEOL JEM 2011 TEM unit with a UTW energy-dispersive X-ray detector (Oxford Instruments) operated at an accelerating voltage of 200 kV and using Gatan DigitalMicrograph 3.4 for data acquisition/manipulation. The samples were dispersed in acetone and deposited on a holey-carbon/Cu grid (300 Mesh). At least 650 individual Pd particles were counted where the Pd particle size (d_{TEM}) quoted in this paper is the surface area-weighted mean

$$d_{TEM} = \frac{\sum_i n_i d_i^3}{\sum_i n_i d_i^2} \qquad \textbf{(4.1)}$$

where n_i is the number of particles of diameter d_i.

4.2.3 Catalytic Procedure

The liquid phase HDH reactions were carried out in a modified, commercial glass reactor (Ken Kimble Reactors Ltd.), equipped with a constant H_2 supply (150 cm^3 min^{-1}, Brooks mass flow-controlled) and a glass impeller (1100 rpm).

A water-recirculating bath (Julabo HD-4) was used to stabilize the reaction temperature at T = 303 ± 1 K, where loss of the reactor liquid contents in the H_2 flow was negligible (< 0.5 % v/v). At the beginning of each experiment, the catalyst and 100 cm^3 of the reactant stock solution were charged and agitated in a He flow (50 cm^3 min^{-1}) while the temperature was allowed to stabilize (15 min); H_2 flow was then introduced (time t = 0 for reaction). The catalyst and organic halogen concentrations were fixed to give a constant halogen/Pd ratio = 900 mol_X mol_{Pd}^{-1}. As blank tests, experiments carried out in the absence of H_2 or over the support alone did not result in any detectable conversion. A non-invasive liquid sampling *via* syringe and in-line filters allowed a controlled removal of aliquots (< 0.5 cm^3) from the reactor. The composition of the reactor liquor was analyzed by gas chromatography using a Perkin-Elmer Auto System XL GC, equipped with an FID and a DB-1 capillary column (J&W Scientific: i.d. = 0.2 mm, length = 50 m, film thickness = 0.33 μm). The reactant and product(s) concentrations in the bulk liquid phase were determined from the total molar balance in the reaction mixture, where the effect of uptake on the support was negligible [41,42]. Taking 2,4-DCP as a representative reactant, the fractional conversion ($X_{2,4\text{-}DCP}$) is defined as

$$X_{2,4\text{-}DCP} = \frac{C_{2,4\text{-}DCP,0} - C_{2,4\text{-}DCP}}{C_{2,4\text{-}DCP,0}} \tag{4.2}$$

where $C_{2,4\text{-}DCP,0}$ and $C_{2,4\text{-}DCP}$ represent the initial concentration of 2,4-DCP and the value at time t, respectively. The fractional selectivity with respect to, for example, 2-CP ($S_{2\text{-}CP}$) is given by

$$S_{2\text{-}CP} = \frac{C_{2\text{-}CP}}{C_{2,4\text{-}DCP,0} - C_{2,4\text{-}DCP}} \tag{4.3}$$

The efficiency of halogen removal is quantified in this study by the fractional degree of dehalogenation (x_X) as determined by

$$x_X = \frac{C_{HX}}{C_X} \tag{4.4}$$

where C_X and C_{HX} are the halogen concentrations associated with the organic reactant and inorganic product, respectively. Repeated reactions with different samples of catalyst/reactant stock solution delivered raw data reproducibility that was better than ± 7 %.

4.3 Results and Discussion

4.3.1 Catalyst Characterization

The total surface area, pore volume, bulk density, porosity and tortuosity values that characterise the Pd/Al_2O_3 catalyst are given in **Table 4.1**.

Table 4.1: Characteristics of the Pd/Al_2O_3 catalyst.

Pd loading (% wt.)	1.2
d_{TEM} (nm)	2.4
Catalyst particle size (μm)	38
ρ (kg m^{-3})	1154
BET Area (m^2 g^{-1})	160
Pore Volume (cm^3 g^{-1})	0.56
Porosity	0.65
Tortuosity	1.54

The BET area (160 m^2 g^{-1}) is within the range (150 - 250 m^2 g^{-1}) of values reported for γ-Al_2O_3 [43]. The porosity characteristics suggest that the HDH reactions should not be accompanied by any significant restrictions in terms of reactant/product diffusion in the interstitial fluid. Indeed, for tortuosity values close to unity, the average path traversed by species within the pores approaches that for diffusion in the bulk fluid [44]. Catalyst reducibility was assessed by TPR and the resultant profile is presented in **Figure 4.1**a. The profile is characterized by a single negative peak (H_2 release) at 355 K that is associated with the decomposition of β-phase Pd hydride formed by the absorption of H_2 in the Pd crystal lattice [5,45]. The absence of a positive peak (H_2 consumption) prior to hydride decomposition suggests the formation of zero-valent Pd at room temperature [46,47]. Reduction of the catalyst under reaction conditions (see dotted line in **Figure 4.1**a) results in Pd hydride formation which can contribute to HDH, as demonstrated elsewhere [45].

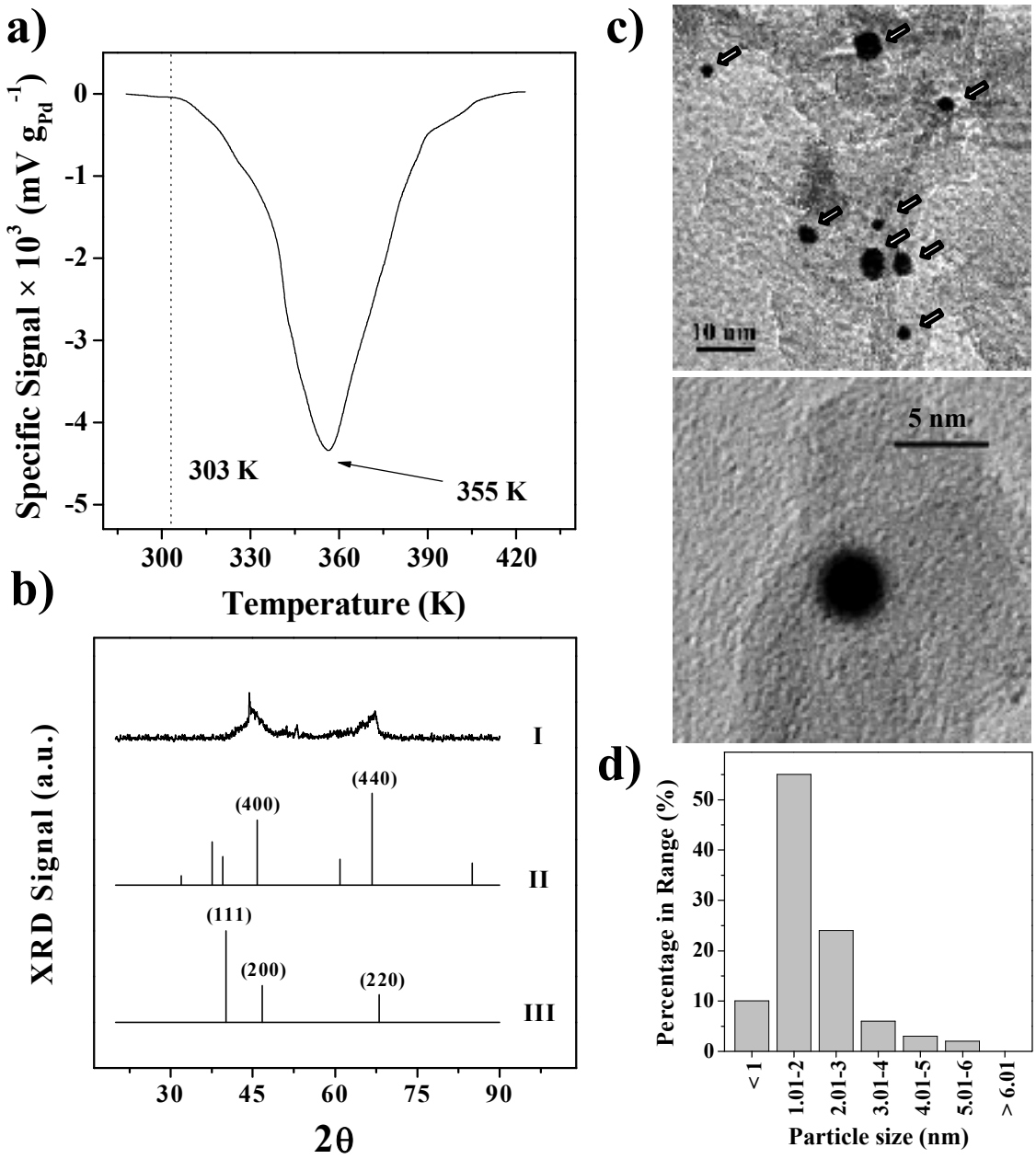

Figure 4.1: a) TPR profile for Pd/Al_2O_3 (dotted vertical line illustrates HDH reaction temperature); b) XRD diffractograms of (I) activated Pd/Al_2O_3 and JCPDS-ICDD reference for (II) γ-Al_2O_3 (Card No. 10-0425) and (III) Pd (Card No. 05-0681); c) Representative high magnification TEM images (individual Pd particles identified by arrows) and d) Pd particle size distribution associated with the activated Pd/Al_2O_3 catalyst.

The hydride stoichiometry (H_{ab}/Pd = 0.15 mol_H mol_{Pd}^{-1}) and associated decomposition temperature (355 K) differ significantly from that recorded [48,49] for bulk Pd, *i.e.* H_{ab}/Pd = 0.69 mol_H mol_{Pd}^{-1} and 384 K. This response is consistent with the presence of a well dispersed nano-scale Pd phase as it has been established that Pd hydride formation and decomposition are dependent on the metal particle size [50,51].

XRD analysis of the activated catalyst generated the diffractogram shown in **Figure 4.1**b (Profile I), characterised by two broad peaks at 2θ = 45.8º and 66.8º corresponding, respectively, to the (400) and (440) main planes associated with cubic γ-Al_2O_3 (JCPDS-ICDD Card No. 10-0425, Profile II). There were no detectable reflections due to Pd (JCPDS-ICDD Card No. 05-0681, Profile III), suggesting the presence of Pd as small ensembles with mean particle size below the XRD detection limit, *i.e.* < 3 - 5 nm [52,53]. Indeed, the representative high magnification TEM micrographs shown in **Figure 4.1**c demonstrate that Pd is present as small particles. The particle size distribution histogram is given in **Figure 4.1**d where it can be seen that all the particles were below 6 nm, with a significant component (65 %) ≤ 2 nm and a surface area-weighted mean particle size of 2.4 nm (**Table 4.1**).

4.3.2 Liquid Phase Catalytic HDH: Consideration of Transport Constraints

The liquid phase catalytic hydrotreatment of all reactants considered in this study was 100 % selective in terms of HDH with no evidence of aromatic ring reduction or hydrogenolytic cleavage of the –OH substituent. Consequently, our catalytic data are not compromised by secondary reactions and facilitate an explicit analysis of solvent effects. With regard to possible transport limitations associated with this three-phase slurry reactor, a full evaluation of transport effects has been given elsewhere [33,41] but details that are pertinent to this study are noted below:

(i) In the bulk fluid, transport constraints associated with the haloarene(s) can be discounted as each reactant is soluble at the concentrations used in this study (= 500 $mmol_{Cl}$ dm^{-3}, ≤ 10 $mmol_{Br}$ dm^{-3}). Regarding H_2 supply, it has been demonstrated previously the absence of H_2 transport limitations for reaction in water at the gas flow rate employed in here, *i.e.* 150 cm^3 min^{-1} [41]. This response extends to reaction in single component organic and water+organic solvent mixtures where the H_2 molar fractions (8×10^{-5} - 22×10^{-5}) exceed that in water (1×10^{-5}) [33].

(ii) Mass-transfer at the liquid/catalyst interface has been evaluated in terms of the Carberry (*Ca*) number which, assuming isothermal conditions, spherical catalyst particle morphology and the absence of concentration gradients, takes the form [54]:

$$Ca = \frac{\rho\, m_{Pd}\, d^2}{12\, C_i\, D_i} \times (R_{HDH})_0 \qquad \textbf{(4.5)}$$

where ρ and d are the bulk catalyst density and particle size, m_{Pd} represents the catalyst Pd loading (0.012 g_{Pd} g^{-1}), C_i and D_i are the bulk liquid concentration ($mmol_i$ dm^{-3}) and diffusivity (m^2 s^{-1}) of compound *i*, and $(R_{HDH})_0$ the initial HDH rate ($mmol_X$ g_{Pd}^{-1} min^{-1}). The diffusivity of H_2 was calculated using the Wilke-Chang method [55] and haloarene diffusivity estimations were dependent on the nature of the solvent and drew on the equations of Hayduk and Laudie [56] (for water) and King *et al.* [57] (for methanol and THF). The associated *Ca* values, varying from 4×10^{-5} (for H_2 in methanol) to 14×10^{-2} (for 2,3-DCP in water), were below the critical limiting value (0.15) [58] and indicate that the chemical/catalytic step is rate-determining.

(iii) Limitations in terms of internal diffusion were estimated by applying the Weisz-Prater number (Φ) criteria:

$$\Phi = \frac{(-R_i)_0\, \rho\, m_{Pd} \left(d/6\right)^2}{C_i\, D_{Eff,i}} \qquad \textbf{(4.6)}$$

where $D_{Eff,i}$ is the effective diffusivity, *i.e.* within the catalyst pores: $D_{Eff,i} = D_i \times (0.65)^2$ [59]. The calculated dimensionless values (≤ 1) confirm that the experimental reaction data were obtained under conditions of kinetic control.

In order to rule out any significant contribution due to deactivation, HDH activity is expressed in terms of initial rates where $x_X \leq 0.25$, an approach that has been successfully applied previously [20,49]. It can be concluded that the catalytic data in this study are free from transport limitations, catalyst deactivation or contributions due to secondary reactions.

4.3.3 Reaction in Methanol: Halophenol Reactivity

The temporal variation of fractional dehalogenation (x_X) is shown in **Figure 4.2** for the three chlorophenol isomers, where C–Cl bond cleavage generated phenol (PhOH) as product. Chlorophenol reactivity can be quantified by the application of pseudo-first order kinetics

$$x_X = \exp\left(k_X t\right) - 1 \tag{4.7}$$

which allows the estimation of k_X (dehalogenation rate constant) as fitting parameter (see lines in **Figure 4.2**).

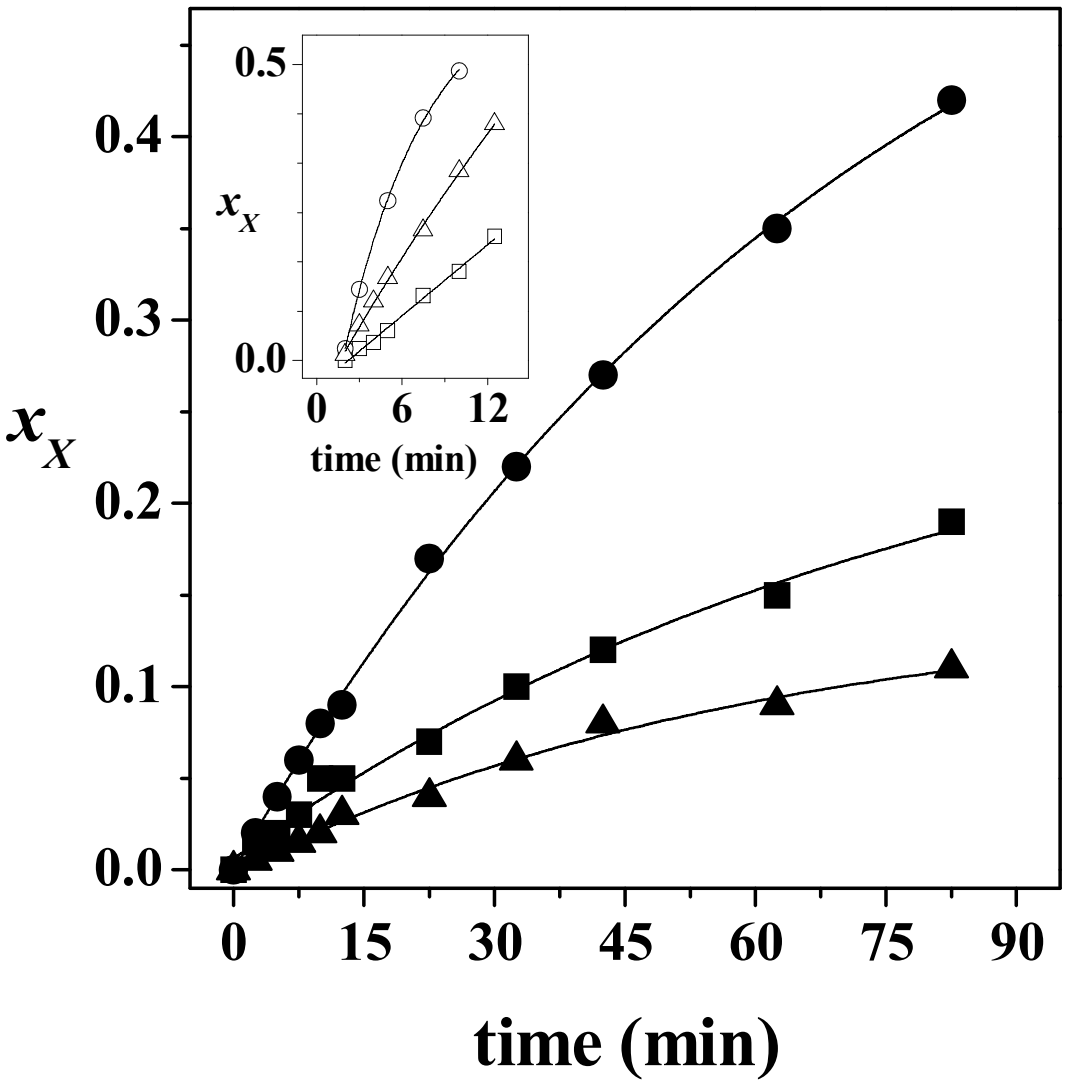

Figure 4.2: Temporal variation of the degree of dehalogenation (x_X) of 2-CP (■), 3-CP (●) and 4-CP (▲) in methanol. Inset: corresponding data for 2-BP (□), 3-BP (○) and 4-BP (△). Note: lines represent fit to eqn. (4.7) ($R^2 \geq 0.998$).

The initial HDH rate ($(R_{HDH})_0$, units: $mmol_X\ g_{Pd}^{-1}\ min^{-1}$) can be then estimated from

$$(R_{HDH})_0 = k_X \frac{C_{X,0}}{W_{Pd}} \quad \textbf{(4.8)}$$

where $C_{X,0}$ is the initial organic halogen concentration ($mmol_X\ dm^{-3}$) and W_{Pd} the Pd concentration ($g_{Pd}\ dm^{-3}$). The results are presented in **Table 4.2**, where the following order of increasing $(R_{HDH})_0$ is established: 4-CP < 2-CP < 3-CP.

Table 4.2: Initial HDH rate ($(R_{HDH})_0$, units: $mmol_X\ g_{Pd}^{-1}\ min^{-1}$) and fitting parameters ($R^2 \geq 0.954$) for solvent dependency (dielectric constant (b_ε), molar volume ($b_{\bar{v}}$) and both properties (b_T)) and fractional contribution of ε_c (Ψ) in the conversion of chloro- and bromo-phenols over Pd/Al_2O_3 in methanol and methanol+water.

Reactant	$(R_{HDH})_0$[a]	$(R_{HDH})_0$[b]	b_ε	$b_{\bar{v}}$	b_T	Ψ
Chlorophenols						
2-CP	37	129	1.66	-1.89	0.89	0.781
3-CP	68	135	1.03	-1.17	0.55	0.781
4-CP	23	124	2.19	-2.48	1.16	0.780
2,3-DCP	16	116	2.38	-2.70	1.27	0.780
2,4-DCP	10	83	2.48	-2.80	1.31	0.780
2,5-DCP	20	89	1.79	-2.06	0.96	0.784
2,6-DCP	21	86	1.90	-2.20	1.02	0.785
3,4-DCP	15	49	1.49	-1.70	0.79	0.781
3,5-DCP	2	16	3.24	-3.74	1.74	0.785
Bromophenols						
2-BP	152	241	0.61	-0.71	0.33	0.785
3-BP	372	647	0.76	-0.88	0.41	0.784
4-BP	248	335	0.39	-0.44	0.21	0.784
2,4-DBP	95	183	0.78	-0.90	0.42	0.785

[a]reaction in pure methanol.
[b]reaction in a 85 % mol water+methanol mixture.

There is now some consensus in the literature that HDH proceeds *via* the electrophilic hydrogen scission of the C–X bond with the formation of a cationic intermediate [60], which is dissociatively adsorbed forming a σ-complex through the carbon atom bearing the highest electron density [4,37].

Serguchev and Belokopytov [61], taking selected chlorobenzenes, calculated the electron densities at each carbon and demonstrated that the values were greater in the presence of ring substituents that were located *meta*- with respect to each other. This observation can account for the higher $(R_{HDH})_0$ recorded here for 3-CP. Moreover, this is also consistent with studies where aromatic chlorines with neighbouring electronegative substituents in the *meta*- position were preferentially removed [62,63]. The higher $(R_{HDH})_0$ for 2-CP when compared with 4-CP suggests that steric effects do not influence HDH activity, which must be governed by the inductive effect of the –OH substituent (by donation of the lone electron pair associated with oxygen to the aromatic ring). Therefore, the *ortho*- C–Cl bond, which is in closer proximity to the hydroxyl substituent, results more susceptible to attack than the *para*- counterpart. A direct comparison of our results with the literature is difficult, given the differences in reaction conditions, catalytic metal and support, where lower chlorine removals have been reported for 2-CP and attributed to steric hindrance [64-68]. It should, however, be noted that in the published studies HDH rate is quoted in terms of (a) halogen removal after a certain time [64,65] or (b) the time needed to achieve total conversion [66-68]. As reaction rate is a function of conversion and, moreover, catalyst deactivation is a feature of prolonged reaction times due to HCl poisoning, the reactivity trends reported in the literature may be compromised by a significant contribution due to deactivation. In contrast, we have chosen the initial ($x_X \leq 0.25$, see section **4.3.2**) HDH rate $(R_{HDH})_0$ as the index to evaluate intrinsic catalyst activity/selectivity and haloarene reactivity.

The HDH of dichlorophenols generated lower $(R_{HDH})_0$ relative to the mono-chlorinated reactants (see **Table 4.2**), a result that is consistent with an electrophilic mechanism where the presence of a second electron-withdrawing (chlorine) substituent has a deactivating effect [8,69]. Moreover, the sequence of decreasing HDH rate (2,6-DCP ≈ 2,5-DCP > 2,3-DCP ≈ 3,4-DCP > 2,4-DCP >> 3,5-DCP) suggests that reactivity is governed by the relative position of both chlorines on the ring. The –OH substituent acts as an electron donor rendering the aromatic ring more reactive to an electrophilic attack at the *ortho*- and *para*- position [70]. Halogens act inductively as electron-attractors but also show an *ortho*- and *para*- directing effect as a consequence of the three lone pair of electrons, which can participate in resonance [70,71]. It follows then that the electron density associated with the ring carbons in dichlorophenols depends on the relative position of the three substituents (–OH and two –Cl) so that electron delocalization effects govern dichlorophenol reactivity.

Hence, 3,5-DCP exhibits the lowest $(R_{HDH})_0$ because of fewer possible resonance structures (4) when compared to the other isomeric forms (between 6 and 11). The possible HDH reaction pathways are illustrated by the simplified scheme shown in **Figure 4.3**a where Cl removal from each DCP isomer can proceed *via* stepwise (k_1, k_2) and/or concerted (k_3) routes.

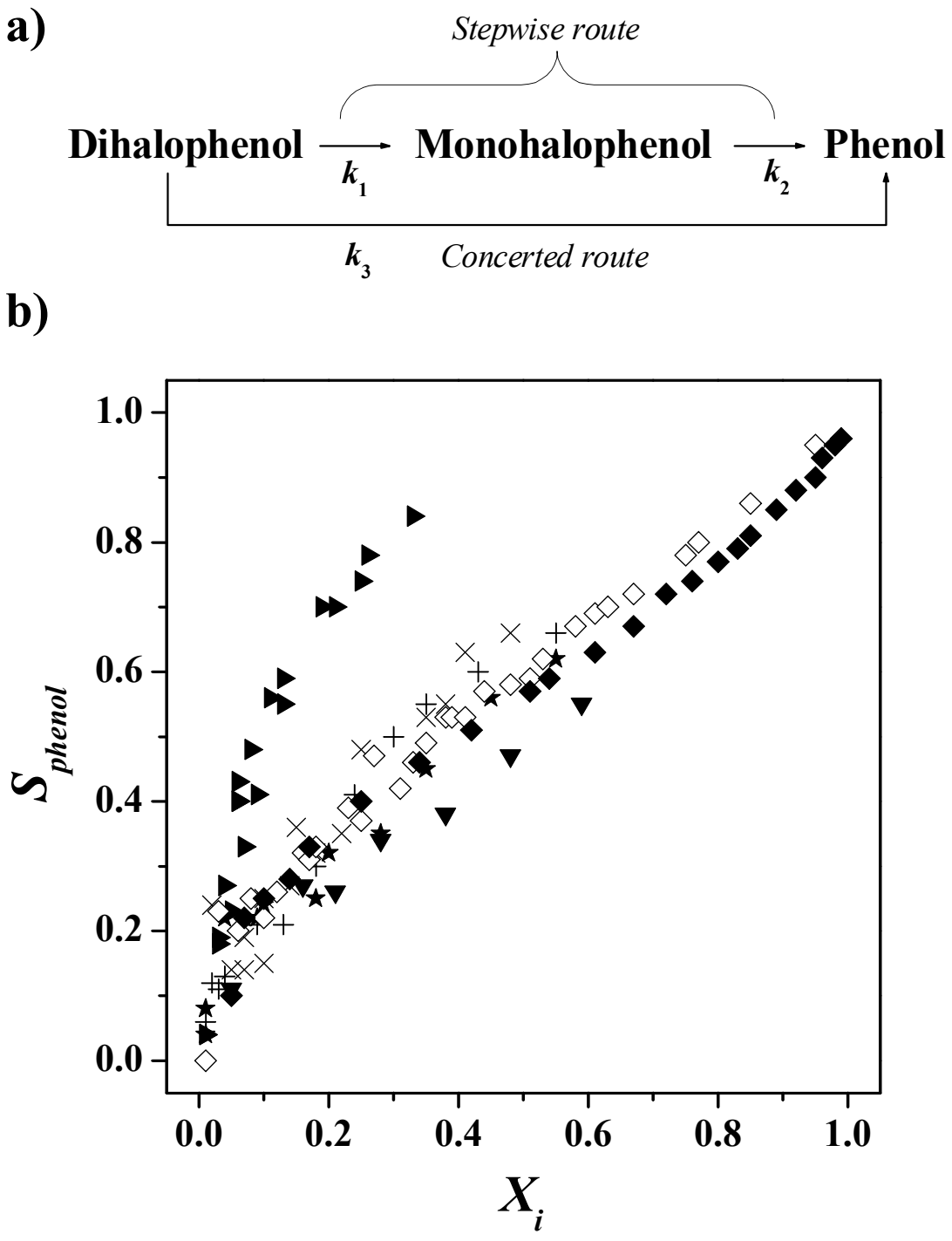

Figure 4.3: a) Simplified dihalophenol HDH mechanism and b) phenol selectivity (S_{phenol}) as a function of reactant conversion (X_i) for the HDH of 2,3-DCP (▼), 2,4-DCP (◆), 2,5-DCP (★), 2,6-DCP (×), 3,4-DCP (▶), 3,5-DCP (+) and 2,4-DBP (◇) in methanol.

At the same degree of conversion, the simultaneous cleavage of both C–Cl bonds leads to higher PhOH content in the product stream and higher dehalogenation efficiency. In the case of the DCP reactants, reaction selectivity was governed by steric effects where (i) 2-CP was systematically isolated from DCP reactants that bore an *ortho*- substituted Cl and (ii) 3-CP was generated from 3,4-DCP. Reaction pathway can be assessed from **Figure 4.3**b, where PhOH selectivity is shown as a function of conversion. In this plot, a data point trend line with a slope approaching unity is indicative of a preferentially stepwise mechanism, as is the case for all the isomers with the exception of 3,4-DCP, which consistently generated higher PhOH selectivity at each conversion. The relative contribution of stepwise (as opposed to concerted) HDH routes for each DCP isomer is best quantified by applying the following relationship [72]:

$$x_{monohalophenol} = \frac{L}{1-M} \times \left[\left(x_{dihalophenol} \right)^{M} - x_{dihalophenol} \right] \qquad \textbf{(4.9)}$$

where

$$L = \frac{k_1}{k_1 + k_3} \quad \therefore \quad M = \frac{k_2}{k_1 + k_3} \qquad \textbf{(4.10)}$$

and the ratio of stepwise to concerted routes (k_1/k_3) can be calculated by

$$\frac{k_1}{k_3} = \frac{1}{1/L - 1} \qquad \textbf{(4.11)}$$

The results of data fitting to eqn. **(4.9)** are presented in **Figure 4.4** (taking 2,4-DCP as representative reactant) and the k_1/k_3 ratios are given in **Table 4.3**. It can be seen that the relative contribution of both routes is dependent on the nature of the reactant isomer where a stepwise mechanism is prevalent for all the isomers with the exception of 3,4-DCP. There is little in the way of published studies of liquid phase dichlorophenol(s) HDC kinetics that have taken into consideration the reaction pathway. It is worth flagging the work of Wei *et al.* [73], who quoted a stepwise to concerted ratio of *ca.* 1.5 for the aqueous phase HDC of 2,4-DCP over (unsupported) Pd-Fe nanoparticles.

Moreover, Shin and Keane have established, for gas phase hydroprocessing of polychlorinated phenols, that the HDC mechanism was dependent on the number and position of the Cl substituents [74-76].

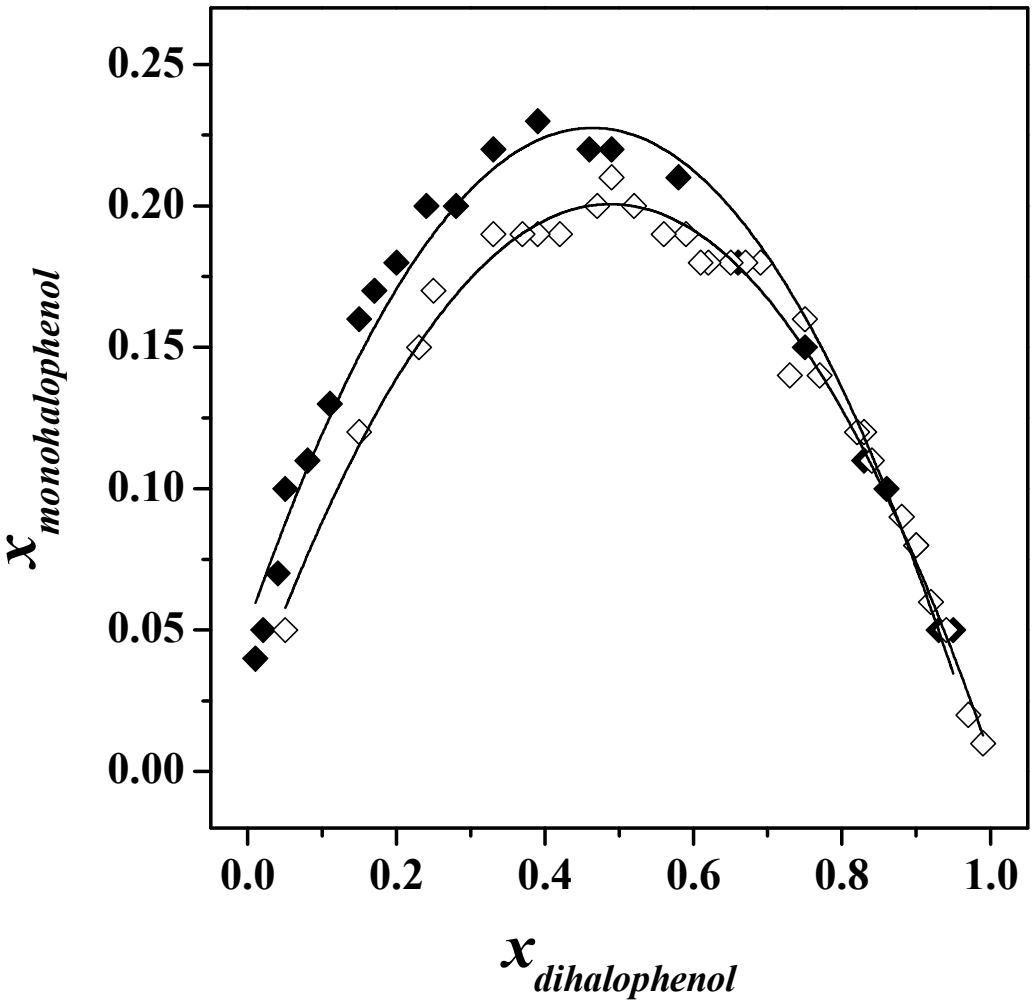

Figure 4.4: Monohalophenol molar fraction ($x_{monohalophenol}$) as a function of dihalophenol molar fraction ($x_{dihalophenol}$) in the HDH of 2,4-DCP (◆) and 2,4-DBP (◇). Note: solid lines represent fit to eqn. (4.9).

Table 4.3: Ratio of stepwise-to-concerted routes (k_1/k_3) in the HDH of dihalophenols over Pd/Al_2O_3 in methanol (see eqns. (4.9 – 4.11)).

Reactant	k_1/k_3
2,3-DCP	13.3
2,4-DCP	2.2
2,5-DCP	5.3
2,6-DCP	4.6
3,4-DCP	0.7
3,5-DCP	8.1
2,4-DBP	3.3

The temporal variation of fractional HDH (x_X) for the bromophenol isomers is shown as an inset to **Figure 4.2** and the extracted rates are given in **Table 4.2**. The $(R_{HDH})_0$ values were appreciably higher (by up to an order of magnitude) when compared with those obtained for chlorophenols. This response can be accounted for on the basis of the bond dissociation energies [77] for C–Cl (400 kJ mol^{-1}) and C–Br (336 kJ mol^{-1}), where the cleavage of the latter is more facile [78,79]. The sequence of increasing HDH rate (2-BP < 4-BP < 3-BP) is again consistent with a higher reactivity in the case of the *meta*- isomer, as established for the chlorinated counterpart. However, a contribution due to steric hindrance is in evidence where 2-BP delivered appreciably lower $(R_{HDH})_0$. Indeed, steric effects are to be expected in the case of bromophenols due to the greater covalent atomic radius of Br (0.121 nm) when compared with Cl (0.099 nm) [71]. It should be noted that Adimurthy *et al.* [80] isolated 2,6-DBP as the only product resulting from the HDH of 2,4,6-tribromophenol over Hβ-zeolite (in methanol) where steric hindrance impeded cleavage of the *ortho*- positioned Br substituents. The HDH of 2,4-DBP (chosen as a representative dibromophenol isomer) delivered an $(R_{HDH})_0$ that was significantly lower than that obtained for each BP reactant but higher than the equivalent 2,4-DCP. The former response can again be accounted for in terms of a deactivating effect due to the second electron withdrawing Br while the latter follows from the more facile hydrogenolytic C–Br bond cleavage. Moreover, PhOH selectivity variation with 2,4-DBP conversion (see **Figure 4.3**b) mirrored that observed for 2,4-DCP while the associated k_1/k_3 ratio (in **Table 4.3**) obtained from data fitting to eqn. **(4.9)** (see **Figure 4.4**) was also close to that recorded for the chlorinated reactant. The latter result suggests that the relative contribution of stepwise/concerted HDH pathways is governed by isomer structure rather than the nature of the halogen substituent, a response which has not been previously reported in the literature.

4.3.4 Solvent Effects in the HDH of Halophenols

Solvent effects were first established by studying the HDH of mono- substituted chlorophenols in methanol+water mixtures. The HDH rates in a representative mixture (85 % mol water) are given in **Table 4.2**, where higher $(R_{HDH})_0$ values (by a factor of up to 5) were obtained in the solvent mixture relative to reaction in methanol. These results are in line with studies in the literature where enhanced HDH rates in methanol+water mixtures with increasing water content have been noted [81-83].

This response has been attributed to a lesser catalyst deactivation as a result of increased solubility of HCl [81] and/or NaCl (formed during HCl neutralization with NaOH) [82,83], which facilitated their removal from the active surface. Nevertheless, Concibido *et al.* [26] recorded a decrease in the HDH rate of tetrachloroethylene over Pd/C at higher water contents (> 50 % mol) due to an irreversible adsorption of the reactant on the carbon support. The same rationale was given by Pozan and Boz [84] who observed a decrease in activity for the conversion of 2,3,5-trichlorophenol over Pd/C with increasing (0 % → 50 % v/v) water content. It should be noted that haloarene uptake on the γ-Al_2O_3 support was negligible in this study and the carbon balance was complete to within ± 5 %.

As HDH proceeds *via* an electrophilic mechanism, a dependence of $(R_{HDH})_0$ on the nature of the solvent can result from differences in the stabilization of the electropositive intermediate due to solute-solvent interactions. Indeed, the author has demonstrated previously ([33] and previous Chapter) that, in the HDH of 2,4-DCP, the critical solvent parameters governing rate are the solvent dielectric constant (ε_c) and molar volume ($\overline{v}_c$). These properties were estimated as follows:

$$\varepsilon_c = \left(\varepsilon_{methanol}\left(1 - x_{water}\right)\right) + \left(\varepsilon_{water}\, x_{water}\right) + \varepsilon^E \qquad \textbf{(4.12)}$$

$$\overline{v}_c = \left(\overline{v}_{methanol}\left(1 - x_{water}\right)\right) + \left(\overline{v}_{water}\, x_{water}\right) + \overline{v}^E \qquad \textbf{(4.13)}$$

where x_{water} is the molar fraction of water, $\varepsilon_{methanol}$ = 32, ε_{water} = 77, $\overline{v}_{methanol}$ = 46 cm^3 mol^{-1} and $\overline{v}_{water}$ = 21 cm^3 mol^{-1}. The ε^E and $\overline{v}^E$ parameters represent the excess properties, which serve to correct deviations associated with the methanol+water mixture from ideal behaviour and numerical values are available in the literature [85,86]. Indeed, when mixing water with alcohols, a reorganization of the overall solution structure occurs with the formation of clusters wherein water accommodates the hydrophilic/hydrophobic organic components *via* H-bonding/physical interactions [87-89]. The continuous formation/destruction of these clusters results in an excess of the thermodynamic properties (including ε_c and $\overline{v}_c$) in the mixture, *i.e.* actual values differ from those predicted on the basis of an ideal mixing rule [90,91].

The ε_c and $\overline{v}_c$ values that we have calculated can be taken as representative of the (thermodynamically) real methanol+water mixtures. The variation of $(R_{HDH})_0$ with ε_c and $\overline{v}_c$ is shown in **Figure 4.5**a and **4.5**b, respectively. The increase in $(R_{HDH})_0$ at higher ε_c can be linked to the increased strength in the ionic (coulomb) solvation forces, while the increase at lower $\overline{v}_c$ can be attributed to the greater number of solvent molecules (per unit volume) available to interact with the (charged) intermediate. Although there are instances in the literature [62,82,92] where HDH rate has been linked to higher ε_c, a quantification of this response is provided here for the first time. Moreover, the possible role of changes in $\overline{v}_c$ has not been considered in published HDH studies where the solvent has been varied. In order to provide an estimation of the relative contribution of both factors to $(R_{HDH})_0$, we have applied empirical relationships:

$$\ln[(R_{HDH})_0] = \ln[a_\varepsilon] + b_\varepsilon \ln[\varepsilon_c] \quad \textbf{(4.14)}$$

$$\ln[(R_{HDH})_0] = \ln[a_{\overline{v}}] + b_{\overline{v}} \ln[\overline{v}_c] \quad \textbf{(4.15)}$$

where a and b are fitting parameters. Considering the direct and inverse relation of $(R_{HDH})_0$ with ε_c and $\overline{v}_c$, respectively, it follows that:

$$\ln[(R_{HDH})_0] = \ln[a_T] + b_T \ln[\varepsilon_c / \overline{v}_c] \quad \textbf{(4.16)}$$

In this expression, b_T is a measure of the overall rate dependence on the reaction medium where, at $b_T = 0$, HDH would be free from solvent contributions and would proceed at $(R_{HDH})_0 = a_T$. It follows that:

$$b_T = b_\varepsilon \Psi + b_{\overline{v}} (1 - \Psi) \quad \textbf{(4.17)}$$

where Ψ represents the fractional contribution of ε_c to variations in $(R_{HDH})_0$. The applicability of eqn **(4.14 - 4.16)** to the HDH of chlorophenols is shown by the solid lines in **Figure 4.5** and the resultant fitting parameters are compiled in **Table 4.2**.

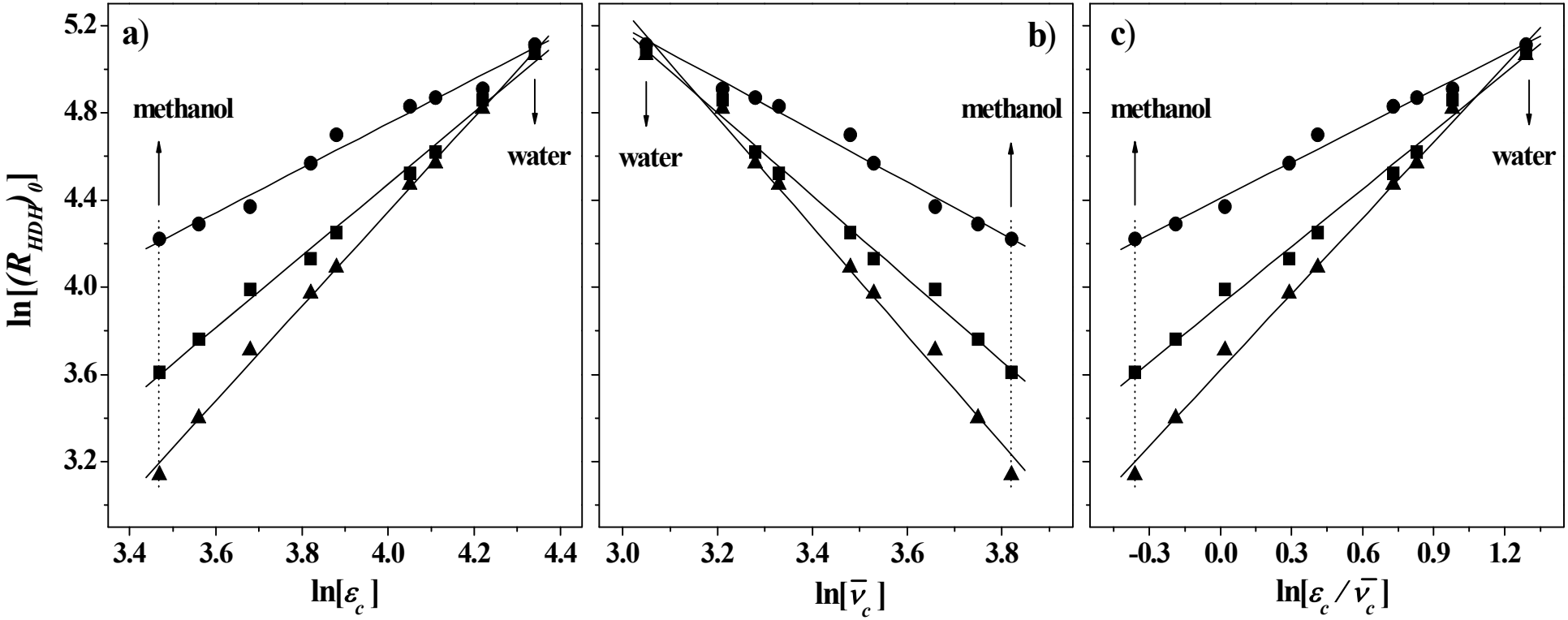

Figure 4.5: Linear dependence of the initial HDH rate ($(R_{HDH})_0$) of 2-CP (■), 3-CP (●) and 4-CP (▲) on the corrected (a) dielectric constant (ε_c), (b) molar volume ($\bar{v}_c$) and (c) ratio of both ($\varepsilon_c / \bar{v}_c$) in water+methanol mixtures. Note: lines represent fit to eqns. (4.14 - 4.16) and dotted lines illustrate abcissa position for pure methanol.

The order of increasing b_T values (3-CP < 2-CP < 4-CP) matches that of decreasing $(R_{HDH})_0$, a result which suggests a greater HDH rate dependence on solvent composition for the less reactive isomer. A striking finding of this study is that Ψ is essentially equivalent (= 0.781 ± 0.001) for the three chlorophenols. The (common) value for Ψ demonstrates that the strength of solute-solvent interactions (measured by ε_c) is more important than the actual number of solvent molecules participating in the solvation process (given by $\overline{v}_c$) and this is independent of the chlorophenol isomer.

Solvent effects were further investigated in the HDH of dichlorophenols and the results are presented in **Table 4.2** and **Figure 4.6**, where it can be seen that $(R_{HDH})_0$ was consistently higher with increasing water content in the solvent. It should be noted that although 2,5-, 2,6- and 3,5-DCP were not soluble in water alone, the model still applies to water+methanol solutions where rate was again enhanced at a higher water content (**Figure 4.6**b). The extracted Ψ values are very close (within ± 0.005) to that established for the monochlorophenol(s), a result which further demonstrates a common HDH rate dependency on solvent ε_c that is independent of the number or position of the Cl substituent(s). Moreover, the same dependence of HDH rate with water content extends to the conversion of bromophenols (see **Table 4.2** and **Figure 4.7**) where the model again applies to a range of water+methanol combinations. It is worth noting that the b_T values (0.21 - 0.42) for the bromo-reactants were lower than those exhibited by chlorophenols, a response which suggests a lesser dependence of debromination on solvent dielectric constant. Nevertheless, the value of Ψ for the bromophenol(s) (0.784 ± 0.001) coincides with that generated for chlorophenol(s), further illustrating that the contribution of ε_c to HDH rate is independent of the halophenol reactant.

The variation of HDH selectivity with solvent composition was assessed by monitoring product distribution as a function of dichlorophenol conversion in methanol+water mixtures. Representative data are presented in **Figure 4.8**, where selectivity with respect to 2-CP is shown for the HDH of 2,3- (I), 2,4- (II), 2,5- (III) and 2,6-DCP (IV) for reaction in mixtures of widely varying water/methanol content. Selectivity/conversion data overlapped for each isomer and was essentially insensitive to solvent composition. This response extends to the HDH of 2,4-DBP, where 2-BP production was again largely independent of the solvent, as illustrated in the inset to **Figure 4.8**II.

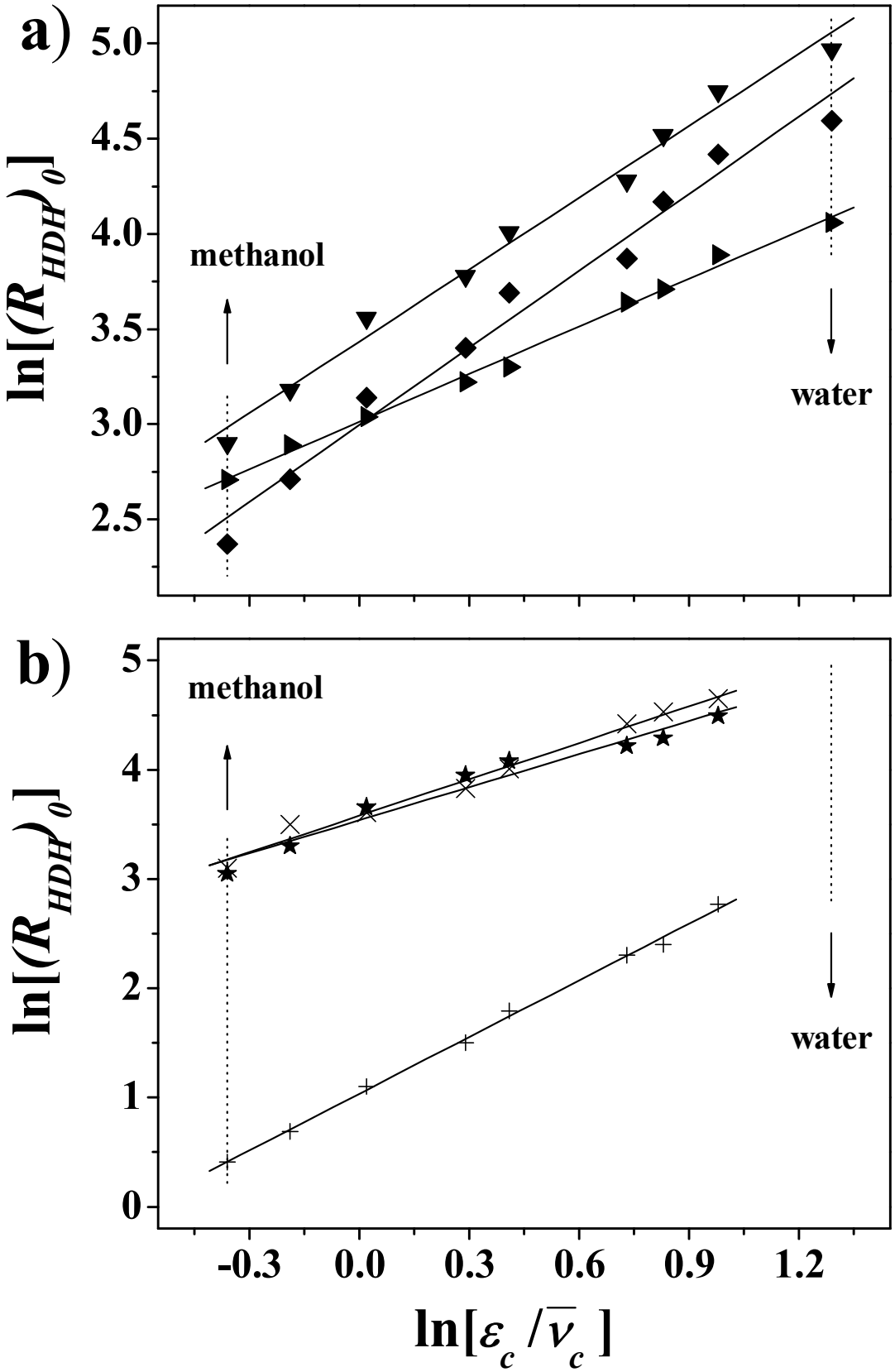

Figure 4.6: Linear dependence of the initial HDH rate ($(R_{HDH})_0$) on the ratio of the (corrected) dielectric constant and molar volume ($\varepsilon_c / \bar{\nu}_c$) in water+methanol mixtures for the conversion of a) 2,3-DCP (▼), 2,4-DCP (◆) and 3,4-DCP (▶) and b) 2,5-DCP (★), 2,6-DCP (×) and 3,5-DCP (+). Note: solid lines represent fit to eqn. (4.16) while dotted lines illustrate abcissa position for pure solvents.

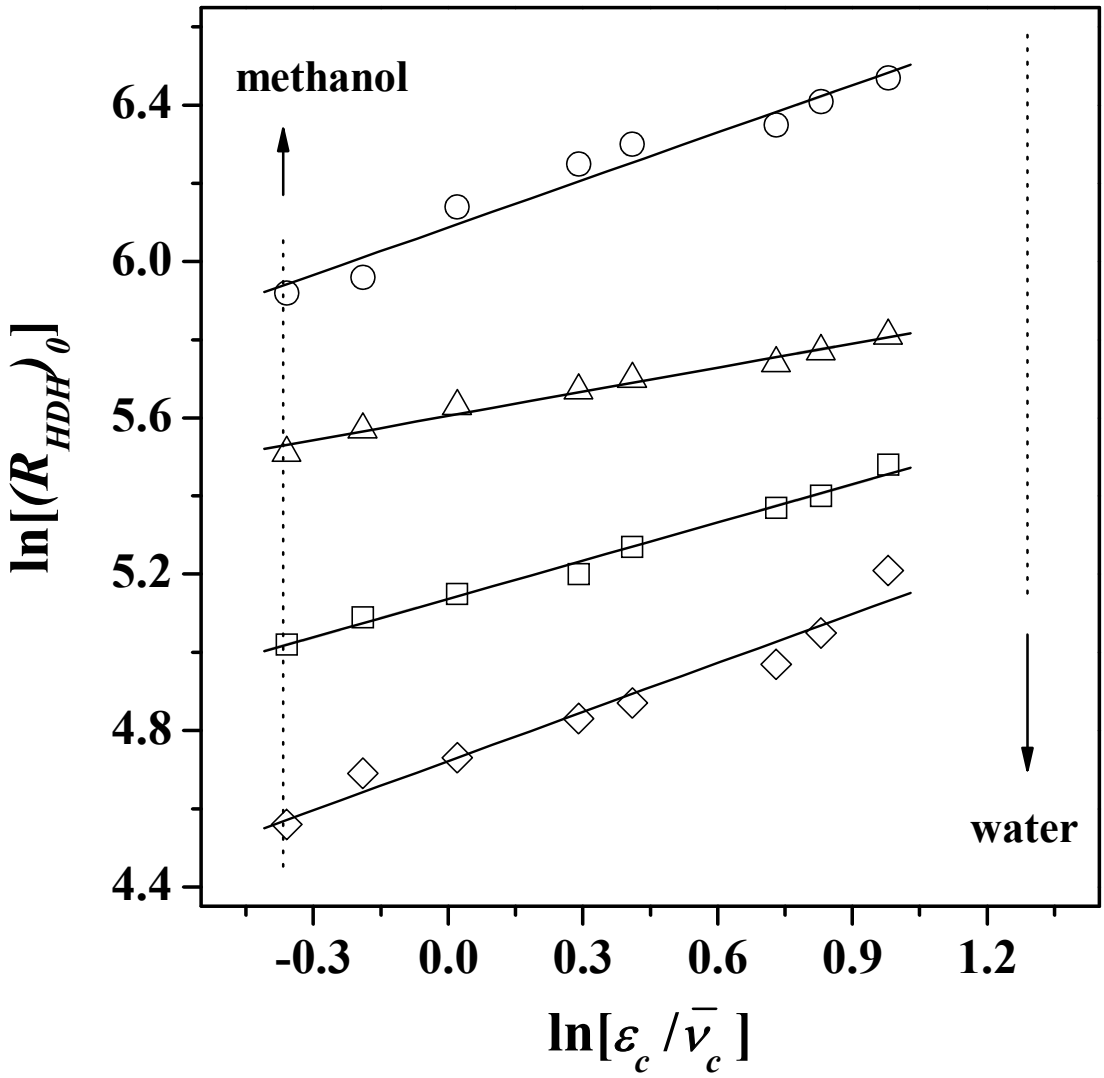

Figure 4.7: Linear dependence of the initial HDH rate ($(R_{HDH})_0$) on the ratio of the (corrected) dielectric constant and molar volume ($\varepsilon_c / \bar{v}_c$) in water+methanol mixtures for the conversion of 2-BP (□), 3-BP (○), 4-BP (△) and 2,4-DBP (☆). Note: solid lines represent fit to eqn. (4.16) while dotted lines illustrate abcissa position for pure solvents.

These results suggest that, for all reactants, each HDH step (see **Figure 4.3**a) is affected to the same degree by changes to the solvent, resulting in equivalent HDH selectivities regardless of the water content. There is some (limited) evidence in the literature of a HDH selectivity dependence on solvent [25,26]. It is worth to highlight the work of Bae *et al.* [92] who, studying the HDC of CCl_4 over Pd/C, recorded a higher selectivity to $CHCl_3$ (97 %) in ethanol than that (74 %) obtained in acetonitrile and this was linked to a proton-donation effect in the case of ethanol. However, in that study the solvent contributed directly to dehalogenation as it served as a hydrogen donor. The results demonstrate, for the first time, that in the absence of secondary reactions HDH selectivity is independent of the solvent.

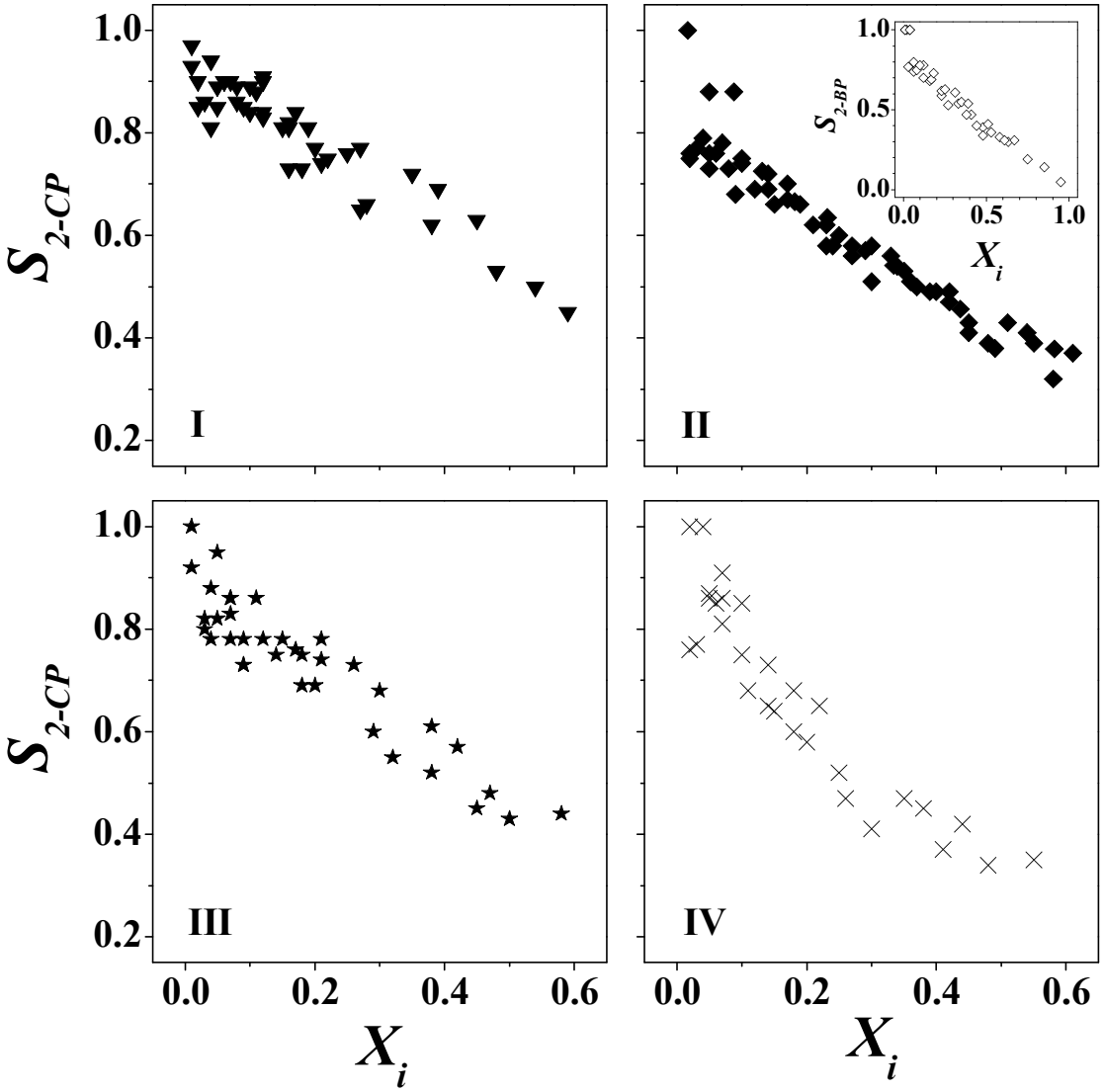

Figure 4.8: 2-CP selectivity ($S_{2\text{-}CP}$) as a function of reactant conversion (X_i) for the HDH of 2,3-DCP (I, ▼), 2,4-DCP (II, ◆), 2,5-DCP (III, ★) and 2,6-DCP (IV, ×) in water+methanol mixtures. Inset to (II) represents 2-BP selectivity ($S_{2\text{-}BP}$) variation with 2,4-DBP conversion (◇).

4.3.5 HDH of Chlorobenzenes

The assessment of solvent effects was extended to a consideration of chlorobenzene(s) HDH, taking CB and 1,3-DCB as model reactants. In this case, water+THF combinations were employed, where any solvent-solute interactions *via* H-bonding can be discounted. The results (presented in **Figure 4.9** and **Table 4.4**) demonstrate that $(R_{HDH})_0$ obtained for chlorobenzenes also increased with increasing water content. As was the case with halophenols, $(R_{HDH})_0$ was consistently higher for the mono- compared with the di-substituted benzene. The dependence of HDH rate on solvent can be again represented in terms of eqn. **(4.16)**, with ε_{THF} = 7, $\bar{v}_{THF}$ = 75 cm^3 mol^{-1} and drawing on reference data [93,94] for the excess properties (see eqns. **(4.12 - 4.13)** in section **4.3.4**).

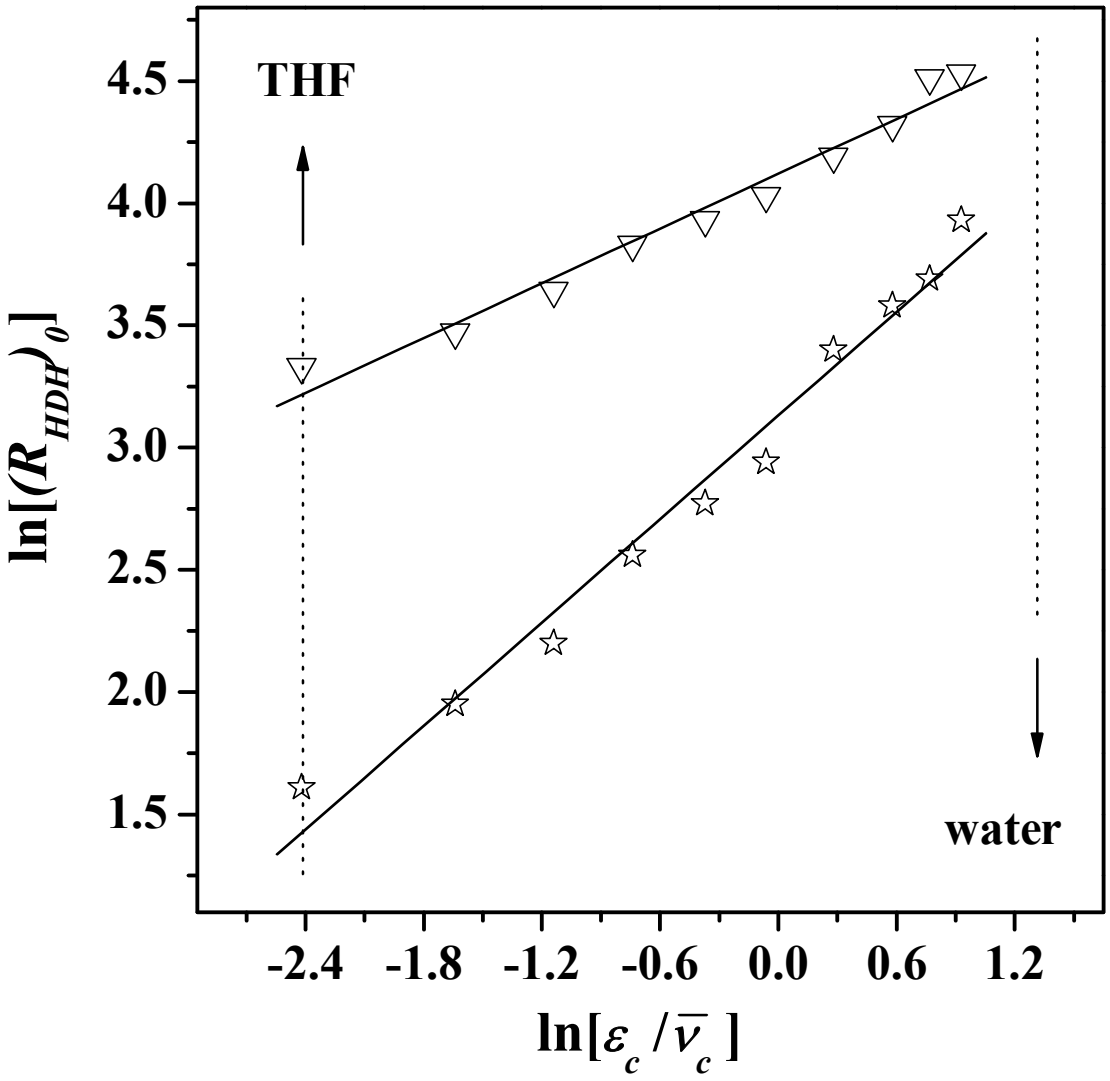

Figure 4.9: Linear dependence of the initial HDH rate ($(R_{HDH})_0$) on the ratio of the (corrected) dielectric constant and molar volume ($\varepsilon_c / \bar{v}_c$) for the conversion of CB (▽) and 1,3-DCB (☆) in water+THF mixtures. Note: solid lines represent fit to eqn. (4.16) while dotted lines illustrate abcissa position for pure solvents.

HDH rate is shown to be governed by solvent dielectric constant where the somewhat greater Ψ values relative to that obtained for halophenols in methanol+water can be accounted for in terms of steric effects in the case of THF, which has a similar molecular size to chlorobenzene(s). This result find indirect support in the work of Xia *et al.* [31] who, studying the HDC of 2,4,4'-trichloro-2'-hydroxyphenylether over Pd/C in various solvents, attributed a lower dechlorination rate in THF to an impeded reactant adsorption on the catalyst surface. The HDH selectivity was, once again, independent of solvent composition (to within ± 0.03, see **Table 4.4**).

These results confirm the wide applicability of this analysis of solvent effects in catalytic HDH where solvent ε_c consistently plays a governing role in determining rate and $\overline{v}_c$ variations represent a secondary consideration.

Table 4.4: Initial HDH rates ($(R_{HDH})_0$, units: $mmol_{Cl}\ g_{Pd}^{-1}\ min^{-1}$) and fitting parameters ($R^2 \geq 0.976$) for solvent dependency (dielectric constant (b_ε), molar volume ($b_{\overline{v}}$) and both properties (b_T)) and fractional contribution of ε_c (Ψ) in the HDH of chlorobenzenes over Pd/Al_2O_3 in THF and water+THF.

Reactant	CB	1,3-DCB[a]
$(R_{HDH})_0$[b]	28	5
$(R_{HDH})_0$[c]	93	51
b_ε	0.62	1.17
$b_{\overline{v}}$	-1.21	-2.27
b_T	0.41	0.78
Ψ	0.885	0.884

[a]at $X = 0.1$, $S_{CB} = 0.46 \pm 0.03$; $S_{benzene} = 0.54 \pm 0.03$.
[b]reaction in pure THF.
[c]reaction in a 85 % mol water in THF mixture.

4.4 Conclusions

In this study, the effect of solvent variations on the liquid phase HDH of a range of haloaromatics has been considered over a Pd/Al_2O_3 catalyst characterised by a well dispersed (Pd mean size = 2.4 nm) metal phase. In the absence of transport limitations, secondary reactions and catalyst deactivation, the initial HDH rates increased in the order: dichlorophenol(s) < monochlorophenol(s) < dibromophenol(s) < monobromophenol(s). This sequence is consistent with an electrophilic aromatic substitution mechanism where (i) higher rates of hydrogenolysis of C–Br relative to C–Cl are the result of the lower C–Br bond dissociation energy and (ii) a second (electron-withdrawing) halogen substituent has a deactivating effect. A dependence of HDH rate on solvent is established with a predominant contribution (*ca.* 80%) due to the dielectric constant of the medium where variation in molar volume is a secondary factor. This effect is attributed to stronger ionic forces at a higher solvent dielectric constant that serve to stabilize the arenium intermediate. This response applies regardless of the nature, number or position of the halogen substituent(s) and also extends to the HDH of chlorobenzene(s) where –OH substituent/solvent interaction(s) do not feature.

In contrast to the observed rate dependence, reaction selectivity was essentially insensitive to changes in solvent composition, suggesting that the possible HDH stepwise/concerted routes are affected to the same extent. The data treatment undertaken herein has provided essential quantification of solvent effects in HDH reactions and this approach is applicable to a range of heterogeneous catalytic systems.

4.5 References

[4.1] V. I. Kovalchuk, J. L. d'Itri, Appl. Catal. A: General, 271, 13 (2004)

[4.2] M. A. Keane, J. Chem. Technol. Biotechnol., 80, 1211 (2005)

[4.3] T. Hara, T. Kaneta, K. Mori, T. Mitsudome, T. Mizugaki, K. Ebitani, K. Kaneda, Green Chem., 9, 1246 (2008)

[4.4] T. Yoneda, T. Takido, K. Konuma, Appl. Catal. B: Environmental, 84, 667 (2008)

[4.5] E. Ding, S. Jujjuri, M. Sturgeon, S. G. Shore, M. A. Keane, J. Mol. Catal. A: Chemical, 294, 51 (2008)

[4.6] J.-H. Kim, P. G. Tratnyek, Y.-S. Chang, Environ. Sci. Technol., 42, 4106 (2008)

[4.7] J. Chae, S. L. Buchwald, J. Org. Chem., 69, 3336 (2004)

[4.8] E.-J. Shin, M. A. Keane, J. Hazard. Mater. B, 66, 265 (1999)

[4.9] S. S. Zinovyev, N. A. Shinkova, A. Perosa, P. Tundo, Appl. Catal. B: Environmental, 55, 49 (2005)

[4.10] E. Díaz, J. A. Casas, Á. F. Mohedano, L. Calvo, M. A. Gilarranz, J. J. Rodríguez, Ind. Eng. Chem. Res., 47, 3840 (2008)

[4.11] S. S. Zinovyev, A. Perosa, P. Tundo, J. Catal., 226, 9 (2004)

[4.12] M. A. Aramendia, V. Boráu, I. M. García, C. Jiménez, F. Lafont, A. Marinas, J. M. Marinas, F. J. Urbano, J. Catal., 187, 392 (1999)

[4.13] G.-B. Liu, L. Dai, X. Gao, M.-K. Li, T. Thiemann, Green Chem., 8, 781 (2006)

[4.14] X. Wang, M. Liang, H. Liu, Y. Wang, J. Mol. Catal. A: Chemical, 273, 160 (2007)

[4.15] M. A. Aramendía, V. Boráu, I. M. García, C. Jiménez, J. M. Marinas, F. J. Urbano, Appl. Catal. B: Environmental, 20, 101 (1999)

[4.16] M. A. Fakhfakh, X. Franck, R. Hocquemiller, B. Figadère, J. Organomet. Chem., 624, 131 (2001)

[4.17] K. Yang, B. Wang, L. Chen, X. Wang, Catal. Commun., 9, 431 (2008)

[4.18] G. Centi, J. Mol. Catal. A: Chemical, 173, 287 (2001)

[4.19] F. J. Urbano, J. M. Marinas, J. Mol. Catal. A: Chemical, 173, 329 (2001)

[4.20] G. Yuan, M. A. Keane, Catal. Today, 88, 27 (2003)

[4.21] L. M. Gómez-Sainero, X. L. Seoane, J. L. G. Fierro, A. Arcoya, J. Catal., 209, 279 (2002)

[4.22] G. Evdokimova, S. Zinovyev, A. Perosa, P. Tundo, Appl. Catal. A: General, 271, 129 (2004)

[4.23] N. C. Concibido, T. Okuda, W. Nishijima, M. Okada, React. Kinet. Catal. Lett., 90, 127 (2007)

[4.24] H.-Y. Wee, J. A. Cunningham, J. Hazard. Mater., 155, 1 (2008)

[4.25] Y. Ukisu, T. Miyadera, React. Kinet. Catal. Lett., 89, 341 (2006)

[4.26] N. C. Concibido, T. Okuda, Y. Nakano, W. Nishijima, M. Okada, Tetrahedron Lett., 46, 3613 (2005)

[4.27] F.-D. Kopinke, K. Mackenzie, R. Koehler, A. Georgi, Appl. Catal. A: General, 271, 119 (2004)

[4.28] Y. Ukisu, Appl. Catal. A: General, 349, 229 (2008)

[4.29] C. Xia, J. Xu, W. Wu, X. Liang, Catal. Commun., 5, 383 (2004)

[4.30] W. Nishijima, Y. Ochi, T.-Y. Tsai, Y. Nakano, M. Okada, Appl. Catal. B: Environmental, 51, 135 (2004)

[4.31] C. Xia, J. Xu, W. Wu, Q. Luo, J. Chen, Q. Zhang, X. Liang, Appl. Catal. B: Environmental, 45, 281 (2003)

[4.32] K. Mackenzie, H. Frenzel, F.-D. Kopinke, Appl. Catal. B: Environmental, 63, 161 (2006)

[4.33] S. Gómez-Quero, F. Cárdenas-Lizana, M. A. Keane, AIChE J., Accepted., (2009)

[4.34] D.-Q. Xu, Z.-Y. Hu, W.-W. Li, S.-P. Luo, Z.-Y. Xu, J. Mol. Catal. A: Chemical, 235, 137 (2005)

[4.35] J. D. Oxley, M. M. Mdleleni, K. S. Suslick, Catal. Today, 88, 139 (2004)

[4.36] M. A. Aramendía, V. Boráu, I. M. García, C. Jiménez, A. Marinas, J. M. Marinas, F. J. Urbano, Appl. Catal. B: Environmental, 43, 71 (2003)

[4.37] K. V. Murthy, P. M. Patterson, M. A. Keane, J. Mol. Catal. A: Chemical, 225, 149 (2005)

[4.38] K. V. Murthy, P. M. Patterson, G. Jacobs, B. H. Davis, M. A. Keane, J. Catal., 223, 74 (2004)

[4.39] C. Menini, C. Park, E.-J. Shin, G. Tavoularis, M. A. Keane, Catal. Today, 62, 355 (2000)

[4.40] M. A. Keane, Appl. Catal. A: General, 271, 109 (2004)

[4.41] G. Yuan, M. A. Keane, Chem. Eng. Sci., 58, 257 (2003)

[4.42] Y. Shindler, Y. Matatov-Meytal, M. Sheintuch, Ind. Eng. Chem. Res., 40, 3301 (2001)

[4.43] M. Trueba, S. P. Trasatti, Eur. J. Inorg. Chem., 17, 3393 (2005)

[4.44] L. Shena, Z. Chen, Chem. Eng. Sci., 62, 3748 (2007)

[4.45] C. Amorim, M. A. Keane, J. Colloid Interface Sci., 322, 196 (2008)

[4.46] C.-B. Wang, H.-K. Lin, C.-M. Ho, J. Mol. Catal. A: Chemical, 180, 285 (2002)

[4.47] G. M. Tonetto, D. E. Damiani, J. Mol. Catal. A: Chemical, 202, 289 (2003)

[4.48] C. Amorim, M. A. Keane, J. Chem. Technol. Biotechnol., 83, 662 (2008)

[4.49] S. Gómez-Quero, F. Cárdenas-Lizana, M. A. Keane, Ind. Eng. Chem. Res., 47, 6841 (2008)

[4.50] N. K. Nag, J. Phys. Chem. B, 105, 5945 (2001)

[4.51] M. Boudart, H. S. Hwang, J. Catal., 39, 44 (1975)

[4.52] S. Díaz-Moreno, D. C. Koningsberger, A. Muñoz-Páez, Nucl. Instrum. Methods Phys. Res., Sect. B, 133, 15 (1997)

[4.53] J. Liu, Microsc. Microanal., 10, 55 (2004)

[4.54] C. N. Satterfield, Heterogeneous Catalysis in Practice, McGraw-Hill, New York, 1980.

[4.55] S. Mukherjee, M. A. Vannice, J. Catal., 243, 108 (2006)

[4.56] R. P. Danner, T. E. Daubert, Manual for Predicting Chemical Process Design Data, Design Institute for Physical Property Data, New York, 1983.

[4.57] C. J. King, L. Hsueh, K.-W. Mao, J. Chem. Eng. Data, 10, 348 (1965)

[4.58] J. R. Anderson, K. C. Pratt, Introduction to Characterization and Testing of Catalysts, Academic Press, London, 1985.

[4.59] J. M. Smith, Chemical Engineering Kinetics, McGraw-Hill, Singapore, 1981.

[4.60] B. F. Hagh, D. T. Allen, Chem. Eng. Sci., 45, 2695 (1990)

[4.61] Y. A. Serguchev, Y. V. Belokopytov, Kinet. Catal., 42, 174 (2001)

[4.62] L. Lassová, H. K. Lee, T. S. A. Hor, J. Mol. Catal. A: Chemical, 144, 397 (1999)

[4.63] L. Lassová, H. K. Lee, T. S. A. Hor, J. Org. Chem., 63, 3538 (1998)

[4.64] T. T. Bovkun, Y. Sasson, J. Blum, J. Mol. Catal. A: Chemical, 242, 68 (2005)

[4.65] V. Felis, C. de Bellefon, P. Fouilloux, D. Schweich, Appl. Catal. B: Environmental, 20, 91 (1999)

[4.66] L. Calvo, A. F. Mohedano, J. A. Casas, M. A. Gilarranz, J. J. Rodríguez, Carbon, 42, 1377 (2004)

[4.67] C. Xia, Y. Liu, J. Xu, J. Yu, W. Qin, X. Liang, Catal. Commun., 10, 456 (2009)

[4.68] J. B. Hoke, G. A. Gramiccioni, E. N. Balko, Appl. Catal. B: Environmental, 1, 285 (1992)

[4.69] E.-J. Shin, A. Spiller, G. Tavoularis, M. A. Keane, Phys. Chem. Chem. Phys., 1, 3173 (1999)

[4.70] F. A. Carey, R. C. Atkins, Organic Chemistry, 5th ed., Mc Graw-Hill, New York, 2003.

[4.71] S. Patai, The Chemistry of the Carbon-Halogen Bond, John Wiley & Sons Ltd., New York, 1973.

[4.72] M. A. Keane, D. Y. Murzin, Catalysis of Organic Reactions: Kinetics of the Hydrodechlorination of Dichlorobenzenes, Marcel Dekker, New York, 2002.

[4.73] J. Wei, X. Xu, Y. Liu, D. Wang, Water Res., 40, 348 (2006)

[4.74] E.-J. Shin, M. A. Keane, Chem. Eng. Sci., 54, 1109 (1999)

[4.75] E.-J. Shin, M. A. Keane, J. Chem. Technol. Biotechnol., 75, 159 (2000)

[4.76] E.-J. Shin, M. A. Keane, Catal. Lett., 58, 141 (1999)

[4.77] D. R. Lide, Handbook of Chemistry and Physics, 90th ed., Taylor and Francis Group, Boca Raton, 2009.

[4.78] F.-D. Kopinke, K. Mackenzie, R. Köhler, Appl. Catal. B: Environmental, 44, 15 (2001)

[4.79] C. A. Marques, O. Rogozhnikova, M. Selva, P. Tundo, J. Mol. Catal. A: Chemical, 96, 301 (1995)

[4.80] S. Adimurthy, G. Ramachandraiah, A. V. Bedekar, Tetrahedron Lett., 44, 6391 (2003)

[4.81] J. L. Benítez, G. del Angel, React. Kinet. Catal. Lett., 66, 13 (1999)

[4.82] N. C. Concibido, T. Okuda, W. Nishijima, M. Okada, Appl. Catal. B: Environmental, 71, 64 (2007)

[4.83] N. C. Concibido, T. Okuda, W. Nishijima, M. Okada, React. Kinet. Catal. Lett., 89, 369 (2006)

[4.84] G. S. Pozan, I. Boz, Environ. Eng. Sci., 25, 1197 (2008)

[4.85] R. L. Smith, S. B. Lee, H. Komori, K. Arai, Fluid Phase Equilib., 144, 315 (1998)

[4.86] J. V. Herráez, R. Belda, J. Solution Chem., 35, 1315 (2006)

[4.87] A. Jouyban, S. Soltanpour, H.-K. Chan, Int. J. Pharm., 269, 353 (2004)

[4.88] R. J. Sengwa, M. Abhilasha, J. Mol. Liq., 123, 92 (2006)

[4.89] S. Sudo, N. Shinyashiki, Y. Kitsuki, S. Yagihara, J. Phys. Chem. A, 106, 458 (2002)

[4.90] T. Sato, A. Chiba, R. Nozaki, J. Mol. Liq., 96-97, 327 (2002)

[4.91] T. Sato, A. Chiba, R. Nozaki, J. Chem. Phys., 110, 2508 (1999)

[4.92] J.-W. Bae, E.-J. Jang, D.-H. Jo, J.-S. Lee, K.-H. Lee, J. Mol. Catal. A: Chemical, 206, 225 (2003)

[4.93] J. N. Nayak, M. I. Aralaguppi, B. V. K. Naidu, T. M. Aminabhavi, J. Chem. Eng. Data, 49, 468 (2004)

[4.94] A. Chaudhari, P. Khirade, R. Singh, S. N. Helambe, N. K. Narain, S. C. Mehrotra, J. Mol. Liq., 82, 245 (1999)

Chapter 5

Liquid Phase Catalytic Hydrotreatment of 2,4-Dichlorophenol over Pd/Al_2O_3: Discontinuous *vs.* Continuous Operation

The work presented in **Chapters 2 - 4** has established the efficacy of Pd/Al_2O_3 in the batch, liquid phase hydrotreatment of haloarenes. In order to extend the applicability of this approach as a waste abatement methodology, it is necessary to consider hydrodechlorination in continuous flow operation. In this Chapter, the feasibility of continuous 2,4-dichlorophenol hydrodechlorination is addressed. The benefits of switching from batch to continuous operation (in terms of hydrogen transport efficiency, hydrodechlorination performance and catalyst lifetime) are demonstrated.

5.1 Introduction

2,4-Dichlorophenol (2,4-DCP) is a common feedstock used in the manufacture of herbicides, pharmaceuticals and dyes [1] with an estimated release into the environment of up to 2×10^4 lb $year^{-1}$ [2]. The low biodegradability of 2,4-DCP (recent biotreatment studies achieving maximum rates of 140 $mg_{2,4\text{-DCP}}\ g_{biomass}^{-1}\ day^{-1}$ [3]) and high associated toxicity [2,4] has placed this chemical on a list of high priority pollutants in terms of treatment [5]. A diversity of detoxification methodologies (*e.g.* photo-oxidation [6] and electrochemical degradation [7]) have been employed where catalytic hydrodechlorination (HDC), the H_2 scission of C–Cl bonds [8,9], has emerged as a progressive and viable approach that facilitates recovery and reuse of raw material [10]. 2,4-DCP HDC has been mainly studied in the liquid phase over carbon [11-18] and alumina [15-20] supported Pd catalysts, given the comparatively greater resistance of this metal to deactivation [21,22]. Structure sensitivity is a feature of HDC over Pd where catalytic performance has been demonstrated to be influenced by the size [23,24] and electronic structure [25,26] of the metal particles. The work to date has focused on discontinuous operation to study reaction kinetics and provide a comparison of catalyst performance where cost and experimental effort has mitigated against the use of continuous reactors [27,28].

Nevertheless, the latter is preferable from a practical point of view and represents a significant step towards industrial implementation, *i.e.* in waste abatement [29]. Continuous operation in chlorophenol(s) HDC has focused on gas phase treatments, a trend which extends to the HDC of chlorobenzenes [30,31] and chloro-methanes [32,33]. Extensive gas phase chlorophenol(s) HDC research has been carried out by Marshall *et al.* [34,35], Halász and co-workers [36] and Keane *et al.* [37-43], who have demonstrated the feasibility of complete chlorine removal over unsupported Ag-Fe [34] and Mg-Pd [35], Pt and Co supported on ZSM-52 [36], Ni/SiO_2 [37-41] and $Au\text{-}Ni/SiO_2$ [42,43]. However, it should be noted that these studies are limited by the requirements of elevated temperatures ($T \geq 473$ K), pressures (up to 250 atm) and/or excess H_2 (400 - 1200 times), which represent a significant energy consumption, a key factor in sustainable process design [44,45]. With regard to liquid phase chlorophenol(s) HDC, it is worth to flag the findings of Calvo and co-workers [46,47] and Diaz *et al.* [48], who have achieved near complete HDC of aqueous 4-chlorophenol over Pd/C in continuous (plug-flow [46,47] and CSTR [48]) reactors under relatively mild reaction conditions ($T \leq 373$ K, 1 - 6 bar) with an excess of H_2 (317 - 1333 times) relative to stoichiometric quantities. Patel and Suresh [49] have recently quoted high efficiencies (*ca.* 80 %) for (continuous) aqueous pentachlorophenol HDC over palladized cellulose discs at room temperature and atmospheric pressure.

In this study, the operational characteristics for aqueous HDC of 2,4-DCP over Pd/Al_2O_3 in a batch reactor are established and then the feasibility/advantages of process scale up to continuous operation is/are considered. To the best of the author's knowledge, this is the first development of a continuous, liquid phase catalytic system for treating toxic 2,4-DCP. Moreover, this work provides (for the first time) a direct comparison of both operational regimes in a catalytic HDC process.

5.2 Experimental

5.2.1 Materials

The catalyst (1.2 % w/w Pd/Al_2O_3) was purchased from Sigma-Aldrich, sieved (ATM fine test sieves) into batches of 38 μm average particle diameter (d) and used as supplied. A full catalyst characterization can be found in earlier reports [18,50] where the presence of metallic Pd was established after room temperature contact with H_2.

The pertinent catalyst structural characteristics are: pH associated with the point of zero charge (pH_{pzc}) = 7.7; bulk density (ρ) = 1154 kg m^{-3}; BET surface area = 160 m^2 g^{-1}; total pore volume = 0.56 cm^3 g^{-1} (porosity = 0.65, tortuosity = 1.54); Pd metal surface area = 208 m_{Pd}^2 g_{Pd}^{-1}; surface area-weighted mean Pd particle size = 2.4 nm. The 2,4-DCP reactant (Aldrich) and NaOH (Riedel-de Haën), both ≥ 99.0 %, were used as received. An aqueous stock solution was prepared with distilled water with fixed concentrations of $C_{2,4\text{-}DCP}$ = 30 $mmol_{2,4\text{-DCP}}$ dm^{-3} and C_{NaOH} = 100 $mmol_{NaOH}$ dm^{-3} (pH = 12.1 at 303 K). The H_2 and He gases used in this study were of ultra high purity (> 99.99 %, BOC).

5.2.2 Discontinuous Reactor

Batch 2,4-DCP HDC reactions were carried out in a modified commercial glass reactor (Ken Kimble Reactors Ltd.); a schematic diagram is provided in **Figure 5.1**a. The system is equipped with a constant H_2 supply (50 - 250 cm^3 min^{-1}, Brooks mass flow controlled) and a glass impeller provided effective agitation (300 - 1300 min^{-1}). A recirculator (Julabo HD-4) was used to stabilize the reaction temperature at T = 303 ± 1 K with water as coolant (293 K); loss of the reactor liquid contents in the H_2 flow was negligible (< 0.5 % v/v). At the beginning of each experiment, the catalyst (0.04 g) and 80 cm^3 of stock solution were charged and agitated in a He flow (50 cm^3 min^{-1}). The temperature was allowed to stabilize (15 min) and H_2 was then introduced (t = 0 for reaction). The pH of the reaction mixture was monitored continuously using a Dow-Corning pencil electrode coupled to a data logging and collection system (Pico Technology Ltd.). Blank tests conducted in He or over the support alone (*i.e.* in the absence of H_2 and/or Pd) did not result in any measurable conversion. A non-invasive liquid sampling system *via* syringe/in-line filters allowed a controlled removal of aliquots (≤ 0.3 cm^3) of reactant/product(s). Upon completion of the reaction, the H_2 flow was replaced by a He purge. The reactant/product liquor was separated from the catalyst, which was retained in the reactor. The catalyst was then washed repeatedly with distilled water until the wash water was near neutral pH.

5.2.3 Continuous Reactor

Continuous HDC reactions were performed in a commercial COFLORE ACR® unit (AMTechuk, see **Figure 5.1**b).

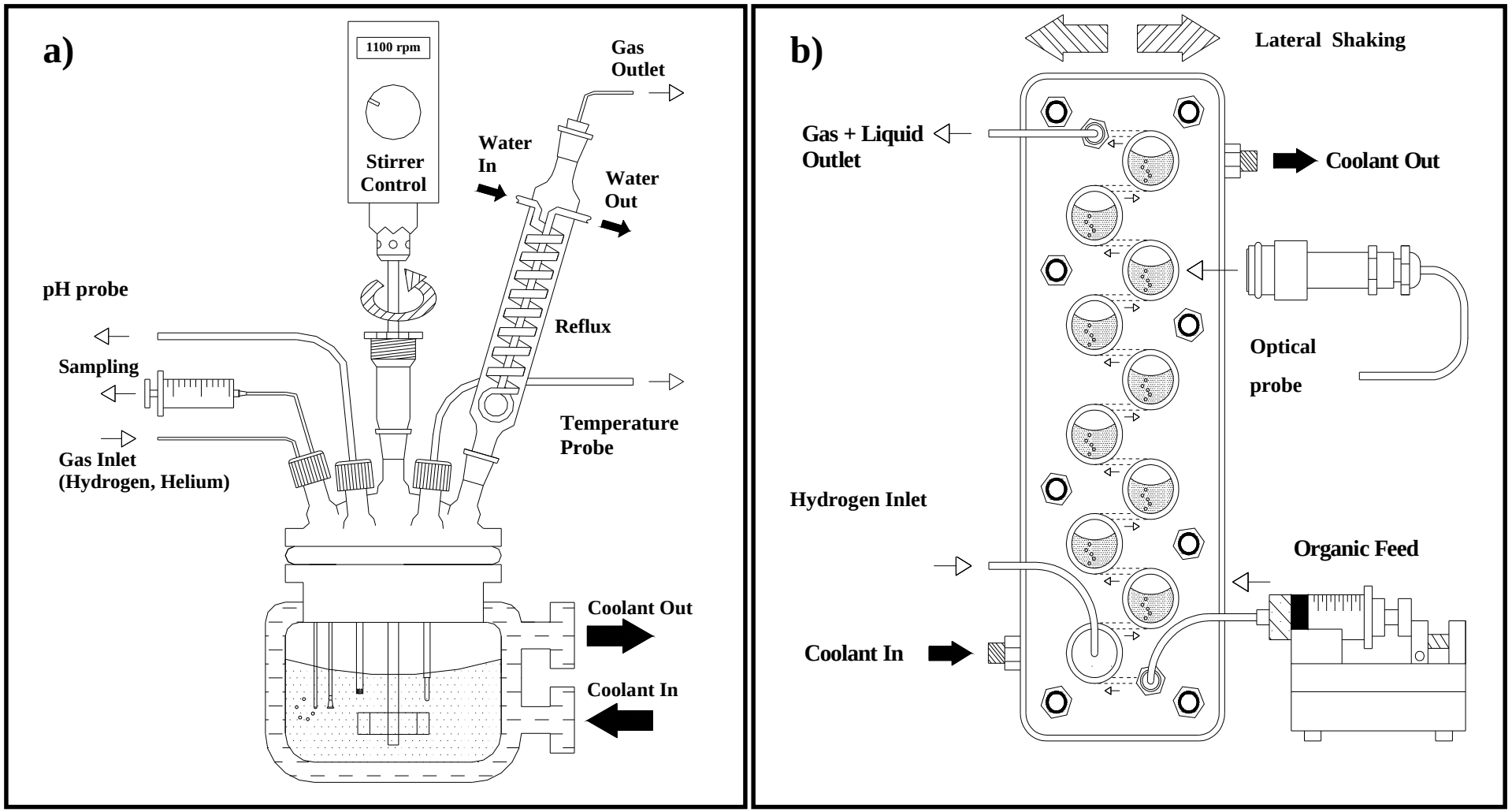

Figure 5.1: Schematic diagram of the three phase slurry a) discontinuous and b) continuous (COFLORE ACR®) reactors.

The reactor contains nine stages where the catalyst (0.04 g) was loaded, each connected in series by channels fitted with 30 μm PTFE filters. The stock 2,4-DCP solution was fed using a Model 100 (kd Scientific) microprocessor-controlled infusion pump (0.4 - 7.6 cm^3 min^{-1}) and a constant volumetric H_2 flow (0 - 60 cm^3 min^{-1}) was provided using a (Brooks) mass flow controller. At steady state operation of constant gas+liquid flow, the available reaction volume (*i.e.* total liquid/solid slurry) was 80 cm^3. The unit was equipped with a mechanical system providing an effective lateral shaking speed (29 - 53 min^{-1}) that helped to maintain the catalyst in suspension. A water bath (Clifton) and a peristaltic pump (Watson-Marlow 502S) were used to stabilize the reaction temperature (303 K) to within ± 2 K, which was measured by an optical sensor (CALEX Electronics Ltd.) fitted to the stage(s) window(s). At the beginning of each run, distilled water was fed to the reactor with a co-current H_2 flow, a lateral shaking speed was fixed and the temperature was allowed to stabilize. The 2,4-DCP stock solution was then introduced and the catalyst/reactant contact time (t) was determined by the volumetric liquid flow rate. The effluent stream was collected for analysis and the pH was also monitored using a Dow-Corning pencil electrode as in the batch operation.

5.2.4 Product Analysis and Evaluation of HDC Activity

Prior to analysis, the samples were neutralized with dilute acetic acid (200 mmol dm^{-3}). The composition of the reaction/product mixture was analyzed by gas chromatography (Perkin-Elmer Auto System XL), employing an FID and a DB-1 (J&W Scientific) capillary column (i.d. = 0.2 mm, length = 50 m, film thickness = 0.33 μm) [14]. The concentration of organic species (2,4-DCP, 2-chlorophenol (2-CP), phenol (PhOH) and cyclohexanone) were determined from the total molar balance in the reaction mixture, where the effect of uptake on the support was negligible [51]. The efficiency of halogen removal is quantified in this study in terms of the fractional degree of HDC (x_{Cl}) as given by

$$x_{Cl} = \frac{n_{HCl}}{n_{Cl}} \qquad \textbf{(5.1)}$$

where n_{Cl} and n_{HCl} are the mmoles of Cl associated with the organic reactant and inorganic product, respectively. Repeated reactions with different samples of catalyst delivered raw data reproducibility that was better than ± 7 %.

5.3 Results and Discussion

5.3.1 Product Distribution: Operation under Catalytic Control

The HDC of aqueous 2,4-DCP over Pd/Al_2O_3 under basic conditions (pH = 12.1) in both, batch and continuous operation, generated 2-CP, as the only partially chlorinated intermediate, and PhOH as the principal product of complete HDC (see **Figure 5.2**). Further ring hydrogenation to yield cyclohexanone was detected at low selectivity levels (≤ 4 %, *i.e.* $(k_3 + k_5 + k_6) <<< (k_1 + k_2 + k_4)$). This response is in accordance with reports in the literature [12,52] where dechlorination of *ortho*-substituted Cl was impeded due to steric hindrance effects. Liquid phase aromatic ring reduction over Pd catalysts is reported to be energetically demanding, requiring higher temperatures (≥ 490 K [53]) and/or pressures (≥ 10 atm [54]) than those used in this study.

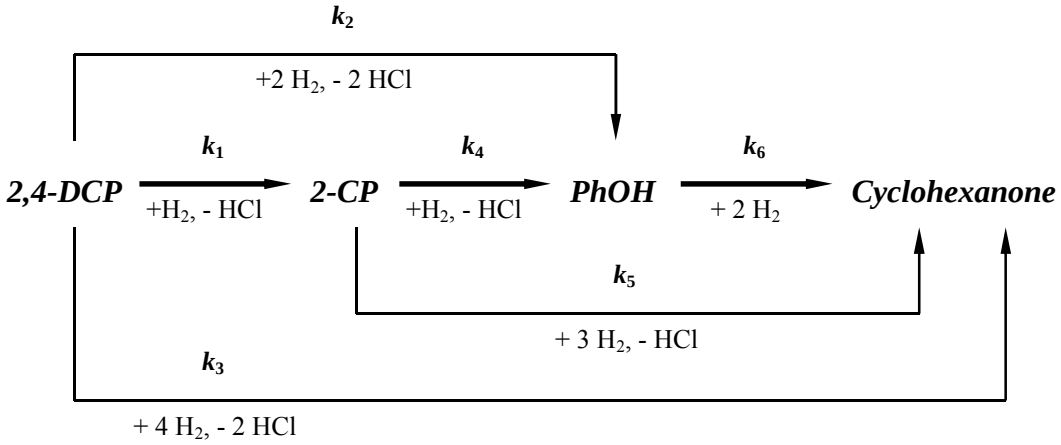

Figure 5.2: Reaction network in the hydrotreatment of 2,4-DCP (bold arrows indicate stepwise mechanism).

In order to evaluate the true catalyst activity, reaction conditions must be first established wherein mass-transfer limitations are negligible and the reactors are operated under kinetic/catalytic control. In a three-phase (gas/liquid/solid) system, the observed rate can be limited by H_2 diffusion through (i) the gas film and/or (ii) the liquid film at the gas/liquid interface.

As pure H_2 gas has been used in this instance, the gas film resistance can be neglected. Diffusion through the liquid film must be enhanced so that the bulk fluid is saturated in H_2 and its concentration ($(C_{H_2})_{bulk}$) approaches the limiting solubility in water (at 1 atm and 303 K, $(C_{H_2})_{saturation} \approx 0.8$ mmol dm^{-3} [50,51]). The H_2 mass transfer rate (N_{H_2}, mmol min^{-1} dm^{-3}) is then proportional to the concentration gradient, as

$$N_{H_2} = \left(k_L a_g\right)\left[(C_{H_2})_{saturation} - (C_{H_2})_{bulk}\right] \quad \textbf{(5.2)}$$

where k_L (m min^{-1}) is the liquid film mass transfer coefficient and a_g (m^2 m^{-3}) the gas/liquid interfacial area per unit volume of liquid; ($k_L a_g$) represents the volumetric H_2 mass transfer coefficient. When operating at constant temperature and pressure, $(C_{H_2})_{saturation}$ is constant and N_{H_2} reaches a maximum value at an optimal ($k_L a_g$). This can be obtained by adjusting the H_2 feed rate and/or the stirring/shaking speed, ensuring a gas/liquid interface equilibrium and facilitating a steady-state H_2 consumption in the bulk liquid [55,56]. The effect of an increase in the H_2 feed rate (I) and stirring/shaking speed (II) on fractional dechlorination (x_{Cl}) is represented in **Figure 5.3** for discontinuous (a) and continuous (b) operation where a constant catalyst loading (relative to the inlet chlorine content) was used (see Experimental section); optimal values are given in **Table 5.1**. In both systems, x_{Cl} was enhanced at higher gas flows and/or agitation speed(s) where the (bulk) pH response was maintained at 12.0 and was equivalent (within ± 0.1) for both systems. The minimum H_2 flow to achieve a constant x_{Cl} (= 0.13) under continuous operation (30 cm^3 min^{-1}, see **Figure 5.3**Ib) was five times lower than that (150 cm^3 min^{-1}, see **Figure 5.3**Ia) needed in the batch system to achieve a lower x_{Cl} (= 0.06). Moreover, in the absence of any agitation there was no detectable HDC activity in the batch reactor while an x_{Cl} = 0.05 was recorded in the continuous flow system (see **Figure 5.3**IIa and **5.3**IIb, respectively). These results suggest a more efficient H_2 diffusion in the continuous reactor and, since k_L is independent of the gas flow rate [55,57], this can be mainly attributed to a greater value of a_g, *i.e.* an extended gas/liquid interface for mass transfer. These results find support in the work of Takić and co-workers [58] who, calculating ($k_L a_g$) for O_3 transfer in aqueous solutions, obtained a higher value in continuous (0.266 min^{-1}) relative to semi-batch (0.198 min^{-1}) operation.

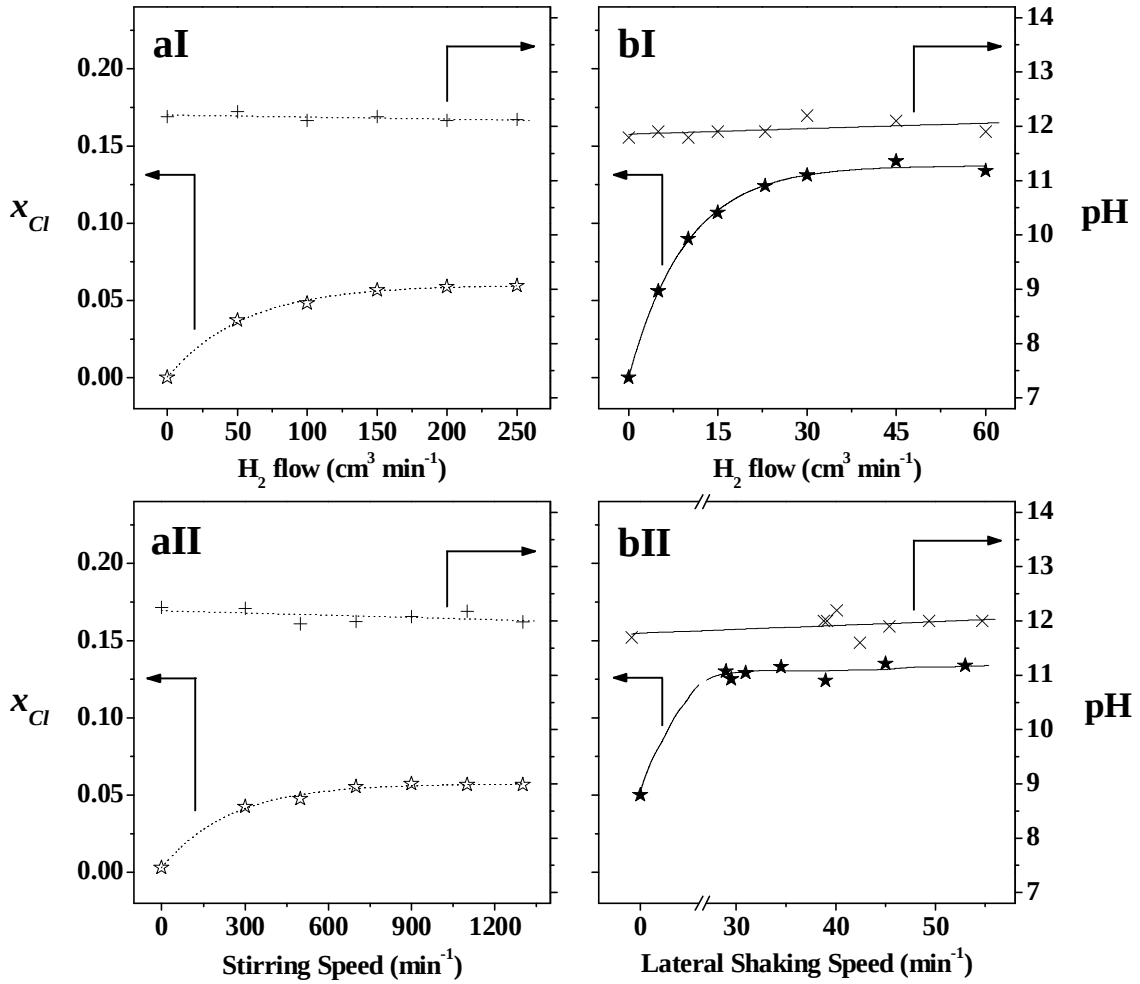

Figure 5.3: Fractional dechlorination (x_{Cl}:☆,★) and associated pH response (+,×) in establishing optimal conditions of (I) H_2 flow and (II) stirring/lateral shaking frequency for 2,4-DCP HDC in a) discontinuous (☆,+) and b) continuous (★,×) operation; t = 16 min.

Table 5.1: Operational and reaction parameters in the HDC of 2,4-DCP over Pd/Al_2O_3 in discontinuous (batch) and continuous reactors.

Regime	**Discontinuous**	**Continuous**
Operational Parameters[a]		
H_2 flow (cm^3 min^{-1})	150	30
Stirring/Shaking speed (min^{-1})	1100	29
Reaction Parameters		
$(R_{HDC})_0$ ($mmol_{Cl}$ g_{Pd}^{-1} min^{-1})	35	65
Ca	0.02	0.03
ϕ	0.03	0.04
η	0.99	0.99
L[b]	0.99	0.66
M[b]	1.00	1.44

[a]refers to optimum values in **Figure 5.3**
[b]from data fit to eqn. **(5.13)**, see **Figure 5.6**

Moreover, Machado *et al.* [59], studying liquid phase nitrobenzene hydrogenation in slurry (batch) and monolith (continuous) reactors, recorded a greater first order rate constant in the latter (0.2 *vs.* 1.4, s^{-1}) and ascribed this to a higher H_2 mass transfer rate when in continuous operation. The results presented in this section establish conditions where both reactors are operated in the absence of external transport limitations (see **Table 5.1**) and H_2 transfer is more effective in the continuous system.

5.3.2 2,4-DCP HDC Rate and Selectivity

HDC activity was evaluated by monitoring x_{Cl} as a function of contact time (t) and the results are presented in **Figure 5.4**. An increase in contact time served to enhance chlorine removal where the (bulk) pH response was invariant (12.1 ± 0.1) and superimposable for both systems. Dehalogenation followed pseudo-first order kinetics according to

$$x_{Cl} = \exp\left(k_{Cl} t\right) - 1 \tag{5.3}$$

where k_{Cl}, the dehalogenation rate constant, is a fitting parameter (see lines in **Figure 5.4**). The initial HDC rate ($(R_{HDC})_0$, units: $mmol_{Cl}\ g_{Pd}^{-1}\ min^{-1}$) was then calculated from:

$$(R_{HDC})_0 = k_{Cl} \frac{n_{Cl}}{W \times m_{Pd}} \tag{5.4}$$

where n_{Cl} represents the inlet chlorine moles ($mmol_{Cl}$), W the mass of catalyst in the reactor (g) and m_{Pd} is the Pd catalyst loading (0.012 $g_{Pd}\ g^{-1}$). The $(R_{HDC})_0$ values are given in **Table 5.1** where a higher value was obtained for the continuous reactor. In order to probe the possible contribution of mass transfer (in terms of internal diffusion) to these results, the Carberry number (Ca) approach was taken to estimate transport resistances in the liquid film at the liquid/catalyst interface which, for spheroidal catalyst particles, at isothermal conditions and constant $C_{2,4\text{-}DCP}$ (*i.e.* absence of heat/mass gradients) takes the form [60]:

$$Ca = \frac{\rho\, m_{Pd}\, d^2}{12\, C_{2,4\text{-}DCP}\, D_{2,4\text{-}DCP}} \times (R_{HDC})_0 \tag{5.5}$$

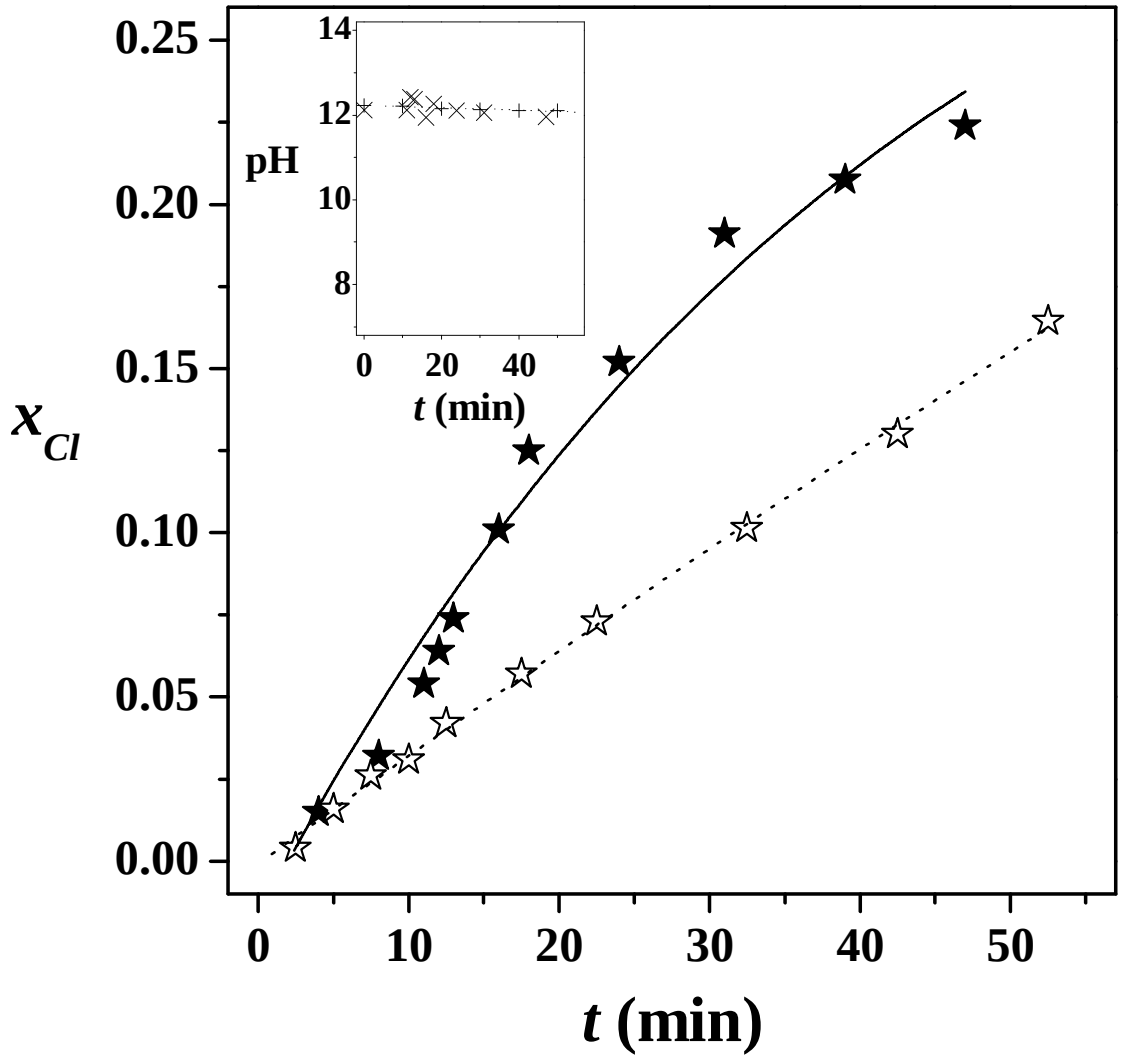

Figure 5.4: Fractional dechlorination (x_{Cl}:☆,★) and pH evolution (inset:+,×) as a function of Pd/Al_2O_3/2,4-DCP contact time (t) in discontinuous (☆,+) and continuous (★,×) operation. Note: lines represent fit to eqn. (5.3).

where ρ and d are the bulk catalyst density and particle size (see Experimental section), $D_{2,4\text{-}DCP}$ is the bulk liquid diffusivity ($m^2\ s^{-1}$), as estimated from Hayduk and Laudie [61]:

$$D_{2,4\text{-}DCP} = \frac{8.621\times10^{-14}}{\left(\eta_{water}\right)^{1.14}\left(\overline{v}_{2,4-DCP}\right)^{0.589}} \qquad \textbf{(5.6)}$$

with η_{water} as the water viscosity (7.97×10^{-4} Pa s at $T = 303$ K [62]) and $\overline{v}_{2,4-DCP}$ as the 2,4-DCP molar volume (0.118 $m^3\ kmol^{-1}$, calculated following [61]); $D_{2,4\text{-}DCP} = 1.03 \times 10^{-9}\ m^2\ s^{-1}$.

Mass transfer limitations within the catalyst pores were estimated by the standard Thiele modulus (ϕ) and effectiveness factor (η) criteria, as given by:

$$\phi = \sqrt{\frac{(R_{HDC})_0 \rho m_{Pd} \left(d/6\right)^2}{C_{2,4\text{-}DCP} D_{Eff,2,4\text{-}DCP}}} \tag{5.7}$$

$$\eta = \frac{1}{\phi}\left(\frac{1}{\tanh(3\phi)} - \frac{1}{3\phi}\right) \tag{5.8}$$

where $D_{Eff,2,4\text{-}DCP}$ is the effective 2,4-DCP diffusivity, *i.e.* within the catalyst pores: $D_{Eff,2,4\text{-}DCP} = D_{2,4\text{-}DCP} \times (0.65)^2$ [27]. The results of these calculations for both reactors (included in **Table 5.1**) are indicative of negligible resistance at the liquid/solid interface (*Ca* limiting value range = 0.1 - 0.15 [28]) with minimal diffusional constraints in the pores ($\phi < 0.5$, $\eta \approx 1$ [55]).

Product composition is presented in **Figure 5.5** for batch (a) and continuous (b) operation, where a decrease in 2,4-DCP concentration with increasing contact time is in evidence but there is a different response in terms of the 2-CP and PhOH concentration profiles for both reactors. As shown in **Figure 5.2**, HDC can proceed *via* stepwise (k_1, k_4) and/or concerted (k_2) routes so that, at a given fractional 2,4-DCP conversion, the simultaneous cleavage of both C–Cl bonds will lead to a higher PhOH content in the product stream and a consequent higher $(R_{HDC})_0$ [50]. Reaction selectivity can be quantified on the basis of the mass balances that define the HDC steps (*i.e.* k_1, k_2 and k_4 in **Figure 5.2**) which, applying pseudo-first order kinetics, take the form:

$$\frac{1}{W}\frac{dx_{2,4\text{-}DCP}}{dt} = -\left(k_1 + k_2\right) x_{2,4\text{-}DCP} \tag{5.9}$$

$$\frac{1}{W}\frac{dx_{2\text{-}CP}}{dt} = k_1 x_{2,4\text{-}DCP} - k_4 x_{2\text{-}CP} \tag{5.10}$$

$$\frac{1}{W}\frac{dx_{PhOH}}{dt} = k_2 x_{2,4\text{-}DCP} + k_4 x_{2\text{-}CP} \tag{5.11}$$

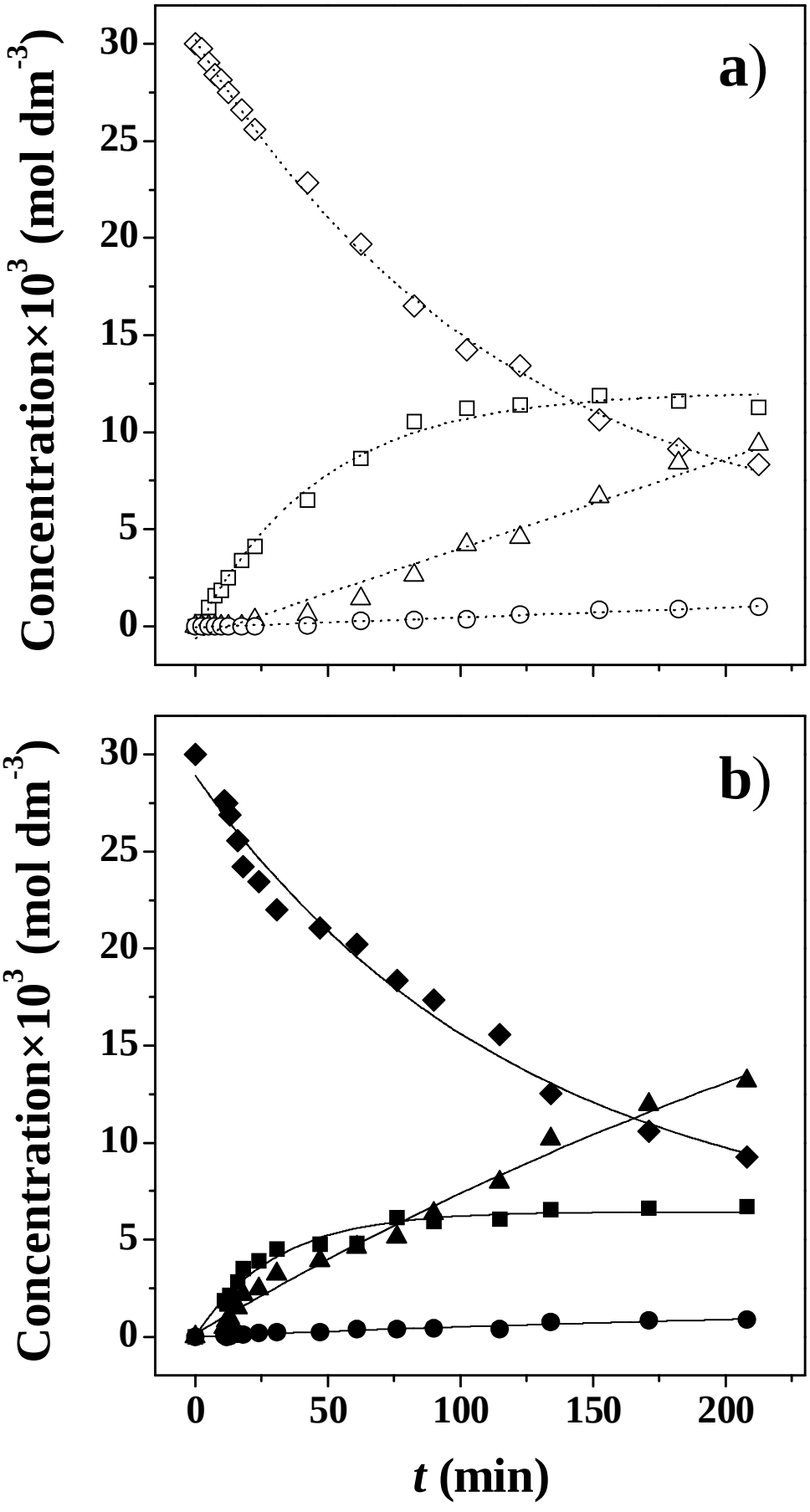

Figure 5.5: Liquid phase composition (in terms of molar concentration of 2,4-DCP (◇,◆), 2-CP (□,■), PhOH (△,▲) and cyclohexanone (○,●)) as a function of Pd/Al_2O_3/2,4-DCP contact time (*t*) in a) discontinuous (open symbols) and b) continuous (solid symbols) operation.

where x_i represent the molar fraction of compound i and k_j is the pseudo first order rate constant for step j. From a combination of eqns. **(5.9)** and **(5.10)**:

$$\frac{dx_{2\text{-}CP}}{dx_{2,4\text{-}DCP}} = \frac{k_1 x_{2,4\text{-}DCP} - k_4 x_{2\text{-}CP}}{-\left(k_1 + k_2\right) x_{2,4\text{-}DCP}} \tag{5.12}$$

which, when integrated gives

$$x_{2\text{-}CP} = \frac{L}{1-M} \times \left[\left(x_{2,4\text{-}DCP} \right)^M - x_{2,4\text{-}DCP} \right] \tag{5.13}$$

where

$$L = \frac{k_1}{k_1 + k_2} \quad \therefore \quad M = \frac{k_4}{k_1 + k_2} \tag{5.14}$$

The significance of the L and M parameters, in terms of HDC mechanism, is summarized in **Table 5.2**. The results of data fitting to eqn. **(5.13)** are presented in **Figure 5.6** where a higher 2-CP content (at the same fractional 2,4-DCP conversion) characterizes discontinuous operation. The extracted values of L and M are given in **Table 5.1**.

Table 5.2: Mechanistic significance of the parameters *L* and *M* (see Figure 5.2 and eqn. (5.14)).

Case	*L*	*M*	Mechanistic Considerations
1	$L = 0$	-	$k_1 = 0$: no contribution due to stepwise HDC.
2	$L \neq 0$		$k_1 \neq 0$: involvement of stepwise HDC.
2a	$0 < L < 1$		$k_2 > 0$: both stepwise and concerted HDC routes possible, the concerted pathway is prevalent when $L \rightarrow 0$.
2b	$L = 1$		$k_2 = 0$: no contribution due to concerted HDC.
3	-	$M = 0$	$k_4 = 0$: no contribution due to sequential HDC, *i.e.* 2-CP HDC to PhOH does not occur.
4		$M \neq 0$	$k_4 \neq 0$: involvement of sequential HDC, *i.e.* 2-CP HDC to PhOH.

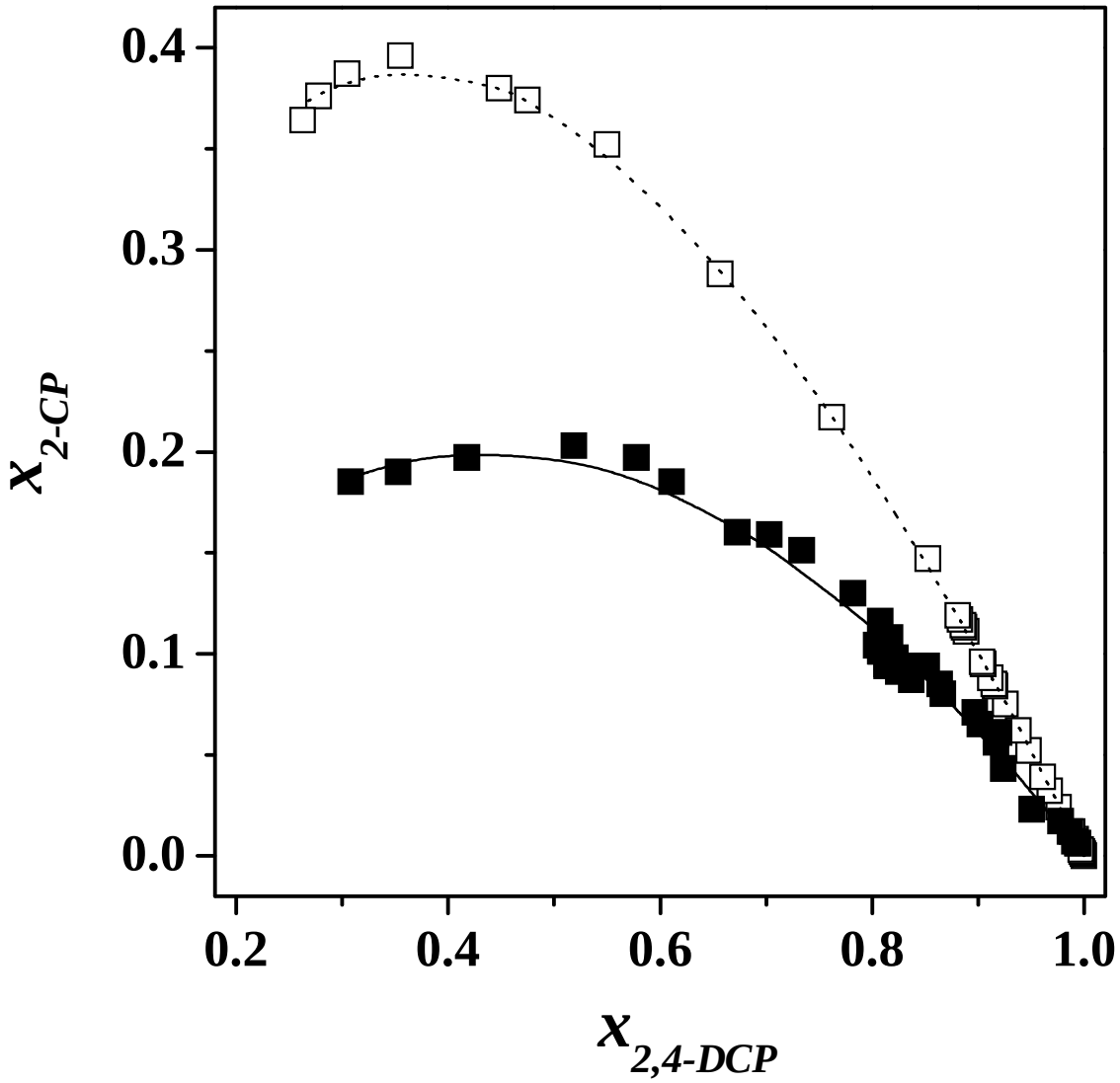

Figure 5.6: Relationship between 2-CP ($x_{2\text{-}CP}$) and 2,4-DCP molar fractions ($x_{2,4\text{-}DCP}$) in discontinuous (□) and continuous (■) operation. Note: lines represent fit to eqn. (5.13).

A strictly consecutive reaction network should yield a value of L close to unity, *i.e.* $k_2 = 0$, and the (significantly) lower L value generated for the continuous reactor is consistent with an enhanced concerted HDC to PhOH. The M value, *i.e.* ≥ 1 for both systems, suggests an equivalent or higher 2-CP HDC relative to 2,4-DCP and this is consistent with an electrophilic reaction mechanism [9,30,63]. The experimental data establish that the hydrogen scission of both C–Cl bonds is promoted to a greater extent in the continuous reactor operated under catalytic control, which leads to higher $(R_{HDC})_0$. In order to account for this response, the reaction pH must be considered as this has been established [19,64] as the critical factor that controls aqueous phase chlorophenol(s) HDC by influencing the nature of the species in solution and the catalyst surface charge.

Under basic conditions (pH = 12), the 2,4-DCP reactant and 2-CP intermediate are dissociated in solution as chlorophenolate species (pK = 7.9 and 8.5, respectively [65]). The catalyst is characterised by pH_{pzc} = 7.7, *i.e.* the pH at which the accessible wetted catalyst surface is electrically neutral. When pH > pH_{pzc} the catalyst surface bears a negative charge which does not favour interaction with (chlorophenolate) anions in solution [66]. A significant HCl component is released during HDC [67,68], with the result that the "local" pH, *i.e.* that associated with the liquid/solid interfacial layer ($pH_{l/s}$), can be quite different from that in the bulk liquid (pH) and at the support surface (pH_{pzc}) [69]. When $pH_{pzc} < pH_{l/s} \leq$ pH (*i.e.* low surface HCl concentration), catalyst interaction with chlorophenolate species is limited but at $pH_{l/s} < pH_{pzc} <$ pH, the catalyst surface develops a positive charge where chlorophenolate interaction(s) are facilitated. Since the bulk pH response is equivalent for both reactors (see inset to **Figure 5.4**), the difference in selectivity response must be linked to a distinct $pH_{l/s}$. It has been demonstrated previously ([69] and **Chapter 2**) that, when $pH_{pzc} < pH_{l/s}$ (= 13), the concerted 2,4-DCP HDC route (*i.e.* k_2 in **Figure 5.2**) is inhibited leading to the selectivity response observed (in **Figure 5.6**) for the batch reactor. It follows that the involvement of the concerted route in the continuous system must be linked to a lower "local" pH value so that $pH_{l/s} < pH_{pzc} <$ pH. This response can be tentatively attributed to a reduced liquid/solid interfacial layer resulting from the continuous flow of liquid over the catalyst particles.

It is known that the thickness of a fluid film on a solid surface is inversely proportional to the relative velocity between them [70,71]. In the batch reactor (see **Figure 5.1**a) the mechanical stirring keeps the slurry in suspension where, considering the fine (38 μm) catalyst size, the solution/particle relative velocity approaches unity [14,70]. On the contrary, in the continuous reactor (**Figure 5.1**b) the catalyst is mainly fluidized by the upstream flow where the lateral shaking represents a secondary source of particle suspension. Therefore, the relative velocity between the liquid and the catalyst must be greater (to overcome deposition/sedimentation) and this results in a "thinner" liquid/solid interfacial layer [72,73]. With a decrease in the volume of this layer, the local HCl concentration is higher and $pH_{l/s} < pH_{pzc} <$ pH. A direct comparison of these results with the available literature on aqueous phase chlorophenol(s) HDC is not feasible as the role of pH in determining reactant/catalyst interactions has not received any explicit treatment.

Nevertheless, it is worth to flag the work of David and Vannice [74] who, studying the semi-batch liquid phase hydrotreatment of 4-chloro-N,N-dibenzylaniline over Pd/C, quoted a shift in reaction selectivity (from exclusive debenzylation to full HDC) when varying bulk solution pH (0.1 → 12) and attributed this to the impact of pH on the catalyst/reactant surface interactions. These results demonstrate that a shift from batch to continuous operation serves to enhance HDC efficiency, which are linked to pH effects at the solid/liquid interface that are sensitive to the mode of operation.

5.3.3 Catalyst Life in Discontinuous vs. Continuous Operation

Batch HDC operation is compromised somewhat in terms of catalyst reuse. A temporal decline in activity is a general feature of HDC reactions and has been attributed to the action of the HCl by-product, which induces metal leaching [75,76], poisoning (*via* electronic modifications) [77-80], sintering [77] and/or coke formation [75,76]. This has been observed regardless of the support (oxide [75-78], carbon [79,80]) or metal (Ni [77,78], Pd [75,79,80], Ru [76]) used. In the case of Pd/Al_2O_3, a decline in HDC activity with reuse in batch liquid operation has been ascribed [15,18] principally to HCl poisoning of small Pd clusters.

HDC performance (in terms of x_{Cl}) in both reactors can be assessed in **Figure 5.7** in terms of the total number of chlorine moles in the feed that had been processed. These results refer to repeated catalyst use in processing successive (up to 10) batches in discontinuous mode and extending continuous operation to arrive at a common total feed processed. It can be seen that the continuous reactor exhibited a continual enhancement in the level of dechlorination (relative to that in discontinuous operation) to deliver a five-fold higher x_{Cl}; bulk solution pH was again invariant. Continuous flow operation serves to extend catalyst life and this can be linked to a more effective transport of the HCl away from the catalyst surface. Urbano and Marinas [81] have also attributed a greater degree of (Pd) catalyst deactivation during HDC in batch (relative to continuous) systems to a prolonged HCl contact with the catalyst surface. The benefits of moving from batch to continuous operation then not only include a more efficient H_2 transport (section **5.3.1**) and an enhanced HDC efficiency (section **5.3.2**) but also extended productive catalyst life.

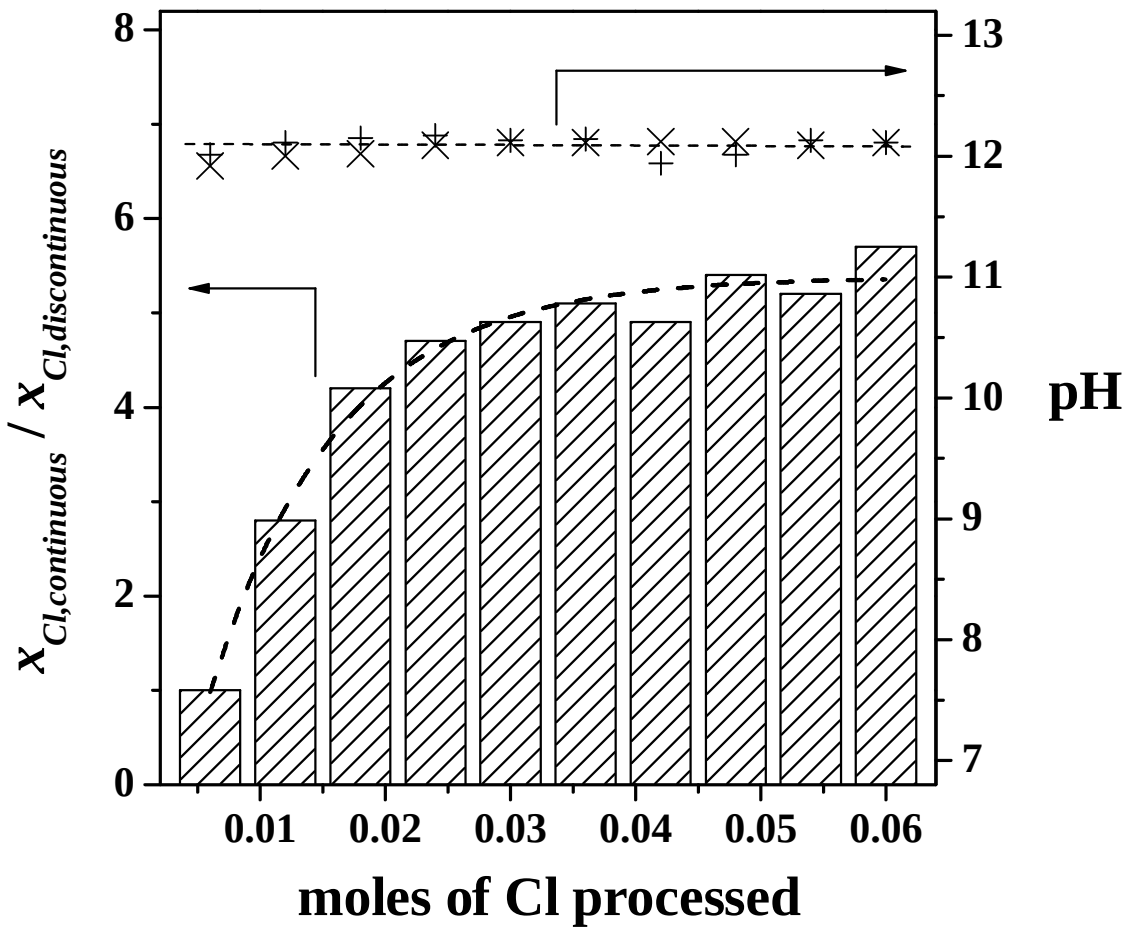

Figure 5.7: Ratio of fractional dechlorination obtained in continuous ($x_{Cl,continuous}$) to discontinuous ($x_{Cl,discontinuous}$) operation as a function of moles of chlorine processed. Note: the associated pH for discontinuous (+) and continuous (×) operation is also given; t = 24 min.

5.4 Conclusions

The liquid phase catalytic HDC of 2,4-DCP (pH = 12.1 ± 0.1, 303 K, 1 atm) over Pd/Al_2O_3 has been studied in batch and continuous flow reactors. Operation of both reactors generated 2-CP as the only partially dechlorinated product, PhOH was the main product of complete HDC and cyclohexanone was isolated in trace quantities (selectivity ≤ 4 %). Reaction conditions have been established for operation in the absence of limitations due to H_2 diffusion, where the continuous reactor delivered a five-fold higher efficiency with respect to H_2 transfer as a result of an enhanced gas/liquid interface. A switch from batch to continuous mode resulted in an increase in HDC rate (and lower 2-CP selectivity) as a result of a decrease in pH at the liquid/solid interface due to the greater relative solution/catalyst velocity. Furthermore, a prolonged productive catalyst life is a feature of continuous operation due to a more effective removal of HCl by-product.

This study establishes the feasibility of operating chloroarene HDC in a continuous flow reactor and can serve as the basis for future process scale-up and/or industrial implementation.

5.5 References

[5.1] F. Muller, L. Caillard, Ullmann's Encyclopedia of Industrial Chemistry. "Chlorophenols", Wiley-VCH Verlag GmbH & Co. KGaA, Weinheim, 2000.

[5.2] USEPA, Advisory Document No. 8EHQ-14302, 2000.

[5.3] M. Dilaver, F. Kargi, Bioresour. Technol., 100, 1459 (2009)

[5.4] P. Kintz, A. Tracqui, P. Mangin, Arch. Toxicol., 66, 298 (1992)

[5.5] USEPA, The Inventory of Sources of Dioxin in the United States. EPA/600/P-98/00A2, 1998.

[5.6] L. Wu, A. Li, G. Gao, Z. Fei, S. Xu, Q. Zhang, J. Mol. Catal. A: Chemical, 269, 183 (2007)

[5.7] H. Cheng, K. Scott, P. A. Christensen, Appl. Catal. A: General, 261, 1 (2004)

[5.8] B. F. Hagh, D. T. Allen, Chem. Eng. Sci., 45, 2695 (1990)

[5.9] Y. A. Serguchev, Y. V. Belokopytov, Kinet. Catal., 42, 174 (2001)

[5.10] E.-J. Shin, M. A. Keane, J. Hazard. Mater. B, 66, 265 (1999)

[5.11] J. B. Hoke, G. A. Gramiccioni, E. N. Balko, Appl. Catal. B: Environmental, 1, 285 (1992)

[5.12] L. Calvo, A. F. Mohedano, J. A. Casas, M. A. Gilarranz, J. J. Rodríguez, Carbon, 42, 1377 (2004)

[5.13] G. S. Pozan, I. Boz, J. Hazard. Mater. B, 136, 917 (2006)

[5.14] G. Yuan, M. A. Keane, Chem. Eng. Sci., 58, 257 (2003)

[5.15] G. Yuan, M. A. Keane, Appl. Catal. B: Environmental, 52, 301 (2004)

[5.16] G. Yuan, M. A. Keane, J. Catal., 225, 510 (2004)

[5.17] G. Yuan, M. A. Keane, Catal. Commun., 4, 195 (2003)

[5.18] G. Yuan, M. A. Keane, Catal. Today, 88, 27 (2003)

[5.19] M. A. Keane, J. Chem. Technol. Biotechnol., 80, 1211 (2005)

[5.20] G. Yuan, M. A. Keane, Ind. Eng. Chem. Res., 46, 705 (2007)

[5.21] G. Centi, J. Mol. Catal. A: Chemical, 173, 287 (2001)

[5.22] P. Albers, J. Pietsch, S. F. Parker, J. Mol. Catal. A: Chemical, 173, 275 (2001)

[5.23] T. Hara, T. Kaneta, K. Mori, T. Mitsudome, T. Mizugaki, K. Ebitani, K. Kaneda, Green Chem., 9, 1246 (2008)

[5.24] B. Aristizábal, C. A. González, I. Barrio, M. Montes, C. M. de Correa, J. Mol. Catal. A: Chemical, 222, 189 (2004)

[5.25] Z. M. de Pedro, L. M. Gómez-Sainero, E. González-Serrano, J. J. Rodríguez, Ind. Eng. Chem. Res., 45, 7760 (2006)

[5.26] R. Gopinath, N. S. Babu, J. V. Kumar, N. Lingaiah, P. S. S. Prasad, Catal. Lett., 120, 312 (2008)

[5.27] J. M. Smith, Chemical Engineering Kinetics, McGraw-Hill, Singapore, 1981.

[5.28] J. R. Anderson, K. C. Pratt, Introduction to Characterization and Testing of Catalysts, Academic Press, London, 1985.

[5.29] H. Hildebrand, K. MacKenzie, F.-D. Kopinke, Global NEST J., 10, 47 (2008)

[5.30] T. Yoneda, T. Takido, K. Konumaa, J. Mol. Catal. A: Chemical, 265, 80 (2007)

[5.31] E. Ding, S. Jujjuri, M. Sturgeon, S. G. Shore, M. A. Keane, J. Mol. Catal. A: Chemical, 294, 51 (2008)

[5.32] J. Feng, B.-W. Zhu, T.-T. Lim, Chemosphere, 73, 1817 (2008)

[5.33] R. F. Bueres, E. Asedegbega-Nieto, E. Díaz, S. Ordóñez, F. V. Díez, Catal. Commun., 9, 2080 (2008)

[5.34] A. Kabir, W. D. Marshall, Green Chem., 3, 47 (2001)

[5.35] T. Yuan, W. D. Marshall, J. Environ. Monit., 4, 452 (2002)

[5.36] J. Halász, S. Mészáros, I. Hannus, React. Kinet. Catal. Lett., 87, 359 (2006)

[5.37] E.-J. Shin, M. A. Keane, Chem. Eng. Sci., 54, 1109 (1999)

[5.38] E.-J. Shin, M. A. Keane, Appl. Catal. B: Environmental, 18, 241 (1998)

[5.39] E.-J. Shin, M. A. Keane, React. Kinet. Catal. Lett., 69, 3 (2000)

[5.40] E.-J. Shin, M. A. Keane, J. Chem. Technol. Biotechnol., 75, 159 (2000)

[5.41] E.-J. Shin, M. A. Keane, Catal. Lett., 58, 141 (1999)

[5.42] G. Yuan, J. Llanos López, C. Loius, L. Delannoy, M. A. Keane, Catal. Commun., 6, 555 (2005)

[5.43] G. Yuan, C. Louis, L. Delannoy, M. A. Keane, J. Catal., 247, 256 (2007)

[5.44] M. A. Keane, J. Chem. Technol. Biotechnol., 82, 787 (2007)

[5.45] J.-C. Charpentier, Chem. Eng. J., 107, 3 (2005)

[5.46] L. Calvo, M. A. Gilarranz, J. A. Casas, A. F. Mohedano, J. J. Rodríguez, Appl. Catal. B: Environmental, 67, 68 (2006)

[5.47] L. Calvo, M. A. Gilarranz, J. A. Casas, A. F. Mohedano, J. J. Rodríguez, J. Hazard. Mater., 161, 842 (2009)

[5.48] E. Díaz, J. A. Casas, A. F. Mohedano, L. Calvo, M. A. Gilarranz, J. J. Rodríguez, Ind. Eng. Chem. Res., 48, 3351 (2009)

[5.49] U. D. Patel, S. Suresh, J. Colloid Interface Sci., 319, 462 (2008)

[5.50] S. Gómez-Quero, F. Cárdenas-Lizana, M. A. Keane, AIChE J., Accepted., (2009)

[5.51] Y. Shindler, Y. Matatov-Meytal, M. Sheintuch, Ind. Eng. Chem. Res., 40, 3301 (2001)

[5.52] G. S. Pozan, I. Boz, Environ. Eng. Sci., 25, 1197 (2008)

[5.53] B. Pawelec, V. La Parola, R. M. Navarro, S. Murcia-Mascaro, J. L. G. Fierro, Carbon, 44, 84 (2006)

[5.54] H. Wang, F. Zhao, Int. J. Mol. Sci., 8, 628 (2007)

[5.55] H. H. Lee, Heterogeneous Reactor Design, Butterworths, London, 1985.

[5.56] N. Frikha, E. Schaer, J.-L. Houzelot, Chem. Eng. J., 124, 19 (2006)

[5.57] A. A. C. M. Beenackers, W. P. M. van Swaaij, Chem. Eng. Sci., 48, 3109 (1993)

[5.58] L. Takić, V. Veljković, M. Lazić, S. Pejanović, J. Serb. Chem. Soc., 72, 847 (2007)

[5.59] R. M. Machado, R. R. Broekhuis, A. F. Nordquist, B. P. Roy, S. R. Carney, Catal. Today, 105, 305 (2005)

[5.60] C. N. Satterfield, Heterogeneous Catalysis in Practice, McGraw-Hill, New York, 1980.

[5.61] R. P. Danner, T. E. Daubert, Manual for Predicting Chemical Process Design Data, Design Institute for Physical Property Data, New York, 1983.

[5.62] D. R. Lide, Handbook of Chemistry and Physics, 90th ed., Taylor and Francis Group, Boca Raton, 2009.

[5.63] F. Alonso, I. P. Beletskaya, M. Yus, Chem. Rev., 102, 4009 (2002)

[5.64] J. Wei, X. Xu, Y. Liu, D. Wang, Water Res., 40, 348 (2006)

[5.65] X. Liu, J. Chen, H. Yu, J. Zhao, J. P. Giesy, X. Wang, Chemosphere, 64, 1619 (2006)

[5.66] J. Vakros, C. Kordulis, A. Lycourghiotis, J. Chem. Soc. Chem. Commun., 17, 1980 (2002)

[5.67] A. Gampine, D. P. Eyman, J. Catal., 179, 315 (1998)

[5.68] Z. C. Zhang, B. C. Beard, Appl. Catal. A: General, 174, 33 (1998)

[5.69] S. Gómez-Quero, F. Cárdenas-Lizana, M. A. Keane, Ind. Eng. Chem. Res., 47, 6841 (2008)

[5.70] J. F. Douglas, J. M. Gasiorek, J. A. Swaffield, Fluid Mechanics, Longman Scientific and Technical, Essex, 1987.

[5.71] S. L. Soo, Fluid Dynamics of Multiphase Systems, Blaisdell Publishing Company, Massachusetts, 1967.

[5.72] C. N. Satterfield, Mass Transfer in Heterogeneous Catalysis, M.I.T. Press, Massachusetts, 1970.

[5.73] J. Levec, S. Goto, Mass Transfer and Kinetics in Three Phase Reactors, Handbook of Heat and Mass Transfer Volume 2: Mass Transfer and Reactor Design, Gulf Publishing Company, Houston, 1986.

[5.74] A. David, M. A. Vannice, J. Catal., 237, 349 (2006)

[5.75] M. I. Cobo, J. A. Conesa, C. M. de Correa, J. Phys. Chem. A, 112, 8715 (2008)

[5.76] K. V. R. Chary, C. S. Srikanth, V. V. Rao, Catal. Commun., 10, 459 (2009)

[5.77] X. Liu, J. Chen, J. Zhang, Ind. Eng. Chem. Res., 47, 5362 (2008)

[5.78] W. Wu, J. Xu, R. Ohnishi, Appl. Catal. B: Environmental, 60, 129 (2005)

[5.79] E. V. Golubina, E. S. Lokteva, V. V. Lunin, N. S. Telegina, A. Y. Stakheev, P. Tundo, Appl. Catal. A: General, 302, 32 (2006)

[5.80] J. W. da Silva, R. E. Bruns, A. J. G. Cobo, Chem. Eng. J., 131, 59 (2007)

[5.81] F. J. Urbano, J. M. Marinas, J. Mol. Catal. A: Chemical, 173, 329 (2001)

Chapter 6

Gas Phase Hydrotreatment of Chlorophenols as an Alternative Route to Cyclohexanone

In order to probe the wider implications of catalytic hydroprocessing using Pd/Al_2O_3, the gas phase continuous flow hydrotreatment of chlorophenols has been considered. This work has focused on the viability of generating cyclohexanone, as a valuable commercial product, from the conversion of mono- and di-chlorophenols. The results of a systematic analysis of cyclohexanone production are presented, focusing on the role of Pd particle size and hydrogen spillover. This alternative route to cyclohexanone is demonstrated to be superior when compared with the traditional phenol hydrogenation approach.

6.1 Introduction

Cyclohexanone (C6ONE) is an important commercial chemical, serving as the raw material in the preparation of Nylon 6 and Nylon 6,6 [1,2], C6ONE-formaldehyde copolymers [3,4] and is used as solvent in the manufacture of herbicides and synthetic resins [5,6]. C6ONE production typically involves (a) oxidation of cyclohexane [7-9], (b) dehydrogenation of cyclohexanol (C6OH) [10-13] or (c) hydrogenation of phenol (PhOH) [14-16] but each of these syntheses presents decided drawbacks. Cyclohexane oxidation generates low C6ONE yields (Y_{C6ONE} = 3 - 4 %) [8,9] and the reactant + O_2 mixture is highly flammable under reaction conditions [7]. C6OH dehydrogenation is endothermic (63 kJ mol^{-1}) and requires high operation temperatures (523 - 573 K) to raise the C6ONE content where PhOH [10,11] and cyclohexene [12,13] are significant by-products (up to 80 % selectivity). PhOH hydrogenation also presents limitations in that, under thermodynamic control, the equilibrium fractional conversion falls below 0.8 at $T \geq 530$ K [10,16] while a higher catalytic conversion is hampered by a temperature-induced desorption of PhOH where $T \geq 433$ K [14,15]. Nevertheless, this is the preferred route where Y_{C6ONE} up to 80 % (with C6OH as by-product) have been recorded over supported Pd catalysts.

A higher selectivity to the ketone over Pd has been linked to the *d*-character of this metal [15], where the complete *d* shell ([Kr] $4d^{10}$) promotes a shielding effect of the valence 5*s* electrons [17] that enhances hydrogenation of PhOH to C6ONE (*via* tautomerization of the 1-cyclohexenol intermediate, see **Figure 6.1**) [18,19]. Nevertheless, the associated C6OH content is still high for industrial applications and at least three distillation columns operating below atmospheric pressure are required to effectively separate C6ONE from the C6OH by-product [20,21]. Recently, C6ONE has been identified as a product from the catalytic hydrodechlorination and further hydrogenation of chlorophenols [22-24]. This transformation involves the consecutive/parallel steps that are shown in **Figure 6.1**. Baumgarten *et al.* [25], studying the gas phase (T = 413 K) hydroprocessing of 2-chlorophenol (2-CP) over polymer supported Pt, correlated a high C6ONE content in the product stream (Y_{C6ONE} = 80 %) with a reduction in Pt electron density due to support effects, which lead to reactant/catalyst interactions that inhibited C6OH formation. Roy and co-workers [26] recorded Y_{C6ONE} values up to 73 % in the batch liquid phase (T = 298 K) reaction of 2,6-dichlorophenol (2,6-DCP) over Pd/Al_2O_3 using H_2 (4 atm) as reductant, while C6OH (16 % yield) was exclusively formed in the presence of $NaBH_4$ as hydrogen donor. C6ONE production from chlorophenols can be regarded as a relatively unexplored synthesis route where metal-support interactions and/or the hydrogen source appear to impact on product distribution/yield. Moreover, chlorophenols are widely available in the industry "pool" as intermediates in agricultural chemicals, pharmaceuticals and dyes [27], which means that they represent a readily available starting material.

The published studies of chlorophenol hydrotreatment have focused on environmental remediation applications in terms of a controlled chlorine removal [28,29]. This report is the first feasibility study directed at (continuous, gas phase) C6ONE production using aqueous solutions as feedstock to achieve a cleaner synthesis [30]. The role of metal particle size has been investigated, considering the catalytic action of bulk Pd as a starting point, before examining alumina and silica supported Pd systems to address the possible contribution of spillover hydrogen. A comprehensive search through the open literature did not unearth any report dealing with the gas phase hydrotreatment of PhOH or chlorophenols over bulk Pd. The benefits of the chlorophenol → C6ONE process are assessed with regard to the conventional synthesis from PhOH. This study is a novel contribution in terms of developing a new efficient route to C6ONE.

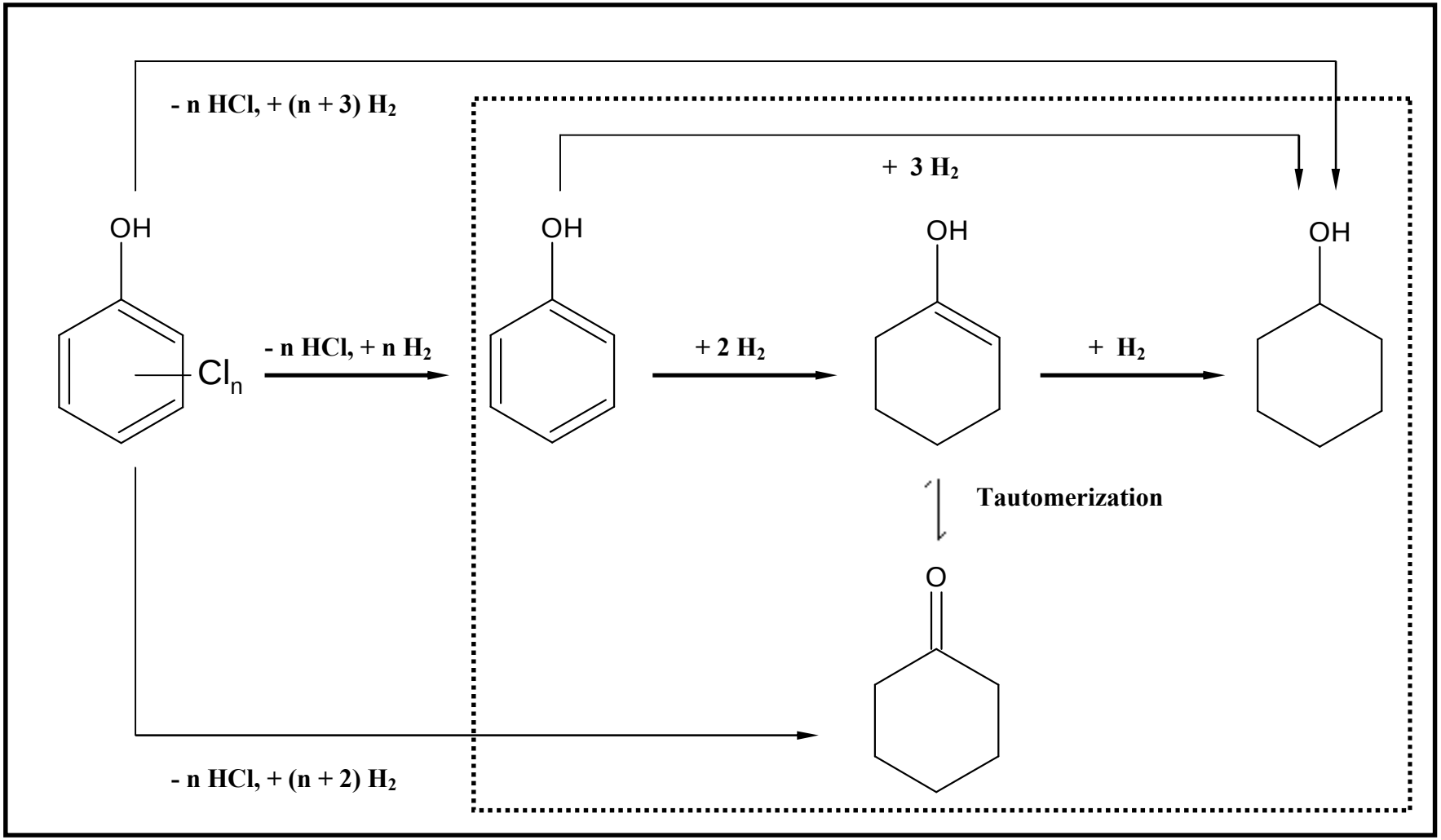

Figure 6.1: Reaction pathway for the production of C6ONE and C6OH *via* PhOH hydrogenation (dotted box) and/or chlorophenols hydrodechlorination+hydrogenation (solid box). Note: stepwise mechanism is identified by bold arrows.

6.2 Experimental

6.2.1 Catalyst Preparation and Activation

PdO (99.998 %) was purchased from Sigma-Aldrich and served as the unsupported Pd precursor. Three supported Pd catalysts have been considered in this study: a commercial (Sigma-Aldrich) 1.2 % w/w Pd/Al_2O_3 (Pd/Al_2O_3-A) and two laboratory synthesised (by impregnation as described elsewhere [31,32]) samples, *i.e.* 6.9 % w/w Pd/Al_2O_3 (Pd/Al_2O_3-B) and 5.2 % w/w Pd/SiO_2. The Pd content (accurate to within ± 2 %) was measured by inductively coupled plasma-optical emission spectrometry (ICP-OES, Vista-PRO, Varian Inc.) from the diluted extract in HF. The Pd/Al_2O_3-A sample was subjected to a thermal treatment to 1273 K (denoted Pd/Al_2O_3-A1) and 573 K (denoted Pd/Al_2O_3-A2) in order to vary Pd particle size as discussed elsewhere ([33] and **Chapter 2**). Prior to reaction, all the catalysts were sieved (ATM fine test sieves) into a batch of 45 μm average particle diameter and activated in a H_2 flow (60 cm^3 min^{-1}) at 1 - 10 K min^{-1} to a final temperature in the range 423 - 523 K (± 1 K), maintaining this temperature for 1.5 h before cooling (if necessary) to 423 K (the reaction temperature).

6.2.2 Catalyst Characterization

Temperature programmed reduction (TPR), H_2 chemisorption and temperature-programmed desorption (H_2-TPD) were performed using the commercial CHEM-BET 3000 (Quantachrome Instruments) unit. The samples were loaded into a U-shaped (i.d. = 3.76 mm, l = 100 mm) quartz cell, contacted (at room temperature) with 5 % v/v H_2/N_2 (17 cm^3 min^{-1}) and activated by TPR as described in section **6.2.1**. The effluent gas passed through a liquid N_2 trap and changes in H_2 consumption/release were monitored by a thermal conductivity detector (TCD) with data acquisition/manipulation using the TPR Win™ software. After TPR, the reduced samples were swept with a 65 cm^3 min^{-1} flow of N_2 for 1.5 h, cooled to room temperature and subjected to H_2 chemisorption using a pulse (50 μl) titration procedure, under conditions where Pd hydride formation does not occur (H_2 partial pressure < 9 Torr [31]). The H_2 pulses were repeated until the signal area was constant and Pd particle size was estimated from H_2 uptake on the basis of dissociative chemisorption (H_2/Pd = 1/2) on (pseudo-)spherical metal particles [34,35].

The samples were then thoroughly flushed (under the same flow of N_2) and H_2-TPD was subsequently conducted by heating the samples to 873 K at 50 K min^{-1}. Hydrogen chemisorption/desorption values were reproducible to within ± 5 % and the values quoted here are the mean. XRD analyses were conducted using a Bruker/Siemens D500 incident X-ray diffractometer with Cu Kα radiation. The samples were scanned at 0.02º $step^{-1}$ over the range 20º ≤ 2θ ≤ 90º (scan time = 5 s $step^{-1}$) and the diffractogram patterns were compared with the JCPDS-ICDD references (Card No. 05-0681 (Pd) and 10-0425 (γ-Al_2O_3)). Selected catalysts were also subjected to transmission electron microscopy (TEM) analysis: JEOL JEM 2011 TEM unit with a UTW energy-dispersive X-ray detector (Oxford Instruments) operated at an accelerating voltage of 200 kV and using Gatan DigitalMicrograph 3.4 for data acquisition/manipulation. The samples were dispersed in acetone and deposited on a holey-carbon/Cu grid (300 Mesh). At least 650 individual Pd particles were counted to generate a surface area-weighted mean value as described previously [36,37].

6.2.3 Catalysis Procedure

The reactants, PhOH (+99.0 %), 2-CP (+99.0 %), 3-CP (98.0 %), 4-CP (+99 %), 2,3-DCP (98.0 %), 2,4-DCP (98.0 %) and 3,4-DCP (99.0 %) were supplied by Sigma-Aldrich and used without further purification. Reactions were carried out under atmospheric pressure *in situ*, immediately after TPR activation, in a fixed bed vertical plug-flow glass reactor (i.d. = 15 mm, l = 600 mm). The catalytic reactor, and operating conditions to ensure negligible heat/mass transport limitations, have been fully described elsewhere [38], but details of relevance to this study are given below. The reactants were delivered (as aqueous solutions) to the reactor *via* a glass/teflon air-tight syringe and a teflon line using a microprocessor controlled infusion pump (Model 100 kd Scientific) where the ratio of catalyst to phenolic flow rate (n_{Pd}/F_{OH}) spanned the range 1 × 10^{-3} - 1.33 mol_{Pd} h mol_{OH}^{-1}. The use of F_{OH} facilitates a direct comparison of process efficiency in terms of Y_{C6ONE} with respect to the "parent" phenolic ring with/without Cl substituent(s). A co-current flow of ultra pure H_2 (60 cm^3 min^{-1}) was monitored using a Humonics (Model 520) digital flowmeter and maintained at a $GHSV$ = 2 × 10^4 h^{-1}. A layer of glass beads above the catalytic bed served as a preheating zone, ensuring that the reactants were vaporized and reached reaction temperature before contacting the catalyst.

The reaction temperature was set at 423 K as it has been established for catalytic operations that PhOH undergoes a temperature-induced desorption where $T \geq 433$ K [14,15]. Moreover, a low operating temperature is critical in the development of a less energy intensive process [39]. Isothermal conditions were maintained by diluting the catalytic bed with (unless otherwise specified) Al_2O_3 (45 μm), where the reaction temperature was continuously monitored by a thermocouple inserted in a thermowell within the catalyst bed. In a series of blank tests, passage of each reactant in a stream of H_2 through the empty reactor or over the support alone, *i.e.* in the absence of Pd, did not result in any detectable conversion. The reactor effluent was frozen in a liquid nitrogen trap for subsequent analysis which was made using a Perkin-Elmer Auto System XL GC, employing a DB-1 (J&W Scientific) capillary column (i.d. = 0.20 mm, l = 50 m, film thickness = 0.33 μm) as described previously [40]. A chlorine mass balance was performed by passing the effluent gas through an aqueous NaOH trap (9×10^{-4} mol dm^{-3}, kept under constant agitation at 400 rpm) with independent pH (Hanna HI Programmable Printing pH Bench-Meter) analysis; HCl was the only inorganic product, as noted elsewhere [41]. Repeated reactions with different samples from the same batch of catalyst delivered raw data reproducibility that was better than ± 8 %. Taking 2,4-DCP as representative reactant, the overall level of hydrodechlorination (and hydrogenation) is quoted as a fractional conversion ($X_{2,4\text{-}DCP}$):

$$X_{2,4\text{-}DCP} = \frac{C_{2,4\text{-}DCP,0} - C_{2,4\text{-}DCP}}{C_{2,4\text{-}DCP,0}} \quad \textbf{(6.1)}$$

where $C_{2,4\text{-}DCP,0}$ and $C_{2,4\text{-}DCP}$ represent the concentration of the reactant in the inlet and outlet stream, respectively. The fractional selectivity to, for example, C6ONE (S_{C6ONE}) is given by

$$S_{C6ONE} = \frac{C_{C6ONE}}{C_{2,4\text{-}DCP,0} - C_{2,4\text{-}DCP}} \quad \textbf{(6.2)}$$

where C_{C6ONE} is the outlet C6ONE concentration and the fractional yield (Y_{C6ONE}) is calculated from:

$$Y_{C6ONE} = X_{2,4\text{-}DCP} \times S_{C6ONE} \quad \textbf{(6.3)}$$

6.3 Results and discussion

6.3.1 Thermodynamic Considerations

It is well established that gas phase PhOH hydrogenation is thermodynamically restricted [10,16]. However, the author could not find any reported thermodynamic data for coupled hydrodechlorination+hydrogenation of chlorophenols. Accordingly, the possibility of thermodynamic limitations in this coupled system has been evaluated considering consecutive reaction steps (taking the mechanism shown in **Figure 6.1**) and drawing on reference equilibrium reaction data [16,42]:

$$K_1 = \frac{\left(P_{monochlorophenol}\right)\left(P_{HCl}\right)}{\left(P_{dichlorophenol}\right)\left(P_{H_2}\right)} = 35.6 \times \exp\left(\frac{17216}{T}\right) \quad \textbf{(6.4)}$$

$$K_2 = \frac{\left(P_{PhOH}\right)\left(P_{HCl}\right)}{\left(P_{monochlorophenol}\right)\left(P_{H_2}\right)} = 2.5 \times \exp\left(\frac{4063}{T}\right) \quad \textbf{(6.5)}$$

$$K_3 = \frac{P_{C6ONE}}{\left(P_{PhOH}\right)\left(P_{H_2}\right)^2} = \left(2.7604 \times 10^{-16}\right) \times \exp\left(\frac{20131}{T}\right) \quad \textbf{(6.6)}$$

$$K_4 = \frac{P_{C6OH}}{\left(P_{C6ONE}\right)\left(P_{H_2}\right)} = \left(3.6844 \times 10^{-7}\right) \times \exp\left(\frac{7897}{T}\right) \quad \textbf{(6.7)}$$

where K_j represent the equilibrium constant of step j, P_i is the partial pressure of *i* (total pressure = 1 atm) and *T* the reaction temperature (K). Eqns. **(6.4)** and **(6.5)** apply to the hydrodechlorination of di- and mono-chlorophenols, respectively, while eqns. **(6.6)** and **(6.7)** apply to the series of partial hydrogenation steps PhOH → C6ONE → C6OH. The values of K_j and the equilibrium conversions (X_i) at reaction temperature (423 K) are given in **Table 6.1**, where it is immediately evident that all steps can be taken as irreversible. Taking into consideration the steps leading to ketone formation (phenolic reactant → C6ONE, $X_i \approx 1$) and consumption (C6ONE → C6OH, $X_i \approx 0.87$), the maximum Y_{C6ONE} under conditions of thermodynamic control is 0.13. It must be noted that this value is the same when using chlorophenol(s) or PhOH as feedstock, *i.e.* the preceding dechlorination step does not affect the equilibrium Y_{C6ONE}.

Table 6.1: Calculated equilibrium constants (K_j) and conversions (X_i) associated with the consecutive steps in the hydrotreatment of chlorophenols and PhOH at T = 423 K (see Figure 6.1 and eqns. (6.4 - 6.7)).

Reaction step	K_j	X_i
dichlorophenol → monochlorophenol	2×10^{20}	1.000
monochlorophenol → PhOH	4×10^{4}	0.995
PhOH → C6ONE	1×10^{6a}	1.000
C6ONE → C6OH	47^{b}	0.865

[a]units: atm^{-2}
[b]units: atm^{-1}

C6ONE production from chlorophenols is then a thermodynamically feasible route where, in order to elevate Y_{C6ONE}, operation under kinetic (rather than thermodynamic) control is critical. Once this is achieved, the next step is to establish reaction conditions where Y_{C6ONE} is higher from the coupled chlorophenol hydrodechlorination+hydrogenation relative to the direct hydrogenation of PhOH.

6.3.2 Reaction over Pd+Al_2O_3

Bulk Pd (physically mixed with Al_2O_3) was chosen as a starting point to consider C6ONE production from chlorophenols and PhOH. This approach has been taken in order to facilitate an explicit examination of the catalytic response exhibited by Pd, avoiding any possible contribution due to metal/support interaction(s) and/or variations in metal particle size, which are known to influence hydrogenation [43-45] and hydrodechlorination [46-48] reactions.

6.3.2.1 Catalyst Characterization

The characteristics of the model (bulk) Pd+Al_2O_3 catalytic system are shown in **Figure 6.2** and **Table 6.2**. The TPR response shown in **Figure 6.2**a (Profile I) generated a single negative peak (H_2 release) at 386 K. This signal can be associated with the decomposition of β-Pd hydride. Room temperature formation of β-Pd hydride is a well established bulk phenomenon where H_2 migrates into the octahedral voids of the Pd crystal lattice where the partial pressure exceeds 0.013 atm [49,50].

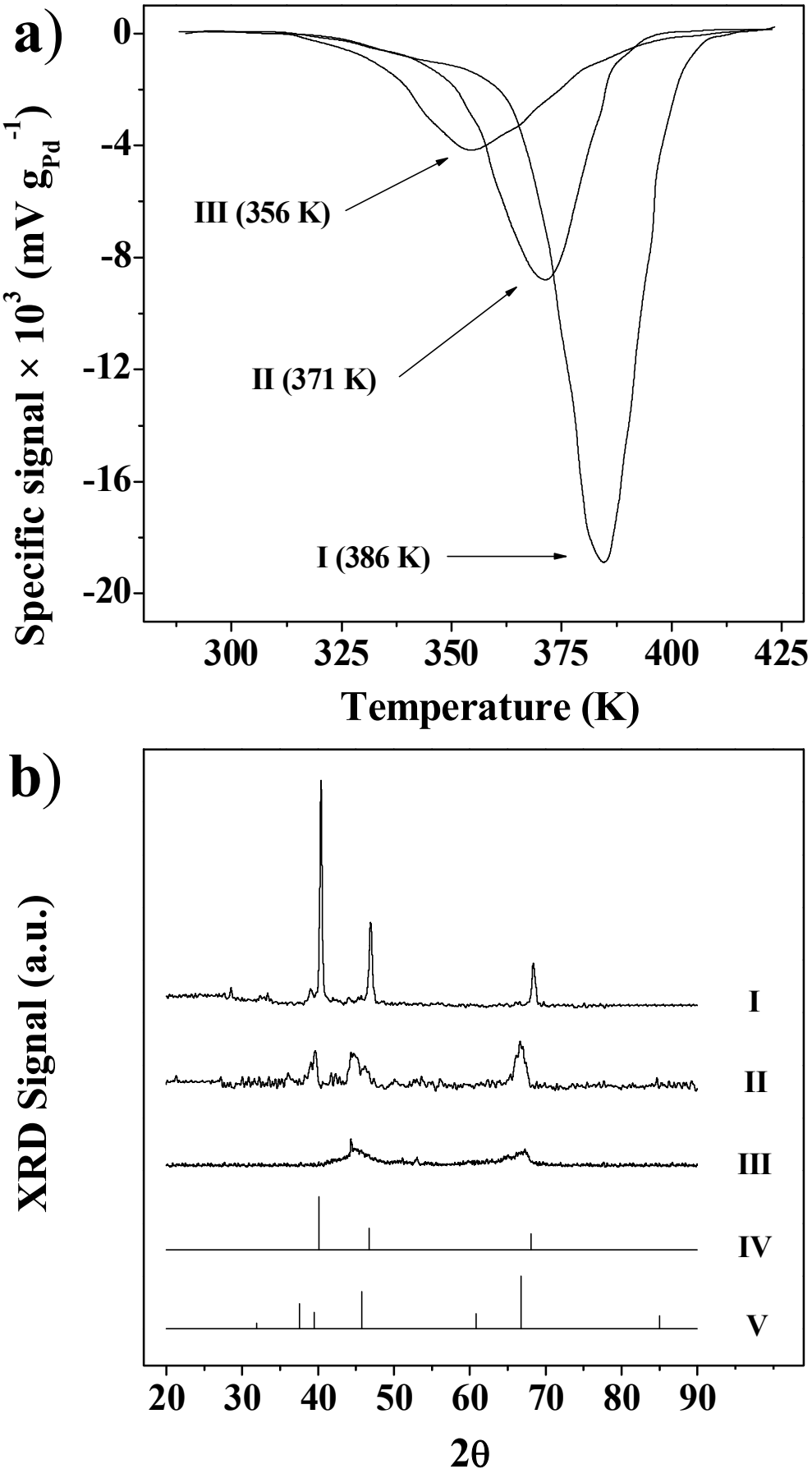

Figure 6.2: a) TPR response and b) XRD patterns for passivated/reduced Pd+Al_2O_3 (I), Pd/Al_2O_3-A1 (II) and Pd/Al_2O_3-A2 (III). Note: XRD includes JCPDS-ICDD reference data for metallic Pd (Card. No. 05-0681, IV) and γ-Al_2O_3 (Card. No. 10-0425, V).

Table 6.2: β-Pd hydride decomposition temperature (TPR T_{max} (K)) and stoichiometry (H_{ab}/Pd), H_2 chemisorption and associated Pd particle size (d_{Chem}) and specific initial C6ONE production rate ($(R'_{C6ONE})_0$) for Pd+Al_2O_3 and Pd/Al_2O_3.

Catalyst	Pd+Al_2O_3	Pd/Al_2O_3-A1[a]	Pd/Al_2O_3-A2[b]
TPR T_{max} (K)	386	371	356
H_{ab}/Pd ($\mu mol_H\ \mu mol_{Pd}^{-1}$)	0.69	0.33	0.15
H_2 chemisorption ($\times 10^{-2}\ \mu mol_{H_2}\ \mu mol_{Pd}^{-1}$)	0.32	8	58
d_{Chem} (nm)	250[c]	13[d]	2[e]
S_{Pd} ($m_{Pd}^2\ g_{Pd}^{-1}$)[f]	2	38	250
$(R'_{C6ONE})_0$ ($\times 10^{-4}\ mol_{C6ONE}\ h^{-1}\ m_{Pd}^{-2}$)	94	68	49

[a]thermal treatment to 1273 K (10 K min^{-1})
[b]thermal treatment to 573 K (10 K min^{-1})
[c]XRD derived Pd particle size = 238 nm
[d]TEM derived Pd particle size = 10 nm
[e]TEM derived Pd particle size = 3 nm
[f]$S_{Pd} = 6 / (\rho_{Pd} \times d_{chem})$ where $\rho_{Pd} = 12.02\ g_{Pd}\ cm_{Pd}^{-3}$

The β-Pd hydride composition can be represented by the ratio H_{ab}/Pd where H_{ab} is the number of absorbed H atoms and the value (= 0.69 $\mu mol_H\ \mu mol_{Pd}^{-1}$, see **Table 6.2**) recorded in this study is in good agreement with those reported previously, *i.e.* 0.66 - 0.73 $\mu mol_H\ \mu mol_{Pd}^{-1}$ [46,51]. There was no detectable H_2 uptake or release by/from the Al_2O_3 support over the same temperature range, which was expected and is consistent with the literature [52,53]. The absence of a positive peak during TPR in advance of H_2 release presupposes the existence of metallic Pd prior to the commencement of the temperature ramp. Indeed, there is evidence in the literature that the reduction of supported [54,55] and unsupported PdO [56] occurs at room temperature. It should be noted that β-Pd hydride decomposition temperature (*i.e.* 386 K) is lower than the activation/reaction temperature (*i.e.* 423 K) and, therefore, the contribution of absorbed H_2 as reactive species during catalysis can be ruled out. Hydrogen chemisorption measurement post-activation delivered an uptake of $0.32 \times 10^{-2}\ \mu mol_{H_2}\ \mu mol_{Pd}^{-1}$ (see **Table 6.2**) with an associated Pd particle size (d_{Chem}) of 250 nm. XRD analysis of the activated sample generated the diffractogram pattern shown in **Figure 6.2**b (Profile I). The profile is characterised by reflections at 2θ = 40.1º, 46.7º and 68.1º corresponding, respectively, to the (111), (200) and (220) planes of cubic Pd (JCPDS-ICDD Card No. 05-0681, Profile IV), demonstrating the presence of zero-valent Pd post-activation at 423 K.

The XRD-derived (based on line broadening using the Scherrer formula) Pd particle size (= 238 nm, see footnote to **Table 6.2**) confirms the value obtained from H_2 chemisorption.

6.3.2.2 Catalytic Hydrotreatment of (Chloro)Phenol(s)

The time-on-stream profiles for the hydrotreatment of chlorophenols are presented in **Figure 6.3**, where C6ONE was the main product (up to 80 % mol). C6OH and PhOH were generated as secondary products with trace quantities (selectivity ≤ 0.02) of chlorophenols isolated in the product stream, *i.e.* conditions of essentially complete hydrodechlorination. A variation in product composition with time on-stream is observed in all cases and can be linked to catalyst poisoning by HCl (as by-product) and/or coke deposition [57,58]. The initial product distribution was evaluated from [59,60]:

$$x_i = x_{i,0} \times \exp\left(-\alpha \times \Delta t\right) \qquad \textbf{(6.8)}$$

where x_i represents molar fraction of i, Δt the integral time and α is a fitting parameter. Non-linear fitting of the experimental data (OriginLab 7.5, see **Figure 6.3**) allows an estimation of the initial molar fractions ($x_{i,0}$) and the corresponding values of initial C6ONE yield ($Y_{C6ONE,0}$) from eqns. **(6.1 - 6.3)**; the results are given in **Table 6.3**. The $Y_{C6ONE,0}$ values recorded for the hydroprocessing of chlorophenols were higher (up to 6 times) than that which would result from thermodynamic control. Moreover, the chlorophenolic feed delivered higher $Y_{C6ONE,0}$ than that obtained from PhOH under the same reaction conditions (see **Figure 6.4** and **Table 6.3**). As shown in **Figure 6.1**, C6ONE production from PhOH occurs *via* the formation and tautomerization of 1-cyclohexenol as intermediate [61,62], where the equilibrium is thermodynamically shifted to the ketone by 75 kJ mol^{-1} [63,64]. In the case of chlorophenols, C6ONE production can proceed through stepwise and/or concerted routes where the latter must be responsible for the greater $Y_{C6ONE,0}$ observed here. If the hydrotreatment of chlorophenols proceeded in a strictly stepwise manner (consecutive hydrodechlorination, hydrogenation and tautomerization steps), Y_{C6ONE} should not exceed that obtained from PhOH.

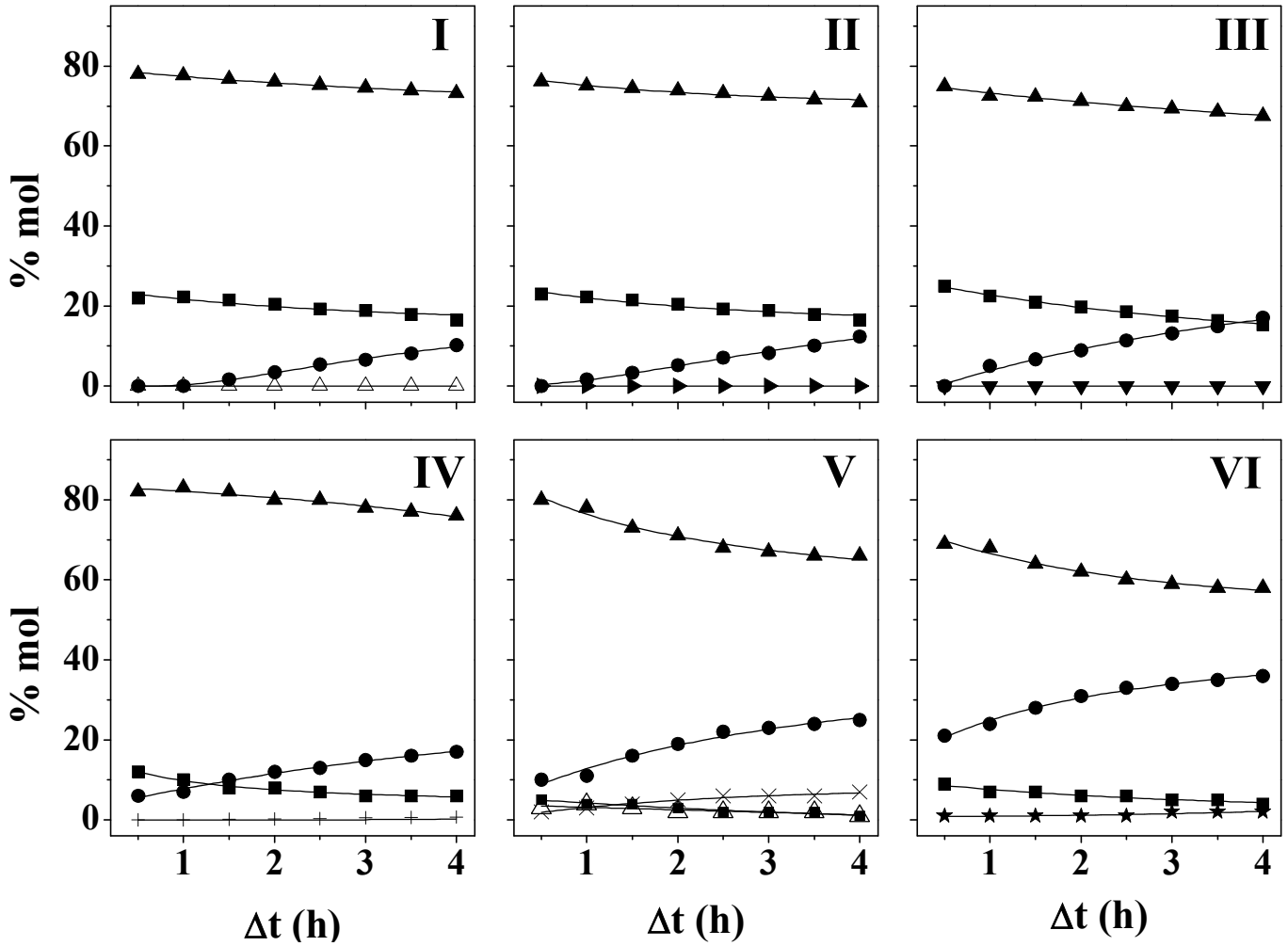

Figure 6.3: Time-on-stream profiles for C6OH (■), C6ONE (▲) and PhOH (●) production *via* hydrodechlorination+hydrogenation of 2-CP (I,△), 3-CP (II,▶), 4-CP (III, ▼), 2,3-DCP (IV,+), 2,4-DCP (V,×) and 3,4-DCP (VI,★) over Pd+Al_2O_3: (n_{Pd}/F_{OH}) = 1.33 mol_{Pd} h mol_{OH}^{-1}. Note: lines represent fit to eqn. (6.8).

Table 6.3: Initial selectivities ($S_{i,0}$) and C6ONE yields ($Y_{C6ONE,0}$) resulting from the hydrotreatment of PhOH and representative chlorophenols over Pd+Al_2O_3; (n_{Pd}/F_{OH}) = 1.33 mol_{Pd} h mol_{OH}^{-1}.

Reactant	$S_{PhOH,0}$	$S_{C6ONE,0}$	$S_{C6OH,0}$	$Y_{C6ONE,0}$
PhOH	-	0.83	0.17	0.62
2-CP	0	0.77	0.23	0.77
3-CP	0	0.76	0.24	0.76
4-CP	0	0.75	0.25	0.75
2,3-DCP	0.07	0.80	0.13	0.80
2,4-DCP[a]	0.10	0.82	0.06	0.82
3,4-DCP[b]	0.19	0.69	0.11	0.69

[a]2-CP present in trace amounts ($S_{2\text{-}CP,0} \leq 0.02$)
[b]3-CP present in trace amounts ($S_{3\text{-}CP,0} \leq 0.01$)

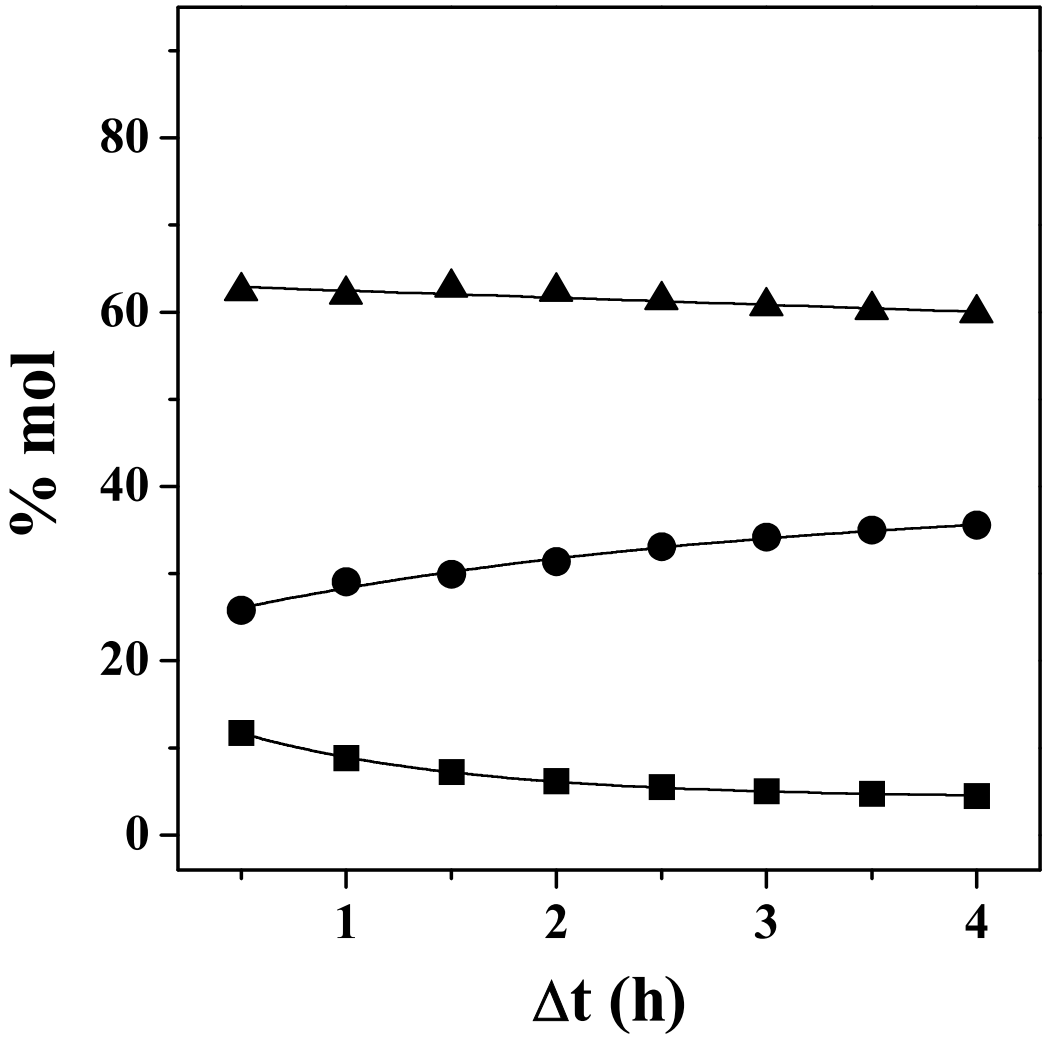

Figure 6.4: Time-on-stream product composition in terms of C6OH (■) and C6ONE (▲) generated *via* the hydrogenation of PhOH (●) over Pd+Al_2O_3: (n_{Pd}/F_{OH}) = 1.33 mol_{Pd} h mol_{OH}^{-1}. Note: lines represent fit to eqn. (6.8).

An alternative route to C6ONE from chlorophenols can involve (electrophilic) attack to the chlorophenol by hydrogen to generate a cationic reaction intermediate that is stabilized by electron delocalization within the aromatic ring [65,66]. The latter includes a contribution due to the lone pair of electrons in the –OH group that stabilises an intermediate bearing the C=O group [67-69], leading to a preferential C6ONE formation. These results support our contention that, operating under catalytic/kinetic control, chlorophenols serve as an effective alternative feed for C6ONE production where $Y_{C6ONE,0}$ increased with increasing Cl substitution following the order PhOH < 2-CP, 3-CP, 4-CP < 2,3-DCP, 2,4-DCP. A lower $Y_{C6ONE,0}$ obtained from the 3,4-DCP isomer suggests that the relative position of the Cl substituents on the ring can influence reaction pathway (concerted *vs.* stepwise mechanism in **Figure 6.1**), impacting on the ultimate C6ONE content. An explicit assessment of Y_{C6ONE} dependence on the nature of the chlorophenol isomer requires reaction conditions where hydrodechlorination is not complete. This was achieved by lowering the contact time (by a factor of 8) and the resultant $Y_{C6ONE,0}$ values are presented in **Figure 6.5**. The hydrotreatment of dichlorophenol(s) generated consistently higher $Y_{C6ONE,0}$ relative to the monochlorophenol reactants. This can be attributed to the greater number of favourable resonance forms (bearing the C=O group) in the dichlorophenol(s) that determines reactivity [42,69]. Taking the monochlorophenols, 2-CP delivered the lowest $Y_{C6ONE,0}$, a response that can be ascribed to steric hindrance effects [28,70].

6.3.3 Structure Sensitivity in the Hydrotreatment of 2,4-DCP: Reaction over Pd+Al_2O_3 and Pd/Al_2O_3

The effect of Pd particle size was considered by comparing the catalytic action of bulk Pd with Pd/Al_2O_3 of varying metal dispersion, taking the hydrotreatment of 2,4-DCP as a representative case.

6.3.3.1 Catalyst Characterization

Metal dispersion was modified by means of a controlled thermal sintering (from 573 K to 1273 K of Pd/Al_2O_3-A; see Experimental section and **Table 6.2**. The TPR activation (prior to reaction) responses are shown in **Figure 6.2**a for Pd/Al_2O_3-A1 (Profile II) and Pd/Al_2O_3-A2 (Profile III). A single negative peak is again observed and, in common with Profile I (Pd+Al_2O_3), can be associated with the decomposition of β-Pd hydride.

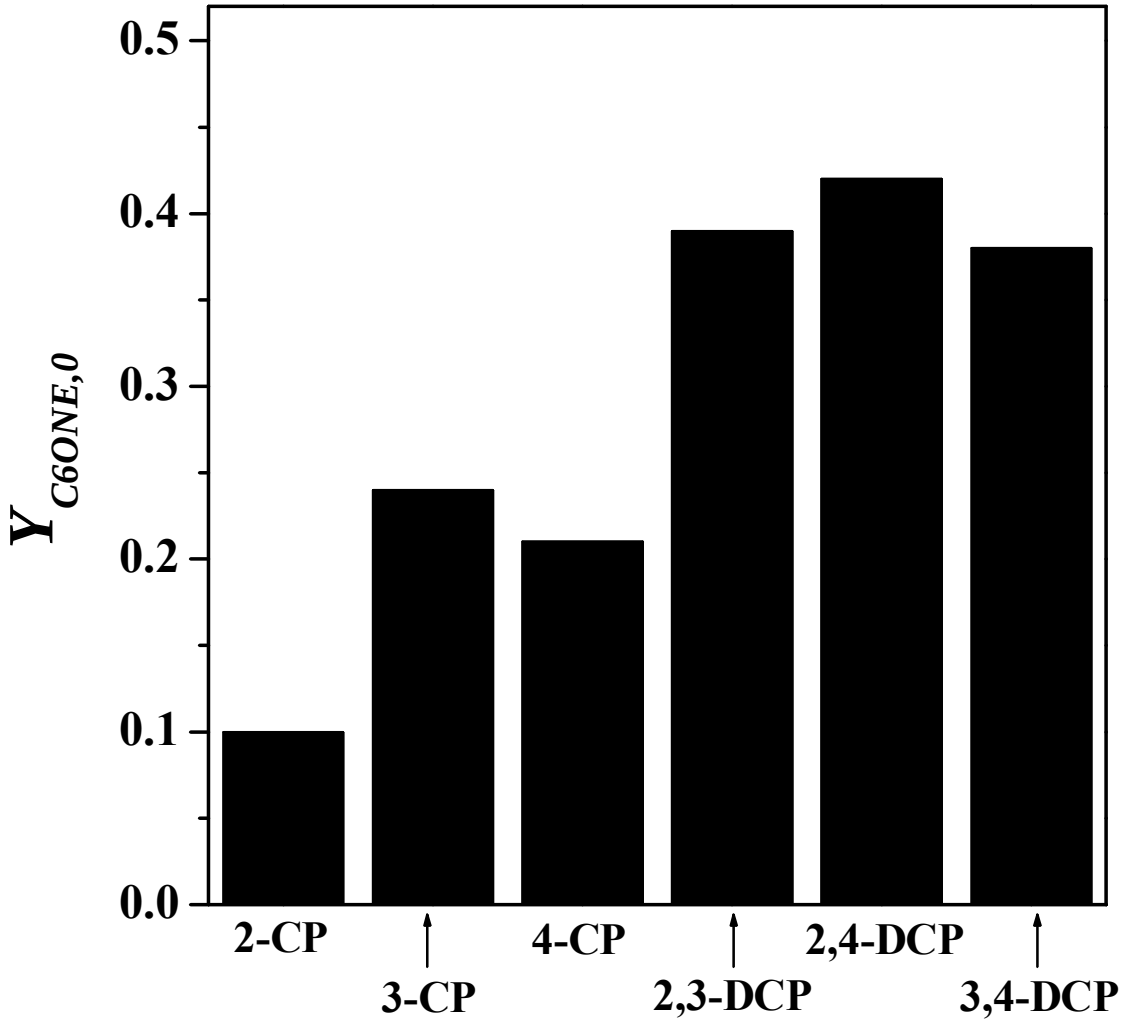

Figure 6.5: Initial C6ONE yield ($Y_{C6ONE,0}$) resulting from the hydrodechlorination+hydrogenation of mono- and di-chlorophenols over Pd+Al_2O_3: (n_{Pd}/F_{OH}) = 0.17 mol_{Pd} h mol_{OH}^{-1}.

Relative to bulk Pd, a lower hydride decomposition temperature (371 K (Pd/Al_2O_3-A1) and 356 K (Pd/Al_2O_3-A2)) was accompanied by a concomitant lower hydrogen content (H_{ab}/Pd = 0.33 μmol_H μmol_{Pd}^{-1} (Pd/Al_2O_3-A1) and 0.15 μmol_H μmol_{Pd}^{-1} (Pd/Al_2O_3-A2)). This suggests smaller Pd particle size for the supported systems where a decrease in H_{ab}/Pd with decreasing Pd size has been established in the literature [71,72]. As hydride formation is a bulk phenomenon, lower particle size is accompanied by an increase in the ratio of surface-to-bulk atoms and the void space available for H_2 diffusion in the Pd cluster is consequently lower. Hydrogen chemisorption for Pd/Al_2O_3-A1 (see **Table 6.2**) was significantly lower (seven-fold) than that recorded for Pd/Al_2O_3-A2 but appreciably (by a factor of 25) greater than that for Pd+Al_2O_3. The associated Pd particle size (d_{Chem}) decreased in the order Pd+Al_2O_3 (250 nm) > Pd/Al_2O_3-A1 (13 nm) > Pd/Al_2O_3-A2 (2 nm).

XRD profiles given in **Figure 6.2**b reveal, in each case, reflections at 2θ = 45.8º and 66.8º corresponding to the (400) and (440) planes associated with cubic γ-Al_2O_3 (JCPDS-ICDD Card No. 10-0425, Profile V). A weak signal due to metallic Pd is in evidence for Pd/Al_2O_3-A1 (Profile II) but there is no detectable response for Pd/Al_2O_3-A2 (Profile III), suggesting the presence of Pd as small ensembles in the latter, with a mean size below the XRD detection limit (< 3 - 5 nm [73,74]). Indeed, representative TEM images of Pd/Al_2O_3-A2 are shown in **Figure 6.6** where nano-scale Pd particles (in the range < 1 to 6 nm) can be seen and exhibit a pseudo-spherical morphology (see image a). There was also evidence of Pd faceting (see high magnification image b) that is diagnostic of some degree of metal/support interactions [75,76]. The surface area-weighted TEM-derived metal particle size (10 nm (Pd/Al_2O_3-A1) and 3 nm (Pd/Al_2O_3-A1)) are in good agreement with the values obtained from H_2 chemisorption (see **Table 6.2**) and serve to confirm the accuracy of the measurements.

6.3.3.2 Catalytic Performance in the Hydrotreatment of 2,4-DCP

$Y_{C6ONE,0}$ as a function of contact time over bulk and supported Pd is presented in **Figure 6.7**a where the values obtained under thermodynamic control (≤ 0.13) are represented by the shaded area. A common trend is evident for the three catalytic systems, *i.e.* a decrease in $Y_{C6ONE,0}$ with decreasing contact time. However, a direct comparison in terms of $Y_{C6ONE,0}$ at a fixed (n_{Pd}/F_{OH}) is not possible as the profiles do not overlap. In order to facilitate an explicit assessment of structure sensitivity, it is necessary to compare specific rates (per m_{Pd}^2) for the three systems. The initial C6ONE production rate $(R_{C6ONE})_0$ was calculated from the mass balance according to

$$(R_{C6ONE})_0 = \frac{dF_{C6ONE}}{dn_{Pd}} = \frac{d\left(Y_{C6ONE,0}\right)}{d\left(n_{Pd}/F_{OH}\right)} \qquad \textbf{(6.9)}$$

and specific rate $(R'_{C6ONE})_0$ was estimated from

$$(R'_{C6ONE})_0 = \frac{(R_{C6ONE})_0}{S_{Pd}} \qquad \textbf{(6.10)}$$

where S_{Pd} is the metal surface area (see **Table 6.2**).

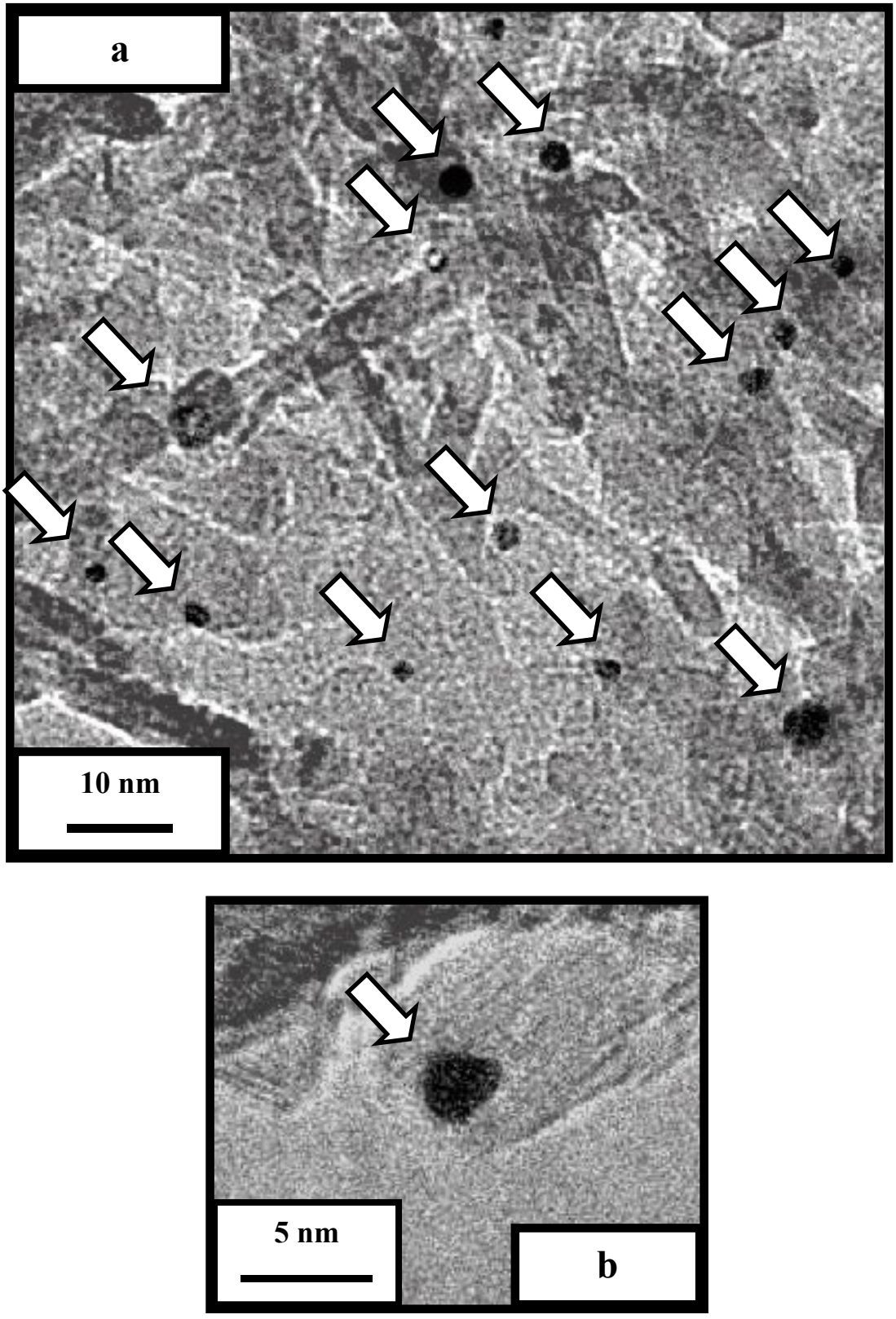

Figure 6.6: Representative a) low and b) high magnification TEM images associated with Pd/Al_2O_3-A2. Note: arrows identify Pd particles.

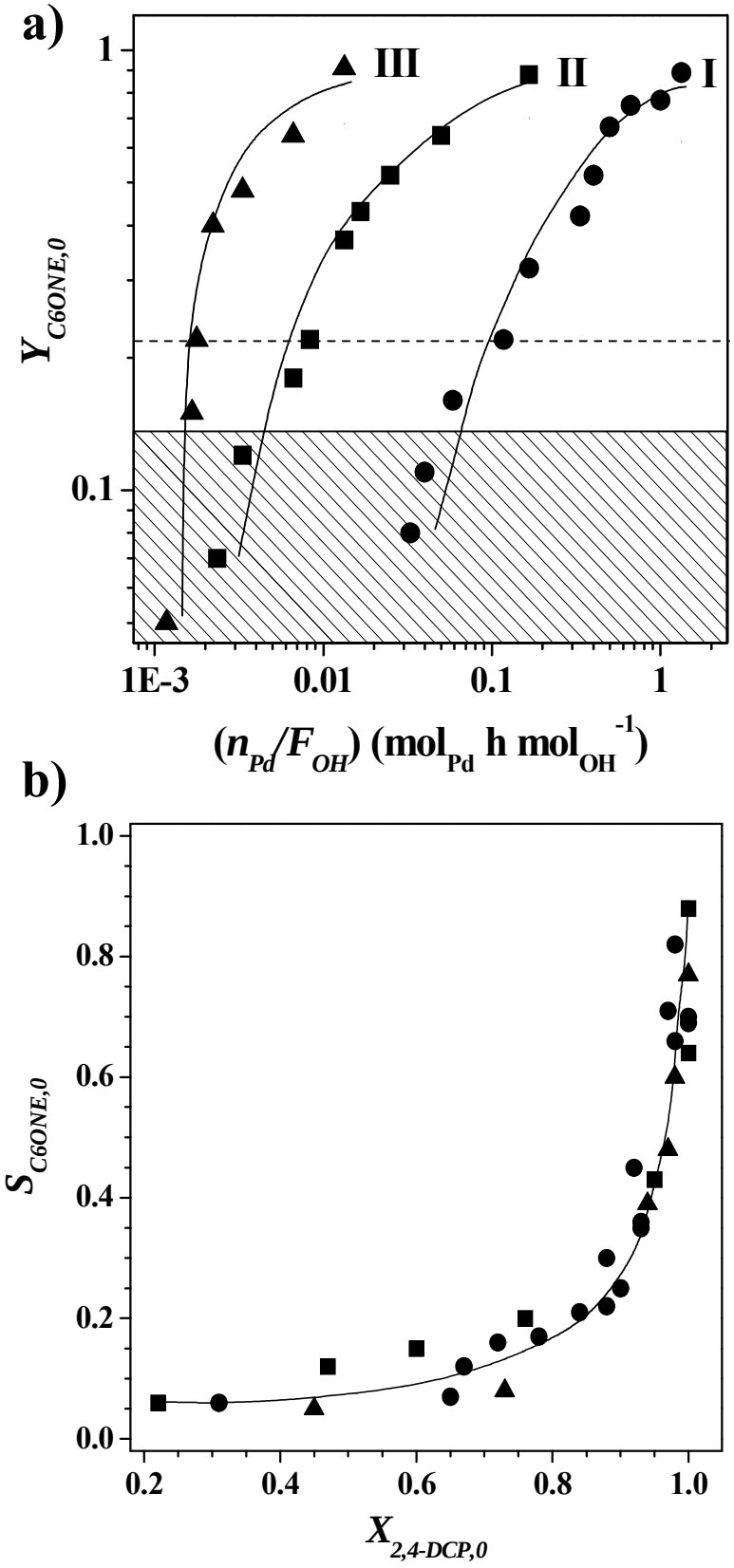

Figure 6.7: a) Initial C6ONE yield ($Y_{C6ONE,0}$) as a function of contact time ((n_{Pd}/F_{OH}), mol$_{Pd}$ h mol$_{OH}^{-1}$) and b) initial C6ONE selectivity ($S_{C6ONE,0}$) as a function of initial 2,4-DCP conversion ($X_{2,4\text{-}DCP,0}$) for hydrodechlorination+hydrogenation over Pd+Al_2O_3 (d_{Chem} = 250 nm, ●), Pd/Al_2O_3-A1 (d_{Chem} = 13 nm, ■) and Pd/Al_2O_3-A2 (d_{Chem} = 2 nm, ▲). Note: shaded area in (a) identifies yields obtained under thermodynamic control ($Y_{C6ONE} \leq 0.13$).

The resultant $(R'_{C6ONE})_0$ values increase in the following order: Pd+Al_2O_3 (94 × 10^{-4} mol_{C6ONE} h^{-1} m_{Pd}^{-2}) > Pd/Al_2O_3-A1 (68 × 10^{-4} mol_{C6ONE} h^{-1} m_{Pd}^{-2}) > Pd/Al_2O_3-A2 (49 × 10^{-4} mol_{C6ONE} h^{-1} m_{Pd}^{-2}). This response is consistent with a higher specific (per m_{Pd}^2) or intrinsic rate for larger mean Pd particle sizes. A direct comparison of these results with the literature is difficult as the observed structure sensitivity applies to coupled hydrodechlorination+hydrogenation and, to the best of the author's knowledge, only the individual processes in isolation have been considered to date. Nevertheless, the results find indirect agreement in those studies [77,78] where larger metal particles have been demonstrated to be more active in the gas phase hydrodechlorination of chlorophenols. In the case of PhOH hydrogenation, structure insensitivity has been reported for supported Pd [18,44,79] but it is worth highlighting the work of Chary *et al*. [80] who recorded a higher turnover frequency (from < 0.01 s^{-1} to 0.52 s^{-1} at T = 453 K) over larger Pd particles (2 - 8 nm) supported on carbon. It is significant that the highest specific rate was obtained for bulk Pd and, in this respect, it is worth to flag the work of Rioux *et al.* [81] and Morato *et al.* [82], who reported higher (gas phase) hydrodechlorination activity over bulk Pd and Ni when compared with the respective carbon-supported systems. The impact of variations in Pd size on the reaction network was assessed from a consideration of the dependence of initial C6ONE selectivity ($S_{C6ONE,0}$) on initial 2,4-DCP conversion ($X_{2,4\text{-}DCP,0}$), as shown in **Figure 6.7**b. It can be seen that the $S_{C6ONE,0}$ *vs.* $X_{2,4\text{-}DCP,0}$ profiles for the three catalytic systems coincide. This result suggests that Pd particle size (or metal support interactions) do not impact significantly on the reaction pathway in terms of a consecutive *vs.* concerted mechanism.

6.3.4 The Role of Spillover Hydrogen in the Hydrotreatment of 2,4-DCP

It has been proposed that the hydrogen mediated conversion of chloroarenes [83,84] and PhOH [85] can be enhanced by contributions due to spillover hydrogen. Spillover hydrogen is generated on supported metals *via* the dissociative chemisorption of H_2 on metal sites and subsequent migration of atomic hydrogen to the support [86,87]. The occurrence of hydrogen spillover has been proposed to be influenced by several factors, including the nature of the support [88,89] and the addition of support as a physical mixture [90,91]. In order to assess the possible contribution of spillover H_2 in this coupled process, Pd/Al_2O_3-B and Pd/SiO_2 were selected because, with the inclusion of additional support, should exhibit different amounts of spillover hydrogen.

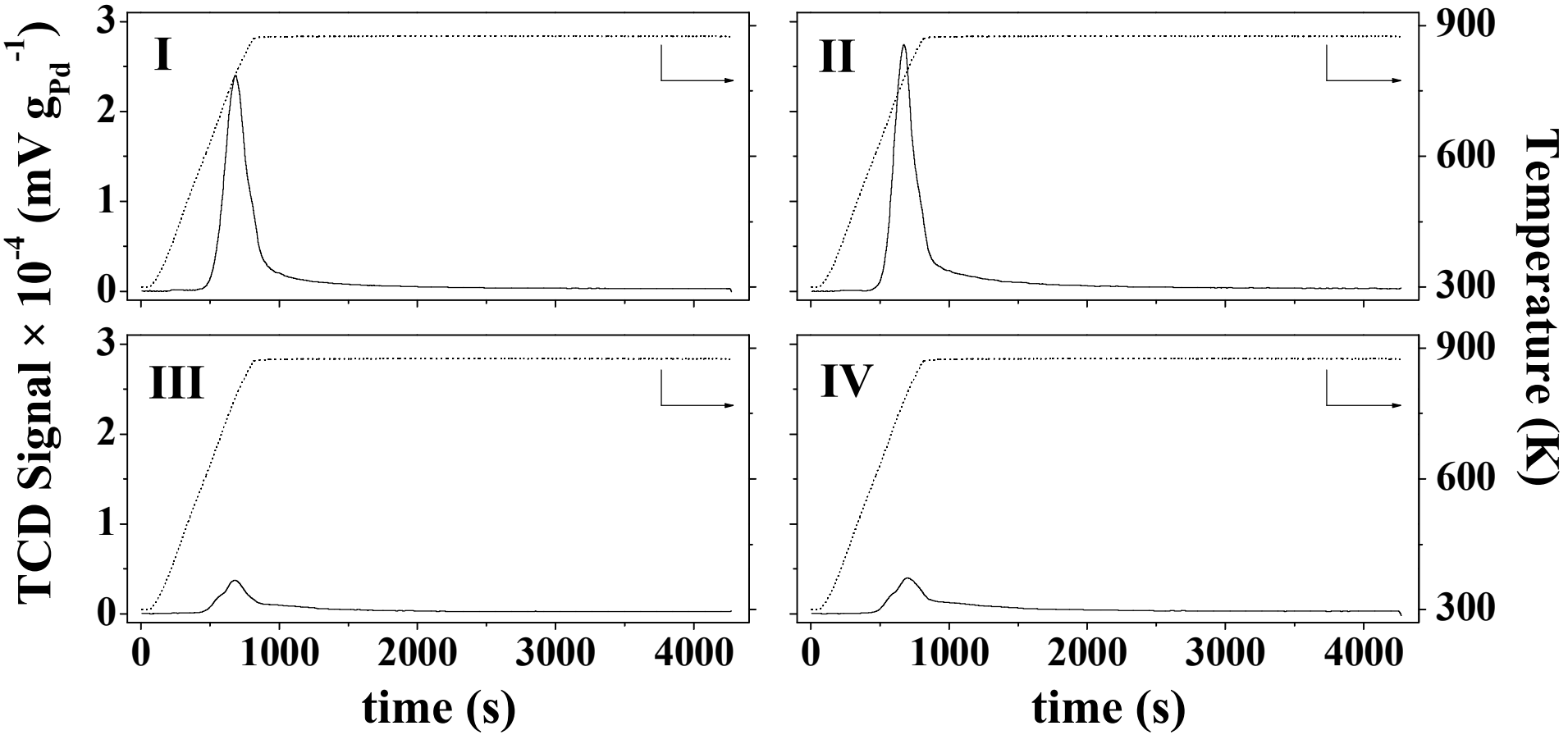

Figure 8: H_2-TPD profiles associated with Pd/Al_2O_3-B (I), Pd/Al_2O_3-B+Al_2O_3 (II), Pd/SiO_2 (III) and Pd/SiO_2+SiO_2 (IV).

Table 6.4: H_2 chemisorption, Pd particle size (d_{Chem}), H_2-TPD T_{max} and associated hydrogen released, and specific initial C6ONE production rate ($(R'_{C6ONE})_0$, $\times 10^{-4}$ mol_{C6ONE} h^{-1} m_{Pd}^{-2}) for Pd/Al_2O_3-B and Pd/SiO_2 (with/without support addition) activated at 523 K (10 K min^{-1}).

Catalytic System	H_2 chemisorption ($\times 10^{-2}$ μmol_{H_2} μmol_{Pd}^{-1})	d_{Chem} (nm)	TPD T_{max} [a] (K)	H_2 desorbed ($\times 10^{-2}$ μmol_{H_2} μmol_{Pd}^{-1})	$(R'_{C6ONE})_0$
Pd/Al_2O_3-B	0.8	66	782	118	72
Pd/Al_2O_3-B+Al_2O_3	0.9		788	128	83
Pd/SiO_2	0.8	62	790	23	25
Pd/SiO_2+SiO_2	1.0		803	30	45

The hydrogen chemisorption values post-TPR are given in **Table 6.4** where the following should be noted: (i) equivalent uptakes obtained with or without addition of support, *i.e.* H_2 chemisorption was only associated with the metal component; (ii) similar Pd particle sizes exhibited by both catalysts (d_{Chem} = 62 - 66 nm). The H_2-TPD profiles that followed chemisorption are given in **Figure 6.8**. In all cases, the profiles presented a positive peak (H_2 release) at $T \geq 780$ K where associated volume of H_2 released exceeded (by up to two orders of magnitude) that taken up in the chemisorption step (see **Table 6.4**). This response certainly suggests release of spillover hydrogen where desorption has been shown to occur at $T \geq 503$ K over Pd catalysts regardless of the oxide support (Al_2O_3 [92,93] or SiO_2 [92,94]). The H_2-TPD profile for Pd/Al_2O_3-B (Profile I) showed a more intense signal and a significantly greater volume of hydrogen desorbed (see **Table 6.4**) when compared with Pd/SiO_2 (Profile III), which is characterised by a comparable Pd loading and size. This can be explained on the basis of the greater capacity of the more acidic Al_2O_3 for spillover hydrogen [88]. Hydrogen spillover species have been viewed as electron donors where an acidic support surface (as electron acceptor) enhances electron transfer to effectively accommodate spillover [95-97]. The profiles generated for the catalyst+support mixtures (**Figure 6.8**, Profiles II and IV) are similar to those corresponding to the catalyst alone but with a significant increase in the volume of hydrogen desorbed (**Table 6.4**). A similar effect has been reported in the literature [52,98] and is consistent with an increase in spillover hydrogen. The possible influence of varying amounts of spillover hydrogen on the catalytic response was assessed by extracting the specific (per m_{Pd}^2) C6ONE production rates for each system and these are given in **Table 6.4**. It can be seen that an enhanced production of C6ONE resulted from an increase in the available surface hydrogen. As all catalytic systems present similar Pd particle sizes and (specific) H_2 uptakes, these results must be explicitly linked to the participation of spillover hydrogen and demonstrate its beneficial role in the conversion of 2,4-DCP to C6ONE over supported Pd catalysts.

6.4 Conclusions

In this contribution, the gas phase (atmospheric pressure, T = 423 K) continuous coupled hydrodechlorination+hydrogenation of chlorophenols over Pd catalysts has been established as a viable route to commercially important C6ONE.

Thermochemical calculations have revealed that hydrodechlorination is not a limiting step for C6ONE production. In the catalytic hydrotreatment of a (chloro-)phenolic feedstock, $Y_{C6ONE,0}$ increased in the order: PhOH < monochlorophenol(s) < dichlorophenol(s). This response is attributed to a facilitated conversion of chlorophenols to C6ONE by resonance stabilization of the electropositive intermediate formed *via* electrophilic hydrogen attack. Taking 2,4-DCP as a representative feed, C6ONE formation is shown to be structure sensitive where, under kinetic control, larger Pd particles (3 → 250 nm) deliver higher specific reaction rates. The reaction pathway was insensitive to Pd size resulting in a common selectivity/conversion profile. Moreover, a correlation between surface hydrogen content and C6ONE production has also been established, demonstrating the beneficial role of spillover hydrogen in the reaction. These results establish the viability of chlorophenol hydroprocessing as a new (gas phase) continuous route to C6ONE, outperforming the conventional PhOH hydrogenation methodology.

6.5 References

[6.1] J. Ritz, H. Fuchs, H. Kieczka, W. C. Moran, Ullmann's Encyclopedia of Industrial Chemistry. "Caprolactam", Wiley-VCH Verlag GmbH & Co. KGaA, Weinheim 2000.

[6.2] M. T. Musser, Ullmann's Encyclopedia of Industrial Chemistry. "Cyclohexanol and Cyclohexanone", Wiley-VCH Verlag GmbH & Co. KGaA, Weinheim, 2000.

[6.3] F. Mustata, I. Bicu, Rev. Roum. Chim., 48, 315 (2003)

[6.4] D. Głowacz-Czerwonka, M. Kucharski, J. Appl. Polym. Sci., 29, 1083 (2006)

[6.5] D. Stoye, Ullmann's Encyclopedia of Industrial Chemistry. "Solvents", Wiley-VCH Verlag GmbH & Co. KGaA, Weinheim, 2000.

[6.6] G. Collin, R. Mildenberg, M. Zander, H. Höke, W. McKillip, W. Freitag, W. Imöhi, Ullmann's Encyclopedia of Industrial Chemistry. "Resins, Synthetic", Wiley-VCH Verlag GmbH & Co. KGaA, Weinheim, 2000.

[6.7] J.-R. Chen, S.-K. Chen, J. Loss Prev. Process Ind., 18, 97 (2005)

[6.8] J. Hao, H. Cheng, H. Wang, S. Cai, F. Zao, J. Mol. Catal. A: Chemical, 271, 42 (2007)

[6.9] L.-X. Xu, C.-H. He, M.-Q. Zhu, S. Fang, Catal. Lett., 114, 202 (2007)

[6.10] E.-J. Shin, M. A. Keane, J. Catal., 73, 450 (1998)

[6.11] D. V. Cesar, C. A. Pérez, V. M. M. Salim, M. Schmal, Appl. Catal. A: General, 176, 205 (1999)

[6.12] H. Nur, H. Hamdan, React. Kinet. Catal. Lett., 66, 33 (1999)

[6.13] V. Z. Fridman, A. A. Davydov, J. Catal., 195, 20 (2000)

[6.14] Y. Z. Chen, C. W. Liaw, L. I. Lee, Appl. Catal. A: General, 177, 1 (1999)

[6.15] N. Mahata, K. V. Raghavan, V. Vishwanathan, C. Park, M. A. Keane, Phys. Chem. Chem. Phys., 3, 2712 (2001)

[6.16] N. Itoh, W.-C. Xu, Appl. Catal. A: General, 107, 83 (1993)

[6.17] Y. Makino, J. Alloys Compd., 408-412, 484 (2006)

[6.18] N. Mahata, V. Vishwanathan, J. Catal., 196, 262 (2000)

[6.19] P. Claus, H. Berndt, C. Mohr, J. Radnik, E.-J. Shin, M. A. Keane, J. Catal., 192, 88 (2000)

[6.20] K. Tan, K. Fujii, M. Nakamura, K. Hanada, in: U.S. Patent (Ed.), 1992.

[6.21] H.-P. Meier, J. van Esbroeck, E. Terweduwe, in: U.S. Patent (Ed.), 1994.

[6.22] T. T. Bovkun, Y. Sasson, J. Blum, J. Mol. Catal. A: Chemical, 242, 68 (2005)

[6.23] J. Morales, R. Hutcheson, I. F. Cheng, J. Hazard. Mater. B, 90, 97 (2002)

[6.24] L. Calvo, M. A. Gilarranz, J. A. Casas, A. F. Mohedano, J. J. Rodríguez, Appl. Catal. B: Environmental, 67, 68 (2006)

[6.25] E. Baumgarten, A. Fiebes, A. Stumpe, React. Funct. Polym., 33, 71 (1997)

[6.26] H. M. Roy, C. M. Wai, T. Yuan, J.-K. Kim, W. D. Marshall, Appl. Catal. A: General, 271, 137 (2004)

[6.27] F. Muller, L. Caillard, Ullmann's Encyclopedia of Industrial Chemistry. "Chlorophenols", Wiley-VCH Verlag GmbH & Co. KGaA, Weinheim, 2000.

[6.28] E.-J. Shin, M. A. Keane, J. Hazard. Mater. B, 66, 265 (1999)

[6.29] E.-J. Shin, M. A. Keane, Catal. Lett., 58, 141 (1999)

[6.30] C. Capello, U. Fisher, K. Hungerbühler, Green Chem., 9, 927 (2007)

[6.31] S. Jujjuri, E. Ding, E. L. Hommel, S. G. Shore, M. A. Keane, J. Catal., 239, 486 (2006)

[6.32] F. Cárdenas-Lizana, S. Gómez-Quero, M. A. Keane, Appl. Catal. A: General, 334, 199 (2008)

[6.33] S. Gómez-Quero, F. Cárdenas-Lizana, M. A. Keane, Ind. Eng. Chem. Res., 47, 6841 (2008)

[6.34] H. H. Lee, Heterogeneous Reactor Design, Butterworths, London, 1985.

[6.35] J. R. Anderson, K. C. Pratt, Introduction to Characterization and Testing of Catalysts, Academic Press, London, 1985.

[6.36] C. Amorim, M. A. Keane, J. Colloid Interface Sci., 322, 196 (2008)

[6.37] F. Cárdenas-Lizana, S. Gómez-Quero, A. Hugon, L. Delannoy, C. Louis, M. A. Keane, J. Catal., 262, 235 (2009)

[6.38] M. A. Keane, P. M. Patterson, J. Chem. Soc., Faraday Trans., 92, 1413 (1996)

[6.39] P. T. Anastas, M. M. Kirchhoff, T. C. Williamson, Appl. Catal. A: General, 221, 3 (2001)

[6.40] G. Yuan, M. A. Keane, Chem. Eng. Sci., 58, 257 (2003)

[6.41] G. Tavoularis, M. A. Keane, J. Mol. Catal. A: Chemical, 142, 187 (1999)

[6.42] E.-J. Shin, M. A. Keane, Chem. Eng. Sci., 54, 1109 (1999)

[6.43] L. M. Sikhwivhilu, N. J. Coville, D. Naresh, K. V. R. Chary, V. Vishwanathan, Appl. Catal. A: General, 324, 52 (2007)

[6.44] C. Park, M. A. Keane, J. Colloid Interface Sci., 266, 183 (2003)

[6.45] S. Scirè, S. Minicò, C. Crisafulli, Appl. Catal. A: General, 235, 21 (2002)

[6.46] C. Amorim, M. A. Keane, J. Chem. Technol. Biotechnol., 83, 662 (2008)

[6.47] R. F. Bueres, E. Asedegbega-Nieto, E. Díaz, S. Ordóñez, F. V. Díez, Catal. Commun., 9, 2080 (2008)

[6.48] R. Gopinath, N. S. Babu, J. V. Kumar, N. Lingaiah, P. S. S. Prasad, Catal. Lett., 120, 312 (2008)

[6.49] J. E. Benson, H. S. Hwang, M. Boudart, J. Catal., 30, 146 (1973)

[6.50] V. Ferrer, A. Moronta, J. Sánchez, R. Solano, S. Bernal, D. Finol, Catal. Today, 107-108, 487 (2005)

[6.51] M. Boudart, H. S. Hwang, J. Catal., 39, 44 (1975)

[6.52] F. Benseradj, F. Sadi, M. Chater, Appl. Catal. A: General, 228, 135 (2002)

[6.53] B. Ngamsom, N. Bogdanchikova, M. A. Borja, P. Praserthdam, Catal. Commun., 5, 243 (2004)

[6.54] F. Pinna, F. Menegazzo, M. Signoretto, P. Canton, G. Fagherazzi, N. Pernicone, Appl. Catal. A: General, 219, 195 (2001)

[6.55] J. A. C. Dias, J. M. Assaf, Appl. Catal. A: General, 334, 243 (2008)

[6.56] C.-W. Chou, S.-J. Chu, H.-J. Chiang, C.-Y. Huang, C.-J. Lee, S.-R. Sheen, T. P. Perng, C.-T. Yeh, J. Phys. Chem. B, 105, 9113 (2001)

[6.57] S. Ordóñez, E. Díaz, F. V. Díez, H. Sastre, React. Kinet. Catal. Lett., 90, 101 (2007)

[6.58] E. López, S. Ordóñez, F. V. Díez, Appl. Catal. B: Environmental, 62, 57 (2006)

[6.59] E.-J. Shin, M. A. Keane, Ind. Eng. Chem. Res., 39, 883 (2000)

[6.60] E.-J. Shin, M. A. Keane, Appl. Catal. B: Environmental, 18, 241 (1998)

[6.61] M. Hronec, Z. Cvengrošová, Š. Holotík, J. Mol. Catal., 91, 343 (1994)

[6.62] H. Li, J. Liu, H. Li, Mater. Lett., 62, 297 (2008)

[6.63] F. A. Carey, R. C. Atkins, Organic Chemistry, 5th ed., Mc Graw-Hill, New York, 2003.

[6.64] H. A. Smith, B. L. Stump, J. Am. Chem. Soc., 83, 2739 (1961)

[6.65] B. F. Hagh, D. T. Allen, Chem. Eng. Sci., 45, 2695 (1990)

[6.66] T. Yoneda, T. Takido, K. Konumaa, J. Mol. Catal. A: Chemical, 265, 80 (2007)

[6.67] L. Khachatryan, S. Lomnicki, B. Dellinger, Chemosphere, 68, 1741 (2007)

[6.68] R. Wang, C.-L. Chen, J. S. Gratzl, Bioresour. Technol., 96, 897 (2005)

[6.69] L. Khachatryan, R. Asatryan, B. Dellinger, J. Phys. Chem. A, 108, 9567 (2004)

[6.70] C. Xia, Y. Liu, J. Xu, J. Yu, W. Qin, X. Liang, Catal. Commun., 10, 456 (2009)

[6.71] G. Fagherazzi, A. Benedetti, S. Polizzi, A. Di Mario, F. Pinna, M. Signoretto, N. Pernicone, Catal. Lett., 32, 293 (1995)

[6.72] N. K. Nag, J. Phys. Chem. B, 105, 5945 (2001)

[6.73] S. Díaz-Moreno, D. C. Koningsberger, A. Muñoz-Páez, Nucl. Instrum. Methods Phys. Res., Sect. B, 133, 15 (1997)

[6.74] J. Liu, Microsc. Microanal., 10, 55 (2004)

[6.75] A. Y. Stakheev, L. M. Kustov, Appl. Catal. A: General, 188, 3 (1999)

[6.76] G. C. Bond, Chem. Soc. Rev., 20, 441 (1991)

[6.77] C. Menini, C. Park, E.-J. Shin, G. Tavoularis, M. A. Keane, Catal. Today, 62, 355 (2000)

[6.78] E.-J. Shin, M. A. Keane, React. Kinet. Catal. Lett., 69, 3 (2000)

[6.79] S. Narayanan, K. Krishna, Appl. Catal. A: General, 174, 221 (1998)

[6.80] K. V. R. Chary, D. Naresh, V. Vishwanathan, M. Sadakane, W. Ueda, Catal. Commun., 8, 471 (2007)

[6.81] R. M. Rioux, C. D. Thompson, N. Chen, F. H. Ribeiro, Catal. Today, 62, 269 (2000)

[6.82] A. Morato, C. Alonso, F. Medina, P. Salagre, J. E. Sueiras, R. Terrado, A. Giralt, Appl. Catal. B: Environmental, 23, 175 (1999)

[6.83] X. Liu, J. Chen, J. Zhang, Ind. Eng. Chem. Res., 47, 5362 (2008)

[6.84] Y. Hashimoto, A. Ayame, Appl. Catal. A: General, 250, 247 (2003)

[6.85] N. Mahata, V. Vishwanathan, J. Mol. Catal. A: Chemical, 120, 267 (1997)

[6.86] A. J. Du, S. C. Smith, X. D. Yao, G. Q. Lu, J. Am. Chem. Soc., 129, 10201 (2007)

[6.87] K. A. Pokrovski, A. T. Bell, J. Catal., 241, 276 (2006)

[6.88] W. C. Conner, J. L. Falconer, Chem. Rev., 95, 759 (1995)

[6.89] P. A. Sermon, G. C. Bond, Catal. Rev.-Sci. Eng., 8, 211 (1973)

[6.90] M. A. Keane, G. Tavoularis, React. Kinet. Catal. Lett., 78, 11 (2003)

[6.91] L. Huang, Y. Zhu, C. Huo, H. Zheng, G. Feng, C. Zhang, Y. Li, J. Mol. Catal. A: Chemical, 288, 109 (2008)

[6.92] I. Witońska, S. Karski, M. Frajtak, N. Krawczyk, A. Królak, React. Kinet. Catal. Lett., 93, 241 (2008)

[6.93] G. Yuan, M. A. Keane, Catal. Today, 88, 27 (2003)

[6.94] K. J. Leary, J. N. Michaels, A. M. Stacy, Langmuir, 4, 1251 (1988)

[6.95] U. Roland, T. Braunschweig, F. Roessner, J. Mol. Catal. A: Chemical, 127, 61 (1997)

[6.96] L. Wang, F. H. Yang, R. T. Yang, Ind. Eng. Chem. Res., 48, 2920 (2009)

[6.97] D. A. Panayotov, J. T. Yates, J. Phys. Chem. C, 111, 2959 (2007)

[6.98] H. Yang, H. Chen, J. Chen, O. Omotoso, Z. Ring, J. Catal., 243, 36 (2006)

Chapter 7

Selective Hydrodechlorination of 2,4-Dichlorophenol over Iron Oxide-Supported Au

In the previous Chapters, catalytic hydrodechlorination has been established as an effective means of detoxifying chlorophenols (in both liquid and gas phase). A common feature of these studies has been the governing role of steric hindrance in determining hydrodechlorination selectivity. Hydrogen scission of the Cl substituent positioned *ortho*- to the –OH group is consistently hampered by steric effects, a feature that is well documented in the published literature. In this Chapter, the action of Au/α-Fe_2O_3 to selectively activate *ortho*- positioned Cl substituent(s) for hydrogen attack is demonstrated, resulting in unique hydrodechlorination selectivities. Catalyst preparation and characterisation is correlated to hydrodechlorination performance.

7.1 Introduction

The presence of chlorophenols in industrial waste streams has been associated with deleterious effects on human health while contributing to ozone depletion and global warming [1,2]. In the past two decades, environmental legislation has become increasingly stringent regarding chlorophenols [2,3]. Several abatement methods have been considered, including photo-oxidation [4,5] (requiring expensive reagents), sono- [6,7] and electro-chemical [8,9] degradation (requiring complex equipment), bioremediation [10,11] (only applicable at low chlorine concentrations, $< 6 \times 10^{-3}$ mol_{Cl} dm^{-3}) and thermal treatments [12,13] (producing toxic by-products). Catalytic hydrodechlorination (HDC), hydrogenolytic C–Cl bond scission, has emerged as a cleaner alternative that facilitates recovery of raw material and operates under mild conditions (even with concentrated feedstock) [14,15]. The HDC of chlorophenols has been studied in both gas (notably over Ni/SiO_2 [16-18]) and liquid (notably over Pd/C [19-21]) phases where the critical role of metal dispersion [18,22] and the nature of the support [14,21] in determining HDC efficiency has been established. As a general observation, steric hindrance effects have been shown to limit HDC, particularly in terms of the cleavage of C–Cl bond(s) positioned *ortho*- with respect to –OH [23-27].

In gas phase operation, Pina *et al.* [24] found that 2-chlorophenol (2-CP) was the only chlorinated intermediate resulting from the HDC of 2,4-dichlorophenol (2,4-DCP) while Shin and Keane [25] isolated 2-CP and 2,6-DCP as products from the HDC of 2,4,6-trichlorophenol (2,4,6-TCP). Regarding liquid phase operation, Calvo and co-workers [26] reported 2-CP as the only chlorinated product from 2,4-DCP HDC whereas Pozan and Boz [27] identified 2-CP, 2,3-DCP and 2,5-DCP as 2,3,5-TCP HDC products. In order to establish HDC as an effective means of chlorophenol(s) detoxification, there is still a need for a catalyst formulation capable of promoting the hydrogenolysis of sterically constrained C–Cl bonds. This has been the ultimate goal of the work that is presented here.

Supported Au catalysts have been recently the focus of a diversity of studies where Au has shown a distinct activity/selectivity response when compared with Pd and/or Pt in alcohol oxidation, alkane isomerization and the hydrogenation of α,β-unsaturated carbonyl groups [28]. Gold particle size has been recognised as a critical variable, where Au clusters $\leq$ 10 nm have been deemed necessary to obtain appreciable activity [29,30]. In this respect, supported Au catalyst synthesis by precipitation methods [30,31] avoids supersaturation of the precursor solution as nucleation occurs on the support surface [32,33], facilitating a more uniform dispersion of smaller Au particles than is obtained from conventional impregnation [34,35]. The choice of support is crucial where higher activities have been achieved using reducible (*e.g.* TiO_2, CeO_2) as opposed to non-reducible (Al_2O_3, SiO_2) metal oxides in hydrogen mediated reactions [34,36]. This response has been linked to enhanced metal/support interactions in the former, which result from (a) the semiconductor (as opposed to insulator) nature of the Au/oxide interface [37] and/or (b) smaller Au particle size with a lower coordination number (*i.e.* increased number of defects) [38]. Hematite (α-Fe_2O_3) has been recently demonstrated to be a superior (reducible) support in the synthesis of active Au catalysts for the hydrogenation of nitroarenes [38], propyne [39] and benzalacetone [40]. In this Chapter, the potential of Au/α-Fe_2O_3 (prepared by deposition-precipitation) to promote the selective hydrogen cleavage of the *ortho*- Cl substituent from 2,4-DCP (as a model reactant) is demonstrated in continuous, gas phase operation. A comprehensive search through the literature did not unearth any study of chlorophenol(s) HDC over α-Fe_2O_3 supported metal catalysts. Moreover, the only reported use of Au (supported on SiO_2 and TiO_2) to promote HDC generated negligible activity [41].

This study represents a novel contribution in that it is the first time that a Au catalyst has been shown to exhibit (i) significant HDC activity and (ii) high selectivity in terms of the HDC of a sterically-hindered Cl substituent.

7.2 Experimental

7.2.1 Support/Catalyst Preparation

The α-Fe_2O_3 support was prepared by precipitation in basic media [42] according to:

$$2[Fe(NO_3)_3 \cdot 9H_2O] + 3Na_2CO_3 \longrightarrow 2Fe(OH)_3 + 6NaNO_3 + 3CO_2 + 15H_2O \quad \textbf{(7.1)}$$

100 cm^3 of aqueous Na_2CO_3 (1 M) were placed in a three-necked round-bottom flask and heated (2 K min^{-1}) in a water bath to 363 K under constant agitation (300 rpm) using a vertically mounted glass impeller. An aqueous solution of $Fe(NO_3)_3 \cdot 9H_2O$ (300 cm^3, 1 M) was then added dropwise *via* a glass/Teflon air-tight syringe and Teflon line (300 cm^3 h^{-1}) by means of a microprocessor-controlled infusion pump (100 kd Scientific). Basic conditions (pH > 7.3) were maintained during precipitation by adding Na_2CO_3 (five additions of 10 g). The pH was measured with a pH meter (Hanna Instruments) equipped with a crystal-body electrode, coupled to a data logging and collection system (Pico Technology Ltd.); calibration was performed with standard buffer solutions (pH 4.0 and 10.0). The solid hydroxide was subsequently aged for 2 h, washed with warm, distilled water (until the pH of wash water reached neutrality) and dehydrated over 3 days at 353 K (2 K min^{-1}) in ultra pure He (60 cm^3 min^{-1}) to form the oxide according to:

$$2Fe(OH)_3 \longrightarrow Fe_2O_3 + 3H_2O \quad \textbf{(7.2)}$$

The red solid was then cooled under the same flow of He, sieved to 75 μm average particle diameter (ATM fine test sieves) and stored under air at room temperature. A 0.81 % w/w Au/α-Fe_2O_3 catalyst was prepared by deposition-precipitation using urea as basification agent. A combination of aqueous urea (*ca.* 100-fold urea excess) and $HAuCl_4$ (300 cm^3, 5×10^{-4} M) was added to the α-Fe_2O_3 support (*ca.* 5 g).

The suspension was stirred and heated (2 K min^{-1}) to 353 K. The pH progressively increased to reach 7.2 after 8 h as a result of the thermally-induced urea decomposition [43]:

$$NH_2\text{-}CO\text{-}NH_2 + 3H_2O \longrightarrow 2NH_4^+ + 2OH^- + CO_2 \quad \textbf{(7.3)}$$

The catalyst was then filtered, washed until the washing water was Cl-free (based on the $AgNO_3$ test) and dried in ultra pure He (60 cm^3 min^{-1}) at 383 K for 3 h. After preparation, the catalyst was sieved to 75 μm average particle diameter (ATM fine test sieves) and stored at 277 K in the dark. The Au loading was determined (to within ± 2 %) by inductively coupled plasma-optical emission spectrometry (ICP-OES, Vista-PRO, Varian Inc.) from the diluted extract of aqua regia.

7.2.2 Support/Catalyst Characterization

The pH associated with the point of zero charge (pH_{pzc}) of the support was determined using the potentiometric mass titration (PMT) technique [44]. Three different masses (0.025, 0.050 and 0.075 g) were immersed in 50 cm^3 0.1 M NaCl to which a known amount of NaOH (0.1 M) was added to adjust the initial pH to *ca.* 11. Titration of the samples was performed under continuous agitation in a He atmosphere with HCl (0.1 M) as titrant. Temperature-programmed reduction (TPR) and H_2 chemisorption/tempetarure-programmed desorption (H_2-TPD) measurements were performed using the commercial CHEM-BET 3000 (Quantachrome Instruments) unit. The samples were loaded into a U-shaped (100 × 3.76 mm) quartz cell, contacted with 5 % v/v H_2/N_2 (17 cm^3 min^{-1}, Brooks mass flow controlled) and subjected to TPR treatment (2 K min^{-1}) to a final temperature in the range 423 K - 1273 K. The effluent gas was directed through a liquid N_2 trap and H_2 consumption/release was monitored by a thermal conductivity detector (TCD) with data acquisition/manipulation using the TPR Win™ software. After TPR, the reduced samples were swept with dry N_2 (65 cm^3 min^{-1}) at the final temperature for 90 min, cooled to room temperature and subjected to H_2 chemisorption analysis (10 μL H_2 pulses) under the same N_2 flow. The H_2 pulses were repeated until the signal area was constant, indicating surface saturation and H_2-TPD was subsequently performed by heating (50 K min^{-1}) the sample to 873 K.

BET area and pore size distribution measurements were performed using the commercial Micromeritics Flowsorb II 2300 unit. Prior to analysis, the samples were outgassed at 423 K for 1 h in 20 cm^3 min^{-1} dry N_2. BET area was obtained in 30 % v/v N_2/He (20 cm^3 min^{-1}) with at least three cycles of N_2 adsorption-desorption using the standard single-point BET method. N_2 adsorption/desorption isotherms were recorded over the relative pressure range $0.05 \leq P/P_0 \leq 0.98$, where the total pore volume and size distribution were obtained using the method of Dollimore and Heal [45]. Hydrogen chemisorption, BET area and pore volumes were reproducible to within ± 5 % and the values quoted in this study are the mean.

The support/catalyst structural features were assessed by X-ray diffraction (XRD) using a Bruker/Siemens D500 incident X-ray diffractometer with Cu Kα radiation. The samples were scanned at 0.02º $step^{-1}$ over the range $20º \leq 2\theta \leq 90º$ (scan time = 5 s $step^{-1}$). The diffractograms were compared with the JCPDS-ICDD references for comparative purposes (Card No. 33-0664 (α-Fe_2O_3); 19-0629 (Fe_3O_4); 06-0696 (Fe); 04-0784 (Au)). Gold particle size/morphology was determined by transmission electron microscopy (TEM) analysis: JEOL JEM 2011 TEM unit with a UTW energy-dispersive X-ray detector (Oxford Instruments) operated at an accelerating voltage of 200 kV and using Gatan DigitalMicrograph 3.4 for data acquisition/manipulation. The samples were dispersed in acetone and deposited on a holey-carbon/Cu grid (300 Mesh). The mean Au particle size is given as a surface area-weighted mean (d_{TEM}) according to:

$$d_{TEM} = \frac{\sum_i n_i d_i^3}{\sum_i n_i d_i^2} \qquad \textbf{(7.4)}$$

where n_i is the number of particles of diameter d_i and $\Sigma\, n_i = 100$.

7.2.3 Catalytic Procedure

The reactants (2-CP, 3-CP, 4-CP, 2,3-DCP, 2,4-DCP, 2,5-DCP, 2,6-DCP, 3,4-DCP, 3,5-DCP and 2,4,6-TCP; ≥ 97 %) and the organic solvents (methanol, ethanol, *n*-propanol, *n*-butanol, *n*-hexane, tetrahydrofuran (THF), cyclohexane; ≥ 99 %) were obtained from Sigma-Aldrich and used as received.

Reactions were carried out under atmospheric pressure, immediately after *in situ* activation, in a continuous flow fixed bed vertical glass reactor (i.d. = 15 mm, l = 600 mm). The catalytic reactor, and operating conditions to ensure negligible heat/mass transport limitations, have been fully described elsewhere [46], but details of direct relevance to this study are given below. The chlorophenol reactants were delivered to the reactor as (unless otherwise specified) aqueous solutions *via* a glass/teflon air-tight syringe and a teflon line using a microprocessor controlled infusion pump (Model 100 kd Scientific) where the molar ratio of Au (n_{Au}) to Cl flow rate (F_{Cl}) spanned the range 2×10^{-3} - 83×10^{-3} mol_{Au} h mol_{Cl}^{-1}. A co-current flow of ultra pure H_2 (60 cm^3 min^{-1}) was monitored using a Humonics (Model 520) digital flowmeter and maintained at a $GHSV$ = 2×10^4 h^{-1}. A layer of glass beads above the catalyst bed served as a preheating zone, ensuring that the reactants were vaporized, reaching reaction temperature (423 K) before contacting the catalyst. Isothermal conditions were maintained by diluting the catalytic bed with ground glass (75 μm), where the reaction temperature was continuously monitored by a thermocouple inserted in a thermowell within the catalytic bed. Passage of each reactant over the support alone, *i.e.* in the absence of Au, did not result in any measurable conversion. The reactor effluent was frozen in a liquid nitrogen trap for subsequent analysis, which was made using a Perkin-Elmer Auto System XL GC, employing a DB-1 (J&W Scientific) capillary column (i.d. = 0.20 mm, l = 50 m, film thickness = 0.33 μm) as described in detailed elsewhere [47]. A chlorine mass balance was performed by passing the effluent gas through an aqueous NaOH trap (9×10^{-4} mol dm^{-3}, kept under constant agitation at 400 rpm) with independent pH (Hanna HI Programmable Printing pH Bench-Meter) analysis; HCl was the only inorganic product as established elsewhere [48]. Repeated reactions with different samples from the same batch of catalyst delivered raw data that were reproducible to within ± 7 %. The fractional selectivity to, for example, 4-CP ($S_{4\text{-}CP}$) is given by

$$S_{4\text{-}CP} = \frac{C_{4\text{-}CP}}{C_{2,4\text{-}DCP,0} - C_{2,4\text{-}DCP}} \qquad \textbf{(7.5)}$$

where $C_{2,4\text{-}DCP,0}$ and $C_{2,4\text{-}DCP}$ represent the inlet and outlet concentrations of 2,4-DCP, respectively, and $C_{4\text{-}CP}$ is the outlet concentration of 4-CP.

7.3 Results and Discussion

7.3.1 Support Characterization

The hematite (α-Fe_2O_3) support was first subjected to a comprehensive programme of characterization in terms of surface area, porosity, reducibility and H_2 chemisorption prior to the addition of gold by deposition-precipitation. Representative SEM images of the (as prepared) support are presented in **Figure 7.1**a where a platelet morphology is in evidence, decorated with small, amorphous ferrihydrite ($Fe_5HO_8{\cdot}4H_2O$) aggregates.

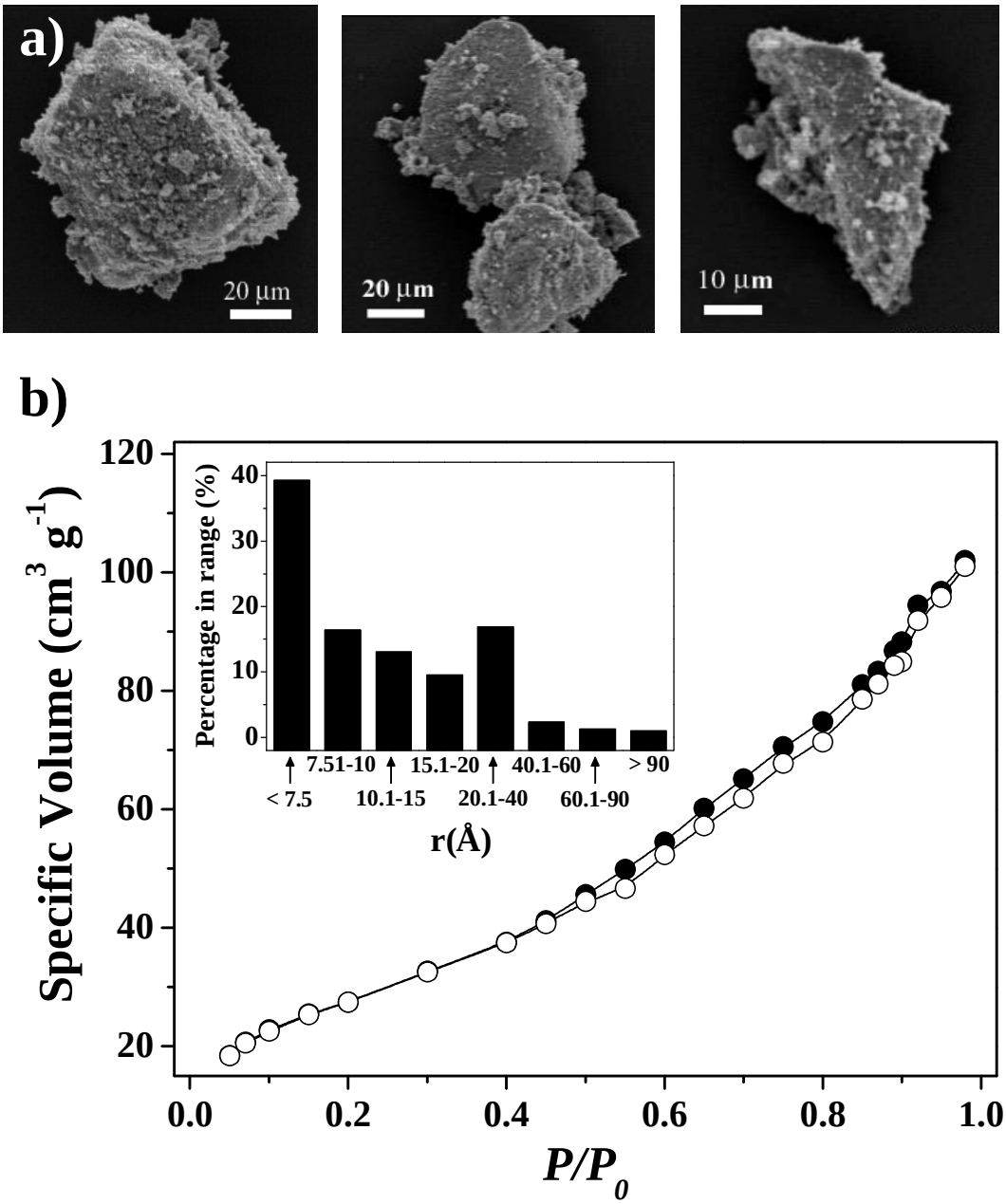

Figure 7.1: a) Representative SEM micrographs and b) N_2 adsorption (●)/desorption (○) isotherms of the hematite (α-Fe_2O_3) support, as prepared. Inset: pore volume distribution from the desorption data.

This morphology is typical in iron (III) oxide(s) synthesised from concentrated (> 0.1 M) Fe^{+3} solutions at $T \geq 363$ K [49], where a metastable $Fe_5HO_8 \cdot 4H_2O$ phase is first formed which, by dehydration [50], produces α-Fe_2O_3 as the thermodynamically stable allotrope [51]. Nitrogen adsorption/desorption isotherms are shown in **Figure 7.1**b and the corresponding total pore volume is given in **Table 7.1**. The isotherms exhibit an hysteresis loop at high relative pressures ($P/P_0 > 0.45$) which, according to type IV IUPAC classification, is indicative of the presence of mesopores. The measurable (≥ 18 $cm^3\ g^{-1}$) N_2 uptake at low relative pressures ($P/P_0 < 0.2$) is characteristic of a micropore component (type I classification) [52]. A contribution of both micro- and meso-pores to the total pore volume gives rise to the bimodal distribution shown as an inset to **Figure 7.1**b. Total porosity is predominantly (*ca.* 78 %) at the micro-scale. The BET surface area (129 $m^2\ g^{-1}$, see **Table 7.1**) falls within the range of values (48 - 252 $m^2\ g^{-1}$) quoted in the literature [53,54]. The pH associated with the point of zero charge (pH_{pzc}) was also measured as a critical property that determines the solution pH requirements to ensure effective precursor-support interactions during catalyst preparation by deposition-precipitation [55]. When pH < pH_{pzc}, the support surface bears a positive charge (due to protonation), favouring interaction with anionic species in solution and a pH in excess of pH_{pzc} results in a surface affinity for cationic species [22,56]. Our experimentally determined pH_{pzc} (= 8.1) is within the range (7.9 - 9.0) reported previously for α-Fe_2O_3 [57,58] and suggests a preferential interaction with anionic Au precursor species at pH < 8.1.

Support reducibility was assessed by a combination of temperature programmed reduction (TPR) and XRD analyses, which are shown in **Figure 7.2**a and **7.2**b, respectively. At room temperature, contact of the support with 5 % v/v H_2/N_2 did not result in any detectable TPR signal (see I in **Figure 7.2**a) and the associated XRD diffractogram (Profile I in **Figure 7.2**b) was consistent with the sole presence of a rhombohedral α-Fe_2O_3 phase (JCPDS-ICCD Card No. 33-0664, Profile V). Reflections at 2θ = 24.1°, 33.2°, 35.6°, 40.9°, 49.5°, 54.1°, 57.6°, 62.4° and 64.0° correspond, respectively, to the (012), (104), (110), (113), (024), (116), (018), (214) and (300) planes. TPR to 1273 K generated a positive (H_2 consumption) TCD response with characteristic T_{max} values at 562 K, 666 K, 965 K and 1183 K (see **Figure 7.2**a).

Table 7.1: Support composition, BET surface area, pore volume and H_2 chemisorption associated with α-Fe_2O_3 (support) and Au/α-Fe_2O_3 (Au/support) at different TPR temperatures.

System	TPR[a]		Support composition[b]	BET ($m^2\ g^{-1}$)	Pore volume ($cm^3\ g^{-1}$)	H_2 chemisorption ($\times 10^6\ mol_{H_2}\ mol_{Fe}^{-1}$)
	Point	Temperature (K)				
Support	I	298[c]	α-Fe_2O_3	129	0.26	-
	II	423		103	0.23	10
	III	673	Fe_3O_4	13	0.03	14
	IV	1273	Fe	3	< 0.01	7
Au/Support	I	298[c]	α-Fe_2O_3	120	0.23	-
	II	423	α-Fe_2O_3[d]	57	0.16	14
	III	673	Fe_3O_4	13	0.04	21
	IV	1273	Fe	3	< 0.01	9

[a]see **Figure 7.2**a (α-Fe_2O_3) and **Figure 7.4**a (Au/α-Fe_2O_3)
[b]based on XRD analysis, see **Figure 7.2**b (α-Fe_2O_3) and **Figure 4**b (Au/α-Fe_2O_3)
[c]as prepared
[d]partial reduction to Fe_3O_4

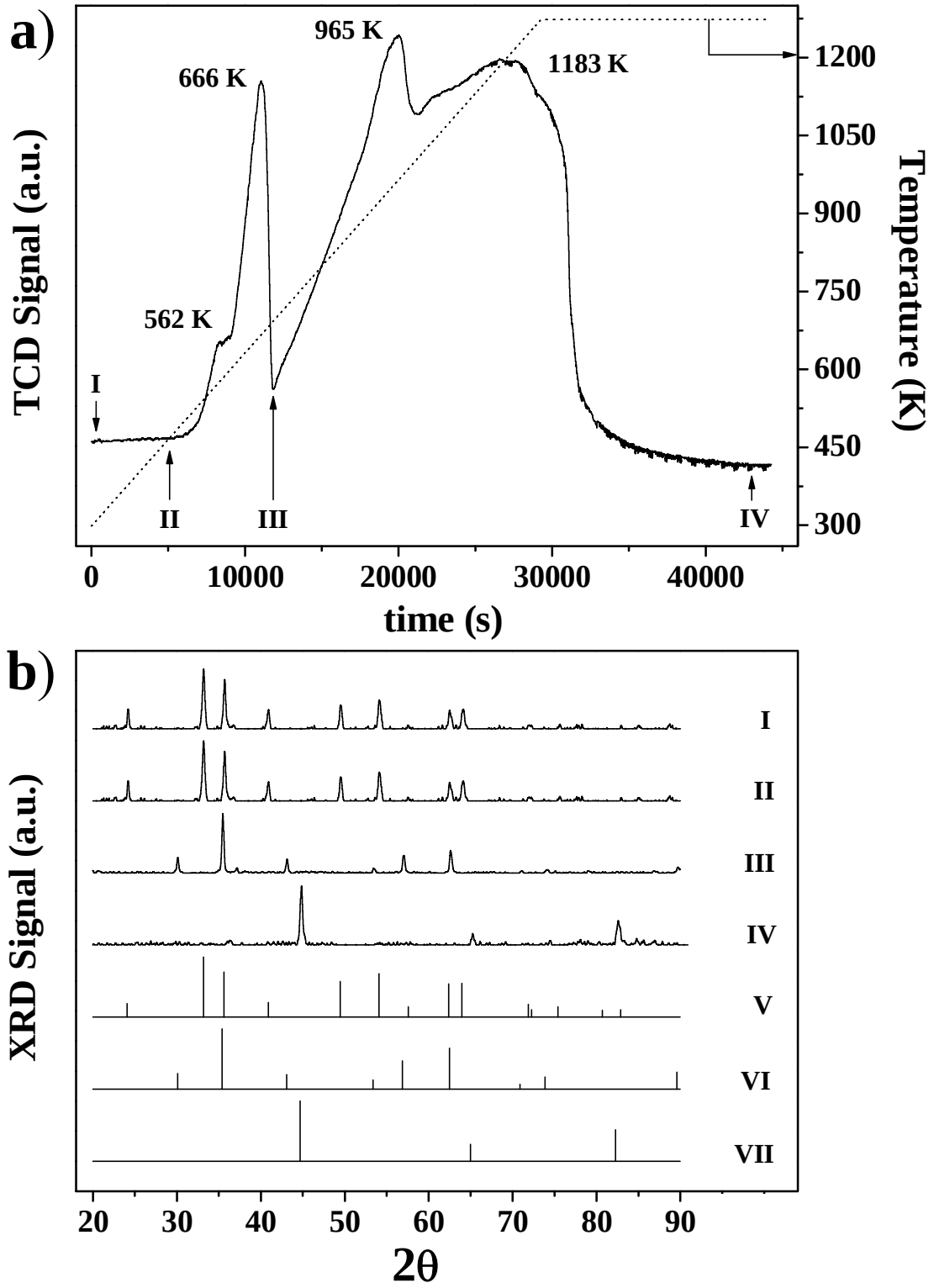

Figure 7.2: a) TPR profile and b) XRD patterns for the hematite (α-Fe_2O_3) support, as prepared (I) and reduced at 423 K (II), 673 K (III) and 1273 K (IV). Note: reference (JCPDS-ICDD) diffractograms for α-Fe_2O_3 (Card No. 33-0664 (V)), Fe_3O_4 (Card No. 19-0629 (VI)) and Fe (Card No. 06-0696 (VII)) are also included.

The first two signals can be associated with the reduction of α-Fe_2O_3 to magnetite (Fe_3O_4) according to:

$$3Fe_2O_3 + H_2 \rightarrow 2Fe_3O_4 + H_2O \quad \textbf{(7.6)}$$

as there is good agreement (within 1 %) between the experimentally determined and theoretical (0.17 $mol_{H_2}\, mol_{Fe}^{-1}$) H_2 consumption for this step. Moreover, XRD profiles post TPR to 423 K (point II in **Figure 7.2**a) and 673 K (point III in **Figure 7.2**a) coincide, respectively, with the patterns for the α-Fe_2O_3 and Fe_3O_4 JCPDS-ICDD standards (Profiles V and VI in **Figure 7.2**b, respectively). The presence of a shoulder (at 562 K) to the main H_2 consumption peak (at 666 K) can be attributed to a lower temperature reduction of (a) $Fe_5HO_8{\cdot}4H_2O$ particles decorating the α-Fe_2O_3 surface (see SEM images in **Figure 7.1**a) and/or (b) surface hydroxyl groups. Indeed, the occurrence of a two stage reduction of α-Fe_2O_3 to Fe_3O_4 has been reported in the literature [51,59] (in the range 633 K - 700 K) and linked to support dehydroxylation with concomitant formation of surface oxygen vacancies. The broader H_2 consumption peaks at 965 K and 1183 K (see **Figure 7.2**a) can be ascribed to a further reduction of Fe_3O_4 to metallic iron according to:

$$Fe_3O_4 + 4H_2 \rightarrow 3Fe + 4H_2O \quad \textbf{(7.7)}$$

Once again, the experimental/theoretical H_2 consumptions were in good agreement (to within 6 %) and the XRD diffractogram of the sample taken to 1273 K (point IV in **Figure 7.2**a) matched that of the JCPDS-ICDD *fcc* Fe reference (Card No. 06-0696, Profile VII in **Figure 7.2**b). The two TPR signals (at 965 K and 1183 K) can be tentatively associated with different reduction requirements associated with surface/structural defects and bulk Fe_3O_4 transformations. Indeed, Pineau *et al.* [60], studying the kinetics of Fe_3O_4 reduction in H_2, demonstrated that the continuous agglomeration of the oxide caused variations in reduction rate and the consequent temperature response during TPR. It should be noted that the support TPR transformations were accompanied by a decrease in BET area and pore volume (see **Table 7.1**). This response can be linked to sample sintering and loss of water, which ultimately generates a low surface area bulk Fe structure [61].

Hydrogen chemisorption measurements for the support at points I - IV (see **Table 7.1**) delivered low uptakes that approached instrumental detection limits.

7.3.2 Catalyst Synthesis and Characterization

Au/α-Fe_2O_3 was prepared by deposition-precipitation and subjected to the same programme of characterization as the support. Temporal variations of solution pH and temperature during the preparation process are shown in **Figure 7.3**, where the pH_{pzc} of α-Fe_2O_3 is indicated by the dashed line. At ambient temperature, the addition of urea and $HAuCl_4$ to α-Fe_2O_3 generated an initial pH of 4.5. A subsequent elevation of temperature was accompanied by an increase in pH (to *ca.* 7.2) due to thermally-induced urea decomposition (see eqn. **(7.3)**). It is known that, in aqueous solution, $AuCl_4^-$ undergoes sequential substitution of Cl^- with OH^- at pH = 4, 4.6, 6.5 and 9, at which point $Au(OH)_4^-$ predominates [55,62]. Accordingly, we can identify our deposited gold precursor as principally $AuCl(OH)_3^-$ species. We avoided the use of a higher solution pH as this has been demonstrated to generate lower Au dispersions [55,63].

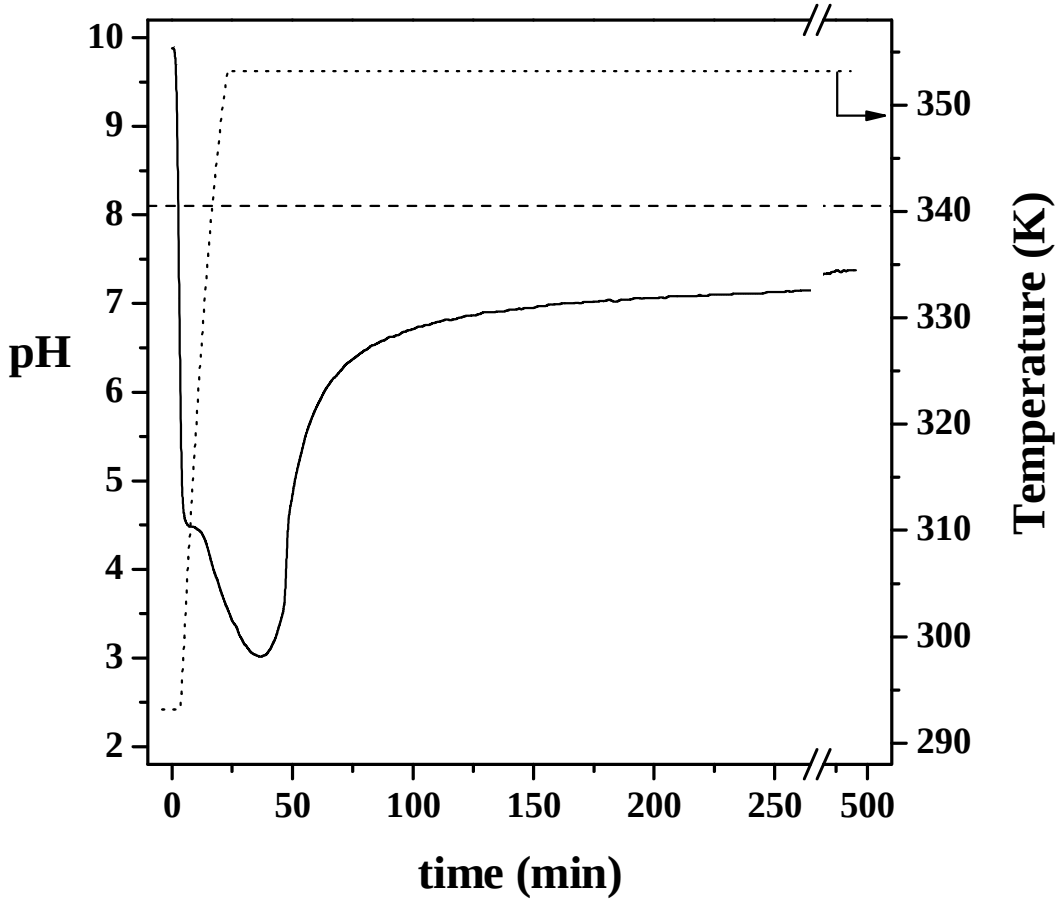

Figure 7.3: Temporal variation of pH (solid line) and temperature (dotted-line) in the synthesis of Au/α-Fe_2O_3. Note: dashed line illustrates pH_{pzc} of the support.

It should be noted that the final pH was less than the pH_{pzc} (= 8.1), favouring anionic Au precursor interaction with the positively charged α-Fe_2O_3 surface. The subsequent period of "aging" (*ca.* 250 min) is known to enhance Au deposition [64]. Catalyst reducibility as assessed by TPR/XRD analyses (see **Figure 7.4**a and **7.4**b, respectively) can be compared directly with the support (see section **7.3.1** and **Figure 7.2**). As in the case of α-Fe_2O_3, there was no detectable room temperature hydrogen consumption by Au/α-Fe_2O_3 (point I in **Figure 7.4**a) and the XRD pattern (Profile I in **Figure 7.4**b) was coincident with the α-Fe_2O_3 JCPDS-ICDD standard (Profile IV). The TPR profile generated for Au/α-Fe_2O_3 (**Figure 7.4**a) differed significantly from that recorded for α-Fe_2O_3 (**Figure 7.2**a) in that all the peaks were shifted to lower temperatures (by up to 200 K). This response suggests a more facile α-Fe_2O_3 reduction due to the presence of Au and is consistent with reports in the literature [65,66]. The occurrence of two TPR peaks for Au/α-Fe_2O_3 at $T \leq 673$ K has been previously reported where the lower temperature signal has been ascribed to the reduction of (a) the Au precursor [66,67] and/or (b) the support [67,68]. In our case, H_2 consumption associated with the first signal (at 363 K) was far greater than that required for Au precursor reduction (19.6 *vs.* 1.5 $mol_{H_2}\,mol_{Au}^{-1}$). This excess in terms of H_2 consumption must be associated with the α-Fe_2O_3 support and can arise from the generation of spillover hydrogen during TPR. Spillover results from a dissociative chemisorption of H_2 to generate atomic hydrogen that migrates to another (accepting) surface, typically from a metal site to an oxide support [69]. Indeed, recent studies have demonstrated (by FTIR) hydrogen spillover at ambient temperature in the case of Au supported on TiO_2 [70] and CeO_2-ZrO_2 [71]. Moreover, Bocuzzi and coworkers [72] have suggested that room temperature spillover hydrogen generated on Au/α-Fe_2O_3 can participate in the superficial reduction of the support. A possible contribution from the lower temperature TPR signal to a partial reduction of α-Fe_2O_3 by spillover hydrogen was probed by XRD (see **Figure 7.4**b). A comparison of the XRD pattern of the as-prepared catalyst (Profile I) with that obtained after TPR to 423 K (Profile II) can be made, focusing on the 2θ range outlined in boxes "c" and "d". It should be noted that the relative intensities of the two main peaks at 2θ = 33.2 º and 35.6º ((104)/(110) planes) in Profile II differ from that which characterises Profile I and the reference α-Fe_2O_3 (see dashed square "c" in **Figure 7.4**b): α-Fe_2O_3 = Profile I = 4/3; Profile II = 3/4.

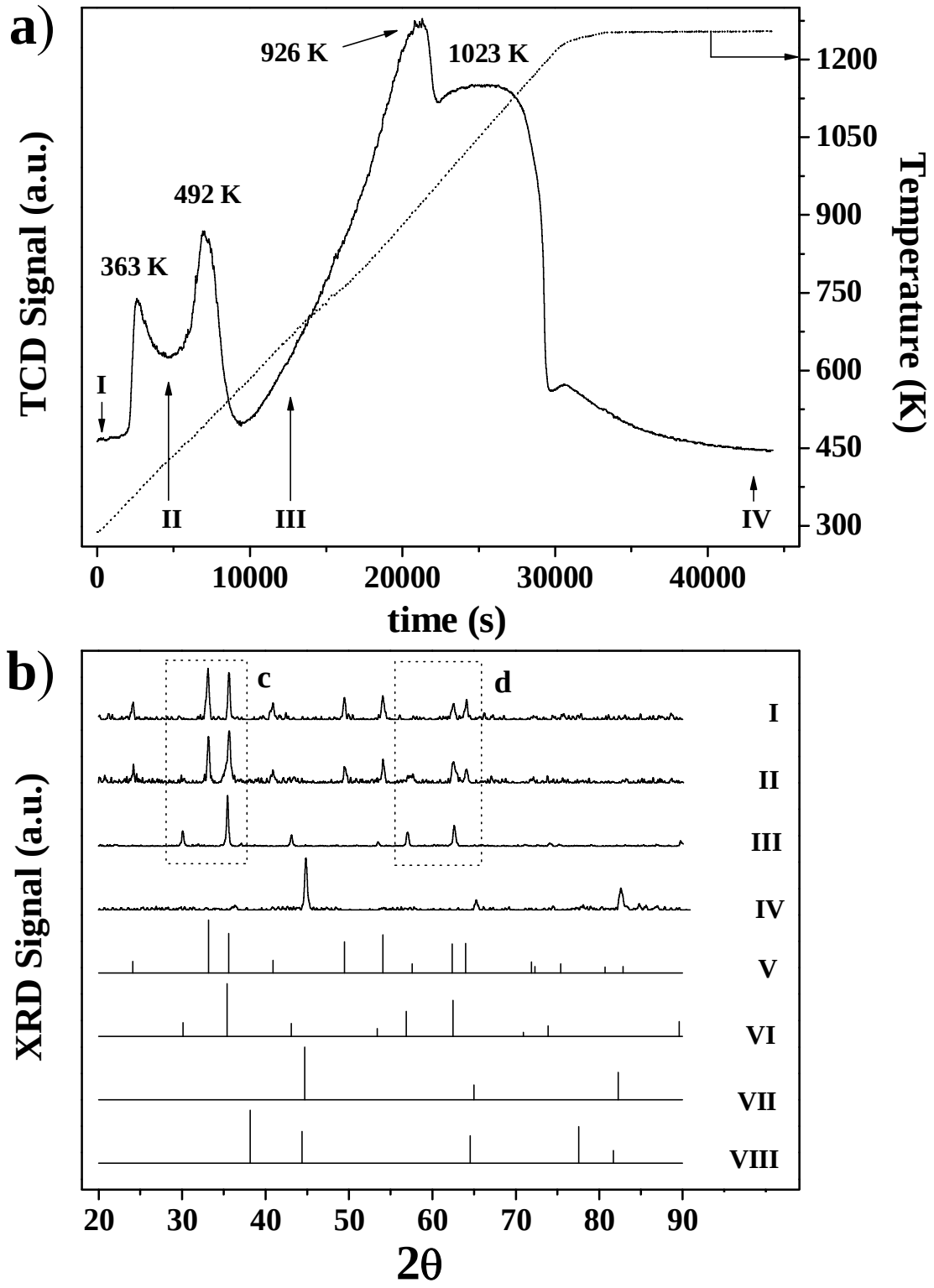

Figure 7.4: a) TPR profile and b) XRD patterns for the Au/α-Fe_2O_3 catalyst, as prepared (I) and reduced at 423 K (II), 673 K (III) and 1273 K (IV). Note: Sections "c" and "d" in b) identify areas for comparison. Reference (JCPDS-ICDD) diffractograms for α-Fe_2O_3 (Card No. 33-0664 (V)), Fe_3O_4 (Card No. 19-0629 (VI)), Fe (Card No. 06-0696 (VII)) and Au (Card No. 04-0784 (VIII)) are also included.

As the XRD peak for the (110) plane for α-Fe_2O_3 coincides with the main characteristic peak for Fe_3O_4 (2θ = 35.4º, (311) plane, Profile VI), this variation in relative intensities suggests a partial reduction of the support. Indeed, a consideration of the XRD signals at 2θ = 62.4 º and 64.0º (planes (214) and (300)) for α-Fe_2O_3 and the (440) plane (at 2θ = 62.5º) for Fe_3O_4 (see dashed square "d" in **Figure 7.4**b) reveals differences in the relative intensities of the characteristic signals for α-Fe_2O_3 with the simultaneous appearance of one of the main peaks for Fe_3O_4. These results demonstrate that, when Au/α-Fe_2O_3 was activated at 423 K, the support was partially reduced to Fe_3O_4. A complete transformation of Au/α-Fe_2O_3 to Au/Fe_3O_4 at 623 K is confirmed by comparing Profile III with the reference Fe_3O_4 in Profile VI. Further reduction to 1273 K resulted in the formation of bulk Fe (see Profile VI in **Figure 7.4**b). The absence in these XRD patterns of any reflections due to Au (JCPDS-ICDD Card No. 04-0784, Profile VIII) can be taken as indicative of the presence of Au as small clusters (XRD detection limit $\leq$ 3-5 nm [73,74]). A measurably higher level of H_2 chemisorption was observed for Au/α-Fe_2O_3 when compared with α-Fe_2O_3 (see **Table 7.1**), albeit the increase in uptake is slight. While it is known that H_2 does not chemisorb on bulk Au (at room temperature) [75], uptake on supported Au particles (< 10 nm) has been reported, notably at step, edge and corner sites [34,76].

The catalyst activation temperature was then fixed at 423 K, where support α-Fe_2O_3 character was largely maintained. The N_2 adsorption/desorption isotherms for the activated/passivated Au/α-Fe_2O_3 (see **Figure 7.5**) deviated somewhat from those recorded for the support (see **Figure 7.1**b). Lower volumes adsorbed/desorbed (particularly where $P/P_0 < 0.4$) and a shift in the hysteresis loop shifted to greater relative pressures ($P/P_0 > 0.65$) characterized Au/α-Fe_2O_3. The associated micropore content of Au/α-Fe_2O_3 was lower, accounting for 65 % of the total pore volume. TEM analysis was performed in order to assess Au size and morphology in the activated catalyst. Representative high magnification micrographs are shown in **Figure 7.6**, where the metal particles exhibited a quasi-spherical shape with diameters $\leq$ 10 nm (see TEM image a). The diffractogram pattern for isolated metal particles (bI and bII) yielded an average *d*-spacing of 0.23 nm, consistent with the (111) main plane of metallic Au (JCPDS-ICDD Card No.: 04-0784).

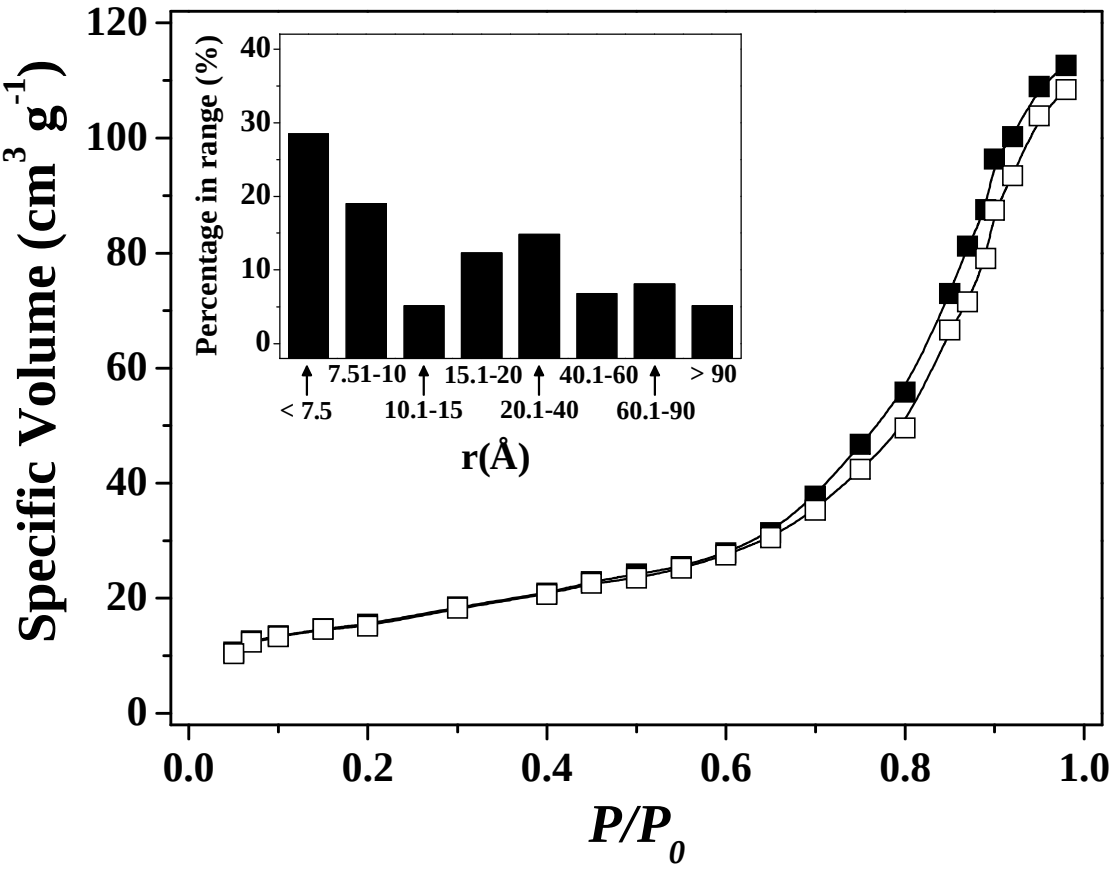

Figure 7.5: Nitrogen adsorption (■)/desorption (□) isotherms of activated (at 423 K) and passivated Au/α-Fe_2O_3. Inset: pore volume distribution from desorption data.

The *d*-spacing obtained for the support (**Figure 7.6**bIII, 0.25 nm) matches the (110) plane of α-Fe_2O_3 (JCPDS-ICDD Card No. 33-0664). The surface area-weighted mean Au particle size was 2.6 nm, which is consistent with the absence of XRD signals due to Au in **Figure 7.4**b (Profile II). Hydrogen content associated with Au/α-Fe_2O_3 was probed further by H_2-TPD analysis and the results are presented in **Figure 7.7**, where the corresponding profile for the support is included for comparative purposes. In both cases, two stages of hydrogen desorption are in evidence (*i.e.* T_{max} = 579 ± 4 K and 700 ± 4 K). A third signal (at 762 K) is present in the profile for α-Fe_2O_3 which, in the case of Au/α-Fe_2O_3, is possibly contained within the broader and more intense higher temperature TPD peak. The total amount of hydrogen desorbed (α-Fe_2O_3: 1×10^{-3} mol_{H_2} mol_{Fe}^{-1}; Au/α-Fe_2O_3: 4×10^{-3} mol_{H_2} mol_{Fe}^{-1}) was appreciably greater (by two orders of magnitude) than that taken up in the chemisorption step (see **Table 7.1**), a response that supports the generation of spillover hydrogen during TPR. The desorption of spillover species has been shown to occur at $T > 503$ K, regardless of the metal/support [77].

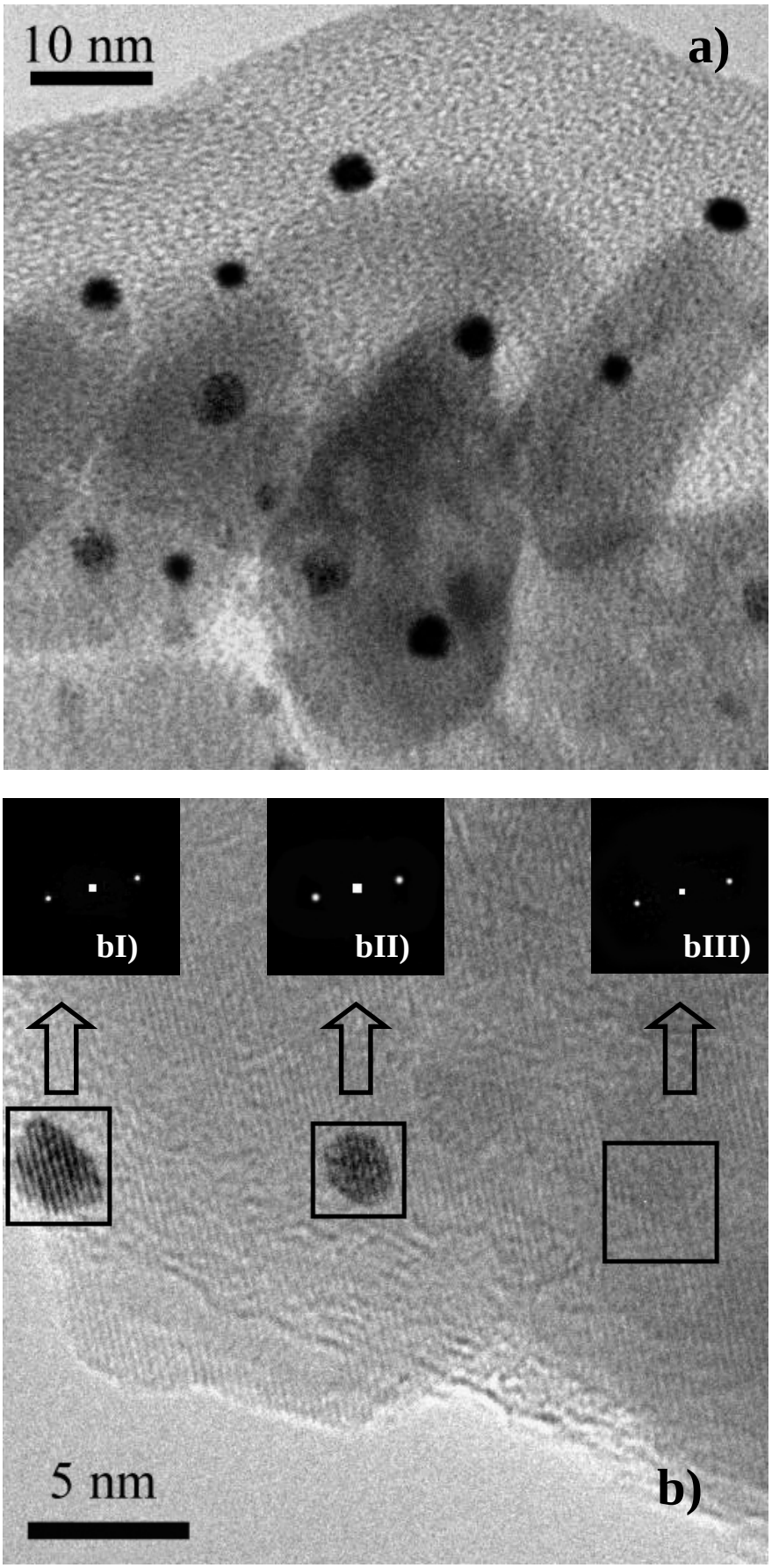

Figure 7.6: Representative high resolution TEM images of activated (at 423 K) and passivated Au/α-Fe_2O_3. Note: diffractogram patterns for isolated Au particles (bI and bII) and α-Fe_2O_3 support (bIII) are included as insets.

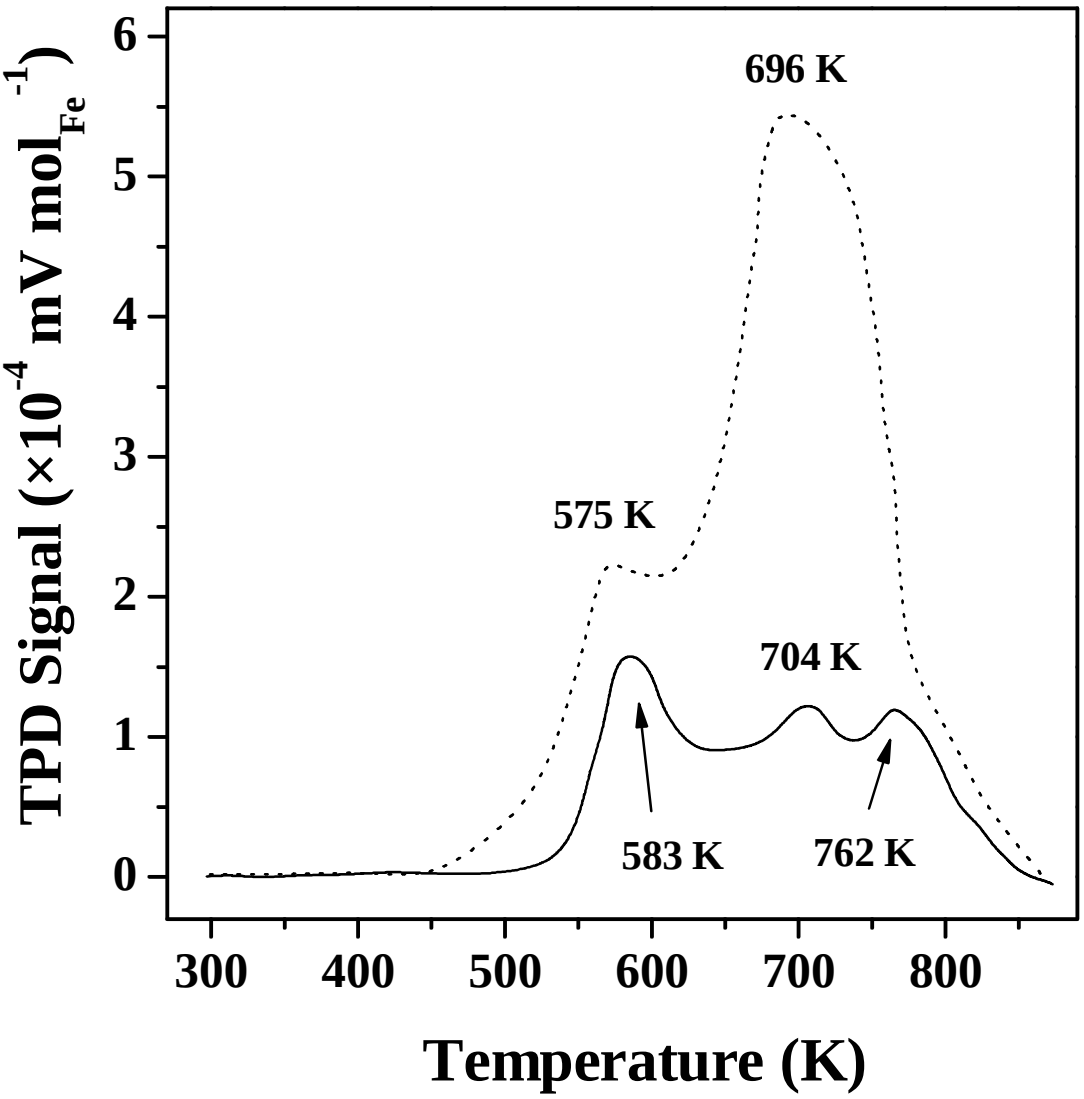

Figure 7.7: Specific (per mol Fe) H_2-TPD profile for α-Fe_2O_3 (solid line) and Au/α-Fe_2O_3 (dotted line) post TPR to 423 K.

The incorporation of Au on α-Fe_2O_3 resulted in a four-fold greater amount of hydrogen released during TPD. The more facile α-Fe_2O_3 reduction in the presence of Au during TPR may be a consequence of this additional surface hydrogen. The catalyst characterization results establish the presence of nanoscale Au (mean size = 2.6 nm) that facilitates a partial reduction of α-Fe_2O_3 to Fe_3O_4 post TPR to 423 K with a significant increase in surface hydrogen content.

7.3.3 Catalytic Activity/Selectivity

The catalytic performance of Au/α-Fe_2O_3 was tested in the HDC of 2,4-DCP: the reaction pathway is shown in **Figure 7.8**.

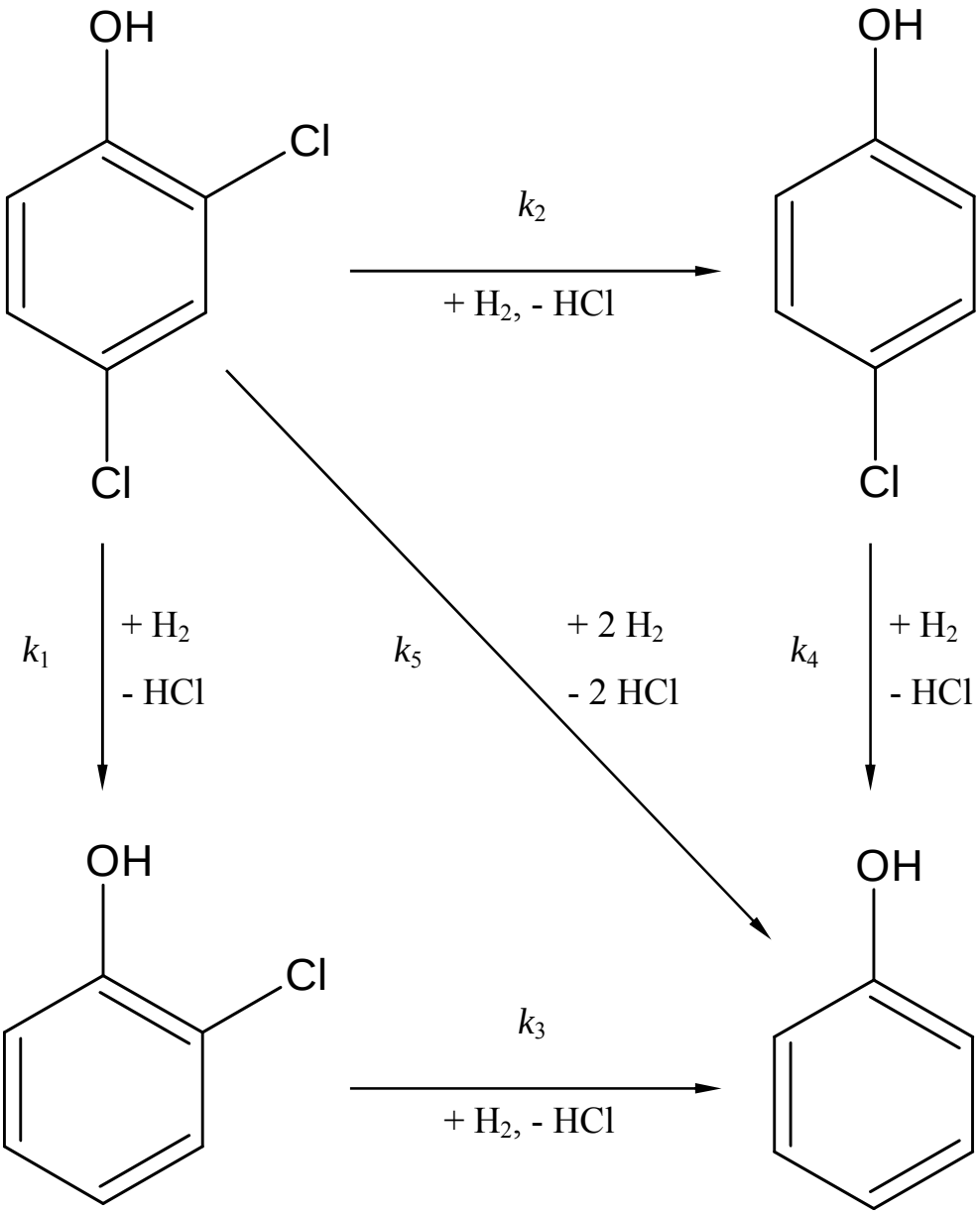

Figure 7.8: Schematic reaction pathway for the HDC of 2,4-DCP.

Chlorine removal can proceed by two stepwise routes, *i.e.* with 2-CP (k_1, k_3) or 4-CP (k_2, k_4) as reaction intermediates, or by the simultaneous removal of both Cl substituents (k_5) leading, in each case, to PhOH as the ultimate product. This is an ideal model system to assess selectivity in terms of *ortho*- as opposed to *para*- Cl attack. 2,4-DCP HDC over Au/α-Fe_2O_3 did not generate any products resulting from aromatic ring hydrogenation and/or dehydroxylation, *i.e.* the catalyst was 100 % selective in terms of chlorine removal. A representative temporal response in terms of outlet stream molar composition is shown in **Figure 7.9**, where it can be seen that 2,4-DCP conversion yielded 4-CP as the principal product.

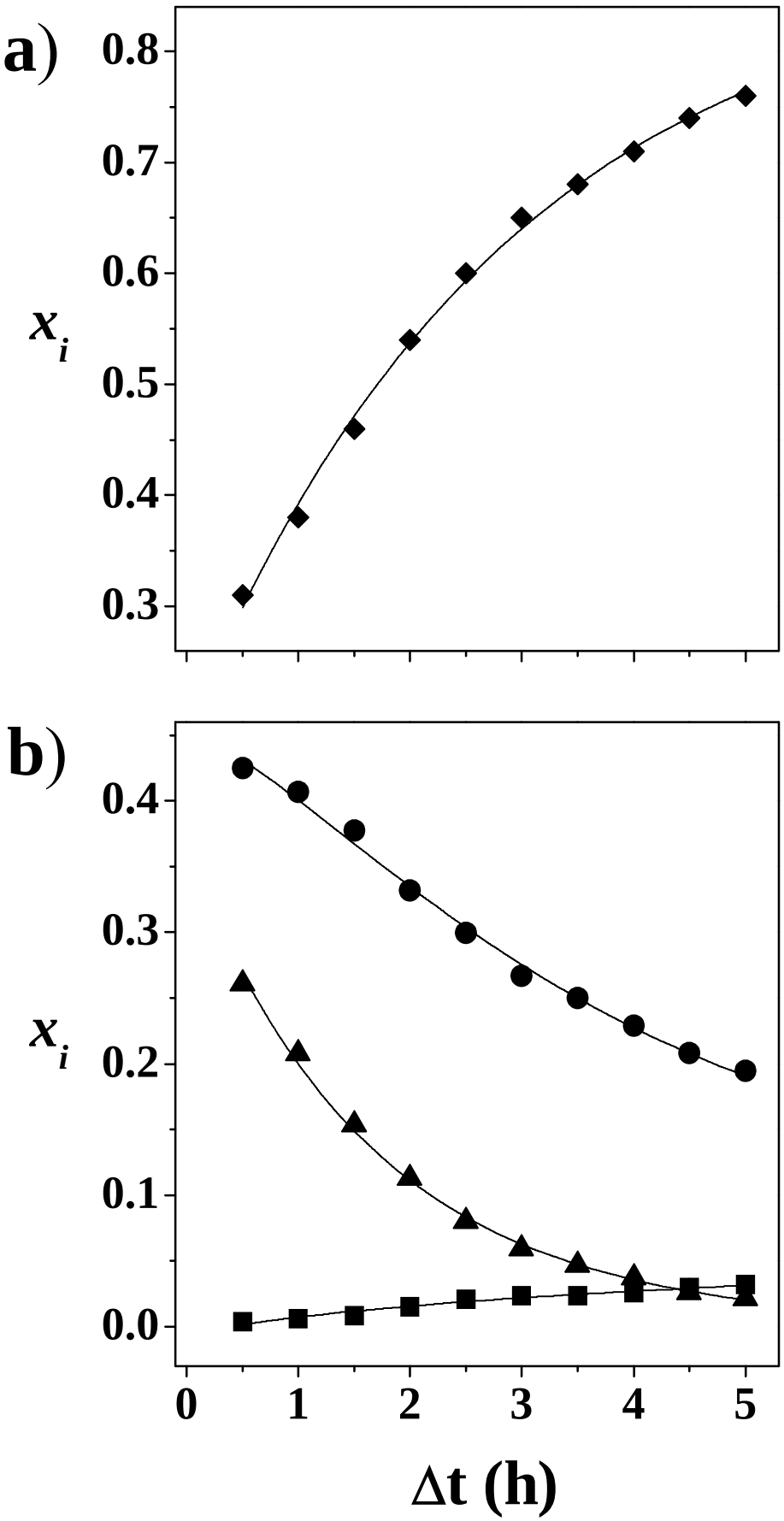

Figure 7.9: Mole fractions (x_i) of a) 2,4-DCP (◆) and b) PhOH (▲), 2-CP (■) and 4-CP (●) as a function of time-on-stream for reaction over Au/α-Fe_2O_3: (n_{Au}/F_{Cl}) = 83 × 10^{-3} mol_{Au} h mol_{Cl}^{-1}. Note: lines represent fit to eqn. (7.8).

From the very outset, it must be stressed that this response is unique in terms of HDC selectivity. The published studies on 2,4-DCP hydrotreatment have uniformly identified steric hindrance effects in the activation/scission of the *ortho*- Cl substituent as governing HDC, leading to the generation of 2-CP as the predominant intermediate, regardless of the phase (gas [17,24] or liquid [26,78]), metal (Ni [17,24], Pd [26,78]) or support (carbon [26], Al_2O_3 [78], SiO_2 [17,24]) used. There was a temporal decline in 4-CP (and PhOH) production that coincided with a decrease in 2,4-DCP conversion with time-on-stream. A time dependent loss of activity is a common feature of catalytic HDC and has been linked to the action of the HCl by-product that can induce metal leaching [79,80], poisoning (*via* electronic modifications) [81-83], sintering [81] and/or coke formation [79,80]. The initial product distribution was calculated from [16,84]:

$$x_i = x_{i,0} \exp\left[-\alpha \, \Delta t\right] \tag{7.8}$$

where $x_{i,0}$ and x_i represent the initial and temporal molar fractions of compound i, Δt is the integral time and α is a fitting parameter; the quality of the data fit ($R^2 \geq 0.992$) can be seen in **Figure 7.9**. In order to relate the catalytic response of Au/α-Fe_2O_3 in terms of HDC pathway (see **Figure 7.8**), the mass balance for each compound was applied assuming pseudo-first order kinetics (H_2 was far in excess of the stoichiometric quantity) for each reaction step which, after integration, gives the following series of equations:

$$x_{2,4\text{-}DCP,0} = \exp\left[-\left(k_1 + k_2 + k_5\right) \times \left(n_{Au} / F_{Cl}\right)\right] \tag{7.9}$$

$$x_{2\text{-}CP,0} = \left(\frac{k_1}{k_3 - \left(k_1 + k_2 + k_5\right)}\right)\left(x_{2,4\text{-}DCP,0} - \exp\left[-k_3 \times \left(n_{Au} / F_{Cl}\right)\right]\right) \tag{7.10}$$

$$x_{4\text{-}CP,0} = \left(\frac{k_2}{k_4 - \left(k_1 + k_2 + k_5\right)}\right)\left(x_{2,4\text{-}DCP,0} - \exp\left[-k_4 \times \left(n_{Au} / F_{Cl}\right)\right]\right) \tag{7.11}$$

$$x_{PhOH,0} = 1 - \left(x_{2,4\text{-}DCP,0} + x_{2\text{-}CP,0} + x_{4\text{-}CP,0}\right) \tag{7.12}$$

where k_j is the pseudo-first order rate constant for step j and n_{Au}/F_{Cl} has the physical meaning of contact time. The results of a non-linear regression of the experimental data to the kinetic model are shown in **Figure 7.10** and the resulting k_j values (mol_{Cl} h^{-1} mol_{Au}^{-1}) are given in **Table 7.2**. The HDC of 2,4-DCP proceeded *via* a preferentially stepwise mechanism (*i.e.* $(k_1 + k_2 + k_3 + k_4) >> k_5$) where the dechlorination of the *ortho*- positioned Cl proceeded at a higher rate than *para*- Cl removal (k_2/k_1 and $k_3/k_4 >> 1$). In contrast, Shin and Keane [17] (over Ni/SiO_2 at 573 K) and Wei and co-workers [85] (over unsupported Pd-Fe at 303 K) observed the opposite trend (*i.e.* k_2/k_1 and $k_3/k_4 << 1$) and ascribed this to rate inhibition due to steric hindrance in the case of *ortho*- Cl. The HDC of the monochlorophenol intermediates proceeded at a higher rate than that of 2,4-DCP: $(k_3 + k_4) >> (k_1 + k_2 + k_5)$. This response is consistent with an electrophilic aromatic substitution where the second (electron-withdrawing) Cl substituent has a deactivating effect [14,86].

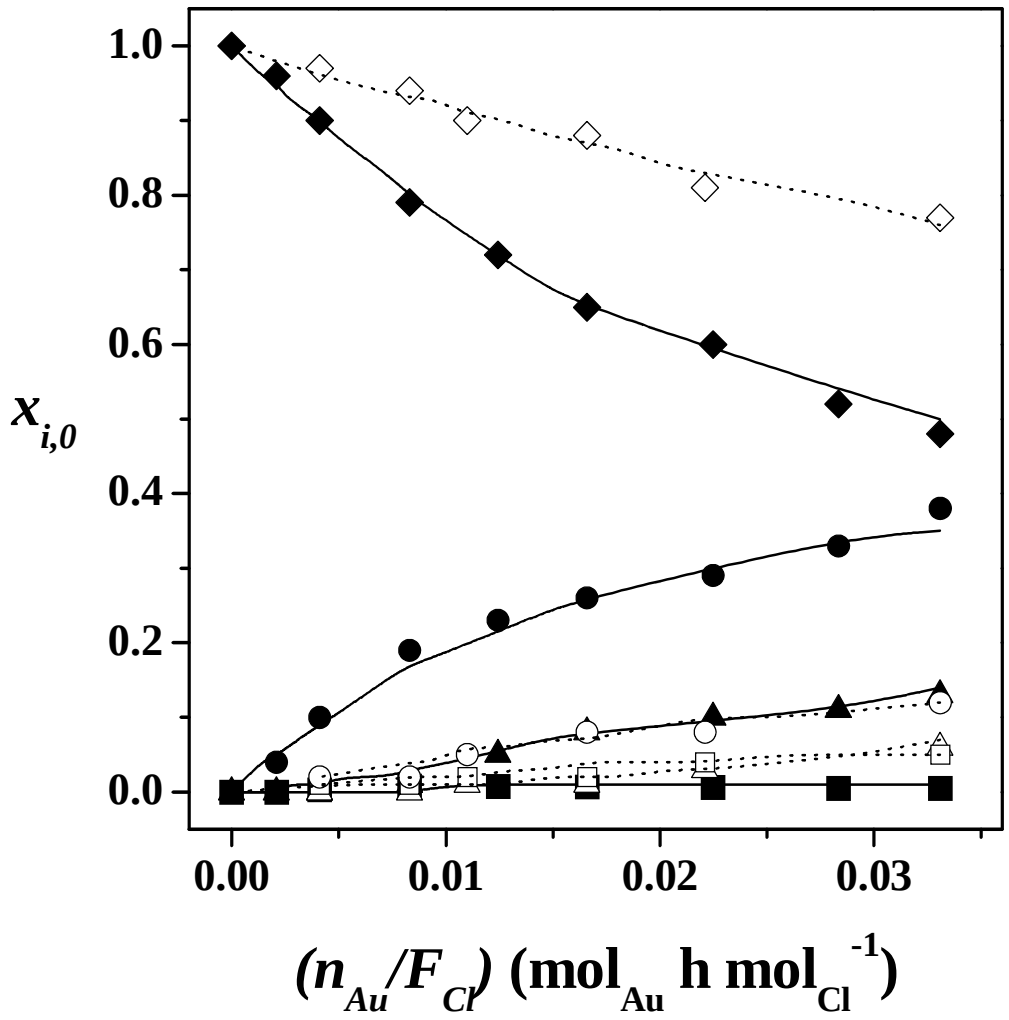

Figure 7.10: Initial mole fractions ($x_{i,0}$) of 2,4-DCP (◆,◇), 2-CP (■,□), 4-CP (●,○) and PhOH (▲,△) as a function of contact time for reaction over Au/α-Fe_2O_3 in water (solid symbols) and THF (open symbols) as solvent. Note: lines represent fit to eqns. (7.9 - 7.12).

Table 7.2: Pseudo-first order rate constants (k_j, $mol_{Cl}\ h^{-1}\ mol_{Au}^{-1}$) for 2,4-DCP HDC over Au/α-Fe_2O_3 (see Figure 7.8 and eqns. (7.9 - 7.12)).

Rate constant	Step	Solvent	
		Water	THF
k_1	2,4-DCP → 2-CP	1.0	2.6
k_2	2,4-DCP → 4-CP	23.4	5.3
k_3	2-CP → PhOH	95.0	22.8
k_4	4-CP → PhOH	20.0	12.5
k_5	2,4-DCP → PhOH	1.8	0.4

In this mechanism, hydrogen attacks the Cl bonded to the aromatic carbon bearing the highest electron density [87], forming a (cationic) reaction intermediate that is stabilized by charge delocalization in the ring [88]. It has been suggested previously [25] that aromatic resonance governs chlorophenol(s) HDC product distribution. However, from this consideration alone, one would expect k_1 to equal k_2 as the number of resonance forms resulting from *ortho*- or *para*- attack of 2,4-DCP is the same (= 4). An alternative or additional factor must then influence product distribution. Indeed, the preferential removal of the *ortho*- Cl suggests that this bond is preferentially activated on Au/α-Fe_2O_3. The unique selectivity response also suggests that the use of a reducible (α-Fe_2O_3) support plays a critical role. Reducible metal oxides (such as TiO_2 and α-Fe_2O_3) are semiconductors as they exhibit a narrower band gap (typically 2 - 3 eV [89]) when compared with non-reducible oxides (*e.g.* Al_2O_3, 9 eV [90]). TPR of α-Fe_2O_3 can then result in the removal of surface oxygen atoms (generating water as by-product) to form vacancies [51,59], which is consistent with the characterization results (see section **7.3.1**). Moreover, there is (XPS/EXAFS) evidence in the literature suggesting that, during TPR of Au/α-Fe_2O_3, the formation of surface oxygen vacancies generates electron-deficient $Au^{+\delta}$ species [91]. Therefore, the author envisions a reaction mechanism involving 2,4-DCP adsorption on (positively) charged Au clusters *via* the lone pair of electrons associated with –OH, facilitating polarization (and activation) of the *ortho*- C–Cl bond as a result of inductive effects. This will render the *ortho*- Cl substituent more susceptible to electrophilic attack than the *para*- counterpart. Such a mechanism requires the involvement of H^+ species and the occurrence of (positively) charged spillover hydrogen has been reported [92].

In section **7.3.2** is has been shown that spillover hydrogen is a feature of Au/α-Fe_2O_3 under the stated activation conditions and there is persuasive evidence in the literature that spillover hydrogen contributes to HDC, notably in the gas phase HDC of 3-CP [86] and chlorobenzenes [80]. A direct comparison of these results with the literature is, however, difficult since this is the first reported study of chlorophenol(s) HDC over a α-Fe_2O_3 based catalyst. Nevertheless, it is worth to flag the work of Shin *et al.* [17,86] who, studying 2,4-DCP HDC over Ni/SiO_2 (*i.e.* a non-reducible support), also suggested this mode of 2,4-DCP/catalyst interaction but, in that case, 4-CP was not generated as product.

The overall specific rate of 2,4-DCP (aqueous solution) conversion ($k_1 + k_2 + k_5$) delivered by Au/α-Fe_2O_3 (11×10^{-4} mol_{Cl} h^{-1} m_{Au}^{-2}, see **Table 7.3**) is close to that reported elsewhere [17] for reaction over Ni/SiO_2 bearing Ni particles with a mean diameter = 1.4 nm size (14×10^{-4} mol_{Cl} h^{-1} m_{Au}^{-2}), where the reaction in the latter case was carried out at a higher temperature (573 K). Such a level of activity for Au/α-Fe_2O_3 can be associated to small Au particle size (2.6 nm) as highly dispersed Au/α-Fe_2O_3 catalysts have been shown to deliver equivalent (and even superior) activity when compared with conventional catalytic systems in the water-gas shift reaction (Cu-Zn/Al_2O_3 [53]) and CO oxidation (Pt/TiO_2 [58]). It must be stressed that this is the first reported study demonstrating significant HDC activity for supported Au. Catalyst performance may also be influenced by the nature of the solvent carrier and it has been demonstrated for the water-gas shift reaction that Au/α-Fe_2O_3 can dissociate water to produce reactive hydrogen species [65,72].

Table 7.3: Specific pseudo-first order 2,4-DCP consumption rate constant (($k_1 + k_2 + k_5$), units: mol_{Cl} h^{-1} m_{Au}^{-2}) and fractional selectivities with respect to PhOH (S_{PhOH}), 2-CP ($S_{2\text{-}CP}$) and 4-CP ($S_{4\text{-}CP}$) at 20 % 2,4-DCP conversion for HDC over Au/α-Fe_2O_3 in different solvents.

Solvent	$(k_1 + k_2 + k_5) \times 10^4$	S_{PhOH}	$S_{2\text{-}CP}$	$S_{4\text{-}CP}$
Water	10.8	0.05	0.03	0.92
Methanol	4.3	0.07	0.04	0.89
Ethanol	5.1	0.05	0.02	0.93
n-Propanol	5.6	0.03	0.04	0.93
n-Butanol	6.7	0.06	0.01	0.93
n-Hexane	2.5	0.05	0.04	0.91
THF	3.8	0.19	0.20	0.61
Cyclohexane	2.4	0.08	0.04	0.88

The possible role of the solvent was also addressed in this study, considering the action of protonated (linear alcohols) and non-protonated (*n*-hexane, THF and cyclohexane) organics as solvent carriers; the results are presented in **Table 7.3**. The catalytic activity associated with all the organic solvents was lower than that recorded in water. This result suggests some level of solvent/2,4-DCP competitive adsorption in the case of the organic carriers. Rate inhibition due to an occlusion of active sites by solvent (alcohols, *n*-heptane) has been reported for the gas phase hydrogenation of PhOH [93] and tetralin [94]. It is worth noting that the HDC rate was higher in the case of the alcohols and, moreover, increased in moving from methanol to *n*-butanol. Alcohol chemisorption on reducible (TiO_2) and non-reducible (Al_2O_3) metal oxides proceeds through interaction between the lone pair of electrons in the alcohol oxygen and a Lewis acid site on the oxide [95,96] with concomitant H^+ abstraction and alcoxide formation, where the ease of oxygen electron donation increases with increasing chain length [23]. The latter is in line with a more facile activation/dissociation of *n*-butanol relative to methanol, generating H^+ species that can promote 2,4-DCP HDC. This response is also consistent with the lower activity registered for *n*-hexane, THF and cyclohexane where H^+ abstraction is not possible. Solvent H^+ donation is a well known phenomenon in liquid phase HDC [97,98] but has not been considered to any significant extent in gas phase reactions. Nevertheless, the work of López *et al.* [99] should be noted, who have recently observed a positive effect with *n*-butanol addition on tetrachloroethylene HDC over Pd/Al_2O_3. In the present case, the use of different solvents had little effect in terms of reaction pathway where, at the same level of 2,4-DCP conversion, product selectivity was essentially the same with the exception of THF, as shown in **Table 7.3**. Application of eqns. **(7.9 - 7.12)** (see **Figure 7.10** and **Table 7.2**) has revealed that the use of THF limits production of 4-CP; $k_2/k_1 = 2$ for THF compared with $k_2/k_1 = 23$ for water. Distinct reaction selectivities when using THF as solvent have also been reported for the hydrogenation of paracetamol [100] and the decomposition of 2-(chloroethyl)ethyl sulphide [101].

These results demonstrate, for the first time, high selectivity in the hydrogenolytic cleavage of a sterically constrained Cl substituent from an aromatic host due to the catalytic action of $Au/\alpha\text{-}Fe_2O_3$. The study was consequently extended to assess this selectivity response for the HDC of a range of mono-, di- and tri-chlorophenols and the results are presented in **Table 7.4**.

Table 7.4: Specific HDC rate constant (k'_{Cl}, units: $mol_{Cl}\ h^{-1}\ m_{Au}^{-2}$) and product composition (in terms of initial molar fractions) for the conversion of representative chlorophenols (in ethanol) over Au/α-Fe_2O_3.

Reactant	$k'_{Cl} \times 10^4$	Product(s)[a]
2-CP	11.6	PhOH (0.37)
3-CP	4.3	PhOH (0.08)
4-CP	4.2	PhOH (0.06)
2,3-DCP	4.4	2-CP (0.01), 3-CP (0.12)
2,4-DCP	5.1[b]	PhOH (0.01), 4-CP (0.15)
2,5-DCP	8.6	2-CP (0.05), 3-CP (0.25)
2,6-DCP	10.0	PhOH (0.31), 2-CP (0.24)
3,4-DCP	2.8	PhOH (0.03), 3-CP (0.02), 4-CP (0.06)
3,5-DCP	3.7	PhOH (0.05), 3-CP (0.05)
2,4,6-TCP	8.5	PhOH (0.10), 4-CP (0.13), 2,4-DCP (0.12)

[a] $(n_{Au}/F_{Cl}) = 0.017\ mol_{Au}\ h\ mol_{Cl}^{-1}$
[b] $k_{Cl} = (k_1 + k_2 + k_5)$, see **Figure 7.8** and eqns. **(7.9 - 7.12)**

A salient feature of the tabulated data is the higher specific HDC rate (k'_{Cl}) exhibited by those reactants bearing *ortho*- Cl substituents. It is worth flagging that 2-CP and 2,6-DCP displayed the highest k'_{Cl} values among the mono- and di-chlorophenol isomers, respectively. The sequence of decreasing k'_{Cl}, *i.e.* 2-CP > 2,6-DCP > 2,4,6-TCP, is again consistent with an electrophilic dechlorination mechanism and a deactivating effect due to the additional electron withdrawing Cl substituent(s). The unique HDC selectivity exhibited by Au/α-Fe_2O_3 is exemplified by the results for the conversion of 2,4,6-TCP where the absence of 2,6-DCP (or 2-CP) as partial HDC products confirms the action of Au/α-Fe_2O_3 to selectively cleave *ortho*- C–Cl bonds. This is further illustrated by the preferential formation of 3-CP (relative to 2-CP) in the HDC of 2,3- and 2,5-DCP. The findings reported and discussed in this study constitute a critical advancement in the selective HDC of chlorophenols where, to date, chloroarenes bearing *ortho*- Cl substituents (*eg.* 2-CP [24,26] and 2,6-DCP [25,102]) have been consistently identified as principal products. This has been attributed to steric hindrance effects that render *ortho*- substituted Cl less susceptible to attack. The results presented here have established a catalytic system (Au/α-Fe_2O_3) that acts to selectively cleave sterically constrained Cl, which will serve to extend the range of possible products generated in the treatment of chloroarene streams. This will facilitate the development of controlled sustainable chloroarene waste recycle to deliver target product(s).

7.4 Conclusions

The synthesis of α-Fe_2O_3 by precipitation (in basic media) and introduction of Au by precipitation-deposition has generated a catalyst that exhibits unique selectivity in hydrodechlorination of chlorophenols. The hematite (α-Fe_2O_3) support can be reduced to magnetite (Fe_3O_4) and metallic Fe during TPR to 673 K and 1273 K, respectively, with a concomitant decrease in BET surface area and pore volume. Support reduction was facilitated by the introduction of Au with a decrease in the requisite temperature by *ca.* 200 K. Based on XRD analysis, TPR of Au/α-Fe_2O_3 to 423 K resulted in a partial reduction of the support to Fe_3O_4. Under these activation conditions, the catalyst bears small ($\leq$ 10 nm), quasi-spherical Au particles (surface area-weighted mean size = 2.6 nm). The activated catalyst exhibited a four-fold increase in surface H_2 content relative to the α-Fe_2O_3 support alone. The gas phase (423 K) catalytic HDC of 2,4-DCP over Au/α-Fe_2O_3 yielded 4-CP as the predominant product *via* a stepwise electrophilic mechanism, ***i.e.*** the *ortho*- Cl substituent was preferentially removed. This response is attributed to the use of a well dispersed Au phase on a reducible support where, under activation conditions, surface oxygen vacancies are created. These induce (*via* electron transfer) the formation of $Au^{+\delta}$ particles, favouring reactant adsorption through the –OH substituent and, ultimately, facilitating activation of the *ortho*- C–Cl bond. The use of water and alcohols as carriers served to elevate HDC activity by generating reactive hydrogen as a result of a dissociative interaction with the catalyst. High selectivity with respect to the cleavage of *ortho*- Cl substituent(s) extends to mono- di- and tri-chlorophenols. These results establish, for the first time, the viability of a selective catalytic hydrogenolysis of sterically constrained Cl substituents. Such control of HDC selectivity represents a critical advancement in the targeted transformation of chlorinated waste.

7.5 References

[7.1] Pollution Handbook 2005: The Esssential Guide to UK and European Pollution Control Legislation, Environmental Protection UK, 2005.

[7.2] USEPA, Advisory Document No. 8EHQ-14302, 2000.

[7.3] F. Muller, L. Caillard, Ullmann's Encyclopedia of Industrial Chemistry. "Chlorophenols", Wiley-VCH Verlag GmbH & Co. KGaA, Weinheim, 2000.

[7.4] M. Pera-Titus, V. García-Molina, M. A. Baños, J. Giméneza, S. Esplugas, Appl. Catal. B: Environmental, 47, 219 (2004)

[7.5] L. Wu, A. Li, G. Gao, Z. Fei, S. Xu, Q. Zhang, J. Mol. Catal. A: Chemical, 269, 183 (2007)

[7.6] R. Kidak, N. H. Ince, Ultrason. Sonochem. , 13, 195 (2006)

[7.7] O. Hamdaoui, E. Naffrechoux, Ultrason. Sonochem., 15, 981 (2008)

[7.8] H. Cheng, K. Scott, P. A. Christensen, Appl. Catal. A: General, 261, 1 (2004)

[7.9] G. Chen, Z. Wang, D. Xia, Electrochim. Acta, 50, 933 (2004)

[7.10] M. Dilaver, F. Kargi, Bioresour. Technol., 100, 1459 (2009)

[7.11] S. Eker, F. Kargi, J. Hazard. Mater., 159, 306 (2008)

[7.12] V. Nicolas, S. Jean-Pierre, Chemosphere, 67, S144 (2007)

[7.13] L. Khachatryan, S. Lomnicki, B. Dellinger, Chemosphere, 68, 1741 (2007)

[7.14] E.-J. Shin, M. A. Keane, J. Hazard. Mater. B, 66, 265 (1999)

[7.15] G. Yuan, M. A. Keane, Ind. Eng. Chem. Res., 46, 705 (2007)

[7.16] E.-J. Shin, M. A. Keane, Appl. Catal. B: Environmental, 18, 241 (1998)

[7.17] E.-J. Shin, M. A. Keane, Chem. Eng. Sci., 54, 1109 (1999)

[7.18] E.-J. Shin, M. A. Keane, React. Kinet. Catal. Lett., 69, 3 (2000)

[7.19] L. Calvo, M. A. Gilarranz, J. A. Casas, A. F. Mohedano, J. J. Rodríguez, J. Hazard. Mater., 161, 842 (2009)

[7.20] C. Xia, Y. Liu, J. Xu, J. Yu, W. Qin, X. Liang, Catal. Commun., 10, 456 (2009)

[7.21] G. Yuan, M. A. Keane, Catal. Today, 88, 27 (2003)

[7.22] S. Gómez-Quero, F. Cárdenas-Lizana, M. A. Keane, Ind. Eng. Chem. Res., 47, 6841 (2008)

[7.23] F. A. Carey, R. C. Atkins, Organic Chemistry, 5th ed., Mc Graw-Hill, New York, 2003.

[7.24] G. Pina, C. Louis, M. A. Keane, Phys. Chem. Chem. Phys., 5, 1924 (2003)

[7.25] E.-J. Shin, M. A. Keane, J. Chem. Technol. Biotechnol., 75, 159 (2000)

[7.26] L. Calvo, A. F. Mohedano, J. A. Casas, M. A. Gilarranz, J. J. Rodríguez, Carbon, 42, 1377 (2004)

[7.27] G. S. Pozan, I. Boz, Environ. Eng. Sci., 25, 1197 (2008)

[7.28] A. S. K. Hashmi, Chem. Rev., 107, 3180 (2007)

[7.29] P. Claus, Appl. Catal. A: General, 291, 222 (2005)

[7.30] A. S. K. Hashmi, G. J. Hutchings, Angew. Chem. Int. Ed., 45, 7896 (2006)

[7.31] G. J. Hutchings, J. Mater. Chem., 19, 1222 (2009)

[7.32] M. L. Toebes, M. K. van der Lee, L. M. Tang, M. H. Huis in‘t Veld, J. H. Bitter, A. J. van Dillen, K. P. de Jong, J. Phys. Chem. B, 108, 11611 (2004)

[7.33] P. Burattin, M. Che, C. Louis, J. Phys. Chem. B, 102, 2722 (1998)

[7.34] M. Okumura, T. Akita, M. Haruta, Catal. Today, 74, 265 (2002)

[7.35] R. J. H. Grisel, P. J. Kooyman, B. E. Nieuwenhuys, J. Catal., 191, 430 (2000)

[7.36] A. C. Gluhoi, M. A. P. Dekkers, B. E. Nieuwenhuys, J. Catal., 219, 197 (2003)

[7.37] A. Sandoval, A. Gómez-Cortés, R. Zanella, G. Díaz, J. M. Saniger, J. Mol. Catal. A: Chemical, 278, 200 (2007)

[7.38] M. Boronat, P. Concepción, A. Corma, S. González, F. Illas, P. Serna, J. Am. Chem. Soc., 129, 16230 (2007)

[7.39] J. A. Lopez-Sanchez, D. Lennon, Appl. Catal. A: General, 291, 230 (2005)

[7.40] C. Milone, C. Crisafulli, R. Ingoglia, L. Schipilliti, S. Galvagno, Catal. Today, 122, 341 (2007)

[7.41] G. Yuan, C. Louis, L. Delannoy, M. A. Keane, J. Catal., 247, 256 (2007)

[7.42] G. Neri, A. M. Visco, S. Galvagno, A. Donato, M. Panzalorto, Thermochim. Acta, 329, 39 (1999)

[7.43] M. Khoudiakov, M. C. Gupta, S. Deevi, Appl. Catal. A: General, 291, 151 (2005)

[7.44] J. Vakros, C. Kordulis, A. Lycourghiotis, J. Chem. Soc. Chem. Commun., 17, 1980 (2002)

[7.45] D. Dollimore, G.R. Heal, J. Colloid Interface Sci., 33, 508 (1970)

[7.46] M. A. Keane, P. M. Patterson, J. Chem. Soc., Faraday Trans., 92, 1413 (1996)

[7.47] G. Yuan, M. A. Keane, Chem. Eng. Sci., 58, 257 (2003)

[7.48] G. Tavoularis, M. A. Keane, J. Mol. Catal. A: Chemical, 142, 187 (1999)

[7.49] M. Žic, M. Ristić, S. Musić, J. Mol. Struct., 834-836, 141 (2007)

[7.50] U. Schwertmann, E. Murad, Clays Clay Miner., 31, 277 (1983)

[7.51] W. K. Jozwiak, E. Kaczmarek, T. P. Maniecki, W. Ignaczak, W. Maniukiewicz, Appl. Catal. A: General, 326, 17 (2007)

[7.52] J. R. Anderson, K. C. Pratt, Introduction to Characterization and Testing of Catalysts, Academic Press, London, 1985.

[7.53] D. Andreeva, V. Idakiev, T. Tabakova, A. Andreev, R. Giovanoli, Appl. Catal. A: General, 134, 275 (1996)

[7.54] J. W. Geus, Appl. Catal. A: General, 25, 313 (1986)

[7.55] F. Moreau, G. C. Bond, Catal. Today, 122, 260 (2007)

[7.56] G. Yuan, M. A. Keane, J. Catal., 225, 510 (2004)

[7.57] M. L. Toebes, J. A. Dillen, K. P. de Jong, J. Mol. Catal. A: Chemical, 173, 75 (2001)

[7.58] M. Haruta, J. New Mater. Electrochem. Syst., 7, 163 (2004)
[7.59] G. Munteanu, L. Ilieva, D. Andreeva, Thermochim. Acta, 291, 171 (1997)
[7.60] A. Pineau, N. Kanari, I. Gaballah, Thermochim. Acta, 456, 75 (2007)
[7.61] A. Pineau, N. Kanari, I. Gaballah, Thermochim. Acta, 447, 89 (2006)
[7.62] F. Moreau, G. C. Bond, A. O. Taylor, J. Catal., 231, 105 (2005)
[7.63] F. Moreau, G. C. Bond, Catal. Today, 122, 215 (2007)
[7.64] A. M. Visco, A. Donato, C. Milone, S. Galvagno, React. Kinet. Catal. Lett., 61, 219 (1997)
[7.65] B. A. A. Silberova, G. Mul, M. Makkee, J. A. Moulijn, J. Catal., 243, 171 (2006)
[7.66] A. Venugopal, M. S. Scurrell, Appl. Catal. A: General, 258, 241 (2004)
[7.67] G. Y. Wang, H. L. Lian, W. X. Zhang, D. Z. Jiang, T. H. Wu, Kinet. Catal., 43, 468 (2002)
[7.68] J. Li, Y. Zhan, X. Lin, Zheng Q, Acta Phys. Chim. Sin., 24, 932 (2008)
[7.69] W. C. Conner, J. L. Falconer, Chem. Rev., 95, 759 (1995)
[7.70] D. A. Panayotov, J. T. Yates, J. Phys. Chem. C, 111, 2959 (2007)
[7.71] S. E. Collins, J. M. Cíes, E. del Río, M. López-Haro, S. Trasobares, J. J. Calvino, J. M. Pintado, S. Bernal, J. Phys. Chem. C, 111, 14371 (2007)
[7.72] F. Boccuzzi, A. Chiorino, M. Manzoli, D. Andreeva, T. Tabakova, J. Catal., 188, 176 (1999)
[7.73] S. Díaz-Moreno, D. C. Koningsberger, A. Muñoz-Páez, Nucl. Instrum. Methods Phys. Res., Sect. B, 133, 15 (1997)
[7.74] J. Liu, Microsc. Microanal., 10, 55 (2004)
[7.75] A. G. Sault, R. J. Madix, C. T. Campbell, Surf. Sci., 169, 347 (1986)
[7.76] J. Słoczyński, R. Grabowski, A. Kozłowska, P. Olszewski, J. Stoch, J. Skrzypek, M. Lachowska, Appl. Catal. A: General, 278, 11 (2004)
[7.77] C. Amorim, M. A. Keane, J. Chem. Technol. Biotechnol., 83, 662 (2008)
[7.78] G. Yuan, M. A. Keane, Appl. Catal. B: Environmental, 52, 301 (2004)
[7.79] M. I. Cobo, J. A. Conesa, C. M. de Correa, J. Phys. Chem. A, 112, 8715 (2008)
[7.80] K. V. R. Chary, C. S. Srikanth, V. V. Rao, Catal. Commun., 10, 459 (2009)
[7.81] X. Liu, J. Chen, J. Zhang, Ind. Eng. Chem. Res., 47, 5362 (2008)
[7.82] E. V. Golubina, E. S. Lokteva, V. V. Lunin, N. S. Telegina, A. Y. Stakheev, P. Tundo, Appl. Catal. A: General, 302, 32 (2006)
[7.83] J. W. da Silva, R. E. Bruns, A. J. G. Cobo, Chem. Eng. J., 131, 59 (2007)
[7.84] E.-J. Shin, M. A. Keane, Ind. Eng. Chem. Res., 39, 883 (2000)

[7.85] J. Wei, X. Xu, Y. Liu, D. Wang, Water Res., 40, 348 (2006)

[7.86] E.-J. Shin, A. Spiller, G. Tavoularis, M. A. Keane, Phys. Chem. Chem. Phys., 1, 3173 (1999)

[7.87] Y. A. Serguchev, Y. V. Belokopytov, Kinet. Catal., 42, 174 (2001)

[7.88] B. F. Hagh, D. T. Allen, Chem. Eng. Sci., 45, 2695 (1990)

[7.89] C. Sol, R. J. D. Tilley, J. Mater. Chem. , 11, 815 (2001)

[7.90] C. Karunakaran, P. Anilkumar, Sol. Energy Mater. Sol. Cells 92, 490 (2008)

[7.91] Z. Hao, L. An, H. Wang, T. Hu, React. Kinet. Catal. Lett., 70, 153 (2000)

[7.92] U. Roland, T. Braunschweig, F. Roessner, J. Mol. Catal. A: Chemical, 127, 61 (1997)

[7.93] E.-J. Shin, M. A. Keane, J. Catal., 73, 450 (1998)

[7.94] A. Guevara, R. Bacaud, M. Vrinat, Appl. Catal. A: General, 253, 515 (2003)

[7.95] S. Cai, K. Sohlberg, J. Mol. Catal. A: Chemical, 193, 157 (2003)

[7.96] B. Shi, H. A. Dabbagh, B. H. Davis, J. Mol. Catal. A: Chemical, 141, 257 (1999)

[7.97] Y. Ukisu, Appl. Catal. A: General, 349, 229 (2008)

[7.98] F.-D. Kopinke, K. Mackenzie, R. Koehler, A. Georgi, Appl. Catal. A: General, 271, 119 (2004)

[7.99] E. López, F. V. Díez, S. Ordóñez, Appl. Catal. B: Environmental, 82, 264 (2008)

[7.100] B. Bachiller-Baeza, A. Guerrero-Ruíz, I. Rodríguez-Ramos, J. Catal., 229, 439 (2005)

[7.101] R. M. Narske, K. J. Klabunde, S. Fultz, Langmuir, 18, 4819 (2002)

[7.102] T. T. Bovkun, Y. Sasson, J. Blum, J. Mol. Catal. A: Chemical, 242, 68 (2005)

Chapter 8

Au/Fe_3O_4: Characterization and Application in Gas Phase Hydrodechlorination

In the previous Chapter, an unprecedented selectivity behaviour of Au with regard to hydrodechlorination of sterically constrained Cl substituents has been established for Au/α-Fe_2O_3. That work is extended further in this Chapter with a consideration of the synthesis, characterization and catalytic performance of Au supported on Fe_3O_4. Two synthesis routes are explored (stepwise *vs.* direct precursor deposition and catalyst activation) and the selective production of 4-chlorophenol from 2,4-dichlorophenol is demonstrated. The benefits of catalytic hydrodehalogenation promoted by Fe_3O_4 supported Au as a waste abatement/recycle methodology are assessed.

8.1 Introduction

Catalytic hydrodechlorination (HDC), the hydrogen mediated scission of C–Cl bond(s), is finding increasing acceptance as a progressive means of chloroarene waste abatement [1]. Catalytic HDC facilitates the recycle and reuse of the parent aromatic without producing hazardous by-products [2] and operates under mild reaction conditions, with lower associated energy requirements relative to standard thermal decomposition [3]. The efficiency of the HDC approach has been assessed in terms of the role temperature [4,5], reactant(s) partial pressure [4,6], catalyst support [5,7], metal dispersion [6,8] and use of additives [9,10] in the (gas phase) treatment of chlorinated dibenzo-*p*-dioxins and furans [9,10], benzenes [4,6,7], toluenes [6] and phenols [5,6,8]. However, further research is required in terms of controlling HDC selectivity, notably in the case of reactions involving chlorophenols where dechlorination is inhibited due to steric hindrance with respect to Cl positioned *ortho*- to the –OH substituent [11,12]. This effect is well illustrated in the case of 2,4-dichlorophenol (2,4-DCP, see reaction pathway in **Figure 8.1**) where, to date, 2-chlorophenol (2-CP) has been consistently isolated as the only partially dechlorinated product for HDC promoted by Pd [13-15], Ni [16,17] or Rh [15] supported on Al_2O_3 [13,15], SiO_2 [16,17] or carbon [14,15] when conducted in either gas [16,17] or liquid [13-15] phase.

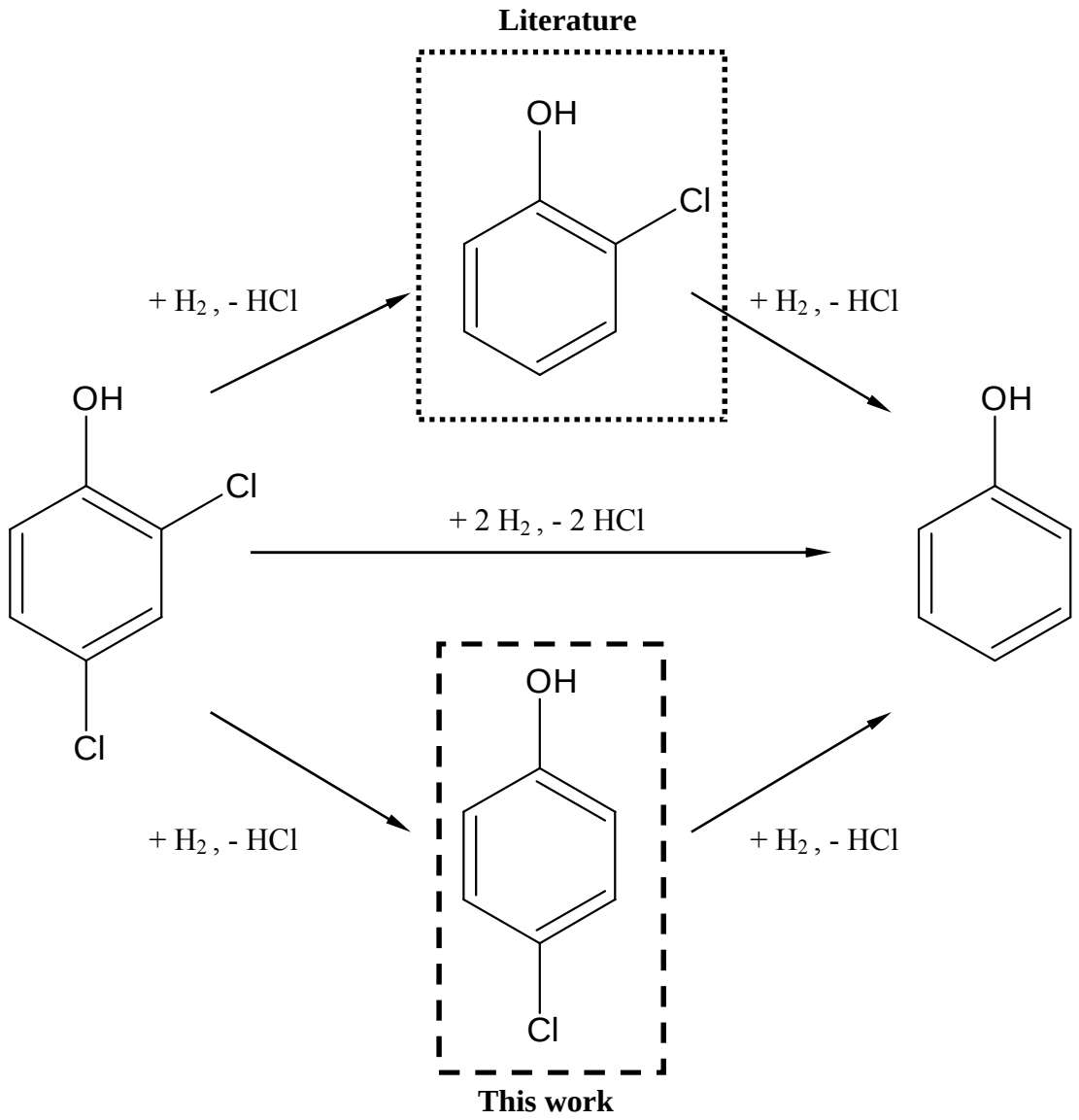

Figure 8.1: Reaction pathway for the HDC of 2,4-DCP.

It should, however, be flagged the work of Yuan *et al.* [18] who achieved a 4-CP selectivity of 13 % for (gas phase) reaction over Ni-Au/TiO_2. 2,4-DCP, the model reactant in this study, has now been placed on the list of high priority pollutants for immediate waste treatment [19]. Incineration as the conventional "end-of-pipe" treatment, requires high temperatures (1200 K - 1500 K) and excess oxygen where products of incomplete combustion, polychlorodibenzodioxins (PCDD) and polychlorodibenzofurans (PCDF) are far more toxic than the chlorinated feed [20,21]. A treatment of 2,4-DCP that facilitates the controlled removal of the *ortho*- Cl substituent represents a far more progressive approach, allowing the recycle of 4-CP.

4-CP is an important raw material in the production of fungicides [22], molluskicides [23], dichlorophene (used as antimicrobial finishing for textiles/paper) [24] and fenticlor (for algae control in water circulating systems) [24]. In **Chapter 7**, the preferential scission of the *ortho*- Cl in a range of mono-, di- and tri-chlorophenols has been achieved using a well dispersed Au phase (mean particle diameter = 2.6 nm) supported on hematite (α-Fe_2O_3). This unique response was accounted for in terms of a selective C–Cl activation at (electron-deficient) $Au^{+\delta}$ particles associated with the partial reduction of α-Fe_2O_3 to magnetite (Fe_3O_4). Those findings are extended in this Chapter to assess the catalytic performance of Au supported on bulk Fe_3O_4 in terms of 4-CP synthesis from 2,4-DCP.

The reported use of Au in HDC applications has been very limited, serving as a promoter of unsupported [25,26] and (Al_2O_3 [26,27], carbon [28-30]) supported Pd in the hydrotreatment of trichloroethene [25,26] and CCl_2F_2 [27-30] and delivering low conversions (≤ 3 %) of 2,4-DCP in the case of Au/SiO_2 and Au/TiO_2 [18]. In general, Au has exhibited low activities in hydrogen mediated reactions when compared with conventional Pd [31] and Pt [32] catalysts. However, Au catalysts have been shown to deliver higher levels of selectivity in the $–NO_2$ group hydrogenation of nitroarenes [33,34] and C=O (as opposed to the C=C) hydrogenation in α,β- unsaturated ketones [35,36]. This catalytic response has been associated with Au particles < 10 nm [37], notably when dispersed on reducible (*e.g.* α-Fe_2O_3, TiO_2, CeO_2) metal oxides [38,39] where Au/support interactions are critical [40]. A thorough search of the literature has failed to unearth any study where Au/Fe_3O_4 has been employed to promote hydrogenolysis reactions. To date, Fe_3O_4 has only been used to support Pd and Au-Pd in the liquid phase HDC of trichloroethene and chlorobenzene [41,42]. In this report, the catalytic action of Au/Fe_3O_4 is assessed focusing, for the first time (in particular), on the selective HDC of 2,4-DCP to 4-CP as a progressive means of waste abatement/recycle.

8.2 Experimental

8.2.1 Catalyst Preparation

Hematite (α-Fe_2O_3) was synthesized by precipitation in basic media as described in the previous Chapter.

Magnetite (Fe_3O_4) was prepared by temperature programmed reduction (TPR) of α-Fe_2O_3 at 2 K min^{-1} to 673 K in a flow of H_2 (60 cm^3 min^{-1}, *GHSV* = 680 h^{-1}). The resultant black powder was flushed in He (60 cm^3 min^{-1}) and cooled to room temperature under the same flow. The Fe_3O_4 was then sieved to 75 μm average particle diameter (ATM fine test sieves) and stored in air at room temperature. Two strategies were used in the preparation of 1 % w/w Au/Fe_3O_4: (i) a stepwise approach where a α-Fe_2O_3 supported Au precursor was first synthesised and then subjected to TPR (2 K min^{-1}) to 673 K (denoted as "Au/Fe_3O_4-step"); (ii) direct synthesis using Fe_3O_4 as support (denoted as "Au/Fe_3O_4-dir"). In both cases, Au was incorporated on the oxide (α-Fe_2O_3 or Fe_3O_4) support by deposition-precipitation, which is known to generate higher metal dispersions (at a common loading) when compared with the less controlled impregnation procedure [34,38]. Aqueous urea (*ca.* 100 fold urea mol excess) was combined with a solution of $HAuCl_4$ (300 cm^3, 5×10^{-4} M) and added to the support (*ca.* 5 g). The suspension was stirred (300 rpm) and heated (2 K min^{-1}) to 353 K. The pH of the suspension was measured using a pH meter (Hanna Instruments) equipped with a crystal-body electrode, coupled to a data logging and collection system (Pico Technology Ltd.); calibration was previously performed with standard buffer solutions (pH 4 and 10). The pH progressively increased to reach *ca.* 7 after 8 h as a result of the thermally-induced urea decomposition [43]. The solids were then filtered, washed with distilled water until the wash water was chlorine-free (based on the $AgNO_3$ test) and dried in He (60 cm^3 min^{-1}) at 383 K for 3 h. After preparation, the samples were sieved to 75 μm average particle diameter and stored at 277 K in the dark. The Au loading was determined (to within ± 2 %) by inductively coupled plasma-optical emission spectrometry (ICP-OES, Vista-PRO, Varian Inc.) from the diluted extract of aqua regia.

8.2.2 Catalyst Characterization

The pH associated with the point of zero charge (pH_{pzc}) of the supports was determined using the potentiometric mass titration technique [44]. Three different masses (0.05, 0.08 and 0.10 g) were immersed in 50 cm^3 0.1 M NaCl to which a known amount of NaOH (0.1 M) was added to adjust initial pH to *ca.* 11. Titration of the samples was performed under continuous agitation in a He atmosphere with HCl (0.1 M) as titrant. Characterization in terms of TPR and H_2 chemisorption was performed using the commercial CHEM-BET 3000 (Quantachrome Instruments) unit.

The samples were loaded into a U-shaped (100 × 3.76 mm) pyrex cell, contacted with 5 % v/v H_2/N_2 flow (17 cm^3 min^{-1}, Brooks mass flow controlled) and subjected to TPR at 2 K min^{-1} to 673 K. The effluent gas was directed through a liquid N_2 trap and H_2 consumption/release was monitored by a thermal conductivity detector with data acquisition and manipulation using the TPR Win™ software. The reduced samples were then swept with dry N_2 (65 cm^3 min^{-1}) at the final temperature for 90 min, cooled to room temperature and subjected to H_2 chemisorption analysis (10 μL pulses). The H_2 pulses were repeated until the signal area was constant, indicating surface saturation. BET surface area and pore volume measurements were performed using a commercial Micromeritics Flowsorb II 2300. Prior to analysis, the samples were outgassed at 423 K for 1 h in 20 cm^3 min^{-1} dry N_2. BET area was obtained in 30 % v/v N_2/He (20 cm^3 min^{-1}) with at least three cycles of N_2 adsorption-desorption using the standard single-point BET method. Total pore volume was recorded at a relative pressure of P/P_0 = 0.95. Hydrogen chemisorption, BET areas and pore volumes were reproducible to within ± 5 % and the values quoted in this study are the mean. Diffuse reflectance UV-Vis (DRS UV-Vis) measurements were conducted using a Perkin Elmer Lambda 35 UV-Vis Spectrometer, where $BaSO_4$ powder served as reference. Absorption profiles were calculated from the reflectance data using the Kubelka-Munk function. Structural features were monitored by X-ray diffraction (XRD) analysis, using a Bruker/Siemens D500 incident X-ray diffractometer with Cu Kα radiation. The samples were scanned at 0.02º $step^{-1}$ over the range 20º ≤ 2θ ≤ 90º (scan time = 5 s $step^{-1}$). The diffractograms were compared with the JCPDS-ICDD references for comparison purposes (Card No. 33-0664 (α-Fe_2O_3); 19-0629 (Fe_3O_4); 04-0784 (Au)). Au particle size/morphology was assessed by transmission electron microscopy (TEM) analysis: JEOL JEM 2011 TEM unit with a UTW energy-dispersive X-ray detector (Oxford Instruments) operated at an accelerating voltage of 200 kV and using Gatan DigitalMicrograph 3.4 for data acquisition/manipulation. The samples were dispersed in acetone and deposited on a holey-carbon/Cu grid (300 Mesh). Up to 400 individual metal particles were counted for each catalyst and the surface area-weighted metal diameter (d_{TEM}) was calculated from:

$$d_{TEM} = \frac{\sum_i n_i d_i^3}{\sum_i n_i d_i^2} \qquad \textbf{(8.1)}$$

where n_i is the number of particles of diameter d_i.

8.2.3 Catalytic Procedure

2,4-DCP was purchased from Sigma-Aldrich (99 %) and used without further purification. Reactions were carried out under atmospheric pressure, in situ immediately after activation, in a fixed bed vertical plug-flow glass reactor (i.d. = 15 mm, l = 600 mm). The catalytic reactor, and operating conditions to ensure negligible heat/mass transport limitations, have been fully described elsewhere [45], but details pertinent to this study are given below. 2,4-DCP was delivered (as an aqueous solution) to the reactor *via* a glass/teflon air-tight syringe and a teflon line using a microprocessor controlled infusion pump (Model 100 kd Scientific), where the molar ratio of Au (n_{Au}) to reactant flow rate (F) spanned the range 0.01 - 0.19 mol_{Au} h $mol_{2,4\text{-}DCP}^{-1}$. A co-current flow of ultra pure H_2 (60 cm^3 min^{-1}) was monitored using a Humonics (Model 520) digital flowmeter and maintained at a $GHSV = 2 \times 10^4$ h^{-1} (*ca.* 700 times in excess of the stoichiometric requirement for conversion of 2,4-DCP to cyclohexane). A layer of glass beads above the catalytic bed served as a preheating zone, ensuring that 2,4-DCP vaporized, reaching reaction temperature (423 K) before contacting the catalyst. Isothermal conditions were maintained by diluting the catalytic bed with ground glass (75 μm). The reaction temperature was continuously monitored by a thermocouple inserted in a thermowell within the catalyst bed. The reactor effluent was frozen in a liquid nitrogen trap for subsequent analysis which was made using a Perkin-Elmer Auto System XL GC, employing a DB-1 (J&W Scientific) capillary column (i.d. = 0.20 mm, l = 50 m, film thickness = 0.33 μm) as described in detailed elsewhere [46]. A chlorine mass balance was performed by passing the effluent gas through an aqueous NaOH trap (9×10^{-4} mol dm^{-3}, kept under constant agitation at 400 rpm) with independent pH (Hanna HI Programmable Printing pH Bench-Meter) analysis; HCl was the only inorganic product, as noted elsewhere [47]. The overall level of HDC is quoted as a fractional conversion ($X_{2,4\text{-}DCP}$):

$$X_{2,4\text{-}DCP} = \frac{C_{2,4\text{-}DCP,0} - C_{2,4\text{-}DCP}}{C_{2,4\text{-}DCP,0}} \qquad \textbf{(8.2)}$$

where $C_{2,4\text{-}DCP,0}$ and $C_{2,4\text{-}DCP}$ represent the inlet and outlet concentrations of 2,4-DCP, respectively. The fractional selectivity to, for example, 4-CP ($S_{4\text{-}CP}$) is given by:

$$S_{4\text{-}CP} = \frac{C_{4\text{-}CP}}{C_{2,4\text{-}DCP,0} - C_{2,4\text{-}DCP}} \quad \textbf{(8.3)}$$

where $C_{4\text{-}CP}$ is the outlet concentration of 4-CP. Repeated reactions with different samples from the same batch of catalyst delivered raw data reproducibility that was better than ± 8 %.

8.3 Results and Discussion

8.3.1 Catalyst Synthesis/Characterization

The characteristics of the two Au/Fe_3O_4 catalysts, in terms of H_2 consumption and associated T_{max} during TPR, subsequent H_2 chemisorption, BET/pore volume and TEM derived surface area-weighted mean Au size (d_{TEM}), are given in **Table 8.1**. A detailed analysis of the data generated for Au/Fe_3O_4-step is given in the following section with a further consideration of the similarities/differences with respect to Au/Fe_3O_4-dir in section **8.3.1.2**.

8.3.1.1 Au/Fe_3O_4-step

The temporal pH/temperature variations in the preparation of $Au/\alpha\text{-}Fe_2O_3$ (precursor for Au/Fe_3O_4-step) are given in **Figure 8.2**a where the pH_{pzc} of the support is identified as a dashed line. The pH_{pzc} represents the pH at which the accessible wetted support surface is electrically neutral so that when pH < pH_{pzc}, the oxide surface bears a positive charge and electrostatic interactions with anions in solution are favoured [48,49]. The experimentally determined pH_{pzc} for $\alpha\text{-}Fe_2O_3$ (= 8.1) is within the range of values (7.9 - 9.0) reported in the literature [50,51]. At room temperature, the addition of the urea and $HAuCl_4$ solution to $\alpha\text{-}Fe_2O_3$ generated an initial pH of 4.5. A subsequent temperature increase was accompanied by an increase in pH (to *ca.* 7.2) due to thermally-induced urea decomposition [43]. It is known that, in aqueous solution, $AuCl_4^-$ undergoes sequential substitution of Cl^- with OH^- at pH = 4, 4.6, 6.5 and 9, at which point $Au(OH)_4^-$ predominates [52,53]. Accordingly, at the final deposition pH, the gold precursor can be identified as principally $AuCl(OH)_3^-$ species. It should be noted that, at this pH, Au precursor interactions with the (positively) charged $\alpha\text{-}Fe_2O_3$ surface are favoured since pH < pH_{pzc}. The subsequent period of "aging" (*ca.* 250 min) was employed to enhance Au deposition [54].

Table 8.1: TPR T_{max} and H_2 consumption, H_2 chemisorption, BET surface area, pore volume, surface weighted-mean Au particle size (d_{TEM}) and associated metal surface area (S_{Au}), ratio of fractional 2,4-DCP conversion after 5 h on-stream ($X_{2,4\text{-}DCP,5h}$) to the initial value ($X_{2,4\text{-}DCP,0}$) and pseudo-first order rate constants (k, k') associated with the activated (673 K, 2 K min^{-1}) Fe_3O_4 supported Au catalysts.

Catalytic System	Au/Fe_3O_4-step	Au/Fe_3O_4-dir
TPR T_{max} (K)	363, 492	563
TPR H_2 consumption ($\times 10^4$ mol_{H_2} g^{-1})	230[a,b]	5 [c,d]
H_2 chemisorption (mol_{H_2} mol_{Au}^{-1})	6×10^{-6}	3×10^{-6}
BET (m^2 g^{-1})	13	11
Pore volume (cm^3 g^{-1})	0.04	0.02
d_{TEM} (nm)	4.5	7.6
S_{Au} (m_{Au}^2 g_{Au}^{-1})[e]	71	42
$X_{2,4\text{-}DCP,5h}/X_{2,4\text{-}DCP,0}$	0.21	0.63
k ($mol_{2,4\text{-}DCP}$ h^{-1} mol_{Au}^{-1})	2.1	0.8
$k' \times 10^{-5}$ ($mol_{2,4\text{-}DCP}$ h^{-1} m_{Au}^{-2})	15.0	9.7

[a]calculated H_2 consumption for α-$Fe_2O_3 \rightarrow Fe_3O_4 = 210 \times 10^{-4}$ mol_{H_2} g^{-1}

[b]calculated H_2 consumption for $Au^{3+} \rightarrow Au^0 = 0.6 \times 10^{-4}$ mol_{H_2} g^{-1}

[c]calculated H_2 consumption for $Fe_3O_4 \rightarrow Fe = 170 \times 10^{-4}$ mol_{H_2} g^{-1}

[d]calculated H_2 consumption for $Au^{3+} \rightarrow Au^0 = 0.9 \times 10^{-4}$ mol_{H_2} g^{-1}

[e]$S_{Au} = 6 / (\rho_{Au} \times d_{TEM})$; $\rho_{Au} = 18.88$ cm^3 g^{-1}

The TPR profile generated for Au/α-Fe_2O_3 is shown in **Figure 8.3**a, which also includes the TPR response exhibited by the α-Fe_2O_3 support (see dotted line) for comparative purposes. The latter is characterised by a principal positive (H_2 consumption) peak at 666 K with a low temperature shoulder at 562 K. These signals can be attributed to the reduction of α-Fe_2O_3 to Fe_3O_4 since the hydrogen consumption associated with this TPR response matched (to ± 1 %) that required (210×10^{-4} mol_{H_2} g^{-1}) for this transformation. Moreover, it has been reported in the literature that the reduction of hematite (to magnetite) requires temperatures in the range 633 K - 700 K [55-58]. Fe_3O_4 is a non stoichiometric oxide containing Fe cations in two different oxidation states ($Fe^{+2}_{(1-x)}Fe^{+3}_{(2+x)}O_{(4+x/2)}$, $0 < x \leq 1$) and presents a spinel structure with associated vacancies/defects [59,60]. The presence of a shoulder (at 562 K) to the main TPR H_2 consumption peak (666 K) can be linked to the removal of hydroxyl groups from the surface of α-Fe_2O_3 prior to (bulk) reduction [60].

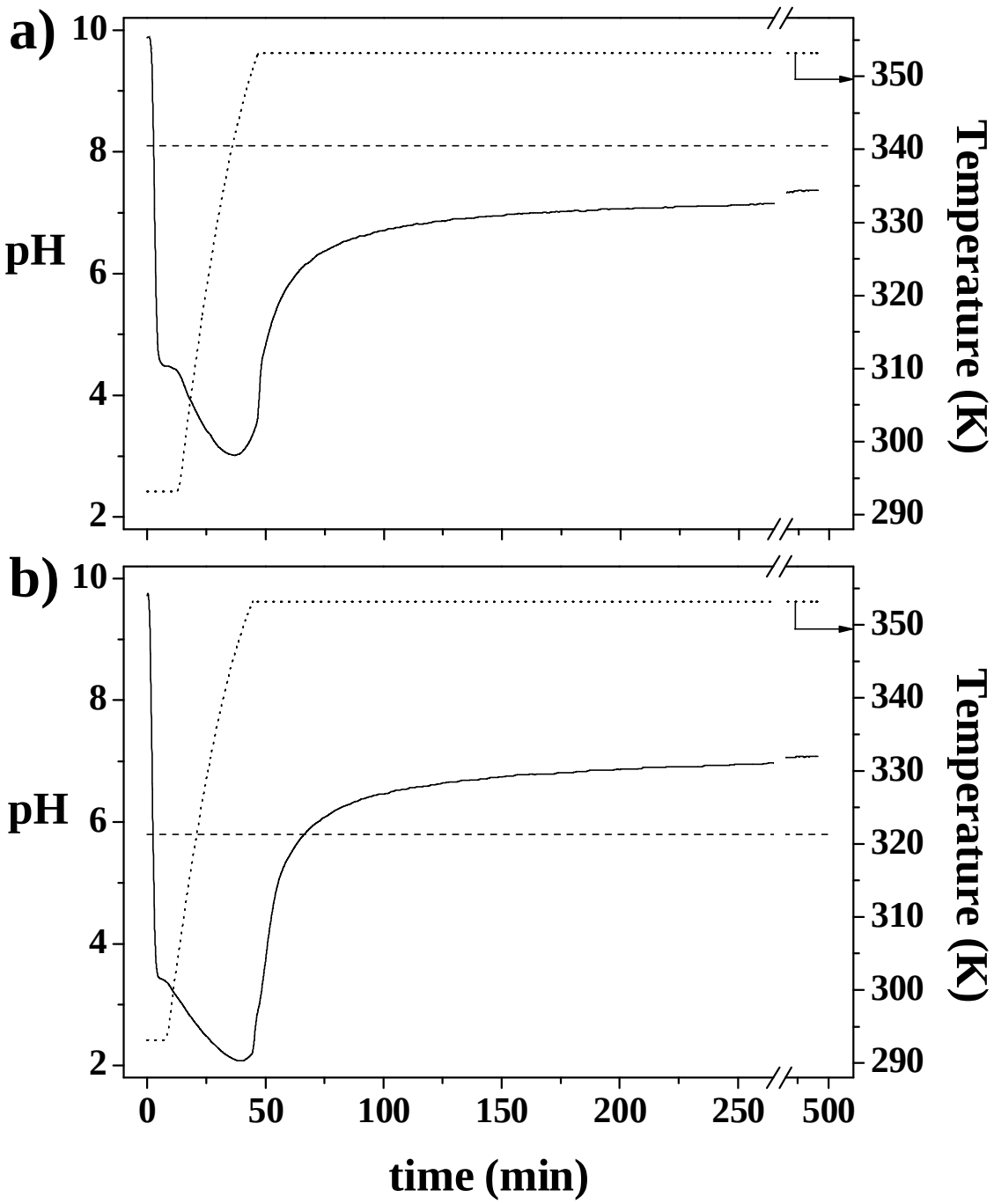

Figure 8.2: Temporal pH and temperature variations in the preparation of (a) Au/α-Fe_2O_3 (precursor of Au/Fe_3O_4-step) and (b) Au/Fe_3O_4-dir. Note: dashed lines identifies pH_{pzc} of the iron oxide supports.

Indeed, Munteanu and co-workers have studied the TPR of hydrated/dehydrated α-Fe_2O_3 and reported a shoulder at 553 K, which was ascribed to the dehydroxylation of iron oxide with concomitant formation of surface oxygen vacancies [61]. In the TPR of Au/α-Fe_2O_3 (solid line in **Figure 8.3**a), the peak maxima are shifted to lower temperatures where the relative peak intensities are quite distinct from those observed for the support.

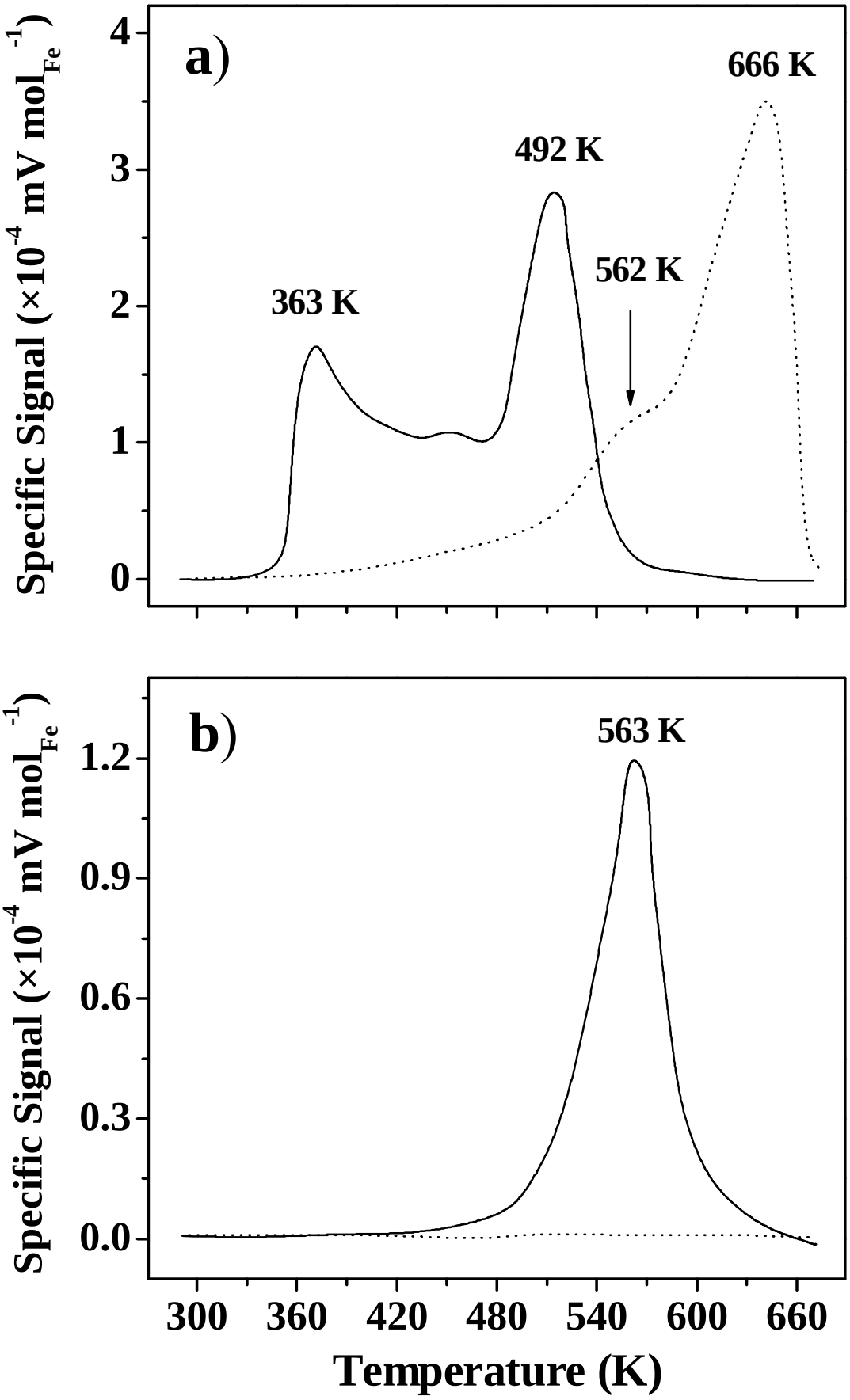

Figure 8.3: TPR profiles for: a) α-Fe_2O_3 (dotted line) and Au/α-Fe_2O_3 (solid line, precursor of Au/Fe_3O_4-step); b) Fe_3O_4 (dotted line) and Au/Fe_3O_4-dir (solid line).

This result is consistent with the literature where it has been established that the presence of Au facilitates the α-Fe_2O_3 → Fe_3O_4 step [56,62]. The experimentally determined H_2 consumption during TPR (230×10^{-4} $mol_{H_2}\ g^{-1}$, see **Table 8.1**) was greater than that required for the combined complete reduction of the α-Fe_2O_3 support (210×10^{-4} $mol_{H_2}\ g^{-1}$) and the Au precursor (0.6×10^{-4} $mol_{H_2}\ g^{-1}$). This "excess" H_2 consumption must be associated with the support and can be attributed to the generation of spillover hydrogen during TPR. Spillover results from a dissociative H_2 adsorption (typically on a metal site) generating atomic hydrogen that migrates to another accepting surface (notably a metal oxide) [63]. Indeed, there is evidence (based on FTIR measurements) of hydrogen spillover formation at ambient temperature for Au supported on TiO_2 [64,65] and CeO_2-ZrO_2 [66]. Moreover, Bocuzzi and coworkers [65] have suggested that room temperature spillover hydrogen generated on Au/α-Fe_2O_3 can participate in the reduction of the support.

The DRS UV-Vis analysis of Au/Fe_3O_4-step is given in **Figure 8.4** (Profile I) where the different regions of the spectrum are identified by vertical dotted lines. In the UV region (< 360 nm [67]), the profile is dominated by a continuum of ill-defined peaks over the range 200 - 330 nm that can be associated with electron transfer from O atoms to Fe^{+3} cations in the Fe_3O_4 lattice [68]. The visible region (between 360 and 820 nm [67]) presents several absorption bands which are due to independent contributions from Fe_3O_4 and Au. The peaks associated with the support appear at 383, 417 and 780 nm and can be linked, respectively, with (i) the presence of Fe^{+3} hydroxide species [69,70], (ii) electron transitions in Fe^{+3} cations [70,71] and (iii) Fe^{+2} → Fe^{+3} charge transfer [68]. The absorption band at *ca.* 572 nm falls within the range (500 - 600 nm) of values quoted in the literature for Au^0 [71,72] and can be taken to be diagnostic of the presence of metallic Au post TPR at 673 K. It should be noted that the occurrence of partially charged $Au_n^{+\delta}$ species has been reported by Deng *et al.* [71] and Pestryakov and co-workers [73] to generate signals at both UV (240 - 275 nm) and visible (360 - 385 nm) wavelengths, which can overlap with those associated with the Fe_3O_4 support (see **Figure 8.4**, Profile I). The presence of positively charged Au species supported on iron oxides (α-Fe_2O_3 [74,75] and Fe_3O_4 [75]) has now been demonstrated (by EXAFS and XPS) and results from electron transfer from the Au sites to the support oxygen vacancies [74].

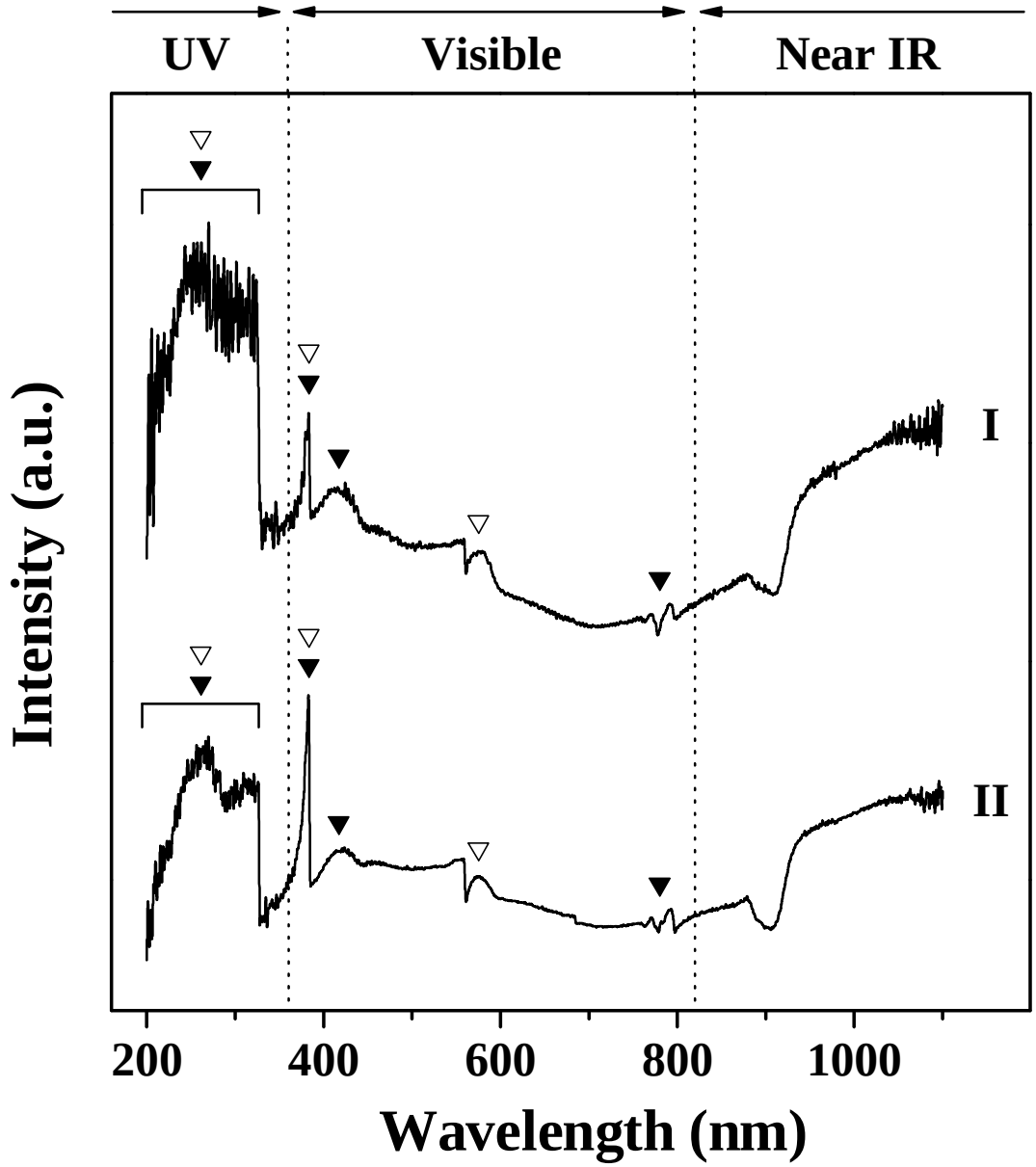

Figure 8.4: DRS UV-Vis spectra of Au/Fe_3O_4-step (I) and Au/Fe_3O_4-dir (II) with associated signals due to the Fe (▼) and/or Au (▽) components. Note: dotted lines illustrate position of the visible region (*i.e.* from 360 nm to 820 nm).

Indeed, the presence of electron-deficient Au particles in Au/Fe_3O_4-step is likely given the formation of oxygen vacancies in the support when activated by TPR to 673 K (see **Figure 8.3**a). XRD analysis was conducted to further study catalyst structure and the resulting diffractogram is shown in **Figure 8.5** (Profile I). The pattern exhibits reflections at 2θ = 30.1º, 35.4º, 43.1º, 53.4º, 56.9º and 62.5º that correspond, respectively with the (220), (311), (400), (422), (511) and (440) planes of Fe_3O_4 (JCPDS-ICDD Card No. 19-0629, Profile IV).

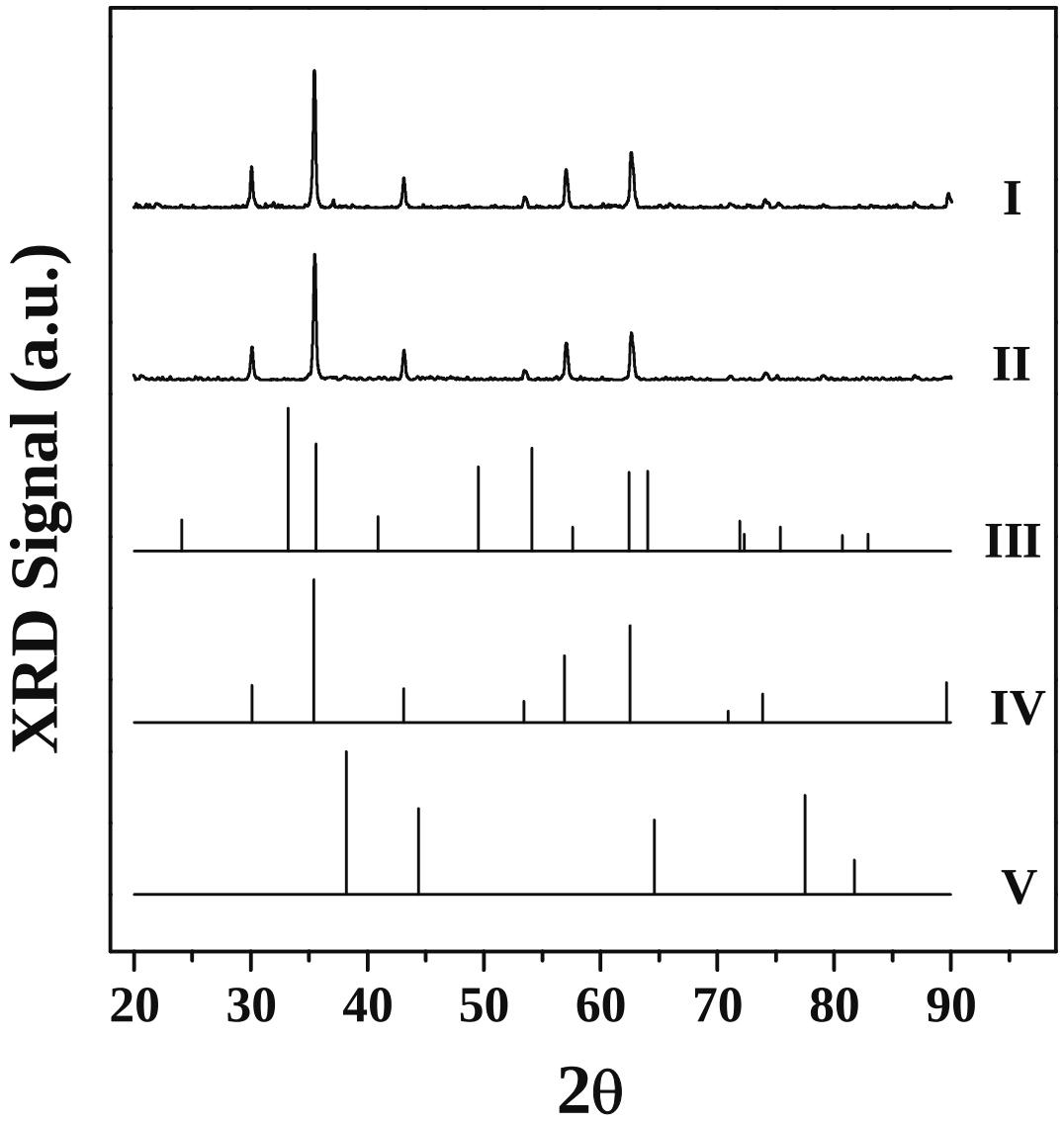

Figure 8.5: XRD profiles for Au/Fe_3O_4-step (I) and Au/Fe_3O_4-dir (II) with the JCPDS-ICDD reference standards for α-Fe_2O_3 (III, Card No. 33-0664), Fe_3O_4 (IV, Card No. 19-0629) and Au (V, Card No. 04-0784).

There are no detectable signals due to α-Fe_2O_3 (JCPDS-ICDD Card No. 33-0664, Profile III), demonstrating complete reduction of the support post TPR of Au/α-Fe_2O_3 to 673 K. The absence of XRD diffractions due to Au (JCPDS-ICDD Card No. 04-0784, Profile V) should be noted and can be attributed to the low metal loading and/or the presence of Au in the form of small clusters (XRD detection limit ≤ 5 nm [76,77]). TEM was consequently performed to establish Au particle size and morphology. Representative micrographs are shown in **Figure 8.6**a (images I and II) where it can be seen that Au is present as pseudo-spherical particles with diameters ≤ 10 nm.

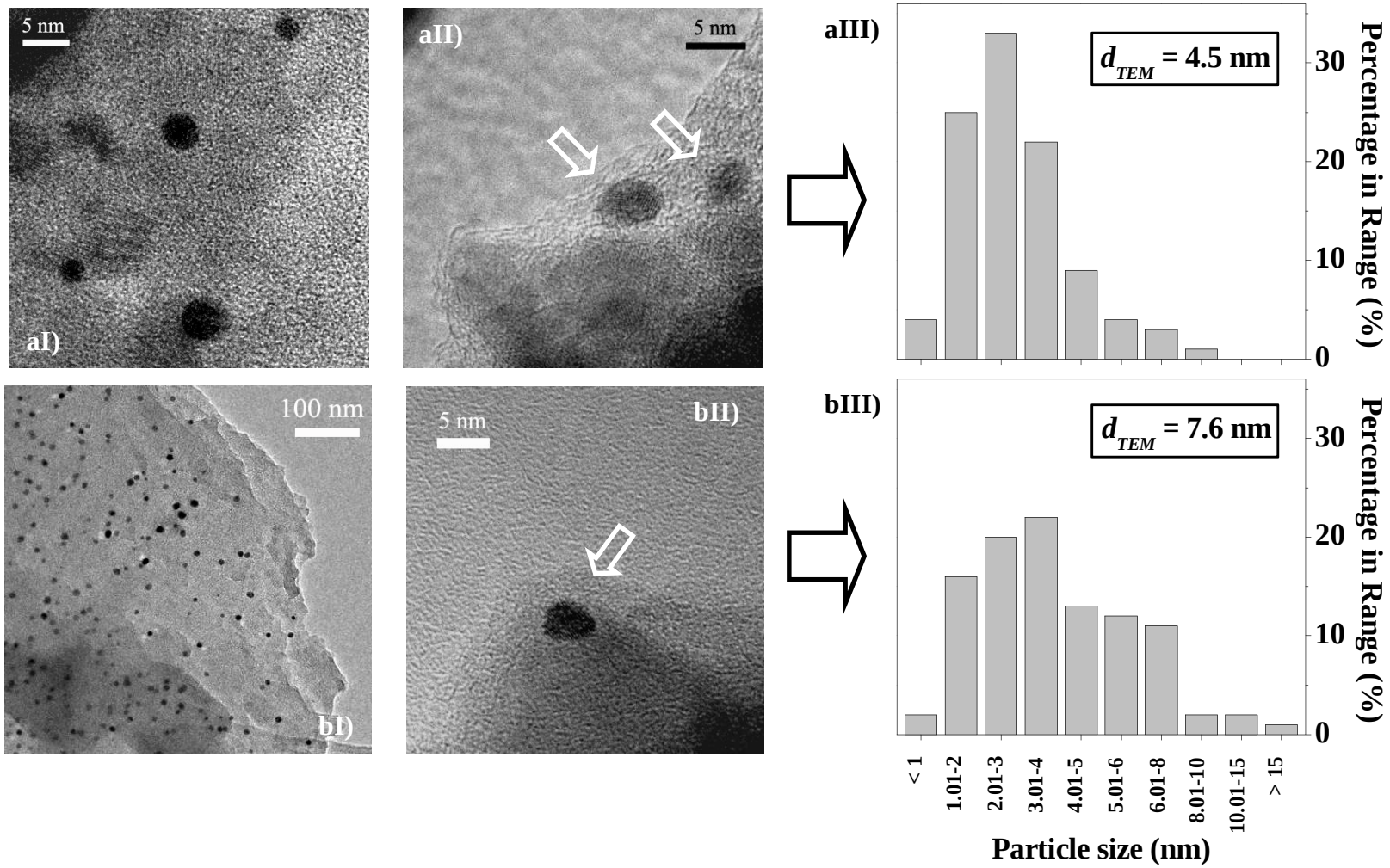

Figure 8.6: Representative TEM images (I,II) and associated Au particle size distribution (III) for reduced/passivated (a) Au/Fe_3O_4-step and (b) Au/Fe_3O_4-dir. Note: surface area-weighted mean Au particle sizes (d_{TEM}) are provided as insets in III.

A near Gaussian distribution of Au particle size (with some tailing over the 5 - 10 nm range, see **Figure 8.6**aIII) characterises the catalyst where the extracted surface area-weighted mean particle size (d_{TEM} = 4.5 nm, see **Table 8.1**) can account for the absence of an XRD signal due to Au. BET area (= 13 m^2 g^{-1}, see **Table 8.1**) and pore volume (= 0.04 cm^3 g^{-1}) are within those values reported elsewhere for Fe_3O_4 (*i.e.* 13 - 32 m^2 g^{-1} and 0.03 - 0.18 cm^3 g^{-1} [58]). The (ambient temperature) hydrogen chemisorption post activation delivered a low uptake (6×10^{-3} mol_{H_2} mol_{Au}^{-1}). It should be noted that this level of H_2 chemisorption was appreciably less than that (0.25 mol_{H_2} mol_{Pd}^{-1}) recorded in this thesis for Pd/Al_2O_3 bearing the same metal loading (1 % w/w) and equivalent mean particle size (4.5 nm) ([49] and **Chapter 2**). The latter observation is in line with the reported [34,78] low capacity of group IB metals for H_2 adsorption, which has been associated with the completely filled *d*-band [79] that results in a high energy barrier for H_2 activation [80]. It is known that H_2 does not chemisorb on bulk Au [81] and any measurable uptake can be attributed to small Au ensembles (≤ 10 nm) where chemisorption occurs predominantly at step, edge and corner sites [38,82].

8.3.1.2 Au/Fe_3O_4-dir

As noted above, a second magnetite supported Au catalyst (Au/Fe_3O_4-dir) was prepared *via* the deposition of the Au precursor directly onto a Fe_3O_4 support, prepared by TPR of α-Fe_2O_3 to 673 K (see experimental section and **Figure 8.3**a). The temporal pH variations in the preparation of Au/Fe_3O_4-dir (see **Figure 8.2**b) are similar to those for Au/α-Fe_2O_3 (precursor of Au/Fe_3O_4-step) in that there is an initial pH drop (to *ca.* 3.4) with subsequent elevation when increasing temperature to 7.0. As this (final) deposition pH is essentially the same as that in the preparation of Au/α-Fe_2O_3 (see **Figure 8.2**a) the nature of the Au precursor can also be taken as mainly $AuCl(OH)_3^-$ species. However, it should be noted that the pH_{pzc} of Fe_3O_4 (= 5.8, consistent with the literature [83]) is lower than the final pH (see **Figure 8.2**b) and, therefore, the Fe_3O_4 surface bears a negative charge [48,49]. As a consequence, interactions with (anionic) Au precursor species are not favoured in this case and deposition occurs principally *via* physical (as opposed to electrostatic) adsorption effects. A similar rationale has been provided by Moreau and Bond [52,53] in their study of Au/TiO_2 prepared by the deposition-precipitation of $HAuCl_4$ at a solution pH higher than the pH_{pzc} of the support.

TPR analysis of Au/Fe_3O_4-dir is shown in **Figure 8.3**b where, once again, the corresponding response for the support alone is included (as a dotted line). The TPR profile for Fe_3O_4 is featureless with no detectable H_2 consumption over the entire temperature range (293 K $\leq T \leq$ 673 K). This result finds agreement in the work of Pineau *et al.* [84] who, studying the TPR of Fe_3O_4 in pure H_2, concluded that its reducibility is highly dependent on the presence of impurities, gas flow and heating rate, with an (apparent) activation energy of up to 200 kJ mol^{-1} over the same temperature range. The TPR profile generated for Au/Fe_3O_4-dir (solid line) is dominated by a single positive peak (at 563 K) where the associated H_2 consumption (5×10^{-4} mol_{H_2} g^{-1}, **Table 8.1**) exceeded that needed to reduce the Au precursor (0.9×10^{-4} mol_{H_2} g^{-1}) but was far less than that required for the complete reduction of Fe_3O_4 to Fe (173×10^{-4} mol_{H_2} g^{-1}). It is important to note that this TPR signal appears at a higher temperature (> 70 K) than those recorded for Au/α-Fe_2O_3. This signal cannot be directly linked to the reduction of the Au precursor which, given the weaker precursor/support interactions that characterise Au/Fe_3O_4-dir (see **Figure 8.2**a), should result in a lower requisite reduction temperature. Moreover, there is persuasive evidence in the literature that Au reduces at room temperature when supported on iron oxides [57]. Wagner *et al.* [85] and Hodge and co-workers [86] reported, using Mössbauer spectroscopy, that Au/α-Fe_2O_3 prepared by inverse co-precipitation (basification of the Au precursor solution) contained over 80 % of Au content in the metallic (fully reduced) state. It is tentatively proposed that the Au precursor in Au/Fe_3O_4-dir is reduced at room temperature where the observed TPR response can be associated with Au-induced support dehydroxylation and/or generation of spillover H_2 (as in the case of Au/α-Fe_2O_3). The literature with regard to TPR analysis of Au/Fe_3O_4 is scant where the available studies do not actually explicitly identify the support as Fe_3O_4. Nonetheless, it is important to note the works of Neri *et al.* [87], who reported a single TPR peak at 408 K (although the authors did not elaborate further) and Zhang and co-workers [88] who recorded TPR signals at 360 K and 450 K that they ascribed to the reduction of Au_xO_y species. The DRS UV-Vis response for Au/Fe_3O_4-dir (**Figure 8.4**, Profile II) was equivalent to that observed for Au/Fe_3O_4-step in that it presents the same absorption bands at the same wavelengths. Furthermore, the XRD diffractogram pattern (**Figure 8.5**, Profile II) exhibited again reflections in the 2θ range 30º - 63º consistent with Fe_3O_4 (Profile IV).

These results suggest that the method of Au/Fe_3O_4 preparation (by stepwise or direct means) does not influence the nature or structural features of the support. This is also demonstrated by the similar BET areas and pore volumes (see **Table 8.1**) exhibited by both (activated) Au/Fe_3O_4 catalysts. However, hydrogen chemisorption on Au/Fe_3O_4-dir was measurably lower relative to Au/Fe_3O_4-step, a response which may reflect differences in Au particle size. Indeed, representative TEM images (I and II) given in **Figure 8.6**b reveal the presence of larger Au particles with a wider size distribution (**Figure 8.6**bIII) in the case of Au/Fe_3O_4-dir. The extracted surface area-weighted mean diameter (d_{TEM} = 7.6 nm) is significantly greater than that of Au/Fe_3O_4-step (= 4.5 nm, see **Table 8.1**). This result indicates that Au dispersion on Fe_3O_4 is sensitive to method of preparation, where smaller Au clusters are obtained by deposition of Au (on α-Fe_2O_3) with subsequent activation. The smaller mean Au size associated with Au/Fe_3O_4-step suggests a stronger interaction of the Au precursor with the α-Fe_2O_3 carrier when compared with Fe_3O_4. This is a direct consequence of the differences between the deposition pH and the pH_{pzc} of the supports (see **Figure 8.2**) and demonstrates the impact of metal/support interactions on the synthesis of nanosized Au catalysts by deposition-precipitation. These results find support in the work of Zanella *et al.* [89] who, studying the mechanism of $HAuCl_4$ deposition-precipitation onto oxide supports, synthesized very large (> 20 nm) Au particles on SiO_2 while smaller (2.5 - 8.1 nm) clusters were formed on Al_2O_3, CeO_2 or TiO_2. They ascribed this response to the low pH_{pzc} of SiO_2 (= 2) that resulted in deleterious support/$AuCl(OH)_3^-$ interactions at their final deposition pH (= 7).

8.3.2 2,4-DCP HDC

The HDC of 2,4-DCP over both Au/Fe_3O_4 catalysts was 100 % selective in terms of Cl removal, with no detectable hydrodehydroxylation or aromatic ring reduction. This result alone is significant because, to date, supported monometallic Au catalysts have exhibited very limited HDC activity. Yuan and co-workers achieved a negligible degree of 2,4-DCP HDC (≤ 3 % conversion) for reaction over Au/SiO_2 and Au/TiO_2 (T = 473 K) where complete HDC to phenol (PhOH) was not observed [18]. Reactant conversion ($X_{2,4\text{-}DCP}$) as a function of time-on-stream is shown in **Figure 8.7**, where both Au/Fe_3O_4 catalysts exhibited a temporal decline in activity to deliver an equivalent fractional conversion (= 0.05) at extended reaction times ($\Delta t > 4$ h).

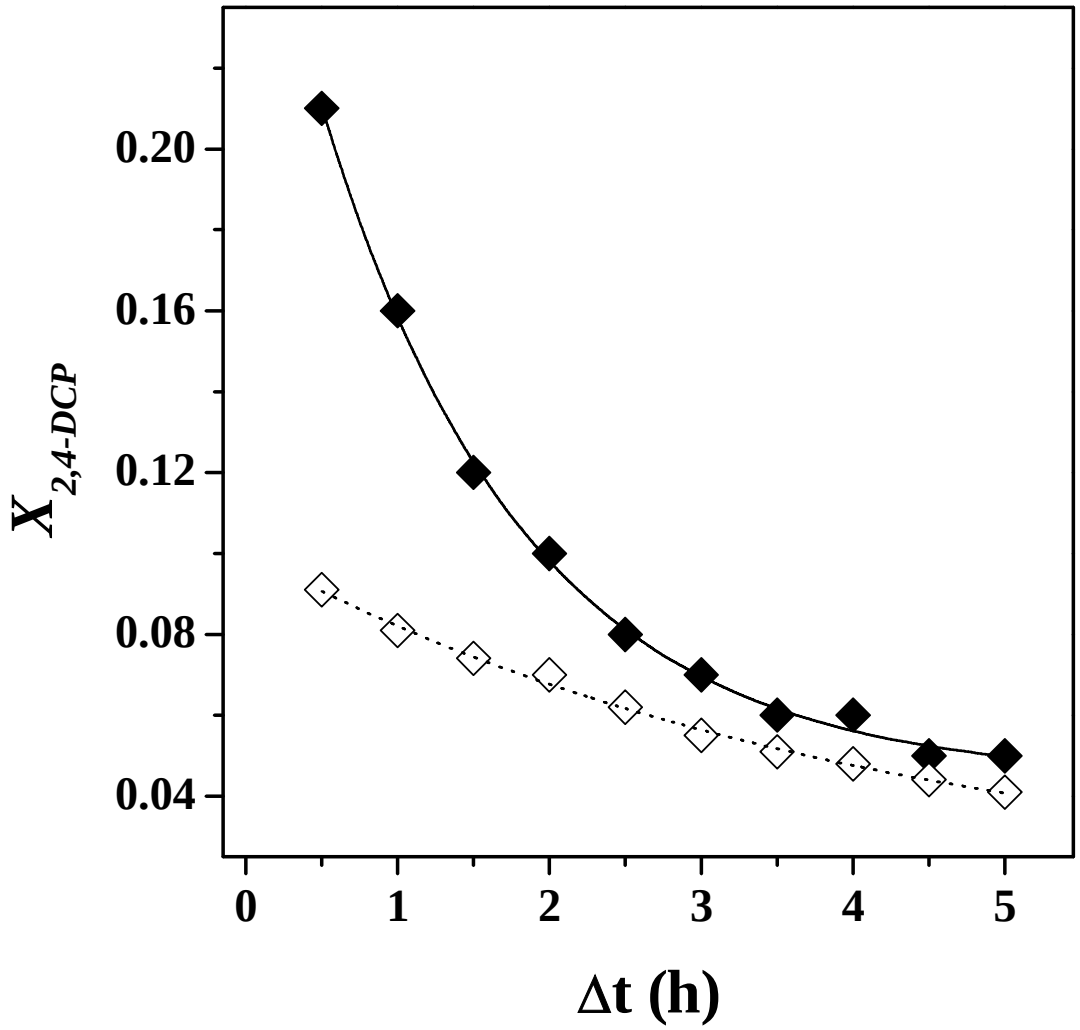

Figure 8.7: Temporal variation of 2,4-DCP fractional conversion ($X_{2,4\text{-}DCP}$) for reaction over Au/Fe_3O_4-step (◆, solid line) and Au/Fe_3O_4-dir (◇, dotted line); (n_{Au}/F) = 0.13 mol_{Au} h $mol_{2,4\text{-}DCP}^{-1}$. Note: lines represent fit to eqn. (8.4).

A measure of initial conversion ($X_{2,4\text{-}DCP,0}$) was calculated from [90]:

$$X_{2,4\text{-}DCP} = X_{2,4\text{-}DCP,0} \exp\left[-\alpha \Delta t\right] \qquad \textbf{(8.4)}$$

where Δt is the integral time and α is a fitting parameter; the quality of the data fit ($R^2 \geq 0.992$) can be seen in **Figure 8.7**. Loss of activity can be quantified in terms of the ratio of the fractional conversion after 5 h on-stream ($X_{2,4\text{-}DCP,5h}$) to the initial value ($X_{2,4\text{-}DCP,0}$): see **Table 8.1**. Deactivation is a general feature associated with catalytic HDC and has been linked to the deleterious action of the HCl by-product that can induce metal leaching [10,91], sintering [92], poisoning [92] and/or coke formation [2,93].

There is some evidence in the literature suggesting that deactivation is structure sensitive where larger (notably Pd) metal particles have been demonstrated to be more resistant to deactivation by HCl [94]. These results are in line with this trend as an appreciably lesser decline in activity characterises HDC over Au/Fe_3O_4-dir (surface area weighted mean particle size = 7.6 nm) relative to Au/Fe_3O_4-step (= 4.5 nm). An explicit assessment of catalytic activity in terms of structure sensitivity requires a comparison of specific rates (*i.e.* normalised per m_{Au}^2). The 2,4-DCP molar balance (on the basis of plug-flow and pseudo-first order kinetics) takes the form:

$$\ln\left[1/\left(1-X_{2,4\text{-}DCP,0}\right)\right] = k \times \left(n_{Au}/F\right) \qquad \textbf{(8.5)}$$

where k ($mol_{2,4\text{-}DCP}$ h^{-1} mol_{Au}^{-1}) is the pseudo-first order kinetic constant and n_{Au}/F (mol_{Au} h $mol_{2,4\text{-}DCP}^{-1}$) has the physical meaning of contact time. The associated linear relationships (forced through the origin) are shown in **Figure 8.8** and the extracted (raw) k values are given in **Table 8.1**. The specific pseudo-first order kinetic constant (k', $mol_{2,4\text{-}DCP}$ h^{-1} m_{Au}^{-2}) was then obtained from:

$$k' = \frac{k}{M_{Au} \times S_{Au}} \qquad \textbf{(8.6)}$$

where M_{Au} and S_{Au} (m_{Au}^2 g_{Au}^{-1}) represents Au atomic mass and metal surface area, respectively (see **Table 8.1**). The resultant k' values demonstrate that 2,4-DCP HDC is structure sensitive where a higher intrinsic activity is associated with Au/Fe_3O_4-step (15×10^{-5} $mol_{2,4\text{-}DCP}$ h^{-1} m_{Au}^{-2}) that bears smaller Au particles relative to Au/Fe_3O_4-dir (10×10^{-5} $mol_{2,4\text{-}DCP}$ h^{-1} m_{Au}^{-2}). In contrast, Keane and coworkers have shown previously [6,8] that larger supported Ni particles deliver higher specific HDC activities and attributed this to an ensemble effect. The structure sensitivity observed here finds agreement in those studies where smaller Au clusters have consistently shown greater activity in hydrogen-mediated reactions [34,95]. The latter has been generally associated with the greater capacity of Au to dissociatively chemisorb H_2 when finely dispersed ($\leq$ 10 nm) [38,82]. Indeed, the characterization measurements have indicated greater H_2 uptake for Au/Fe_3O_4-step (see **Table 8.1**).

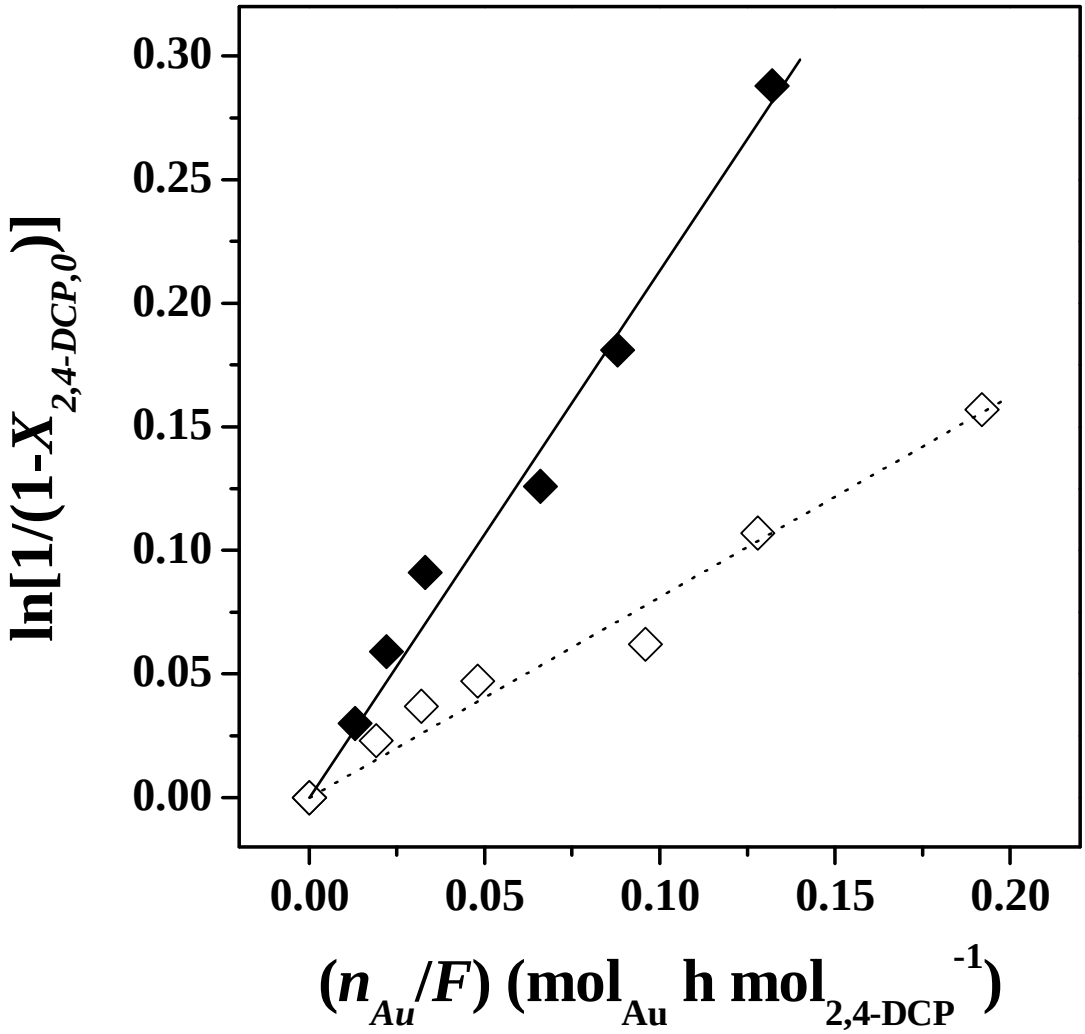

Figure 8.8: Pseudo-first order kinetic plot for 2,4-DCP HDC over Au/Fe_3O_4-step (◆, solid line) and Au/Fe_3O_4-dir (◇, dotted line); T = 423 K. Note: lines represent fit to eqn. (8.5).

Product distribution over both Au/Fe_3O_4 catalysts was also time dependent as shown in **Figure 8.9** where selectivity was increasingly shifted in favour of partial dechlorination with increasing time-on-stream (see **Figure 8.9**a) and 4-CP was the principal product (**Figure 8.9**b). This response, *i.e.* preferential removal of the *ortho*- Cl substituent, is unique when compared with the literature where 2-CP has been consistently reported as the major intermediate in the HDC of 2,4-DCP (over Ni/SiO_2 [96], Pd/C [97] and unsupported Pd-Fe nanoparticles [98]), a result that has been attributed to steric hindrance effects. The HDC of haloarenes proceeds *via* an electrophilic mechanism with the formation of a positively charged intermediate [99]. The preferential removal of the *ortho*- Cl suggests that this bond is preferentially activated on Au/Fe_3O_4, where the use of a reducible (Fe_3O_4) support must play a critical role.

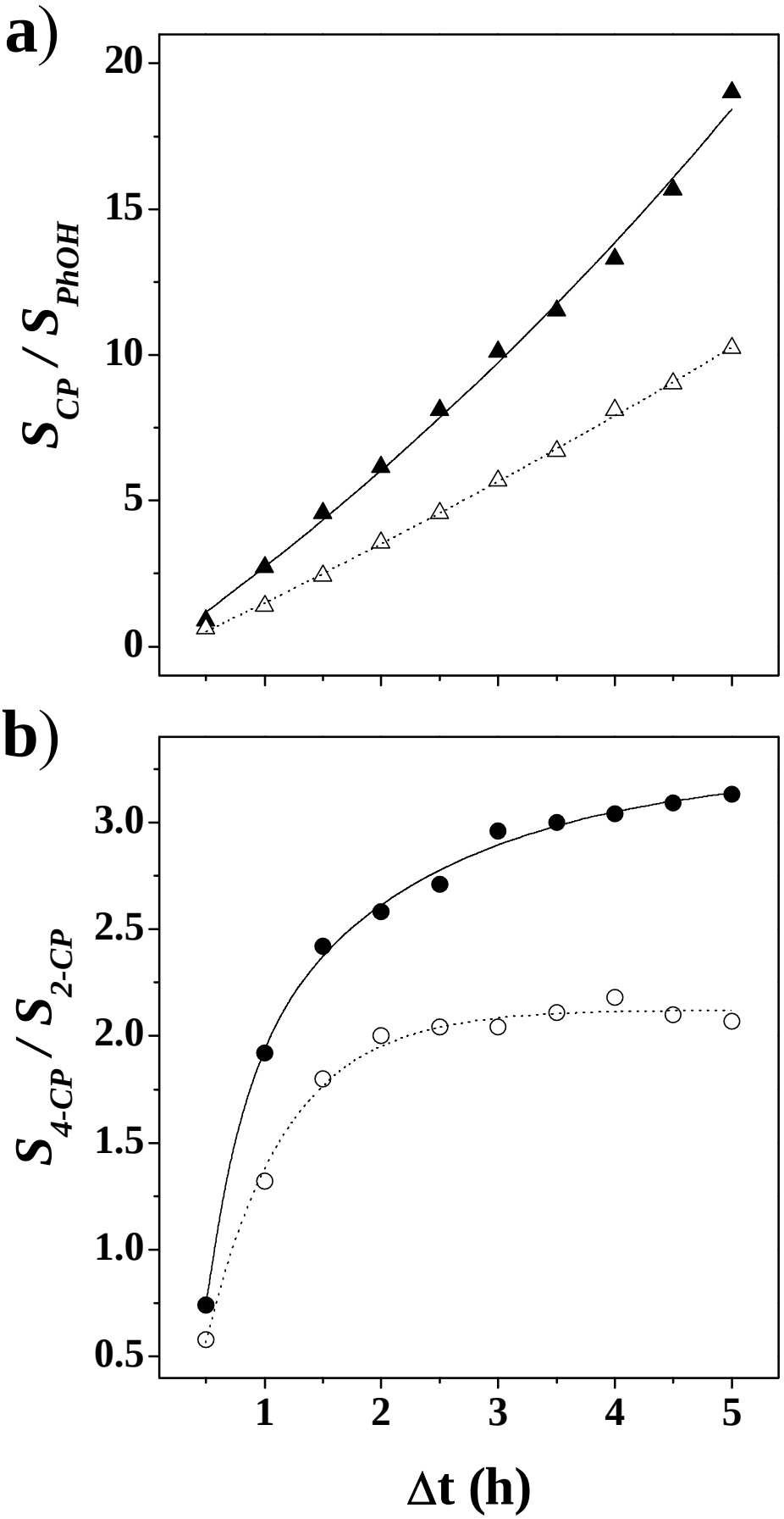

Figure 8.9: Ratio of product selectivity (S_i) in terms of a) CP *vs.* PhOH (▲,△) and b) 4-CP *vs.* 2-CP (●,○) as a function of time-on-stream for HDC over Au/Fe_3O_4-step (solid symbols/lines) and Au/Fe_3O_4-dir (open symbols/dotted lines); (n_{Au}/F) = 0.13 mol_{Au} h $mol_{2,4\text{-DCP}}^{-1}$.

Reducible metal oxides (such as TiO_2 and α-Fe_2O_3) are semiconductors as they exhibit a narrower band gap (2 - 3 eV) when compared with non-reducible oxides (*e.g.* Al_2O_3, 9 eV) [100]. As a consequence, activation of these materials (in H_2 or CO) can result in the removal of surface oxygen atoms to form vacancies [61,101]. Indeed, XPS/EXAFS measurements have demonstrated the occurrence of oxygen vacancies on the support which consequently generates electron-deficient $Au^{+\delta}$ species [75,102]. A TPR-induced generation of support oxygen vacancies with concomitant formation of electron-deficient Au particles is a feature of both (activated) Au/Fe_3O_4 catalysts (see TPR profiles in **Figure 8.3** and DRS UV-Vis spectra in **Figure 8.4**). Therefore, the author envisions a reaction mechanism involving 2,4-DCP adsorption on (positively) charged Au clusters *via* the lone pair of electrons associated with –OH, facilitating polarization (and activation) of the *ortho*- C–Cl bond as a result of inductive effects. This renders the *ortho*- Cl substituent more susceptible to electrophilic attack than the *para*- counterpart. Shin and Keane [96] also suggested this mode of 2,4-DCP/catalyst interaction for reaction over Ni/SiO_2 (a non-reducible support) but, in that case, 4-CP was not generated as product. An electrophilic mechanism requires the involvement of H^+ species and the occurrence of (positively) charged spillover hydrogen has been reported [103]. Indeed, the characterization results suggest the formation of spillover hydrogen during TPR and there is persuasive evidence in the literature that spillover hydrogen contributes to the gas phase HDC of chloroarenes [91]. It should be noted that 4-CP formation was favoured to a greater extent over Au/Fe_3O_4-step when compared with Au/Fe_3O_4-dir at extended reaction times (see **Figure 8.9**b). The latter suggests that reaction selectivity is also structure sensitive and this can be tentatively linked to the lower (electropositive) charge density associated with the larger Au clusters in Au/Fe_3O_4-dir. Zhang *et al.* [95], in the hydrogenation of 1,3-butadiene, found a distinct selectivity response (from butene to butane) over Au/ZrO_2 catalysts with varying Au particle size (3.5 - 8.0 nm) and ascribed this to a depletion in the charge of the metal clusters (lower Au^{+3}/Au^0 ratio).

The selective removal of the *ortho*- Cl substituent from 2,4-DCP represents an unprecedent advancement in the implementation of HDC processes where, to date, *ortho*-chlorinated phenol(s) have been isolated as principal partially dechlorinated product(s) due to the inability of conventional systems (Ni/SiO_2 [11,16], Pd/C [12,14,97]) to remove sterically hindered Cl from the parent phenolic ring.

The model catalyst considered in this study (Au/Fe_3O_4) promotes the transformation of aqueous 2,4-DCP (a common industrial waste stream [104,105]) into high-value 4-CP, a critical starting reactant for the synthesis of various fine chemicals [22-24]. This unique selectivity shown by Au/Fe_3O_4 demonstrates the potential of HDC as part of a progressive means of waste recycle in the generation of targeted chloroarene isomers.

8.4 Conclusions

Au/Fe_3O_4 catalysts have been prepared by (i) synthesis of Au/α-Fe_2O_3 with subsequent TPR to 673 K (Au/Fe_3O_4-step) and (ii) direct deposition of Au on Fe_3O_4 (Au/Fe_3O_4-dir). Both activated catalysts present similar characteristics in terms of BET area (11 - 13 $m^2\ g^{-1}$), total pore volume (0.02 - 0.04 $cm^3\ g^{-1}$) and DRS UV-Vis/XRD features. TEM measurements demonstrate that Au/Fe_3O_4-step exhibited a narrower Au size distribution and a smaller (surface area-weighted) mean size (= 4.5 nm) than Au/Fe_3O_4-dir (= 7.6 nm). This is a consequence of differences in the pH_{pzc} of the supports (with respect to the final deposition pH during Au introduction), which result in stronger (*i.e.* electrostatic) Au precursor/support interactions in the case of Au/α-Fe_2O_3 (precursor of Au/Fe_3O_4-step) when compared with Au/Fe_3O_4-dir. The application of both catalysts to promote the continuous, gas phase hydroprocessing of 2,4-DCP generated 4-CP as the principal product. HDC over Au/Fe_3O_4 is structure sensitive where a greater specific activity (15×10^{-5} $mol_{2,4\text{-}DCP}\ h^{-1}\ m_{Au}^{-2}$) is delivered by Au/Fe_3O_4-step, bearing smaller Au particles than Au/Fe_3O_4-dir (10×10^{-5} $mol_{2,4\text{-}DCP}\ h^{-1}\ m_{Au}^{-2}$). The formation of 4-CP from 2,4-DCP is unprecedented in the literature where steric hindrance has been proposed to govern HDC leading to 2-CP as the principal partially dechlorinated product. This selectivity response can be accounted for in terms of a preferential activation of the *ortho*- C–Cl bond at electron-deficient Au particles. This work demonstrates, for the first time, that Au/Fe_3O_4 is an active catalytic system in chloroarene HDC applications, facilitating the dechlorination of *ortho*- positioned Cl. Taking aqueous 2,4-DCP as a model industrial waste stream, HDC over Au/Fe_3O_4 produces 4-CP which is a critical compound in the synthesis of several commercially important fine chemicals, *i.e.* effective transformation of toxic waste into valuable material.

8.5 References

[8.1] F. Murena, F. Gioia, J. Hazard. Mater., 162, 661 (2009)

[8.2] C. A. González, M. Bartoszek, A. Martin, C. M. de Correa, Ind. Eng. Chem. Res., 48, 2826 (2009)

[8.3] Z. M. de Pedro, L. M. Gómez-Sainero, E. González-Serrano, J. J. Rodríguez, Ind. Eng. Chem. Res., 45, 7760 (2006)

[8.4] G. Tavoularis, M. A. Keane, J. Chem. Technol. Biotechnol., 74, 60 (1999)

[8.5] E.-J. Shin, M. A. Keane, J. Hazard. Mater. B, 66, 265 (1999)

[8.6] C. Menini, C. Park, E.-J. Shin, G. Tavoularis, M. A. Keane, Catal. Today, 62, 355 (2000)

[8.7] W. Wu, J. Xu, R. Ohnishi, Appl. Catal. B: Environmental, 60, 129 (2005)

[8.8] E.-J. Shin, M. A. Keane, React. Kinet. Catal. Lett., 69, 3 (2000)

[8.9] Y. Mitoma, N. Tasaka, M. Takase, T. Masuda, H. Tashiro, N. Egashira, T. Oki, Environ. Sci. Technol., 40, 1849 (2006)

[8.10] M. I. Cobo, J. A. Conesa, C. M. de Correa, J. Phys. Chem. A, 112, 8715 (2008)

[8.11] E.-J. Shin, M. A. Keane, J. Chem. Technol. Biotechnol., 75, 159 (2000)

[8.12] G. S. Pozan, I. Boz, Environ. Eng. Sci., 25, 1197 (2008)

[8.13] G. Yuan, M. A. Keane, Ind. Eng. Chem. Res., 46, 705 (2007)

[8.14] L. Calvo, A. F. Mohedano, J. A. Casas, M. A. Gilarranz, J. J. Rodríguez, Carbon, 42, 1377 (2004)

[8.15] G. Yuan, M. A. Keane, Catal. Commun., 4, 195 (2003)

[8.16] G. Pina, C. Louis, M. A. Keane, Phys. Chem. Chem. Phys., 5, 1924 (2003)

[8.17] G. Yuan, J. Llanos López, C. Loius, L. Delannoy, M. A. Keane, Catal. Commun., 6, 555 (2005)

[8.18] G. Yuan, C. Louis, L. Delannoy, M. A. Keane, J. Catal., 247, 256 (2007)

[8.19] USEPA, The Inventory of Sources of Dioxin in the United States. EPA/600/P-98/00A2, 1998.

[8.20] R. Weber, T. Sakurai, H. Hagenmaier, Appl. Catal. B: Environmental, 20, 249 (1999)

[8.21] N. Visez, J.-P. Sawerysyn, Chemosphere, 67, S144 (2007)

[8.22] P. Ackermann, P. Margot, F. Müller, Ullmann's Encyclopedia of Industrial Chemistry. "Fungicides, Agricultural", Wiley-VCH Verlag GmbH & Co. KGaA, Weinheim, 2005.

[8.23] H.-J. Schnorbach, H.-D. Matthaei, F. Müller, Ullmann's Encyclopedia of Industrial Chemistry. "Molluskicides", Wiley-VCH Verlag GmbH & Co. KGaA, Weinheim, 2008.

[8.24] W. Paulus, Ullmann's Encyclopedia of Industrial Chemistry. "Phenol Derivates", Wiley-VCH Verlag GmbH & Co. KGaA, Weinheim, 2005.

[8.25] M. S. Wong, P. J. J. Alvarez, Y.-L. Fang, N. Akçin, M. O. Nutt, J. T. Miller, K. N. Heck, J. Chem. Technol. Biotechnol., 84, 158 (2009)

[8.26] M. Nutt, J. Hughes, M. Wong, Environ. Sci. Technol., 39, 1346 (2005)

[8.27] M. Legawiec-Jarzyna, A. Srebowata, Z. Karpinski, React. Kinet. Catal. Lett., 79, 157 (2003)

[8.28] M. Bonarowska, J. Pielaszek, V. A. Semikolenov, Z. Karpiński, J. Catal., 209, 528 (2002)

[8.29] M. Bonarowska, B. Burda, W. Juszczyk, J. Pielaszek, Z. Kowalczyk, Z. Karpiński, Appl. Catal. B: Environmental, 35, 13 (2001)

[8.30] M. Bonarowska, J. Pielaszek, W. Juszczyk, Z. Karpiński, J. Catal., 195, 304 (2000)

[8.31] F. Cárdenas-Lizana, S. Gómez-Quero, M. A. Keane, Catal. Commun., 9, 475 (2008)

[8.32] A. S. K. Hashmi, Chem. Rev., 107, 3180 (2007)

[8.33] M. Boronat, P. Concepción, A. Corma, S. González, F. Illas, P. Serna, J. Am. Chem. Soc., 129, 16230 (2007)

[8.34] F. Cárdenas-Lizana, S. Gómez-Quero, N. Perret, M. A. Keane, Gold Bulletin, 42, 124 (2009)

[8.35] B. Campo, G. Santori, C. Petit, M. Volpe, Appl. Catal. A: General, 359, 79 (2009)

[8.36] E. Bus, R. Prins, J. A. van Bokhoven, Catal. Commun., 8, 1397 (2007)

[8.37] A. S. K. Hashmi, G. J. Hutchings, Angew. Chem. Int. Ed., 45, 7896 (2006)

[8.38] M. Okumura, T. Akita, M. Haruta, Catal. Today, 74, 265 (2002)

[8.39] A. C. Gluhoi, M. A. P. Dekkers, B. E. Nieuwenhuys, J. Catal., 219, 197 (2003)

[8.40] A. Sandoval, A. Gómez-Cortés, R. Zanella, G. Díaz, J. M. Saniger, J. Mol. Catal. A: Chemical, 278, 200 (2007)

[8.41] H. Hildebrand, K. Mackenzie, F.-D. Kopinke, Environ. Sci. Technol., 43, 3254 (2009)

[8.42] H. Hildebrand, K. MacKenzie, F.-D. Kopinke, Global NEST J., 10, 47 (2008)

[8.43] M. Khoudiakov, M. C. Gupta, S. Deevi, Appl. Catal. A: General, 291, 151 (2005)

[8.44] J. Vakros, C. Kordulis, A. Lycourghiotis, J. Chem. Soc. Chem. Commun., 17, 1980 (2002)

[8.45] M. A. Keane, P. M. Patterson, J. Chem. Soc., Faraday Trans., 92, 1413 (1996)

[8.46] G. Yuan, M. A. Keane, Chem. Eng. Sci., 58, 257 (2003)

[8.47] G. Tavoularis, M. A. Keane, J. Mol. Catal. A: Chemical, 142, 187 (1999)

[8.48] G. Yuan, M. A. Keane, J. Catal., 225, 510 (2004)

[8.49] S. Gómez-Quero, F. Cárdenas-Lizana, M. A. Keane, Ind. Eng. Chem. Res., 47, 6841 (2008)

[8.50] M. L. Toebes, J. A. Dillen, K. P. de Jong, J. Mol. Catal. A: Chemical, 173, 75 (2001)

[8.51] M. Haruta, J. New Mater. Electrochem. Syst., 7, 163 (2004)

[8.52] F. Moreau, G. C. Bond, Catal. Today, 122, 260 (2007)

[8.53] F. Moreau, G. C. Bond, A. O. Taylor, J. Catal., 231, 105 (2005)

[8.54] A. M. Visco, A. Donato, C. Milone, S. Galvagno, React. Kinet. Catal. Lett., 61, 219 (1997)

[8.55] G. Y. Wang, H. L. Lian, W. X. Zhang, D. Z. Jiang, T. H. Wu, Kinet. Catal., 43, 468 (2002)

[8.56] A. Venugopal, M. S. Scurrell, Appl. Catal. A: General, 258, 241 (2004)

[8.57] B. A. A. Silberova, G. Mul, M. Makkee, J. A. Moulijn, J. Catal., 243, 171 (2006)

[8.58] J. Li, Y. Zhan, X. Lin, Zheng Q, Acta Phys. Chim. Sin., 24, 932 (2008)

[8.59] T.-J. Park, S. Sambasivan, D. A. Fischer, W.-S. Yoon, J. A. Misewich, S. S. Wong, J. Phys. Chem. C, 112, 10359 (2008)

[8.60] W. K. Jozwiak, E. Kaczmarek, T. P. Maniecki, W. Ignaczak, W. Maniukiewicz, Appl. Catal. A: General, 326, 17 (2007)

[8.61] G. Munteanu, L. Ilieva, D. Andreeva, Thermochim. Acta, 291, 171 (1997)

[8.62] S. Scirè, C. Crisafulli, S. Minicò, G. G. Condorelli, A. di Mauro, J. Mol. Catal. A: Chemical, 284, 24 (2008)

[8.63] W. C. Conner, J. L. Falconer, Chem. Rev., 95, 759 (1995)

[8.64] D. A. Panayotov, J. T. Yates, J. Phys. Chem. C, 111, 2959 (2007)

[8.65] F. Boccuzzi, A. Chiorino, M. Manzoli, D. Andreeva, T. Tabakova, J. Catal., 188, 176 (1999)

[8.66] S. E. Collins, J. M. Cíes, E. del Río, M. López-Haro, S. Trasobares, J. J. Calvino, J. M. Pintado, S. Bernal, J. Phys. Chem. C, 111, 14371 (2007)

[8.67] D. R. Lide, Handbook of Chemistry and Physics, 90th ed., Taylor and Francis Group, Boca Raton, 2009.

[8.68] J. J. Fripiat, Advanced Techniques for Clay Mineral Analysis, Elsevier, New York, 1982.

[8.69] B. Qiao, Y. Deng, Appl. Catal. B: Environmental, 66, 241 (2006)

[8.70] P. Marturano, L. Drozdová, G. D. Pirngruber, A. Kogelbauer, R. Prins, Phys. Chem. Chem. Phys., 3, 5585 (2001)

[8.71] W. Deng, C. Carpenter, N. Yi, M. Flytzani-Stephanopoulos, Top. Catal., 44, 199 (2007)

[8.72] A.C. Gluhoi, X. Tanga, P. Marginean, B. E. Nieuwenhuys, Top. Catal., 39, 101 (2006)

[8.73] A. N. Pestryakov, V. V. Lunin, A. N. Kharlanov, D. I. Kochubey, N. Bogdanchikova, A. Y. Stakheev, J. Mol. Struct., 642, 129 (2002)

[8.74] Z. Hao, L. An, H. Wang, T. Hu, React. Kinet. Catal. Lett., 70, 153 (2000)

[8.75] J. Hua, K. Wei, Q. Zheng, X. Lin, Appl. Catal. A: General, 259, 121 (2004)

[8.76] S. Díaz-Moreno, D. C. Koningsberger, A. Muñoz-Páez, Nucl. Instrum. Methods Phys. Res., Sect. B, 133, 15 (1997)

[8.77] J. Liu, Microsc. Microanal., 10, 55 (2004)

[8.78] M. Bron, D. Teschner, A. Knop-Gericke, F. C. Jentoft, J. Kröhnert, J. Hohmeyer, C. Volckmar, B. Steinhauer, R. Schlögl, P. Claus, Phys. Chem. Chem. Phys., 9, 3559 (2007)

[8.79] P. Claus, Appl. Catal. A: General, 291, 222 (2005)

[8.80] B. Hammer, J. K. Nørskov, Nature, 376, 238 (1995)

[8.81] A. G. Sault, R. J. Madix, C. T. Campbell, Surf. Sci., 169, 347 (1986)

[8.82] J. Słoczyński, R. Grabowski, A. Kozłowska, P. Olszewski, J. Stoch, J. Skrzypek, M. Lachowska, Appl. Catal. A: General, 278, 11 (2004)

[8.83] Y.-C. Chang, D.-H. Chen, Macromol. Biosci., 5, 254 (2005)

[8.84] A. Pineau, N. Kanari, I. Gaballah, Thermochim. Acta, 456, 75 (2007)

[8.85] F. E. Wagner, S. Galvagno, C. Milone, A. M. Visco, L. Stievano, S. Calogero, J. Chem. Soc., Faraday Trans., 93, 3403 (1997)

[8.86] N. A. Hodge, C. J. Kiely, R. Whyman, M. R. H. Siddiqui, G. J. Hutchings, Q. A. Pankhurst, F. E. Wagner, R. R. Rajaram, S. E. Golunski, Catal. Today, 72, 133 (2002)

[8.87] G. Neri, A. M. Visco, S. Galvagno, A. Donato, M. Panzalorto, Thermochim. Acta, 329, 39 (1999)

[8.88] F. Zhang, Q. Zheng, K. Wei, X. Lin, H. Zhang, J. Li, Y. Cao, Catal. Lett., 108, 131 (2006)

[8.89] R. Zanella, L. Delannoy, C. Louis, Appl. Catal. A: General, 291, 62 (2005)

[8.90] E.-J. Shin, M. A. Keane, Ind. Eng. Chem. Res., 39, 883 (2000)

[8.91] K. V. R. Chary, C. S. Srikanth, V. V. Rao, Catal. Commun., 10, 459 (2009)

[8.92] X. Liu, J. Chen, J. Zhang, Ind. Eng. Chem. Res., 47, 5362 (2008)

[8.93] E. López, S. Ordóñez, F. V. Díez, Appl. Catal. B: Environmental, 62, 57 (2006)

[8.94] M. A. Aramendia, V. Boráu, I. M. García, C. Jiménez, F. Lafont, A. Marinas, J. M. Marinas, F. J. Urbano, J. Catal., 187, 392 (1999)

[8.95] X. Zhang, H. Shi, B.-Q. Xu, Catal. Today, 122, 330 (2007)

[8.96] E.-J. Shin, M. A. Keane, Chem. Eng. Sci., 54, 1109 (1999)

[8.97] G. S. Pozan, I. Boz, J. Hazard. Mater. B, 136, 917 (2006)

[8.98] J. Wei, X. Xu, Y. Liu, D. Wang, Water Res., 40, 348 (2006)

[8.99] Y. A. Serguchev, Y. V. Belokopytov, Kinet. Catal., 42, 174 (2001)

[8.100] C. Sol, R. J. D. Tilley, J. Mater. Chem. , 11, 815 (2001)

[8.101] M. Boaro, M. Vicario, J. Llorca, C. de Leitenburg, G. Dolcetti, A. Trovarelli, Appl. Catal. B: Environmental, 88, 272 (2009)

[8.102] G. J. Hutchings, M. S. Hall, A. F. Carley, P. Landon, B. E. Solsona, C. J. Kiely, A. Herzing, M. Makkee, J. A. Moulijn, A. Overweg, J. C. Fierro-Gonzalez, J. Guzman, B. C. Gates, J. Catal., 242, 71 (2006)

[8.103] U. Roland, T. Braunschweig, F. Roessner, J. Mol. Catal. A: Chemical, 127, 61 (1997)

[8.104] USEPA, Advisory Document No. 8EHQ-14302, 2000.

[8.105] P. Kintz, A. Tracqui, P. Mangin, Arch. Toxicol., 66, 298 (1992)

Chapter 9

Summary and Future Work

The results presented in this PhD thesis demonstrate the feasibility of catalytic hydrodehalogenation (HDH) as a viable and practical process for the treatment (and recycle) of toxic haloarene waste. The main challenges outlined in **Chapter 1** have been comprehensively tackled and the most significant findings are identified below, with suggested future research directions.

9.1 General Conclusions

In **Chapter 2**, structure sensitivity in batch, aqueous phase (T = 303 K) HDH has been explicitly established in the case of 2,4-dichlorophenol (2,4-DCP) conversion over bulk Pd and Pd supported on Al_2O_3. A range of Pd particle sizes (1.6 - 13.1 nm) was achieved by controlled thermal treatment (423 - 1273 K at 1 - 50 K min^{-1}). Dechlorination over smaller Pd particles delivered the highest specific activity (up to 0.67 $mmol_{Cl}$ m_{Pd}^{-2} min^{-1}) under conditions where bulk Pd was completely inactive. Reaction selectivity has been shown to be independent of Pd dispersion under basic pH (= 13) conditions. In contrast, for reaction under acidic conditions (pH = 3), smaller Pd clusters yielded greater 2-chlorophenol (2-CP) selectivity as a result of repulsion with a supported Pd–H^+ adduct. Reaction over bulk Pd (*i.e.* in absence of metal/support interactions) resulted in the lowest 2-CP selectivity. Given the impact of the reaction medium on HDH performance, the effect of the solvent was considered in **Chapter 3**, using water and a range of organics (linear alcohols, cyclohexane, *n*-hexane, benzene and THF) with varying properties in terms of solvent-solvent and reactant-solvent interactions. A detailed analysis of mass transport limitations has been presented where HDH over a porous (0.56 cm^3 g^{-1}), well dispersed (2.4 nm) Pd/Al_2O_3 is free from H_2/2,4-DCP transfer restrictions. In the absence of secondary reactions and catalyst deactivation, selectivity is shown to be independent of the solvent while a change in reaction mixture composition has a significant impact on dechlorination rate, with the highest activity (up to 88 $mmol_{2,4\text{-}DCP}$ g_{Pd}^{-1} min^{-1}) recorded in water. A systematic analysis of solvent properties revealed that the latter was induced by the simultaneous change in the dielectric constant (ε) and molar volume ($\bar{v}$), where ε represents the major contribution (≈ 80 %).

This response also applies when using water+organic mixtures as the reaction medium. The work included in this thesis constitutes the first reported instance where solvent effects in hydrodechlorination have been comprehensively demonstrated and, quantified. These effects are illustrated in **Chapter 4**, where the Pd/Al_2O_3 promoted HDH of mono- and dichlorophenols, selected bromophenols and chlorobenzenes is examined in water+methanol mixtures. HDH mechanism is established as an electrophilic aromatic substitution. The hydrogenolysis of C–Br bond(s) is promoted at a greater rate (by up to an order of magnitude) relative to C–Cl due to the lower associated bond dissociation energy while the presence of a second (halogen) substituent has a deactivating effect, *i.e.* serves to deplete electron density in the aromatic ring. Higher initial HDH rates were observed with increasing water content in the solvent mixture and this is principally related to an increase in ε, with *ca.* 80 % contribution regardless of the reactant considered. The HDH of dichlorophenols, 2,4-dibromophenol and dichlorobenzene follow a predominantly stepwise mechanism where, in all cases, selectivity levels are independent of the solvent composition, *i.e.* suggesting that each step in such mechanism (consecutive *vs.* simultaneous dehalogenation) is influenced to the same extent.

The efficacy of discontinuous HDH over Pd/Al_2O_3 to detoxify haloarene solutions is established in **Chapters 2 - 4**. The consequence of a shift to continuous operation, of direct relevance to industrial implementation, is considered in **Chapter 5** where aqueous 2,4-DCP hydrodechlorination is selected as model system. Under conditions where batch and continuous operation are operated under kinetic control, a more efficient (five-fold) H_2 transfer is found in the latter system and attributed to an extended gas/liquid interface available for mass transport. Higher dechlorination rates and increased selectivity to phenol were obtained in continuous flow due to a difference in the "local" pH at the liquid/solid interface relative to batch operation. Furthermore, productive catalyst lifetime was extended in the continuous reactor due to the more effective removal of HCl from the catalyst surface. These findings constitute the first reported direct evidence for the benefits of continuous HDH operation.

A further shift in reaction phase/temperature, from liquid (T = 303 K) to gas (T = 423 K), resulted in the formation of cyclohexanone (C6ONE) as principal product from the chlorophenols hydrotreatment over Pd/Al_2O_3. C6ONE, is a high value product with important applications, *e.g.* as precursor for Nylon 6,6 and various co-poplymers. A detailed evaluation of the continuous, gas phase conversion of chlorophenols to C6ONE using unsupported/supported (Al_2O_3, SiO_2) Pd catalysts is provided in **Chapter 6**. A thermodynamic analysis demonstrates the feasibility of this production route. Operating under kinetic control, the hydroprocessing of chlorophenols over bulk $Pd+Al_2O_3$ physical mixture generates higher yield of C6ONE relative to conventional phenol hydrogenation. This is accounted for in terms of a direct chlorophenol $\rightarrow$ C6ONE pathway that is facilitated by electron delocalization in the reaction intermediate generated *via* electrophilic H_2 attack to C–Cl bond(s). Structure sensitivity in C6ONE production is demonstrated for 2,4-DCP with higher specific rates (from 49×10^{-4} to 94×10^{-4} mol_{C6ONE} h^{-1} m_{Pd}^{-2}) associated with larger Pd particles (3 nm $\rightarrow$ 250 nm). Reaction selectivity is structure insensitive in that C6ONE selectivity at the same conversion is equivalent for reaction over bulk and supported Pd catalysts. Moreover, the beneficial contribution due to hydrogen spillover in elevating C6ONE production rates has also been demonstrated.

The resistance of *ortho*- Cl substituent(s) to H_2 cleavage is a common feature of the chlorophenols HDH data presented in **Chapters 2 - 6** and is well established in the literature. In **Chapter 7**, the use of Au (supported on α-Fe_2O_3) as the HDH agent is shown to deliver quite distinct dechlorination selectivities. The characterization results demonstrate that the α-Fe_2O_3 support is reduced to Fe_3O_4 during TPR to 673 K and the introduction of Au (by deposition precipitation) facilitates this transformation by reducing the requisite temperature by *ca.* 200 K. Au/α-Fe_2O_3 activation to 423 K results in the formation of quasi-spherical small Au clusters (surface area-weighted mean particle size = 2.6 nm) and the occurrence of spillover hydrogen is established: Au/α-Fe_2O_3 exhibited four-fold greater hydrogen content (relative to α-Fe_2O_3). The gas phase hydrotreatment of 2,4-DCP generated 4-CP as the principal product through a (predominantly) stepwise electrophilic mechanism. This selectivity response (preferential cleavage of the sterically constrained *ortho*- positioned Cl) is attributed to reactant adsorption through the –OH substituent on $Au^{+\delta}$ particles, which renders the *ortho*- Cl more susceptible to hydrogen scission *via* inductive effects.

The role of the carrier has also been considered in **Chapter 7** where solvent dissociation (in the case of water and alcohols) generates reactive hydrogen that contributes to activity. Selectivity in the cleavage of sterically-constrained Cl substituents is demonstrated for a range of mono-, di- and tri-chlorophenol reactants, representing a unique control of HDH selectivity associated with Au/α-Fe_2O_3. This behaviour is examined further in **Chapter 8**, which considers the preparation of Fe_3O_4 supported Au catalysts by two synthesis routes: (i) stepwise Au deposition on α-Fe_2O_3 with consecutive reduction (Au/Fe_3O_4-step) and (ii) direct Au deposition on Fe_3O_4 (Au/Fe_3O_4-dir). Both catalysts presented the same characteristics in terms of XRD, DRS UV-Vis and BET/pore volume features and only differed with respect to the (surface area-weighted) particle sizes: Au/Fe_3O_4-step = 4.5 nm; Au/Fe_3O_4-dir = 7.6 nm. The HDH of (aqueous) 2,4-DCP results in the production of 4-CP with a high degree of selectivity (up to 90 %) where smaller Au particles are intrinsically more active (up to 2 $\times$ 10^{-4} mol_{Cl} h^{-1} m_{Au}^{-2}). As 4-CP is an important intermediate in the production of fungicides and molluskicides, this final Chapter provides further evidence of the potential of catalytic HDH, not only as a waste treatment tool, but also as a synthetic route for industrial processes.

The research developed and conclusions drawn in this dissertation, with respect to the benefits of catalytic HDH, can be summarized as: (i) progressive green technology in terms of product reuse (C6ONE, 4-CP) and mild operating conditions, (ii) applicability to treat concentrated feedstock, (iii) selective removal of the halogen content through the judicious choice of reaction conditions (acid *vs.* basic solutions) or catalyst (small *vs.* larger metal clusters, Pd *vs.* Au) and (iv) flexible and facile implementation in either batch or continuous operation. In short, this PhD thesis demonstrates the fundamentals for the establishment of HDH as a progressive and feasible approach for chloroarene waste abatement.

9.2 Future Directions

9.2.1 Study of Catalyst Deactivation

Deactivation is a general feature of catalytic HDH as, indeed, can be seen from the short literature review presented in **Table 9.1**.

Table 9.1. A compilation of relevant recent (2000 to present) literature concerning catalyst deactivation during HDH.

Phase	Metal	Support	Reactant	Cause of Deactivation	Reference
Gas	Ni	Al_2O_3, SiO_2 TiO_2, ZrO_2	Dichloromethane	Poisoning	[1]
		SiO_2	Trichlorophenols	Poisoning Site Occlusion	[2]
			1,2-Dichlorobenzene 1,2-Dibromobenzene	Poisoning	[3]
			Chlorobenzenes Bromobenzenes Chlorophenols	Poisoning Coking	[4]
	Pd	Al_2O_3	Tetrachloroethylene Dichloromethane Chlorobenzene	Coking	[5]
			Trichloroethylene	Poisoning	[6]
			Chlorobenzene	Poisoning	[7]
		Al_2O_3, SiO_2 TiO_2, ZrO_2	Dichloromethane	Poisoning	[1]
		TiO_2	Dichloromethane Tetrachloroethylene Chloroform	Poisoning Coking	[8]
	Pd M-Pd[a]	SiO_2	Chlorobenzenes	Poisoning	[9,10]
	Pt	Al_2O_3	Chlorobenzenes	Poisoning Blocking	[11]
		NaX Zeolite	Carbon tetrachloride	Poisoning Blocking	[12]
	Ru	Nb_2O_5	1,2,4-Trichlorobenzene	Coking Leaching Poisoning	[13]
Liquid	Ni	Al_2O_3, Carbon, SiO_2	Chlorobenzene	Poisoning	[14]
		SiO_2	Chlorobenzene	Poisoning Sintering	[15]
	Pd	Al_2O_3	Dioxins	Coking Leaching	[16]
		Al_2O_3, Carbon	2,4-Dichlorophenol	Poisoning	[17-19]
		Carbon	Chlorobenzene	Poisoning	[20]
			Tetrachloroethylene	Coking Poisoning	[21]
		TiO_2	Pentachlorophenol	Poisoning	[22]
	Pt	Al_2O_3	Chlorobenzenes	Poisoning Blocking	[11]

[a]M = Sr, Ba and lanthanides

It should be noted that catalyst deactivation during HDH has been reported regardless of the phase (gas, liquid), metal (Ni, Pd, Pt, Ru), support (reducible/non-reducible oxides, carbon) or halo-reactant (chlorinated, brominated) considered. The main causes of deactivation proposed include coke formation, sintering of metal nanoparticles, active site occlusion and (most commonly) poisoning due to interaction(s) between the metal and the inorganic acid (HCl or HBr) formed as by-product. Many of these putative causes have been largely suppositions and few of the studies in **Table 9.1** have actually supported these proposals with reliable experimental evidence: see the works of Keane *et al.* [3,19], López *et al*. [5] and de Souza *et al.* [12]. There is a definite need for a comprehensive experimental investigation of the exact source(s) and mechanism(s) of deactivation in order to develop efficient catalytic formutations/processes. In this respect, catalyst characterization in terms of (i) TEM/XRD (for particle size analysis) and (ii) TPR-TPD, TPO and porosity measurements pre- and post-reaction (for carbon deposition) are required. Furthermore, XPS/XANES/EXAFS should provide a better insight into changes in the electronic state of the supported metal particles upon contact with HCl/HBr.

9.2.2 Exclusive Aromatic Ring Hydrogenation

In **Chapters 6** and **8**, the advantages of HDH in terms of product recycle/reuse has been demonstrated in the conversion of 2,4-DCP into (commercially important) C6ONE and 4-CP. The possibility of a selective reduction of the aromatic ring without substituent(s) hydrogenolysis has not received any treatment in the literature, albeit such a transformation has several practical applications. Taking chlorobenzene as a representative haloarene reactant, it may be possible to produce chlorocyclohexane, which is used in the synthesis of industrially important cyclohexene [23]. The same reasoning applies to the selective hydrogenation of, *e.g.* toluene and phenol, where the corresponding methylcyclohexane and cyclohexanol products serve as intermediates in the production of cellulose ethers [24] and Nylon 6 [25], respectively. Homogeneous [26-33] and heterogeneous [31,34-37] catalysts based on Rh [26-28,30-36] and Ru [29,31,32] have now been used for the ring hydrogenation of arenes (notably toluene [26-31,33-36], styrene [30,35,36], ethylbenzene [30,35,36] and xylene(s) [28,29,33,34,36]) and derivates containing heteroatoms (notably cresol(s) [34,36], phenol [26,34,36], anisole [26,27,34,36] and benzoic acid [32,37]) over a wide range of conditions (294 K $\leq T \leq$ 393 K [26,34], 1 atm $\leq P \leq$ 80 atm [26,33]).

However, there is a dearth of studies that have considered exclusive aromatic hydrogenation in the presence of halogen substituents. In this respect, it is worth flagging the work of Okano *et al.* [33] who, in using Rh complexes immobilised over phosphinated silica (at T = 298 K and P = 80 atm), reported the first study (in 1982) of the selective ring reduction of chlorobenzene and ascribed this to the action of Rh^{+1}, *i.e.* the metal retained its oxidized nature after immobilisation and H_2 activation. Therefore catalysts based on nanosized Ru, which present the same electronic configuration as Rh^{+1} ([Kr] $4d^8$) when fully reduced, could be considered as a potential starting point for such a study. The use of Os (with a similar configuration as Ru) should also be considered as an alternative catalytic metal with as of yet limited applications in hydrogenation reactions (as an heterogeneous catalyst).

9.2.3 Hydrotreatment of Polyhalogenated Aromatics

While simple model reactants (*i.e.* chloro- and bromophenols, chlorobenzenes) have been used throughout this thesis, the conclusions drawn may well be applied to the hydrotreatment of polyhalogenated systems. The HDH of hexachlorobenzene [38-41], pentachlorophenol [42-49] and polychlorinated dibenzo-*p*-dioxins and dibenzofurans [16,50-52] has now been successfully achieved over Fe [49,50], Ni [40-43,48], Pd [16,38,44-47,52] and Rh [51] supported on carbon [38,45,51,52], Al_2O_3 [16,41,47,52], SiO_2 [42,43,46,48] and TiO_2 [45,52]. Such promising results from the literature warrant further research and, along with those presented in this work, serve to demonstrate the potential of catalytic HDH as the best means of polyhalogenated waste abatement/recycle.

9.2.4 Hydrogen -Mediated Reactions Using Heterogeneous Au Catalysts

The unique catalytic properties of Au have been demonstrated in **Chapters 7** and **8** where the selective removal of *ortho*- substituted Cl substituents has been established as a result of electronic effects combined with preferential adsorption through the –OH group. These results can be added to the growing literature on selective H_2-mediated reactions involving Au-based catalysts (see the works of Louis *et al.* [53,54], Claus *et al.* [55,56], Bond *et al.* [57,58], Gluhoi *et al.* [59-61] and Andreeva *et al.* [61,62]). The selective hydrogenation of arenes bearing oxygen-containing functional groups represents a challenging catalytic system where the unique selectivity of Au catalysts can be harnessed.

This work can follow the approach adopted in projects to which the author of this thesis has actively contributed, involving the selective reduction of nitroarenes to targeted amine products [63-68].

9.3 References

[9.1] B. Aristizábal, C. A. González, I. Barrio, M. Montes, C. M. de Correa, J. Mol. Catal. A: Chemical, 222, 189 (2004)

[9.2] E.-J. Shin, M. A. Keane, J. Chem. Technol. Biotechnol., 75, 159 (2000)

[9.3] K. V. Murthy, P. M. Patterson, G. Jacobs, B. H. Davis, M. A. Keane, J. Catal., 223, 74 (2004)

[9.4] C. Menini, C. Park, E.-J. Shin, G. Tavoularis, M. A. Keane, Catal. Today, 62, 355 (2000)

[9.5] E. López, S. Ordóñez, F. V. Díez, Appl. Catal. B: Environmental, 62, 57 (2006)

[9.6] F.-D. Kopinke, K. Mackenzie, R. Köhler, Appl. Catal. B: Environmental, 44, 15 (2003)

[9.7] R. Gopinath, N. S. Babu, J. V. Kumar, N. Lingaiah, P. S. S. Prasad, Catal. Lett., 120, 312 (2008)

[9.8] C. A. González, M. Bartoszek, A. Martin, C. M. de Correa, Ind. Eng. Chem. Res., 48, 2826 (2009)

[9.9] E. Ding, S. Jujjuri, M. Sturgeon, S. G. Shore, M. A. Keane, J. Mol. Catal. A: Chemical, 294, 51 (2008)

[9.10] S. Jujjuri, E. Ding, S. G. Shore, M. A. Keane, J. Mol. Catal. A: Chemical, 272, 96 (2007)

[9.11] Y. Hashimoto, A. Ayame, Appl. Catal. A: General, 250, 247 (2003)

[9.12] A. G. F. de Souza, A. M. P. Bentes, A. C. C. Rodrigues, L. E. P. Borges, J. L. F. Monteiro, Catal. Today, 107-108, 493 (2005)

[9.13] K. V. R. Chary, C. S. Srikanth, V. V. Rao, Catal. Commun., 10, 459 (2009)

[9.14] W. Wu, J. Xu, R. Ohnishi, Appl. Catal. B: Environmental, 60, 129 (2005)

[9.15] X. Liu, J. Chen, J. Zhang, Ind. Eng. Chem. Res., 47, 5362 (2008)

[9.16] M. I. Cobo, J. A. Conesa, C. M. de Correa, J. Phys. Chem. A, 112, 8715 (2008)

[9.17] G. Yuan, M. A. Keane, J. Catal., 225, 510 (2004)

[9.18] G. Yuan, M. A. Keane, Appl. Catal. B: Environmental, 52, 301 (2004)

[9.19] G. Yuan, M. A. Keane, Catal. Today, 88, 27 (2003)

[9.20] E. V. Golubina, E. S. Lokteva, V. V. Lunin, N. S. Telegina, A. Y. Stakheev, P. Tundo, Appl. Catal. A: General, 302, 32 (2006)

[9.21] R. F. Bueres, E. Asedegbega-Nieto, E. Díaz, S. Ordóñez, F. V. Díez, Catal. Commun., 9, 2080 (2008)

[9.22] J. W. da-Silva, R. E. Bruns, A. J. G. Cobo, Chem. Eng. J., 131, 59 (2007)

[9.23] H. A. Wittcoff, B. G. Reuben, J. S. Plotkin, Industrial Organic Chemicals, 2nd ed., Witey-Interscience Publication, New Jersey, 2004.

[9.24] K. Verschueren, Handbook of Environmental Data on Organic Chemicals, Van Nostrand Reinhold, New York, 1983.

[9.25] M. T. Musser, Ullmann's Encyclopedia of Industrial Chemistry. "Cyclohexanol and Cyclohexanone", Wiley-VCH Verlag GmbH & Co. KGaA, Weinheim, 2000.

[9.26] P. Giannoccaro, M. Gargano, A. Fanizzi, C. Ferragina, M. Aresta, Appl. Catal. A: General, 284, 77 (2005)

[9.27] K. H. Park, K. Jang, H. J. Kim, S. U. Son, Angew. Chem. Int. Ed., 46, 1152 (2007)

[9.28] K. B. Sidhpuria, H. A. Patel, P. A. Parikh, P. Bahadur, H. C. Bajaj, R. V. Jasra, Appl. Clay Sci., 42, 386 (2009)

[9.29] M. H. G. Prechtl, M. Scariot, J. D. Scholten, G. Machado, S. R. Teixeira, J. Dupont, Inorg. Chem., 47, 8995 (2008)

[9.30] B. Léger, A. Denicourt-Nowicki, H. Olivier-Bourbigou, A. Roucoux, Inorg. Chem., 47, 9090 (2008)

[9.31] P. J. Dyson, Dalton Trans., 2964 (2003)

[9.32] H. Wang, F. Zhao, Int. J. Mol. Sci., 8, 628 (2007)

[9.33] T. Okano, K. Tsukiyama, H. Konishi, J. Kiji, Chem. Lett., 603 (1982)

[9.34] I. S. Park, M. S. Kwon, N. Kim, J. S. Lee, K. Y. Kang, J. Park, Chem. Commun., 5667 (2005)

[9.35] C. Bianchini, V. Dal Santo, A. Meli, S. Moneti, M. Moreno, W. Oberhauser, R. Psaro, L. Sordelli, F. Vizza, Angew. Chem. Int. Ed., 42, 2636 (2003)

[9.36] V. Mévellec, A. Nowicki, A. Roucoux, C. Dujardin, P. Granger, E. Payen, K. Philippot, New J. Chem., 30, 1214 (2006)

[9.37] T. Harada, S. Ikeda, Y. H. Ng, T. Sakata, H. Mori, T. Torimoto, M. Matsumura, Adv. Funct. Mater., 18, 2190 (2008)

[9.38] F. Murena, F. Gioia, J. Hazard. Mater., 162, 661 (2009)

[9.39] A. Ghaffar, M. Tabata, Appl. Catal. B: Environmental, 86, 152 (2009)

[9.40] Y. A. Serguchev, Y. V. Belokopytov, Kinet. Catal., 42, 174 (2001)

[9.41] B. F. Hagh, D. T. Allen, Chem. Eng. Sci., 45, 2695 (1990)

[9.42] E.-J. Shin, M. A. Keane, J. Hazard. Mater. B, 66, 265 (1999)

[9.43] E.-J. Shin, M. A. Keane, Catal. Lett., 58, 141 (1999)

[9.44] U. D. Patel, S. Suresh, J. Colloid Interface Sci., 319, 462 (2008)

[9.45] J. W. da Silva, R. E. Bruns, A. J. G. Cobo, Chem. Eng. J., 131, 59 (2007)

[9.46] T. T. Bovkun, Y. Sasson, J. Blum, J. Mol. Catal. A: Chemical, 242, 68 (2005)

[9.47] H. M. Roy, C. M. Wai, T. Yuan, J.-K. Kim, W. D. Marshall, Appl. Catal. A: General, 271, 137 (2004)

[9.48] E.-J. Shin, M. A. Keane, React. Kinet. Catal. Lett., 69, 3 (2000)

[9.49] A. Kabir, W. D. Marshall, Green Chem., 3, 47 (2001)

[9.50] J.-H. Kim, P. G. Tratnyek, Y.-S. Chang, Environ. Sci. Technol., 42, 4106 (2008)

[9.51] Y. Mitoma, N. Tasaka, M. Takase, T. Masuda, H. Tashiro, N. Egashira, T. Oki, Environ. Sci. Technol., 40, 1849 (2006)

[9.52] Y. Ukisu, T. Miyadera, Appl. Catal. B: Environmental, 40, 141 (2003)

[9.53] A. Hugon, L. Delannoy, C. Louis, Gold Bulletin, 41, 127 (2008)

[9.54] L. Delannoy, N. Weiher, N. Tsapatsaris, A. M. Beesley, L. Nchari, S. L. M. Schroederb, C. Louis, Top. Catal., 44, 263 (2007)

[9.55] C. Mohr, H. Hofmeister, P. Claus, J. Catal., 213, 86 (2003)

[9.56] P. Claus, Appl. Catal. A: General, 291, 222 (2005)

[9.57] F. Moreau, G. C. Bond, Catal. Today, 122, 260 (2007)

[9.58] F. Moreau, G. C. Bond, Catal. Today, 122, 215 (2007)

[9.59] A.C. Gluhoi, X. Tanga, P. Marginean, B. E. Nieuwenhuys, Top. Catal., 39, 101 (2006)

[9.60] A. C. Gluhoi, M. A. P. Dekkers, B. E. Nieuwenhuys, J. Catal., 219, 197 (2003)

[9.61] D. Andreeva, I. Ivanov, L. Ilieva, M. V. Abrashev, R. Zanella, J. W. Sobczak, W. Lisowski, M. Kantcheva, G. Avdeev, K. Petrov, Appl. Catal. A: General, 357, 159 (2009)

[9.62] L. Ilieva, G. Pantaleo, I. Ivanov, A. M. Venezia, D. Andreeva, Appl. Catal. A: General, 65, 101 (2006)

[9.63] F. Cárdenas-Lizana, S. Gómez-Quero, N. Perret, M. A. Keane, Gold Bulletin, 42, 124 (2009)

[9.64] F. Cárdenas-Lizana, S. Gómez-Quero, M. A. Keane, Catal. Commun., 9, 475 (2008)

[9.65] F. Cárdenas-Lizana, S. Gómez-Quero, M. A. Keane, Appl. Catal. A: General, 334, 199 (2008)

[9.66] F. Cárdenas-Lizana, S. Gómez-Quero, M. A. Keane, ChemSusChem, 1, 215 (2008)

[9.67] F. Cárdenas-Lizana, S. Gómez-Quero, M. A. Keane, Catal. Lett., 127, 25 (2009)

[9.68] F. Cárdenas-Lizana, S. Gómez-Quero, A. Hugon, L. Delannoy, C. Louis, M. A. Keane, J. Catal., 262, 235 (2009)